

University of St Andrews



Full metadata for this thesis is available in
St Andrews Research Repository
at:

<http://research-repository.st-andrews.ac.uk/>

This thesis is protected by original copyright

2

AN INVESTIGATION INTO
THE SOLID STATE
FLUORESCENCE OF SOME
ORGANIC AZO PIGMENTS

A thesis presented to the University of St. Andrews
for the degree of Doctor of Philosophy

By

Simon Martyr



September 2001

University of St. Andrews



I, Simon Martyr, hereby certify that this thesis has been composed by me, that is an accurate representation of the work undertaken by me in the University of St. Andrews since my admission as a Research Student on 1st October 1997, and that it has not been accepted in any previous application for any Higher Degree or professional qualification.

September 2001

Signed.

I hereby certify that Simon Martyr has fulfilled the regulations appropriate to the Degree.

September 2001

Signed

In submitting this thesis to the university of St. Andrews I understand that I am giving permission for it to be made available for use in accordance with the regulations of the University Library for the time being in force, subject to any copyright vested in the work not being affected nearby. I also understand that the title and abstract will be published, and that a copy of the work may be made and supplied to any bona fide library or research worker.

Acknowledgements

I'd like to thank the following people.

Mr supervisor, Dr. David Smith for all his help and encouragement throughout my Ph.D. and writing of this thesis, especially through the difficult times.

The guys at Ciba, Dr. Greig Chisholm, Dr. Iain Fraser And Professor Ian Macpherson for their constant help and for putting up with my constant questions.

Professors Ewan Smith and Andrews Mills at the University of Strathclyde for all their help and letting me use their nice machines.

All the technical staff at St. Andrews, including Sylvia for the elemental analyses and Melanja for help with all the NMR stuff.

Drs Elizabeth McClean and Simon Teat at Daresbury, Phil Lightfoot at St. Andrews and Alan Kennedy at Strathclyde for trying to get the single crystal structures of those stubborn bis-azo pigments (not the easiest thing in the world to do to say the least).

Drs Phil Lightfoot and Alex Slawin for the monoazo crystal structures.

Past group members, Drs Colin French, Colin Morton and Rick White.

Louis "mopatop" Rogers for all his help and advice and use of his laptop and Ivor Bull for putting me up rent free while writing up the final stages of my thesis.

Various others such as James Errey, Tim Jones, Leon Jackson, Dave Elias and Paul "Mr Spok" Wheatley for providing me with a constant source of amusement (usually at their expense).

The EPSRC and Ciba Speciality Chemicals for the funding.

Abstract

Several novel yellow, orange and red diarylide fluorescent azo pigments were synthesised from *o*-dianisidine and 2,2'-dichlorobenzidine with coupling components based on a cyclic 1,3-diketone or 1,3-diester skeleton. Fluorescence and absorption properties of these pigments in solution and the solid state were studied and compared with those of several known commercial diarylide pigments. The novel diarylide pigments show varying levels of fluorescence in the solid state and solution, the most intense being compound (65).

Particle size measurements were also studied using transmission electron microscopy. It has been shown that for those pigments which exhibited solid-state fluorescence, smaller particle sizes resulted in a greater fluorescence intensity.

Due to inherent difficulties in growing crystals suitable for single crystal diffraction from diarylide pigments, powder X-ray diffraction was used to study novel pigments in the hope of gaining information relating to distances between adjacent layers of molecules and side-by-side separation of molecules. This proved problematic in numbers of cases, due to the complexity of the powder XRD traces. Several crystal structures for commercial pigments were already known, so detailed examinations of these structures were carried out to investigate if any relationship exists between crystal structure and solid-state fluorescence. Where growing crystals of the diarylide pigments has proved to be problematic, monoazo analogues of the diarylide pigments were synthesised, characterised and studied by single crystal X-ray diffraction; other monoazo analogues where crystal structures were already known were studied. It is found that correlations between the mono and the corresponding bis-azo (diarylide) pigments have to be treated cautiously. Trends such as bond lengths and through-space interatomic distances were reasonably consistent, but comparisons of torsion angles and crystal packing are not necessarily meaningful. The main cause of solid-state fluorescence in the pigments is thought to be reduced intermolecular interactions due to distances between the molecules in the lattice.

Legend

NMR	Nuclear magnetic resonance
XRD	X-ray diffraction
δ	Chemical shift (ppm)
s	singlet
br s	broad singlet
d	doublet
m	multiplet
UV	Ultra-violet
ϵ	Molar absorption coefficient
m.p.	Melting point
DMF	<i>N,N</i> -Dimethylformamide
DMSO	Dimethylsulfoxide
THF	Tetrahydrofuran
DCB	<i>o</i> -dichlorobenzidine
PO13	Pigment Orange 13
PO34	Pigment Orange 34
PO16	Pigment Orange 16
PR254	Pigment Red 254
PV19	Pigment Violet 19
PY12	Pigment Yellow 12
PY13	Pigment Yellow 13
PY14	Pigment Yellow 14
PY17	Pigment Yellow 17
PY63	Pigment Yellow 63
PY83	Pigment Yellow 83
PY101	Pigment Yellow 101
PY8501	Pigment Yellow 8501

Contents

1.0 Introduction.....	1
1.1 Pigments and Dyes	1
1.2 Organic and Inorganic Pigments	2
1.3 Organic Pigments.....	2
1.3.1 Non-azo pigments.....	3
1.3.2 Phthalocyanine Pigments.....	3
1.3.3 Quinacridone Pigments.....	3
1.3.4 Perylene and Perinone Pigments	4
1.3.5 2 <i>H</i> , 5 <i>H</i> -Pyrrolo[3,4- <i>c</i>]pyrrole-1,4-dione (DPP) Pigments	5
1.3.6 Azo Pigments.....	6
1.4 Ketohydrazone Tautomerism and Hydrogen-Bonding in the Solid State	6
1.5 Coupling Components	8
1.6 Monoazo Pigments	8
1.7 Bis-Azo Pigments	9
1.8 Lightfastness and Weatherfastness in Azo Pigments	10
1.9 Diazotisation.....	11
1.10 Coupling	11
1.11 Polymorphism.....	12
1.12 Hue.....	12
1.13 Fluorescence and Phosphorescence.....	13
1.14 Pigment Orange 16	17
1.15 Solid-State Fluorescence of PO16.....	17
1.15.1 Solid-state Fluorescence in Pigments Structurally Similar to PO16	18
1.16 Solid-state Fluorescence in Other Pigments	19
1.16.1 Pigment Yellow 101	19
1.16.2 Solid-state Fluorescence (1,4-Diketopyrrolo[3,4- <i>c</i>]pyrroles (DPPs)	20
1.16.3 Solid-state Fluorescence of Perylene Dyes.....	21
1.16.4 Pigment Yellow 8501	22
1.16.5 Dicyanopyrazine Dyes.....	25
1.16.6 Aromatic Dicarboxamides	26
1.17 Patent Information on Other Pigments With Solid-State Fluorescence	29
2.0 Aims and Objectives.....	30
2.1 Organic Electroluminescent Devices and Displays	30
2.2 Special Effects Printing	30
2.3 Security Printing	31

3.0 Results and Discussion	33
3.1 Synthesis of Novel Diarylide Pigments	36
3.2 Prior Art - Crystal Structure Analysis of Diarylide Pigments	39
3.2.2 PY13 (44).....	41
3.2.3 PY14 (45).....	43
3.2.4 PY63(46).....	44
3.2.5 PY83 (48).....	46
3.3 Non-Commercial Diarylide Pigments	48
3.3.1 (43).....	48
3.4 Crystal Structure Analysis of Novel Diarylide Pigments	50
3.5 Synthetic Mono-Azo Analogues.....	50
3.5.1 2-[(2-Chlorophenyl)hydrazono]-3-oxo- <i>N</i> -phenylbutyramide (73).....	52
3.5.2 2-[(2-Chlorophenyl)hydrazono]-3-oxo-3, <i>N</i> -diphenylpropionamide (74).....	54
3.5.3 Novel Mono-Azo Compounds.....	56
3.5.4 2-[(2-Methoxyphenyl)hydrazono]-3-oxo- <i>N</i> -phenylbutyramide (71)	56
3.5.5 2-[(2-Methoxyphenyl)hydrazono]- <i>N</i> -(2,4-dimethylphenyl)-3-oxobutyramide (72)59	
3.5.6 2-[(2-Methoxyphenyl)hydrazono]-5,5-dimethylcyclohexane-1,3-dione (68) and 5- [(2-methoxyphenyl)hydrazono]-2,2-dimethyl-1,3-dioxan-4,6-dione (69)	62
3.6 Intermolecular Interactions and Crystal Packing Trends in Known Diarylide Pigments	66
3.6.1 PY12 (42).....	66
3.6.2 PY13 (44).....	67
3.6.3 PY14 (45).....	68
3.6.4 PY63 (46).....	69
3.6.5 PY83 (48).....	70
3.6.6 (43).....	71
3.7 Quantitative Fluorescence Measurements of Pigments	73
3.7.1 Solid-State Fluorescence	74
3.7.2 Solution Fluorescence.....	78
3.8 Quantitative Absorption Measurements of Pigments	82
3.8.1 Solution and Solid-State Absorption Measurements	82
3.9 Comparison of Fluorescence and Absorption Data	82
3.10 Particle Size Measurements	93
3.11 Powder X-ray diffraction studies.....	94
3.12 Conclusions.....	111
3.12.1 Crystal Structure and Packing and Effect on Solid-State Fluorescence	112
3.12.2 Particle Size and Effect on Fluorescence.....	113
3.13 Further Work	114
4.0 Experimental.....	116

4.1 General.....	116
4.11 X-ray Diffraction	117
4.12 Single crystal X-ray diffraction	125
4.2 Problems with Manufacture and Synthesis of PO16 and Similar Pigments.....	127
4.3 General Method for Synthesis of Bis-azo Pigments.....	131
4.4 General Method for Synthesis of Monoazo Pigments	135
4.5 Ciba Method for Synthesis of Bis-azo Pigments	139
4.6 Crystal Growth Techniques	139
4.6.1 Bis-azos.....	139
4.7 Solid-State Fluorescence Measurements	139
4.8 Solution Fluorescence and Absorption Measurements.....	140
4.9 Solid State Absorption Measurements.....	140

References 141

Appendices..... 145

2-[(Methoxyphenyl)hydrazono]-3-oxo- <i>N</i> -phenylbutyramide (74).....	145
2-[(2-Methoxyphenyl)hydrazono]- <i>N</i> -(2,4-dimethylphenyl)-3-oxo-butylamide (75).....	152
2-[(2-Methoxyphenyl)hydrazono]-5,5-dimethylcyclohexane-1,3-dione.....	159
5-[(2-methoxyphenyl)hydrazono]-2,2-dimethyl-1,3-dioxan-4,6-dione (72).....	166
Electron Microscopy Photographs.....	173

1.0 Introduction

1.1 Pigments and Dyes

The general aspects of this topic have been discussed intensively in two recent texts.^{1,2}

Synthetic colourants are either classified as pigments or dyes. Pigments are inorganic or organic, coloured, white or black materials that are practically insoluble in the medium in which they are incorporated and cannot be washed out of the medium, even from the surface. Dyes, unlike pigments, do dissolve during their application and in the process lose their crystal or particulate structure. It is by their physical characteristics rather than by chemical composition that pigments are differentiated from dyes.³

In many instances, the chemical structures of dyes and pigments are very similar. As pigments are required to be insoluble, it is necessary to avoid solubilizing groups in the molecule.

Certain classes of pigment may be practically insoluble in one medium, yet soluble to a certain extent in another. Partial solubility of a pigment is a function of the application medium and processing conditions, especially that of the processing temperature. Important application properties of pigments and/or pigmented systems, such as hue, tinctorial strength, migration, recrystallisability, heat stability, lightfastness and weatherfastness are often determined by the packing of molecules within the crystal, crystal shape and size (morphology) and by the pigment crystal surface. The usefulness of a colourant as a commercial pigment is dependent on its interaction with the application medium under the conditions in which it is incorporated in the medium and subsequently processed.³

1.2 Organic and Inorganic Pigments

In some application areas, inorganic pigments are used to an appreciable extent, frequently in combination with organic pigments. However, a comparison between the two classes of pigments shows some fundamentally important differences between the two classes.¹

Most inorganic pigments are extremely weatherfast and many have excellent hiding power. Their rheology is usually an advantage, being superior to that of most organic pigments under comparable conditions. However, with the exception of a select few (Molybdate Red, Chrome Yellow, cadmium-based pigments and titanium dioxide) inorganic pigments provide dull shades in comparison to organic pigments. Due to toxicity concerns, alternatives to cadmium-based pigments are being looked at.³

Poor tinctorial strength and lack of brilliance restrict the use of inorganic pigments in printing inks. There are areas of application, however, where it is hardly, if at all, possible to replace the inorganic species by an organic pigment. The ceramics industry, for example, requires extreme heat stability, which precludes the use of organic compounds. Thus, the organic and inorganic classes of pigment are generally considered complementary rather than competitive.¹

1.3 Organic Pigments

Organic pigments can generally be classified into two main groups, the azo and the non-azo pigments. The latter, in the main, are polycyclic pigments. The commercially important group of azo pigments can be further classified according to structural characteristics, such as by the number of azo groups or by the type of diazo or coupling component (section 1.5 page 8). Polycyclic pigments may be classified by the number and the type of rings that constitute the chemical type.

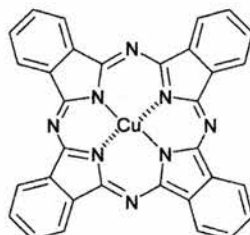
1.3.1 Non-azo pigments

There are several different classes of non-azo pigment. A few important classes are listed below.

1.3.2 Phthalocyanine Pigments

The phthalocyanine structure,⁴ a tetraazatetrabenzoporphine, provides the basis of all phthalocyanine pigments. This molecule can chelate with a large variety of metals under various coordination conditions. However only copper (II) complexes in the main are of practical importance as pigments. Colours range from green to blue. Excellent general chemical and physical properties, combined with a reasonable cost, give them the largest market share of any organic pigments.¹

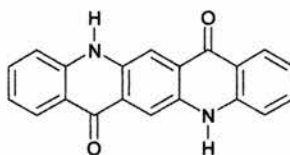
Shown below is copper phthalocyanine blue (1)⁵ which is the copper (II) complex of tetraazatetrabenzoporphine. This pigment complex is used in a wide range of applications. Lightfastness is good enough for automotive paints but it is inexpensive to make so it can also be used for printing inks and plastics.



(1)

1.3.3 Quinacridone Pigments

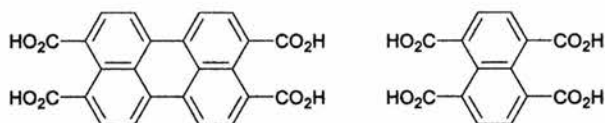
The quinacridone structure is a linear system of five annellated rings.^{6,7} These pigments perform like phthalocyanine pigments. Outstanding light and weatherfastness, solvent resistance and migration resistance justify the somewhat high market price in applications for high-grade industrial coatings, such as automotive finishes, plastics and special printing inks. Shown below is an example of a commercially available quinacridone pigment, Pigment Violet 19 (2).



(2)

1.3.4 Perylene and Perinone Pigments

Perylene and perinone pigments are chemically related. They are derived respectively from perylene-3,4,9,10-tetracarboxylic acid (3) and naphthalene-1,4,5,8-tetracarboxylic acid (4) are shown below.



(3)

(4)

Commercially available types provide good to excellent lightfastness and weatherability although some of them, however, darken upon weathering.³ A number of them have excellent heat stability, which renders them suitable for spin dyeing. Spin dyeing is a technique that falls between the plastics and textiles industries. In contrast to textile colouration, the material to be extruded is coloured before the fibre is made. Spin dyeing falls into three different categories.³

*Melt spinning*¹ – This is used with thermoplastic materials such as polyesters, polyamides or polypropylene. The polymer is melted in the extruder and then pressed through a spinnerette. It solidifies by cooling as it falls vertically through a shaft to the bottom of the extruder. Pigments incorporated into these materials are therefore expected to exhibit excellent heat stability. As a rule, pigment preparations for this application are first incorporated (mixed) into a “carrier”, which may be identical or similar to the polymer which is to be extruded.

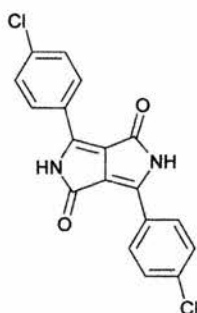
*Wet Spinning*¹ – This technique is characterised by spinning a filtered viscous polymer mass, dissolved in a suitable solvent, into contact with a precipitation or coagulation bath. Polyacrylonitrile, polyvinyl acetate and cellulose acetate are processed by this method. Thermal requirements for pigments are less stringent than

for melt spinning. However the pigments are expected to be fast (chemically resistant) to the solvents and chemicals used.

*Dry Spinning*¹ – The polymer, dissolved in a suitable solvent and the solution then filtered, is pressed through spinnerettes and, in an anaerobic environment, pulled by vacuum through a heated shaft. The polymer solidifies as the solvent evaporates. The requirements of this process regarding the heat stability of pigments are much less stringent than in melt spinning. However, like wet spinning, pigments must be fast to the solvents used. Polyacrylonitrile, triacetate and polycarbonate are processed by this method.

1.3.5 2H, 5H-Pyrrolo[3,4-c]pyrrole-1,4-dione (DPP) Pigments

In the early 1980s, Ciba discovered a new type of heterocyclic pigment^{8,9} based on a symmetrical chromophore, the 1,4-diketopyrrolo[3,4-c]pyrrole system (R = alkyl, aryl, Cl, Br, CF₃). The basic skeleton of this newly developed group of pigments consists of two annellated five-membered rings each of which contains an amide moiety in the ring (5).

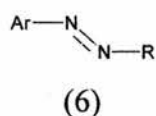


(5)

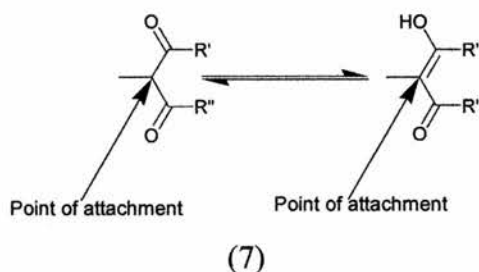
This class of pigment has some commercially used representatives, one of them with great importance in the market, Pigment Red 254 (PR254) (5).¹ In full shades and white reductions i.e. mixed with titanium dioxide, the pigments afford shades in the colour range from orange to medium and bluish reds. The pigments are primarily used in high-grade industrial coatings, including automotive finishes and in plastics, because of their excellent lightfastness and weatherfastness and their good heat stability.¹

1.3.6 Azo Pigments

Azo pigments carry an azo function, $-N=N-$, between two sp^2 hybridised carbon atoms, the azo group being a chromophore in its own right. They are based on the formula (6)²



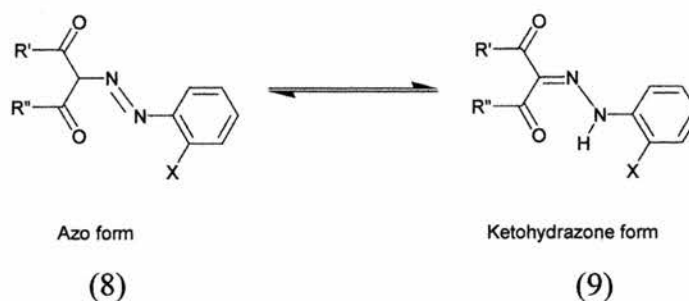
in which Ar is an aromatic or heteroaromatic moiety and R is either an aromatic unit or represents the function (7)



An alkyl or aryl group is usually attached in the R'' position. Most current commercially important pigments are derivatives with $R'' = CH_3$. R' is most commonly $-NH-Ar$, in which Ar may be either benzenoid or heteroaromatic.¹

1.4 Ketohydrazone Tautomerism and Hydrogen-Bonding in the Solid State

There is a possibility of ketohydrazone tautomerism in azo pigments depending upon the coupling component which is used, e.g.

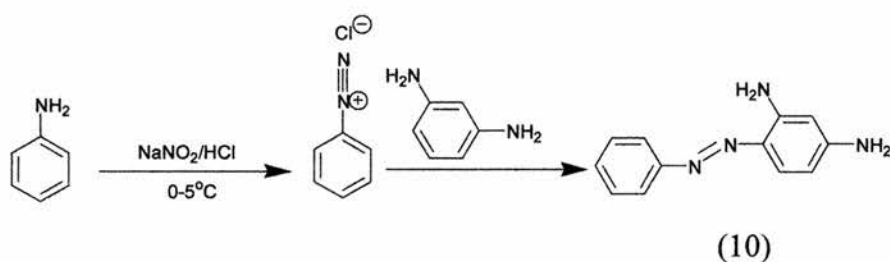


Scheme 1

It has been found (from X-ray crystallography and NMR) that a significant number of azo pigments exist in the ketohydrazone form (9).¹⁰⁻¹² It has been suggested that the ketohydrazone form is more thermodynamically stable due to the increased hydrogen bonding (both intramolecular and intermolecular) present both in solution and the solid state.¹¹⁻¹³

Azo pigments are conveniently subdivided into mono and bis-azo pigments (although bis-azo pigments are sometimes referred to as disazo pigments in the pigment industry). Compounds containing more than two azo groups have failed to gain commercial importance. The synthesis of azo pigments is economically attractive, because the standard sequence of diazonium salt formation and subsequent reaction with a wide choice of coupling components allows access to a wide variety of products.¹

The first important event in the history of azo pigments was the discovery of the diazotisation reaction by Griess in 1858.¹⁴ In 1875, Caro and Witt¹⁵ synthesised chrysoïdin (10) (scheme 2), the first azo dye, through a reaction sequence of diazotisation and coupling, a technique which continues to be used today.



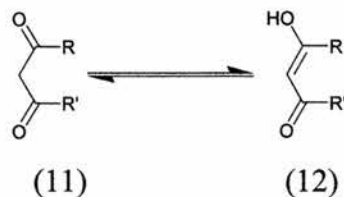
Scheme 2

Azo pigments are typically formed by a reaction sequence of diazotisation and coupling, involving a primary aromatic amine, and a nucleophilic aromatic or aliphatic compound with an active methylene group referred to as a *coupling component*.²

1.5 Coupling Components

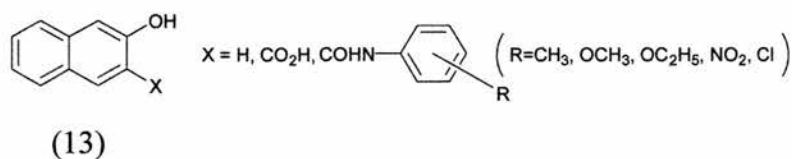
The technically most significant groups of coupling components are:¹

a) Compounds containing activated methylene groups of the type (11)

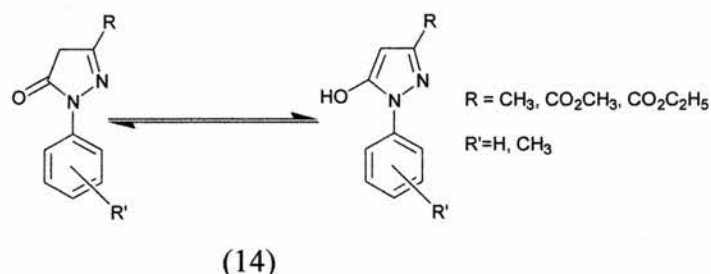


Scheme 3

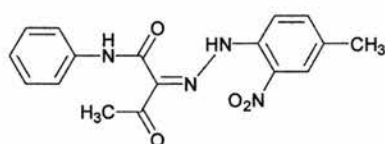
b) 2-Naphthol, 3-hydroxy-2-naphthoic acid, or their derivatives (13) (especially amides).



c) Pyrazolone derivatives (14).



1.6 Monoazo Pigments



Pigment Yellow 1 - an example of a monoazo pigment

(15)

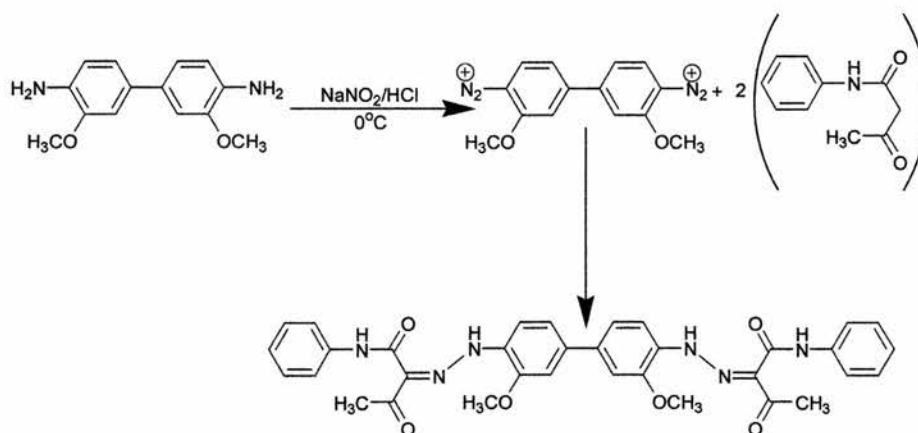
These pigments are potentially tautomeric but infra-red, X-ray and ¹³C NMR spectra indicate that the hydrazone tautomer^{11,16} readily predominates in the solid state and in the usual NMR solvents (section 1.4 page 6).

All members of this pigment family share good lightfastness, but this is combined with poor solvent and migration resistance. These properties define the limit of their application. Monoazo pigments are used extensively in air-dried alkyd resins and in

emulsion paints, and certain inks used in flexo and screen-printing. Other applications are in letterpress and offset inks.¹

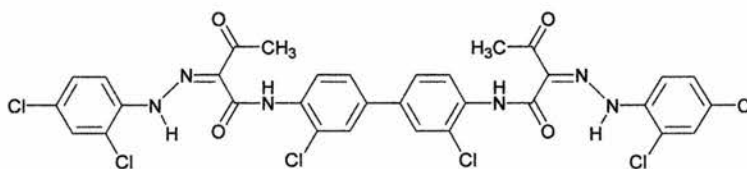
1.7 Bis-Azo Pigments

There is a dual classification system based on differences in the starting materials. The first and most important group includes compounds which are derived from diaminobiphenyls e.g.¹



Scheme 4

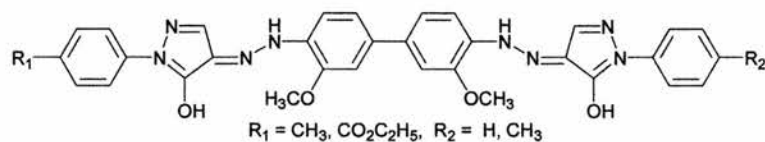
The second group, bisacetoacetic arylide pigments, is based on bis (acetoacetic amide), e.g. a diaminobiphenyl is reacted with a coupling component to form a bis (acetoacetic amide) which is then reacted with a diazotised amine.¹



Pigment Yellow 16, an example of a bisacetoacetic amide pigment

(16)

Acetoacetic arylamides and 1-arylpyrazol-5-ones are the two most common types of coupling component. The former affords diarylide yellow pigments e.g. (16) whilst the latter produces bisazopyrazolone pigments e.g. (17).



(17)

1.8 Lightfastness and Weatherfastness in Azo Pigments

Little is known about the relation between chemical constitution and lightfastness/weatherfastness of pigments, although it is clear that the fastness is primarily defined by the chemistry of the molecule. Various pigments, for example, undergo degradation upon exposure to light, irrespective of whether they are crystalline or in solution. The surrounding medium – the vehicle in which a pigment is applied – also affects the stability of a compound to light : the tendency of optically excited pigment molecules to react with their surroundings varies with the vehicle in which they are applied.¹⁷

High-grade pigments cannot generally be studied in solution, because they are insoluble in almost all solvents.

In azo pigments, a straightforward correlation may be established between the lightfastness and weatherfastness on the one hand and the substitution pattern on the other hand.¹⁷ Resistance to light and weather is generally improved by electron acceptors that are introduced through the diazo component (nitro groups, alkoxy carbonyl groups), even more so in combination with electron donors (methoxy or methyl groups) in the phenyl moiety of the coupling component.¹⁷ Obviously, the substitution pattern of the aromatic system, especially that of the diazo component, has a major impact on the molecule; light-and-weather-fastness properties tend to improve in the sequence *meta* – *para* – *ortho* substitution. In the same order, the formation of intermolecular and intramolecular hydrogen bonds is probably facilitated.¹⁷

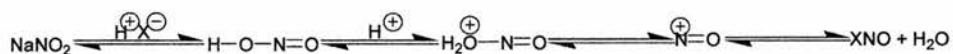
1.9 Diazotisation

Diazotisation² is the reaction of a primary aromatic amine with a nitrosating agent, such as sodium nitrite or, to a lesser extent, nitrosylsulfuric acid, nitrous gases, or organic nitrites in an aqueous acidic solution at a temperature between 0 and 5°C, and converting the amine to its diazonium salt. The arylammonium ion is unable to undergo diazotisation since the crucial step in the diazotisation mechanism is the electrophilic nitrosation of the free amino group.^{2,18}



Scheme 5

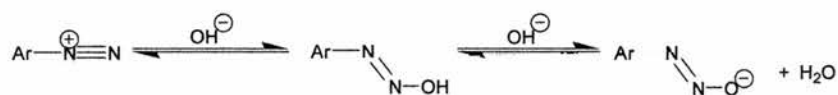
The diazotisation reaction requires an additional quantity of acid; formation of the active nitrosating agent XNO proceeds via the underlying equilibrium.²



Scheme 6

1.10 Coupling

The coupling reaction involves electrophilic substitution of an enol: although it is necessary to add bases or buffers to the reaction mixture in order to maintain a constant pH and to optimise the outcome of the coupling process, it is not normally necessary to use a strong base which deprotonates the enol prior to coupling. Highly basic solutions do not permit coupling in aqueous media (this only applies to acetoacetarylamide couplings) as they convert the diazonium compound to a *trans* diazotate ion, which does not couple.²



Scheme 7

Weakly acidic or weakly basic conditions thus provide the optimum conditions.¹ Buffers such as sodium acetate, magnesium oxide and potassium carbonate may be used. Alternatively, as in the large-scale commercial process used by Ciba, a dilute (3 to 6%) sodium hydroxide solution is constantly added during the coupling reaction.

1.11 Polymorphism

Forces of mutual attraction between molecules or ions of many organic compounds which prevail as solid compounds frequently transform the individual molecules into different crystal structures. A large number of organic pigments are *polymorphous* i.e. they occur in more than one modification or crystal structure, despite identical chemical composition. The quinacridone pigment Pigment Violet 19 (PV19) (2) displays at least three different modifications.⁷ Different polymorphs can be detected by means of powder X-ray diffraction.

The thermodynamic stability is a feature unique to each of the individual crystal structures of a chemical compound. Transforming an unstable modification into a stable one may require a certain amount of activation energy, but the process always offers an ultimate energetic advantage. Energy levels may vary considerably between different crystal modifications. One important commercial pigment which exhibits polymorphism is copper phthalocyanine (1). At least 5 polymorphs are known.¹⁹ Alpha and beta forms are the most important commercially. The alpha is the kinetic product, formed by rapid precipitation from oleum into water. The more thermodynamically stable beta form is obtained by heating the alpha form in a high boiling aromatic solvent. The alpha form is red-shade blue (used in paints), the beta form is green-shade blue (used as the cyan in three-colour printing).¹⁹

1.12 Hue

The appearance of colour is associated with electronic excitation within a molecule caused by absorption of electromagnetic radiation in the visible region of the electromagnetic spectrum.² Electrons are elevated from the ground state energy level to an excited state by absorbing selected frequencies of incident radiation, thus giving the molecule the shade of the resulting complementary colour. Electronic excitation also occurs with vibrational and rotational transitions and this is responsible for the appearance of more or less broad absorption bands. An absorption band is said to undergo a *bathochromic* shift if a comparison of different spectra shows it has shifted

to a longer wavelength. A shift to shorter wavelengths is termed a *hypsochromic* shift.²

The hue is primarily defined by the pattern of *chromophores*. A chromophore is a system of conjugated double bonds (π -electron systems) which is responsible for the absorption of visible light.

Azo pigments, like all azo compounds, can be viewed as systems in which electron donors and electron acceptors are connected via a chromophore, e.g. the azo group ($-\text{N}=\text{N}-$), to form a system of conjugated double bonds.

1.13 Fluorescence and Phosphorescence

A molecule or ion in an excited state can lose the absorbed energy in the following ways;

- a) Radiationless transitions, such as internal conversion (IC) or intersystem crossing (ISC).
- b) Emission of radiation (fluorescence and phosphorescence).
- c) Photochemical reactions.

Processes of type (a) and (b) are represented in a so called *Jablonski diagram*²⁰ (figure 1) which is a scheme of the essential energy levels (see page 15). The lowest vibrational energy levels of electronic excited states are indicated by thick horizontal lines; other horizontal lines represent associated vibrational levels. A molecule (or ion) in the ground state S_0 will be brought to an excited singlet state, either S_1 or S_2 , by absorption of light. Radiationless transitions are shown by wavy lines in a Jablonski diagram. Vibrational deactivation (denoted as vd in the diagram) (vertical wavy lines) leads to the lowest vibrational level of the respective excited singlet electronic state or to lower singlet states. Intersystem crossing (ISC) (horizontal wavy lines) leads to triplet excited states (see page 15). Internal conversion (IC) is the process by which the electronic energy is converted into vibrational energy of the

molecule itself without a change of multiplicity. Emission of radiation from the lowest vibrational level of the excited state S_1 to any of the vibrational levels of the ground state is called *fluorescence*. Emission of radiation from the lowest triplet state T_1 to the ground state is called *phosphorescence*. If both types of radiation are discussed or observed, or it is not known whether the radiation is fluorescence or phosphorescence, the term *luminescence* is used.

The term phosphorescence²¹ refers to processes in which there is a change of multiplicity. Many examples of phosphorescence involve triplet – singlet transitions and are preceded by processes in which an excited singlet state is converted into an excited triplet state. In order to display phosphorescence, molecules primarily excited to the S_1 singlet state must convert to the lowest level of their triplet manifold (T_1) by the radiationless process of intersystem crossing (ISC). From T_1 they can slowly emit radiation (phosphorescence), or they can return to the S_0 level without emission by intersystem crossing (ISC). Formally, a triplet state cannot convert into a singlet state because an electron spin cannot reverse in a transition (it is a forbidden transition). The radiative transition is not totally forbidden, however, as the mechanism that was responsible for the ISC also breaks the selection rule. This mechanism is referred to as spin-orbit coupling.²¹ This occurs where the magnetic field arising from an electron's orbital motion around the nucleus interacts with the spin magnetic moment of the electron, and flips it to a new orientation. The strength of the orbitally generated magnetic field increases as the nuclear charge increases. The molecule is therefore able to emit weakly, and the emission may continue long after the original state was formed. Phosphorescence spectra are also usually shifted bathochromically, but more so than is observed in fluorescence. The reason for this is that the energy of the triplet state T_1 is usually below that of the singlet S_1 . Therefore, phosphorescence takes place at higher wavelengths than fluorescence.

Absorption of radiation normally occurs from the lowest vibrational level of the electronic ground state and leads to one of the vibrational levels of an electronic excited state. Fluorescence generally takes place from the lowest vibrational level of the first excited state (S_1)* and results in the electron dropping to one of the

vibrational levels of the ground state. The fluorescence spectrum, in ideal cases, is therefore a mirror image of the absorption spectrum, but shifted to longer wavelengths (Stokes' rule).²¹

With the exception of phosphorescence, all radiation processes are very fast. First order rate constants for these processes have the following orders of magnitude:²¹

Light absorption	10^{15}s^{-1}
vd	$\geq 10^{12}\text{s}^{-1}$
fluorescence	10^6 to 10^9s^{-1}
phosphorescence	10^{-2} to 10^4s^{-1}

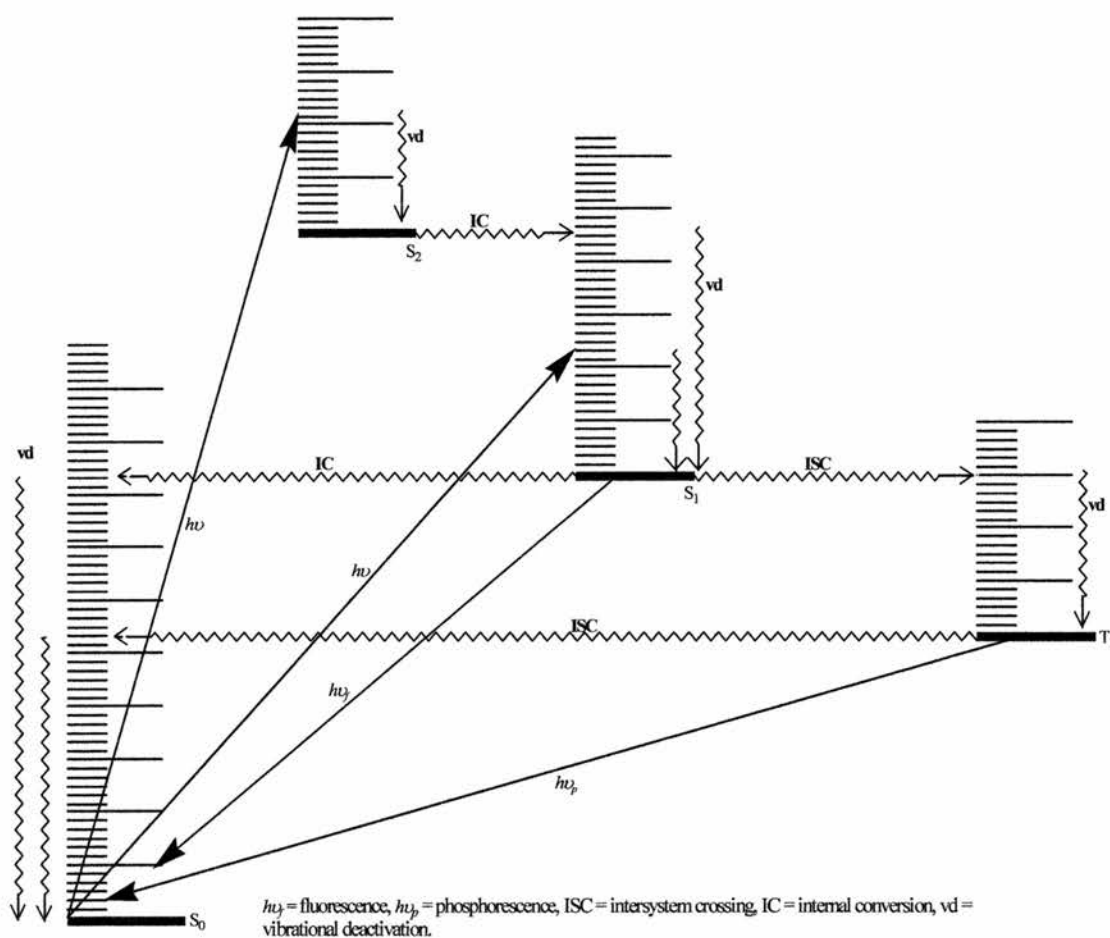
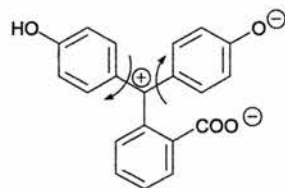


Figure 1-Jablonski Diagram

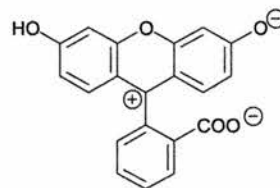
Most fluorescent organic compounds are characterised by a rigidity of their structure that prevents the energy of the excited states from being lost by torsional vibrations of

the molecule. The classic example is fluorescein²² (19) which is highly fluorescent. In contrast, phenolphthalein²³ (18) shows no fluorescence because in this compound the excited state loses energy by internal conversion (vibrations of the benzene rings), a process not possible to the same extent in fluorescein due to the ether bridge.



Phenolphthalein

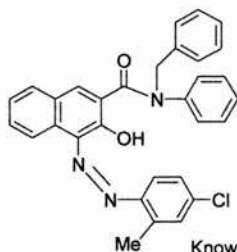
(18)



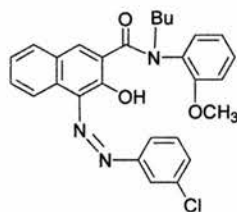
Fluorescein

(19)

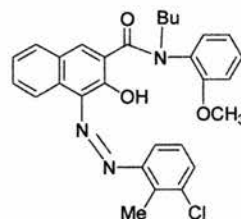
Also some azo pigments are fluorescent in the solid state.^{24,25}



(20)



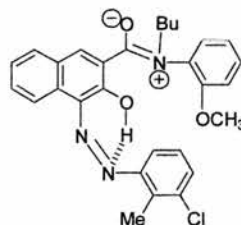
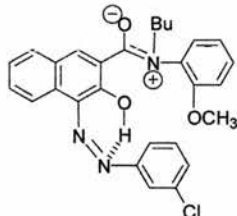
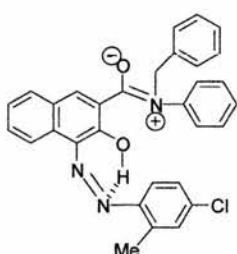
(21)



(22)

Known examples of fluorescent organic azo pigments

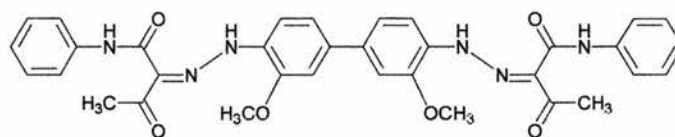
These pigments are also known to have very poor lightfastness, which presumably has precluded their industrial use. It is reasonable to assume that these pigments all have rigid non-planar structures, which hinder vibrational deactivation and fluorescence is the more likely path for energy dissipation. One could speculate that all these structures could adopt a planar conformation and have an extensive hydrogen bonded network if they are illustrated in the following mesomeric forms.



Shown in this form, there is restricted rotation about the amide carbon-nitrogen bond which could contribute towards the planarity of the structures.

1.14 Pigment Orange 16

Structurally based on 3,3'-dimethoxybenzidine as the diazo component, Pigment Orange 16 (PO16) (**23**) is also known as Dianisidine Orange.



Pigment Orange 16

(**23**)

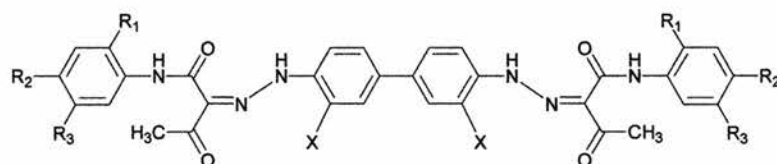
At present, the pigment enjoys some importance in Europe, the USA and Japan. The largest area of application for PO16 (**23**) is in the printing ink industry.¹ The pigment is used to adjust the shades of Pigment Yellow 12 (PY12) type diarylide yellow pigments, to which it is most closely related as far as performance is concerned. Such blends are used in low-cost packaging and speciality inks. The chemical structure of PY12 is identical to that of PO16 (**23**) with the exception that 3,3'-dichlorobenzidine is used as the diazo component (see later). PO16 (**23**) is not lightfast and durable enough to be used in industrial paints although it is used in decorative paints. In this respect, it performs even more poorly than PY12.¹ Low-cost production, however, makes it a suitable colourant for rubber and textile printing.

1.15 Solid-State Fluorescence of PO16

Recently it was discovered by Ciba that PO16 (**23**) exhibited fluorescent characteristics in the solid state.²⁶ PO16 (**23**) has been known and manufactured for years and is a well-established pigment throughout the industry. This was a totally unexpected event, and has prompted a renewed investigation into PO16 (**23**) and other similar pigments for their solid-state fluorescent properties.

1.15.1 Solid-state Fluorescence in Pigments Structurally Similar to PO16

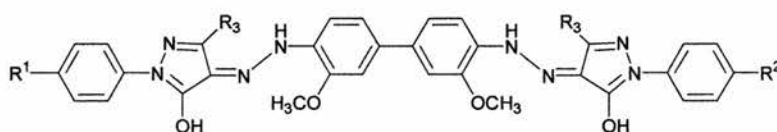
Recently, two patents submitted by the Sun Chemical Corporation^{27,28} claimed to observe solid-state fluorescence in the following pigments:



(24)

Pigment	X	R ₁	R ₂	R ₃
PY12	Cl	H	H	H
PY13	Cl	CH ₃	CH ₃	H
PY14	Cl	CH ₃	H	H
PY17	Cl	OCH ₃	H	H
PY63	Cl	Cl	H	H
PY83	Cl	OCH ₃	H	OCH ₃
PO16	OCH ₃	H	H	H

Table 1



(25)

Pigment	R ₁	R ₂	R ₃
PO13	H	H	CH ₃
PO34	CH ₃	CH ₃	CH ₃

Table 2

It is known by Ciba that PY12, PY14, PO16 (23) and PY63 are fluorescent in the solid state and in solution.²⁶ However analysis by Ciba has found structurally similar pigments such as PY13 and PY83 not to be fluorescent. The patent claims that not

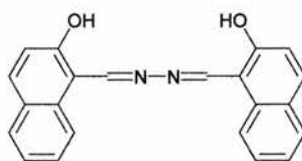
only PO16 was fluorescent but has also claimed PO13 and PO34 are fluorescent^{27,28} although it gives no data in reference to this.

1.16 Solid-state Fluorescence in Other Pigments

Solid-state fluorescence has been encountered in other pigments, the most important ones are discussed below.

1.16.1 Pigment Yellow 101

The oldest known example of a fluorescent pigment is PY101¹ (**26**) which has been known since 1899 as a fluorescent dye and was used later as a pigment for the mass colouration of viscose. It is obtained by condensing 2 moles of 2-hydroxy-1-naphthaldehyde with one mole of hydrazine.

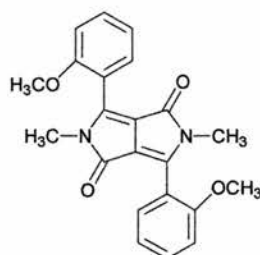


(26)

PY101 (**26**) produces uncommonly brilliant yellow shades. It is referred to as a fluorescent pigment and in this respect it is quite rare among available organic pigments. The vast majority of industrial fluorescent pigments are in fact fluorescent dyes which are dissolved in suitable media such as thermosetting resins i.e. individual molecules in solid solution.¹ Some of these provide good migration resistance through chemical interaction between dye and resin. PY101 (**26**), on the other hand, is a crystalline pigment, although it shows somewhat less fluorescence than resin-based dyes.

1.16.2 Solid-state Fluorescence (1,4-Diketopyrrolo[3,4-*c*]pyrroles (DPPs))

Some derivatives of DPP have been found to be fluorescent in the solid state.²⁹ An important derivative is the compound below (27) (the bis-*o*-methoxy derivative) as it has been found to crystallise in two different modifications (an example of polymorphism).

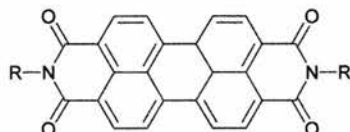


(27)

The first is the more thermodynamically stable form, with a strong solid-state fluorescence, and the other (metastable) form shows a weak solid-state fluorescence. Complete structural information has been obtained by Langhals *et al.*²⁹ so there are comprehensive data on lattice packing. In the metastable compound (the weakly fluorescent molecule) the chromophores are stacked one over the other, so that there are strong interactions between the chromophores. Langhals³⁰ proposes that these interactions will not only cause a bathochromic shift in the solid-state absorption but also a rather strong coupling of the electronic energy to lattice vibrations. The coupling could enhance an energy transfer to lattice vibrations and therefore fluorescence quenching can occur. In the other form, the chromophores are laterally shifted relative to one another so that there is only a little interaction. Consequently, excitation energy persists until fluorescence occurs.

1.16.3 Solid-state Fluorescence of Perylene Dyes

A second system that exhibited solid-state fluorescence comprised some perylene dyes, in particular perylene-3,4:9,10-tetracarboxylic bisimides (**28**).³⁰⁻³³

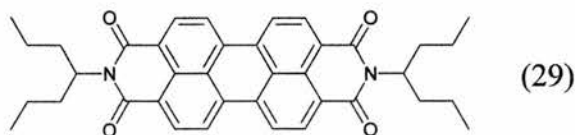


(28)

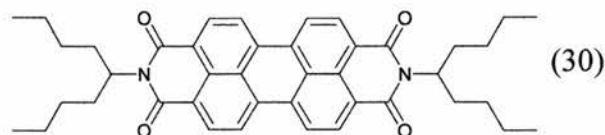
These dyes are very photostable and strongly fluorescent in solution. The fluorescence of the dyes is not as strong in the solid state as in solution, and the fluorescence is influenced very little by the substituents on the nitrogens. Because of this, the perylene dyes proved to be a good probe for studying crystal packing effects with different *N*-substituted derivatives.

There are two major types of pigment with this chromophore, a black-blue with no visible fluorescence, and one showing weak red fluorescence. Crystal structure analysis has been performed with both types which indicate that in both the chromophores are parallel stacked and laterally displaced.³⁰ An exception is the dye below, which has a brilliant red solid-state fluorescence (**30**).³⁰

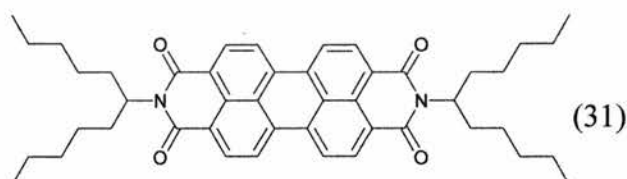
This solid-state fluorescence is a great deal stronger than that of (**31**) as well as that of the shorter chain analogue (**29**) (shown below).



(29)



(30)



(31)

It has been shown by powder X-ray diffraction that all these compounds are crystalline. The difference in packing between these compounds is demonstrated by the application of mechanical stress to the powders.³⁰ Whilst the crystalline structure of (29) and (31) persist after pulverisation, (30) becomes amorphous.

Langhals³⁰ suggests that the strong interaction of the chromophores is not only the basis of the rather stable structure of (29) and (31) but is also responsible for fluorescence quenching via the coupling of electronic excitation to lattice vibrations. However, in the highly fluorescent (30) the chromophore interactions are weak which results in a highly intense solid-state fluorescence and in a breakdown of lattice structure on the application of mechanical stress.

The relationship between the lattice packing and the solid-state fluorescence is supported by the investigation of a further type of packing in fluorescent perylene dyes.³⁰ Another perylene dye, similar to (29-31), with two 1-octylnonyl substituents on the nitrogens, is orange, has an intense solid-state fluorescence, and has a similar fluorescence intensity to perylene dyes in dilute solutions. Crystals of this last dye have been found not to be very ordered or densely packed, this being caused by the flexibility of the alkyl side chains. Structural information obtained shows that the packing is like a sandwich of chromophores with alkyl chains between them. Therefore the chromophores are isolated by alkyl chains and very little interactions between chromophores can occur. This is similar to the fluorescent perylene dyes in solution where the chromophores will be “sandwiched” between solvent molecules.³⁰

1.16.4 Pigment Yellow 8501

Pigment Yellow 8501³⁴ (32) has been found to have very intense solid-state fluorescence, up to five times greater than PO16 (23). Figure 2 (see below) shows a crystal packing diagram of PY8501.

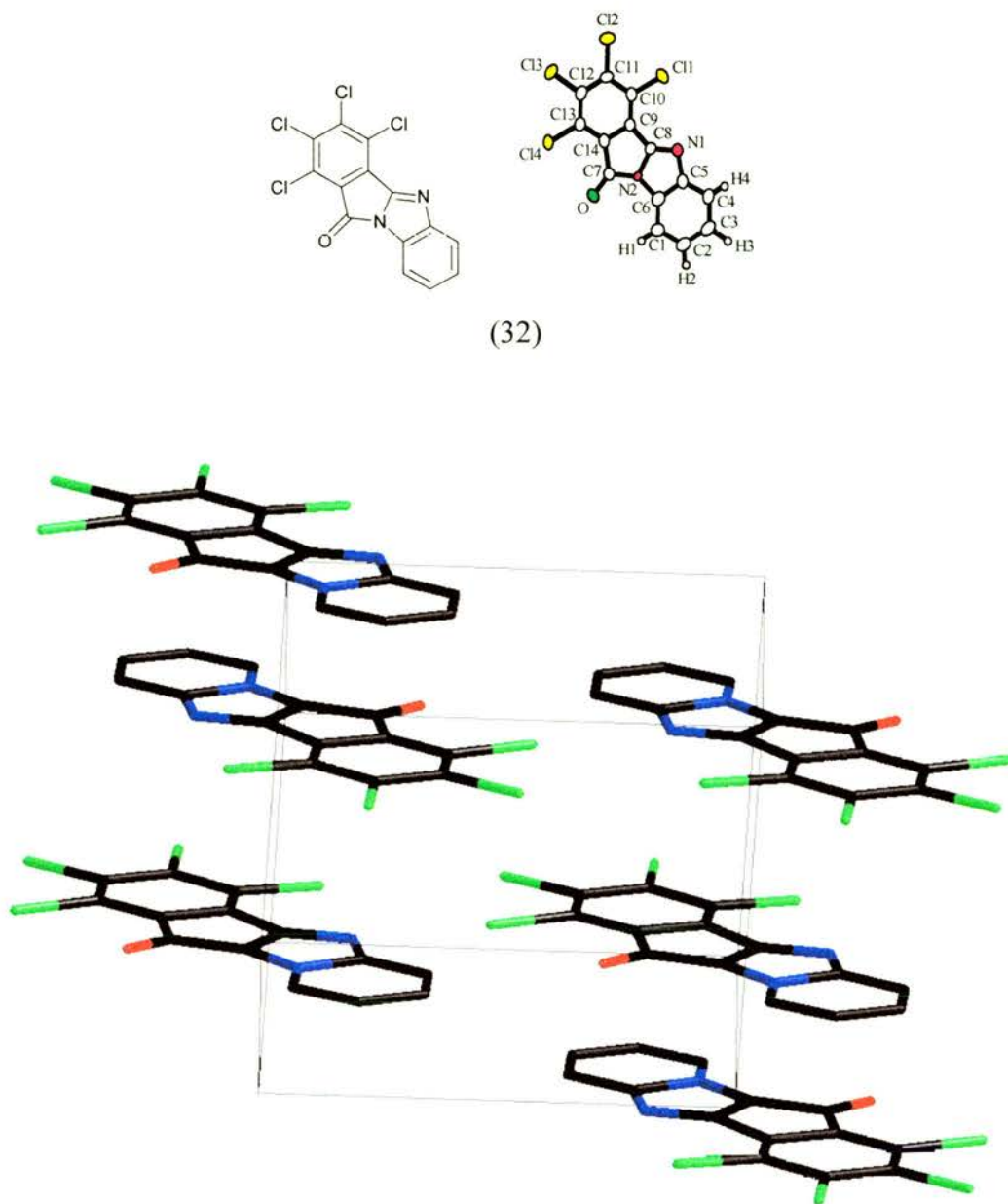


Figure 2 – Crystal packing diagram of PY8501 (32)

The diagram below (figure 3) illustrates interatomic distances and interatomic bond angles of the non-hydrogen atoms, as well as the atomic numbering. Examination of the three N2-C bond lengths reveals that they are abnormally shorter than expected for a trivalent nitrogen, i.e. 1.472Å. In particular, the N2-C8 bond is exceptionally short, i.e. 1.388(4)Å. The deviation of N2 from the C6-C7-C8 plane is only 0.002Å, thereby indicating that the three covalent bonds of N2 are in the same plane.

Furthermore, the sum of the bond angles around N2 is 359.9°. From all the above, the N2 atom is in effect essentially sp^2 in nature.³⁴

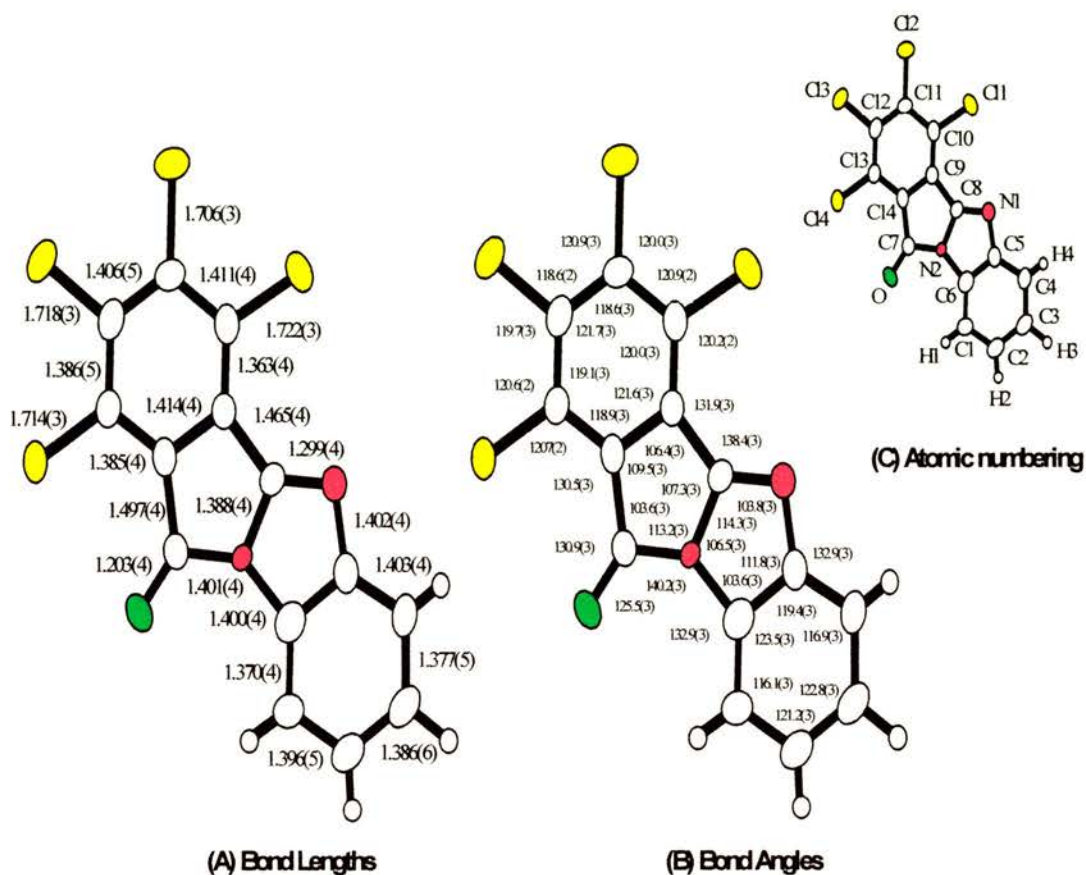


Figure 3 - Intramolecular distances and bond angles involving the non-hydrogen atoms. (A) Distances are in Angstrom (Å) and (B) angles in degrees(°). Estimated standard deviations are given in parentheses. (C) Atomic numbering is also indicated again for convenience.

The Cl(2) atom takes position over the centre of the aromatic C1 to C6 ring of the next stacking molecule (figure 4). The separation between Cl(2) and the aromatic ring is approximately 3.44(4)Å, which agrees with the sum of the van der Waals radii for a chlorine and aromatic ring. Of the four Cl-C bonds, the Cl(2)-Cl(1) bond is notably short, at 1.706(3)Å. Taking this together with the knowledge that a chlorine on an aromatic ring can be electron donating via a mesomeric effect, it was hypothesized by Otani³⁴ that a weak charge-transfer type of interaction exists along the stacking direction.

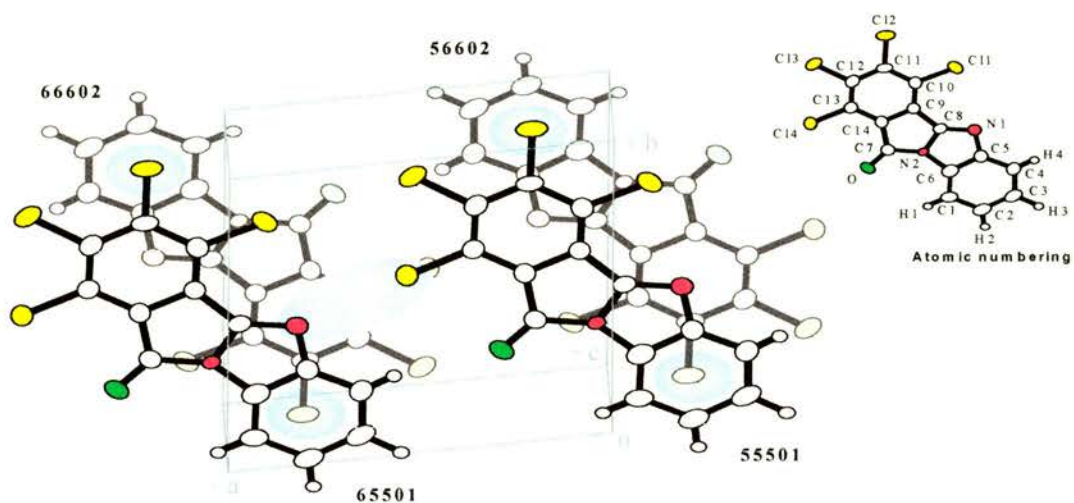
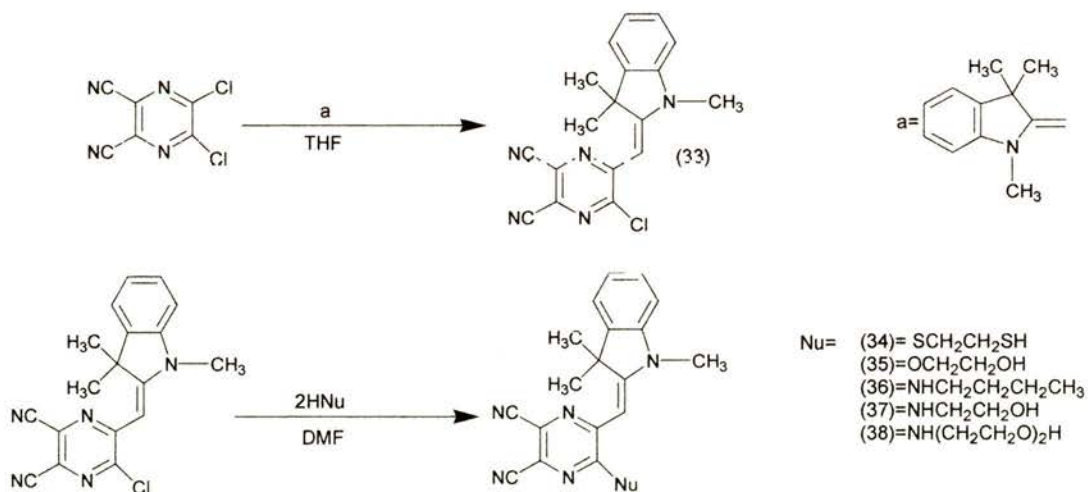


Figure 4- Molecular packing arrangement projected from the stacking direction. Interactions on the stacking direction and between the stacking columns are emphasized by the pale-blue ellipsoids

1.16.5 Dicyanopyrazine Dyes

The dyes below ³⁵ (33-38) have been found to be fluorescent both in solution and the solid-state.



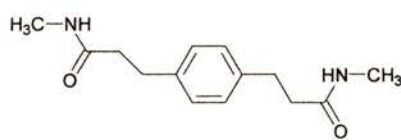
Scheme 8

It is interesting to note that dye (34) showed green fluorescence in solution, but red fluorescence in the solid state. Similar results were observed for (35) and (36). Comparison of the λ_{\max} of the fluorescence in solution and the solid state showed a hypsochromic shift (from solution to solid-state). In solution the λ_{\max} of dyes

undergo hypsochromic shifts resulting from a weakening of intermolecular π - π interactions.³⁵

1.16.6 Aromatic Dicarboxamides

Secondary dicarboxamides (**39-41**) have been found to be fluorescent in solution and the solid state.^{36,37} They are known to pack in the solid-state as one-dimensional hydrogen-bonded tapes or as two-dimensional hydrogen-bonded sheets. In the case of *N,N'*-dimethylarenedicarboxamides the rod-like arene dicarboxamides (**39-41**) form one-dimensional tapes in which the up-down translational arrangement of amide-hydrogen bonding allows extended chains of neighbouring atoms to adopt either face-to-face or edge-to-face geometries. These differences in crystal packing might be expected to influence the excited-state behaviour of the arenedicarboxamides in the crystalline state. The crystal structures of (**39-41**) are shown below:^{36,37}



(39)

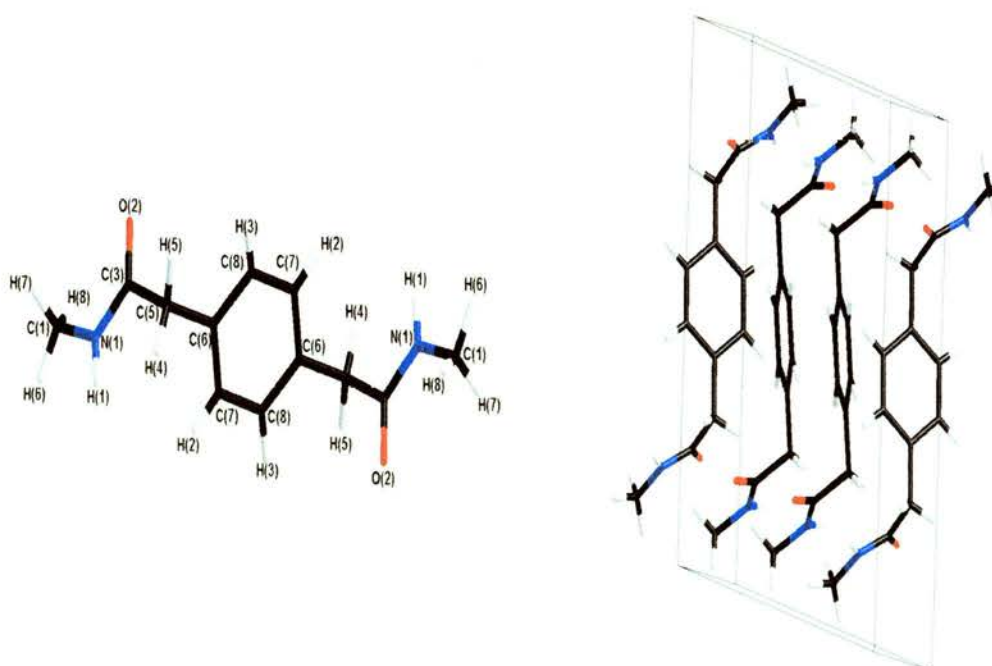


Figure 5- Crystal structure and packing diagram of (39)

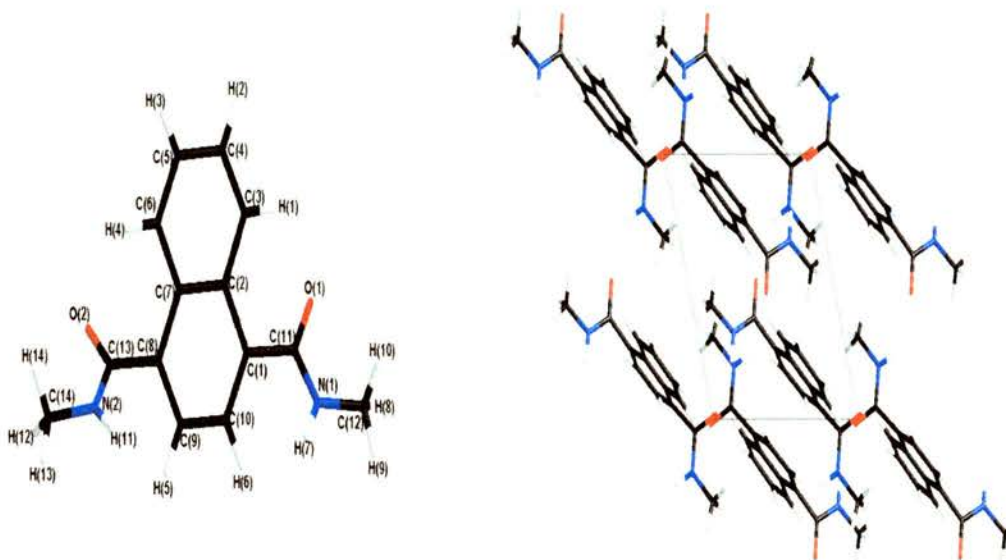
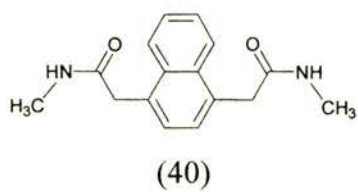
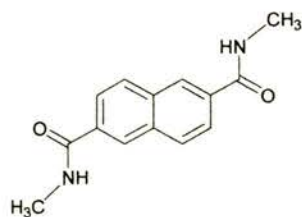


Figure 6- Crystal structure and packing diagram of (40)



(41)

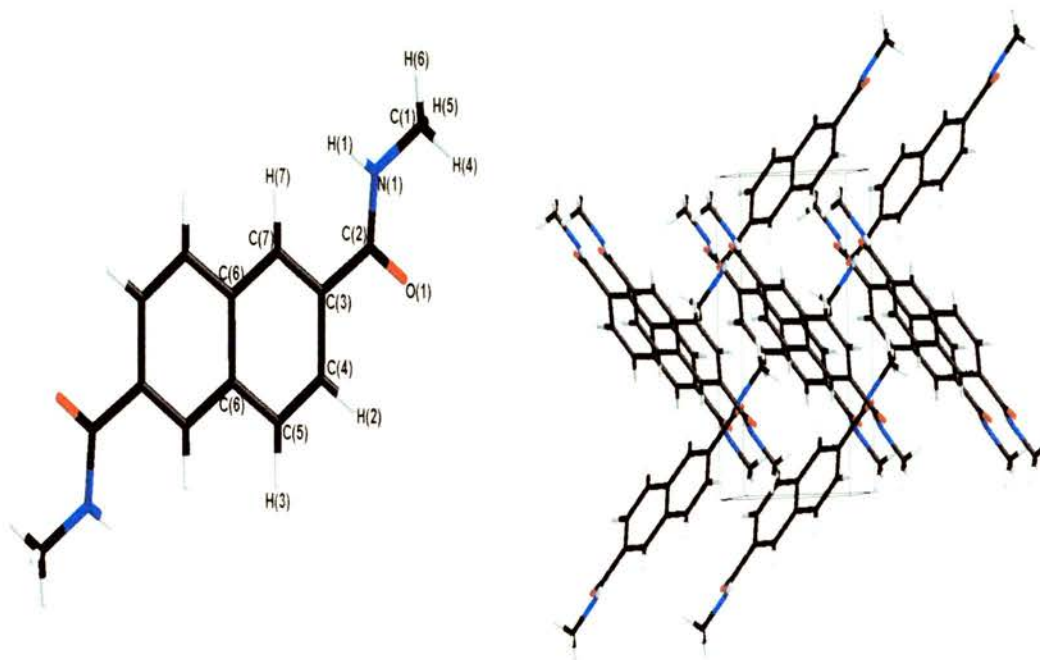


Figure 7- Crystal structure and packing diagram of (41)

Fluorescence spectra were also obtained for powdered and for melted samples.³⁶ The fluorescence spectra of (41) in the powder are broad and structureless with maxima at longer wavelengths than that of the long wavelength band of the single crystal.

It is interesting to note that there are not many arene-arene or chromophoric interactions in this molecule either of which could be a cause of fluorescence quenching.

1.17 Patent Information on Other Pigments With Solid-State Fluorescence

Several recent patents have been published in the literature claiming pigments of various types^{38,39} (DPP derivatives, perylene derivatives, phthalocyanine derivatives and isoindoline derivatives) with good to excellent solid-state fluorescence although no fluorescence data are given. However these are “blanket” claims and no reference is made to any one pigment. In all cases a large number of different compounds are claimed with no clear indication as to which pigments are in fact fluorescent.

2.0 Aims and Objectives

Azo pigments such as PO16 (23) (page 17) and structurally similar pigments such as PY12 (table 1 page 18) have been used extensively in the pigment industry for years due to their stability, low cost and good lightfastness.¹ Now it has been discovered that both PO16 (23) and PY12 are fluorescent, this could potentially afford a source of low cost fluorescent pigments on an industrial scale that would have a whole new range of applications.

Fluorescent pigments may find application in:

2.1 Organic Electroluminescent Devices and Displays

Electroluminescence has been subject to interest for several decades because of its many applications in areas such as telecommunications or information displays.⁴⁰ During the last decade, an explosive growth of activity in the area of organic electroluminescence has occurred, stimulated by the promise of light-emitting plastics for the fabrication of large, inexpensive and efficient screens to be used in different applications.⁴¹⁻⁴³ Such devices have advantages over current inorganic based devices in that they have improved emission intensity, a greater range of hues can be obtained and they operate at a lower voltage. A significant challenge for this type of device is matching the durability of inorganic materials.

2.2 Special Effects Printing

Materials which fluoresce under specific lighting conditions e.g. daylight or UV light are desirable not only to provide eye-catching decorative effects for packaging, but also to provide durable fluorescent inks/paints for safety equipment, signs etc. Current fluorescent inks and paints are made with “pigments” which are actually dyes in a polymer matrix and ground to give a powder. As such, whilst they may be applied in the same way as pigments, their durability is that of dyes.

2.3 Security Printing

There is a need to develop new fluorescent pigments that give novel effects. Such effects may be overt or covert and requiring detection. Fluorescent pigments provide a neat solution to this demand. The ability to affect the strength of emission by some form of “curing” process e.g. simple heat treatment is particularly desirable as it may allow a “secondary” image to be hidden in a printed area. The “secondary” image would be formed by the curing process and would ideally only be visible via some means of detection e.g. UV light.

The aims of the project are to ascertain why PO16 (**23**) and similar pigments are fluorescent and to determine what molecular and/or solid-state features influence this fluorescence, in the hope that this can aid synthesis of new fluorescent pigments in the future and optimise their fluorescence.

Synthetic analogues will be used to investigate how molecular changes affect fluorescence intensity. Also, analogues will be prepared with a view to investigating how rigidity, planarity, π - π stacking, intramolecular and/or intermolecular hydrogen bonding affect fluorescence with structures being tailored to augment these effects.

To look at the solid-state effects single crystal X-ray studies are proposed. Where this proves impracticable “indirect” routes such as powder X-ray diffraction electron microscopy and “monoazo” analogues will be used.

Monoazo analogues correspond to “half” of the pigment molecules. These smaller molecules do not suffer from the insolubility problems associated with the pigments themselves, and in certain cases single crystal X-ray analysis have been reported in the literature. The intention is to synthesise a series of such model azo compounds for NMR, X-ray and fluorescence studies.

Fluorescence studies will be used (both in solution and the solid-state) along with UV/Visible absorption (again in solution and the solid state). The differences between solid-state and solution absorption, solid-state fluorescence and solid-state

absorption and solution fluorescence and solution absorption will be examined to gain more information about the nature of the fluorescence.

3.0 Results and Discussion

As stated earlier (see introduction) it was found that some members of the diarylide pigment series showed solid-state fluorescence whilst others do not. It was decided to perform qualitative tests on a wide series of diarylide pigments (which were all well known commercially used pigments with the exception of (43)^{44,45} to see whether they fluoresced in the solid state (i.e. they were subjected to UV irradiation and the effects were observed with the naked eye).

Rather surprisingly quite a large number of the commercial pigments displayed solid-state fluorescence, as claimed in the recent Sun patents (page 18). From table 2 one might suspect that subtle changes in the molecular structure affected the solid-state fluorescence of these pigments. It posed the question: what were the critical factors for solid-state fluorescence?

These might be as follows : -

1) Substitution on the phenyl rings (i.e. those with their origins in the coupling component)

There is no substitution on the “end” phenyl rings of PY12 (42) or PO16 (23); however there is substitution at the 2-position in (45) and (46) at the 2- and 4-positions of (44) and (47) and at the 2- and 5- positions of (48). Looking at these systems, the pigments with the most intense fluorescence were the pigments with the least degree of substitution on the “end” phenyl rings. All the pigments with two substituents on the “end” phenyl ring did not appear to be fluorescent under the naked eye. The question thus arises as to whether the two “ends” of the molecule have to be planar in order for solid-state fluorescence to be observed, and does an *ortho*-substituent on these phenyl rings interfere with such planarity?

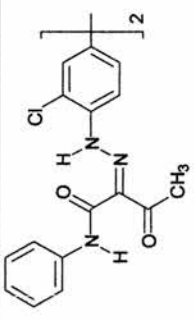
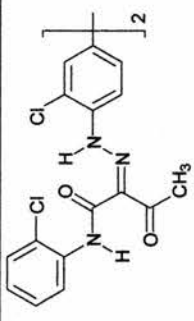
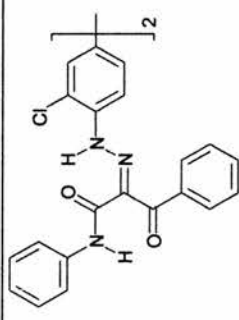
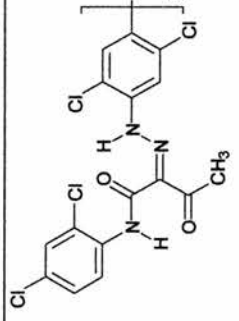
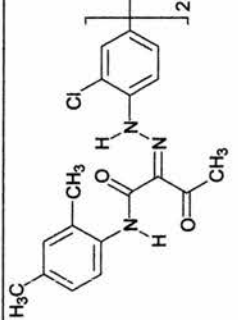
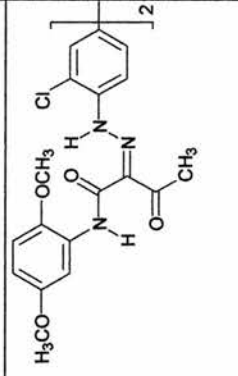
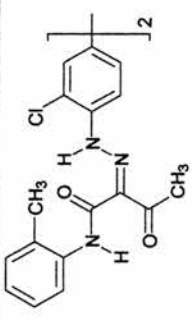
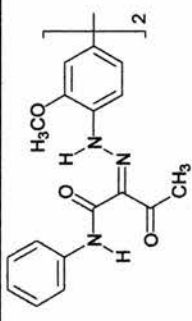
Pigment	Structure	Solid-state fluorescence under UV lamp	Pigment	Structure	Solid-state fluorescence under UV lamp
PY12 (42)		Yes	PY63 (46)		Yes
(43) ^{44,45}		Yes	PY81 (47)		No
PY13 (44)		No	PY83 (48)		No
PY14 (45)		Yes	PO16 (23)		Yes

Table 3

2) Central biphenyl moiety: (*o*-dianisidine or 2,2'-dichlorobenzidine)?

Did the central biphenyl moiety and its substituents have an effect on the solid-state fluorescence, i.e. did *o*-dianisidine or *o*-dichlorobenzidine-based pigments give higher fluorescence intensities? The fluorescence intensity of (23) is much greater than that of PY12 (42) (with the naked eye). Since only one pigment in table 3 is derived from *o*-dianisidine, however, further investigation was required in order to establish the generality or otherwise of this effect.

3) The possibility of intramolecular hydrogen bonding.

To what extent was hydrogen bonding present in these pigments? The more intramolecular hydrogen bonding present, the greater the likelihood that the individual molecules would be rigid or contain rigid segments, and would thus deny a route for fluorescence quenching via vibrational deactivation.

4) Intermolecular interactions

How efficiently do the molecules pack throughout the crystal lattice? The more efficiently the molecules pack the greater the chance of intermolecular hydrogen bonds and π - π interactions. Matsuoka³⁵ *et al.* have attributed fluorescence quenching to π - π interactions.

How important was the planarity of individual molecules, or of parts of individual molecules, in the crystal lattice? How would this affect the crystal packing and would it affect the fluorescence?

3.1 Synthesis of Novel Diarylide Pigments

To investigate the importance or otherwise of the terminal rings being planar, and/or coplanar with the ketohydrazone moiety, a series of new diarylides was synthesised, using coupling components (49-53) (table 4) which contain one or more tetrahedral carbons and so cannot adopt a planar conformation. Along with these, diarylides derived from barbituric acid (53) were synthesised: (53) is known to couple with diazonium salts⁴⁶ and the resulting “end-groups” in the pigments may or may not be planar depending on the preferred tautomer adopted by the “end-groups” in the solid state, and steric interactions within the crystal lattice.

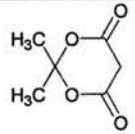
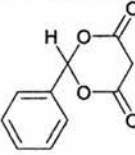
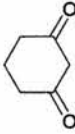
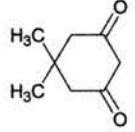
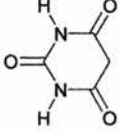
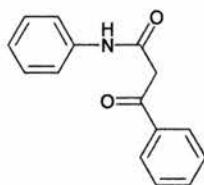
Coupling Component	Structure
Meldrum's acid (49)	
2-phenyl-1,3-dioxan-4,6-dione ⁴⁷ (50)	
Cyclohexane-1,3-dione (51)	
Dimedone (52)	
Barbituric acid (53)	

Table 4

Also extended colour ranges might be possible using these coupling components which might afford different coloured fluorescent pigments.

Also 2-benzoylacetanilide (**54**) was investigated due to the presence of another phenyl group on the coupling component. One such non-commercial pigment was already known (**43**)^{44,45} (see table 2 page 18).



(54)

Also both *o*-dianisidine (**55**) and *o*-dichlorobenzidine (**56**) were used as basis for a comparison between pigments based on these backbones. For the reason 2',4'-dimethylacetoacetanilide (**57**) was also used.

Again qualitative tests were carried out on these synthetic pigments to see whether they fluoresced in the solid state (i.e. they were subjected to UV irradiation and any fluorescence was observed with the naked eye). Table 5 (page 38) shows the results. It should be noted that two of these pigments (**60**)⁴⁶ and (**66**)⁴⁸ have been cited in the literature.

All the synthetic analogues showed solid-state fluorescence. Looking at (**62**) [the *o*-dianisidine analogue of PY13 (**44**)] is particularly interesting. PY13 (**44**) shows no fluorescence under the UV lamp whilst (**62**) is again quite intensely fluorescent. Some, but not all *o*-dichlorobenzidine-based pigments are more intensely fluorescent than the *o*-dianisidine based pigments. There seemed to be no obvious correlation based on qualitative assessment between the correspondingly-substituted *o*-dichlorobenzidine- and *o*-dianisidine- based pigments and fluorescence intensity. Due to this, it was decided to focus on the solid-state nature of the pigments. A number of crystal structures for diarylide pigments had already been solved, so here was an opportunity to examine existing crystal data.

Pigment	Structure	Solid state fluorescence under UV lamp	Pigment	Structure	Solid state fluorescence under UV lamp	Pigment	Structure	Solid state fluorescence under UV lamp
(58)		Yes	(62)		Yes	(66) ⁴⁸		Yes
(59)		Yes	(63)		Yes	-	-	-
(60) ⁴⁶		Yes	(64)		Yes	-	-	-
(61)		Yes	(65)		Yes	-	-	-

Table 5

3.2 Prior Art - Crystal Structure Analysis of Diarylide Pigments

3.2.1 PY12 (42)^{49,50}

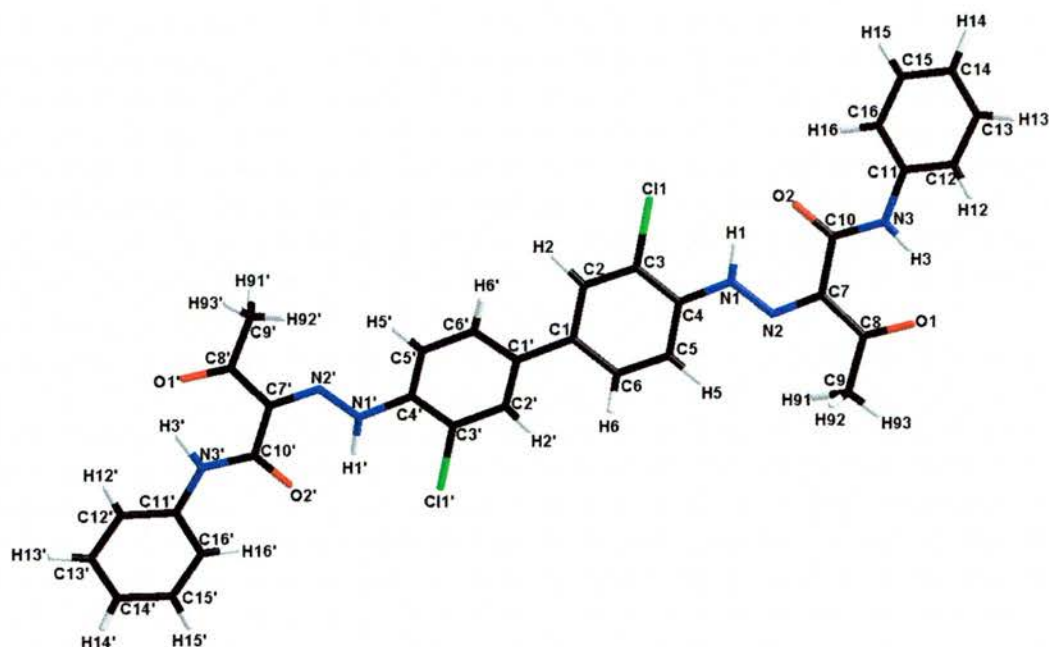
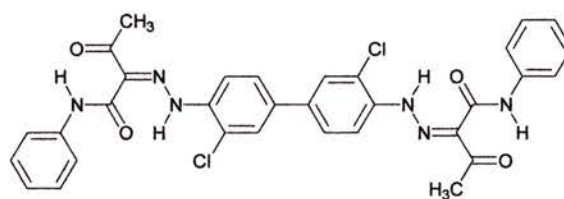


Figure 8 - Crystal structure diagram of PY12 (42)



(42)

The first striking feature in the structure of PY12 (42) is that the molecule does not possess a crystallographic centre of symmetry. The torsion angle between C2-C1-C1'-C6' in PY12 (42) is $-26(1)^\circ$ and as a consequence the whole molecule is twisted. Was this “biphenyl-twist” a critical factor in the solid-state fluorescence of PY12 (42)? One of the end phenyl groups of the PY12 (42) molecule is not coplanar with the adjacent amidic functionalities, the dihedral angle being $-27(1)^\circ$. The phenyl group in the other half of the molecule is essentially coplanar with the adjacent amidic functionalities, the dihedral angle being $-1(1)^\circ$.

So one “half” of the molecule is essentially planar and the other half is “twisted”. The whole molecule is itself twisted like a “corkscrew”. Was the out of plane phenyl group in “one half” of the molecule also critical to solid-state fluorescence? The bond length C1-C1' is 1.49(1)Å which is similar to the corresponding bond length in biphenyl itself⁵¹⁻⁵⁶ [1.50(2)Å] in which the rings are coplanar in the crystal. Decadeutero-biphenyl is also planar. However, a second polymorph exists for decadeutero-biphenyl in which there is a torsion angle of 10.1(2)°.⁵⁷⁻⁵⁹ There is evidence to show that PY12 (**42**) adopts the keto-hydrazone tautomeric form. The bond lengths N2'-C7' and N2-C7 demonstrate C=N bond character and the bond lengths N1-N22 and N1'-N2' show N-N single bond character. Also the interatomic distances between the molecules (shown below) would allow for weak hydrogen bonding.⁶⁰

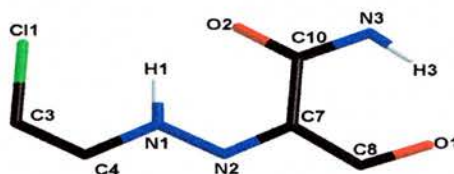


Figure 9

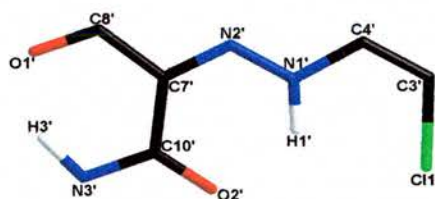


Figure 10

Atoms	Distance/Å
Cl1-H1	2.45(8)
O2-H1	1.83(7)
O1-H3	1.95(5)
Cl1'-H1'	2.45(9)
O2'-H1'	1.87(7)
O1'-H1'	1.72(7)

Table 6

3.2.2 PY13 (44)⁵⁰

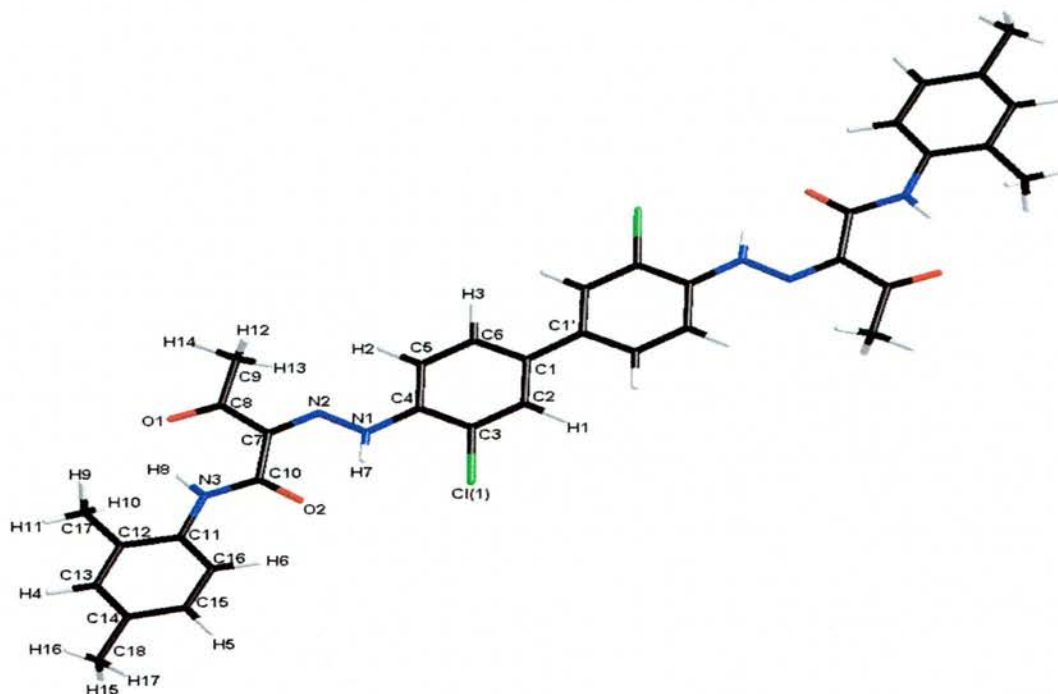
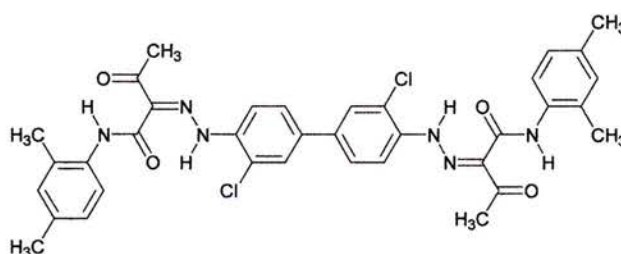


Figure 11- Crystal structure diagram of PY13 (44)



(44)

It is important to remember at this stage that PY13 (44) is not fluorescent. The two halves are related by a crystallographic centre of symmetry halfway along the C1–C1' bond, i.e. the central biphenyl moiety is planar. The chromophore adopts the keto-hydrazone tautomeric form as shown by bond lengths between the relevant atoms and there is weak hydrogen bonding between H1 and O2, H3 and O1, and H1 and Cl(1) which aids the molecule in retaining an approximately planar overall conformation with only very small deviations (non-zero torsion angles along the C4–N1 [$-179.3(2)^\circ$], C10–N3 [$(179.9(2)^\circ)$], C10–C7 [$(-1.0(4)^\circ)$] and C11–N3 [$(176.9(2)^\circ)$ bonds]).

Possible intramolecular hydrogen bonds are as follows :

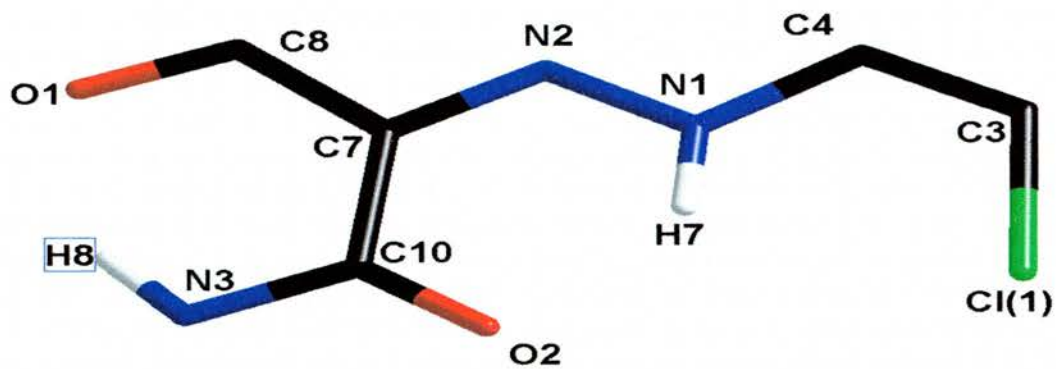


Figure 12

Atoms	Distance/Å
Cl(1)-H7	2.6(1)
O2-H7	1.89(5)
O1-H8	1.86(5)

Table 7

3.2.3 PY14 (45)⁵⁰

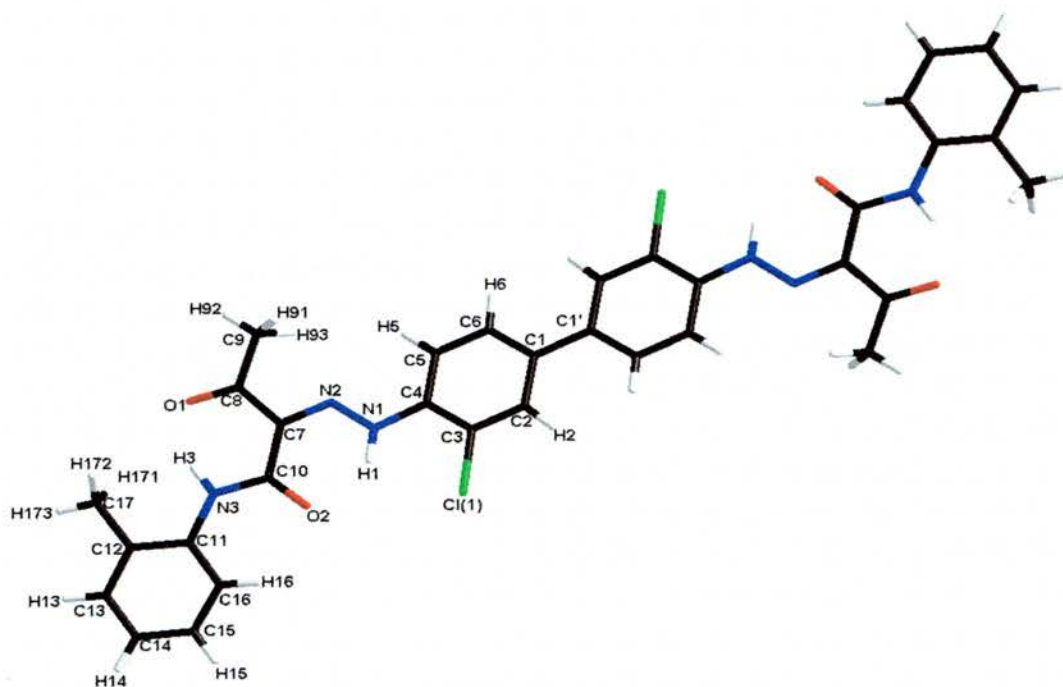
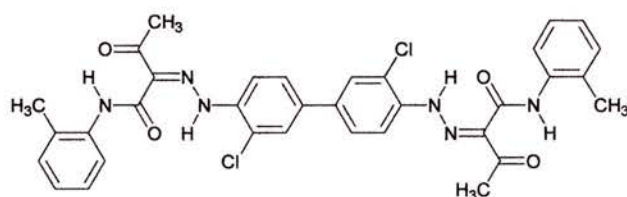


Figure 13 - Crystal structure diagram of PY14 (45)



(45)

This differs from PY13 (44) only in one respect, namely that one methyl substituent is missing from each of the “end” phenyl groups. Again the molecule is centrosymmetric and exists as the keto-hydrazone tautomer and similar hydrogen bonding is seen here as in PY12 (42) and PY13 (44).

The molecule as a whole is effectively planar as shown by the selected torsion angles C4-N1-N2-C7 [179.4(2)°], C10-N3-C11-C12 [(179.5(2)° and C10-N3-C11-C16 [-0.2(4)°].

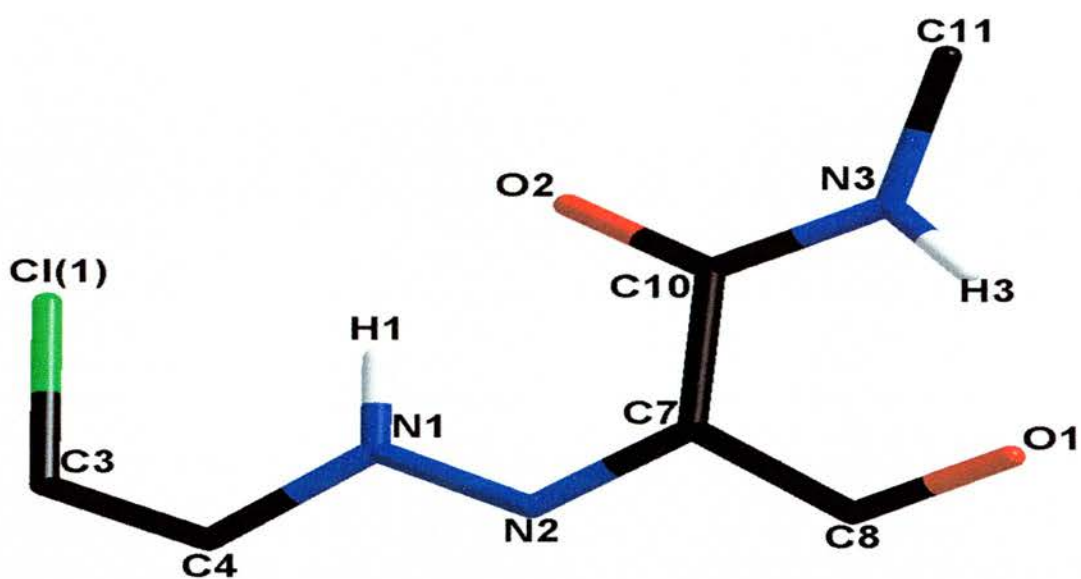


Figure 14

Atoms	Distance/Å
Cl(1)–H1	2.60(7)
O2–H1	1.89(3)
O1–H3	1.82(4)

Table 8

3.2.4 PY63(46)⁵⁰

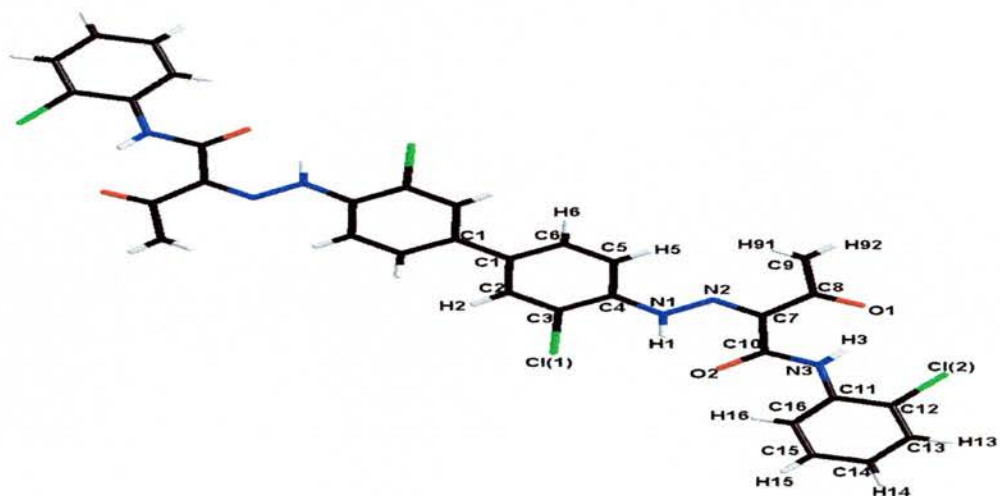
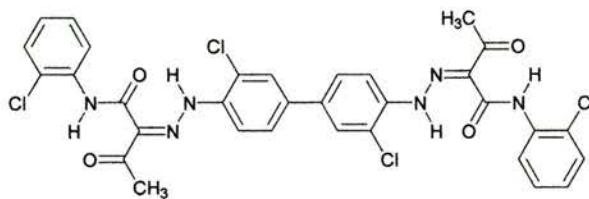


Figure 15 - Crystal structure diagram of PY63 (46)



(46)

Again the molecule is centrosymmetric and exists as the ketohydrazone tautomer and hydrogen bonding trends are repeated.

PY63 (**46**) is approximately planar as shown by the selected torsion angles C4–N1–N2–C7 [179.2(4)°], C10–N3–C11–C12 [178.9(4)°] and C10–N3–C11–C16 [2.1(7)°]. It should be repeated that PY63 (**46**) is fluorescent in the solid–state.

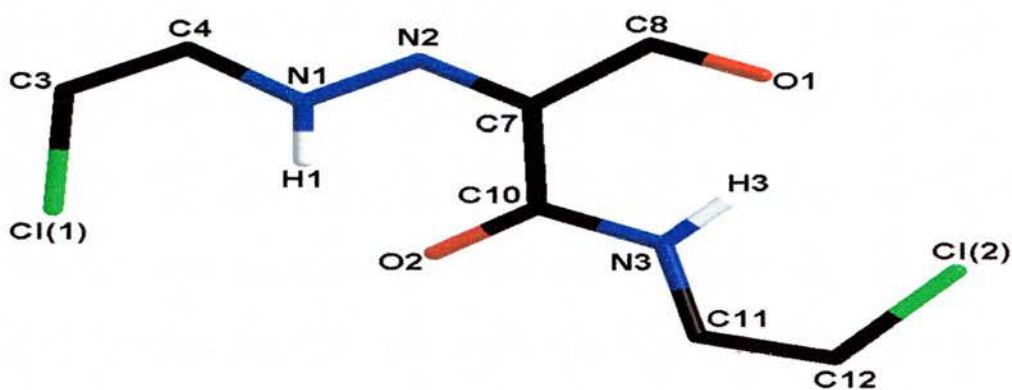


Figure 16

Atoms	Distance/Å
Cl(1)–H1	2.62(7)
O2–H1	1.91(6)
O1–H3	1.88(6)

Table 9

3.2.5 PY83 (48)⁴⁵

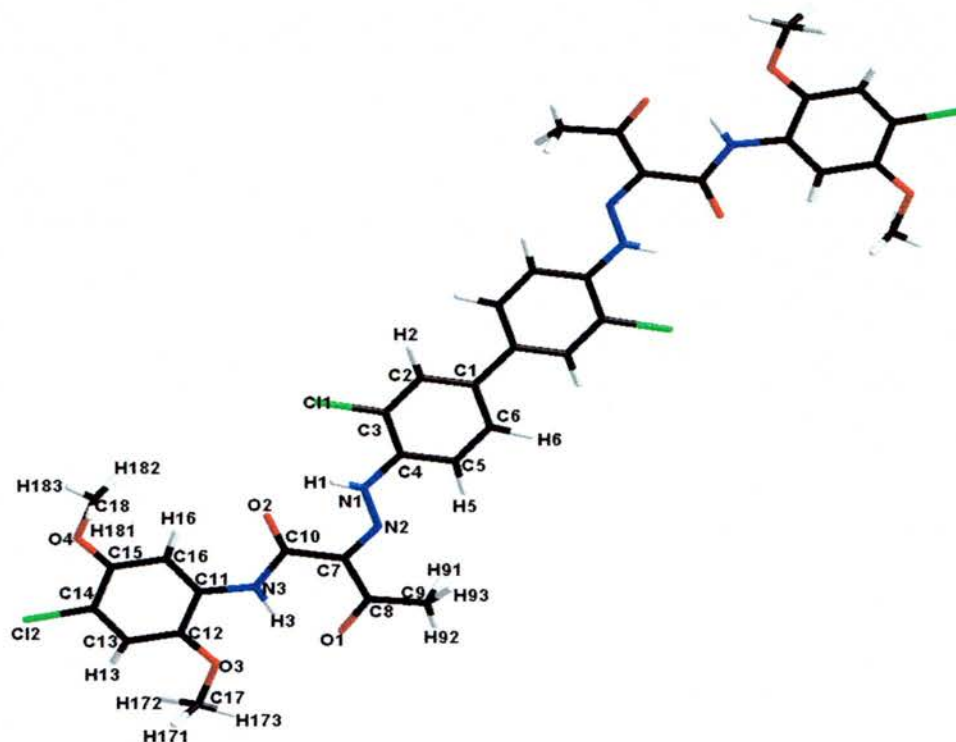
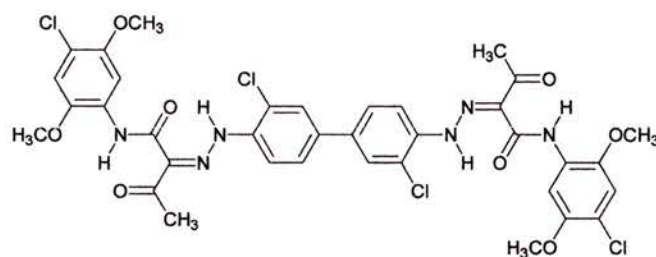


Figure 17 - Crystal structure diagram of PY83 (48)



(48)

As for PY13 (44), PY14 (45) and PY63 (46), PY83 (48) is centrosymmetric and exists as the keto-hydrazone tautomer. Hydrogen bonding trends are also similar.

PY83 (48) is approximately planar as shown by the selected torsion angles C4–N1–N2–C7 [177(1)°], C10–N3–C11–C12 [176(1)°] and C10–N3–C11–C16 [0(2)°]. PY83 (48) is not fluorescent in the solid state.

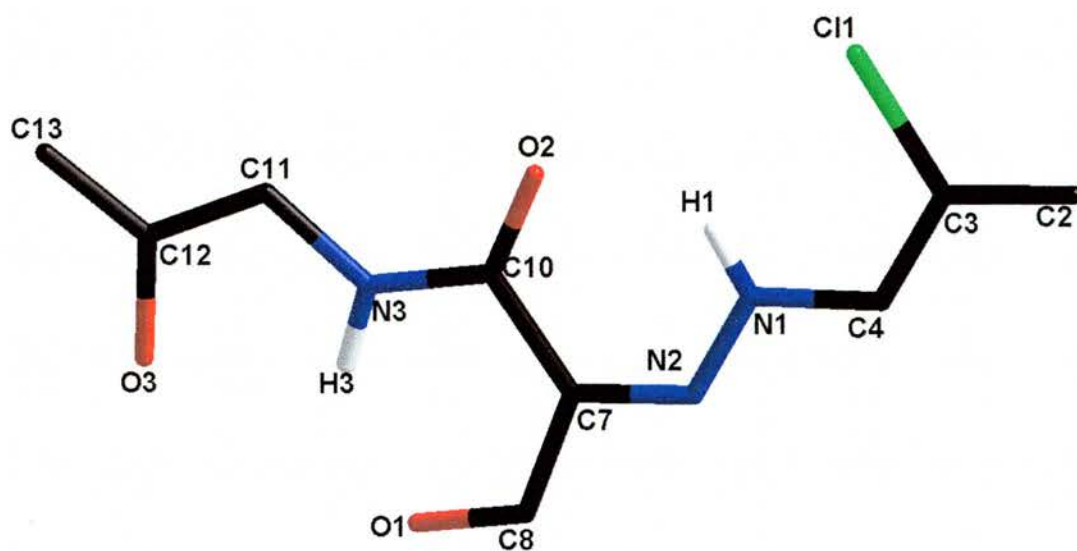


Figure 18

Atoms	Distance/Å
C1(1)-H1	2.5(3)
O2-H1	1.9(1)
O1-H3	1.8(1)

Table 10

3.3 Non-Commercial Diarylide Pigments

3.3.1 (43)⁴⁵

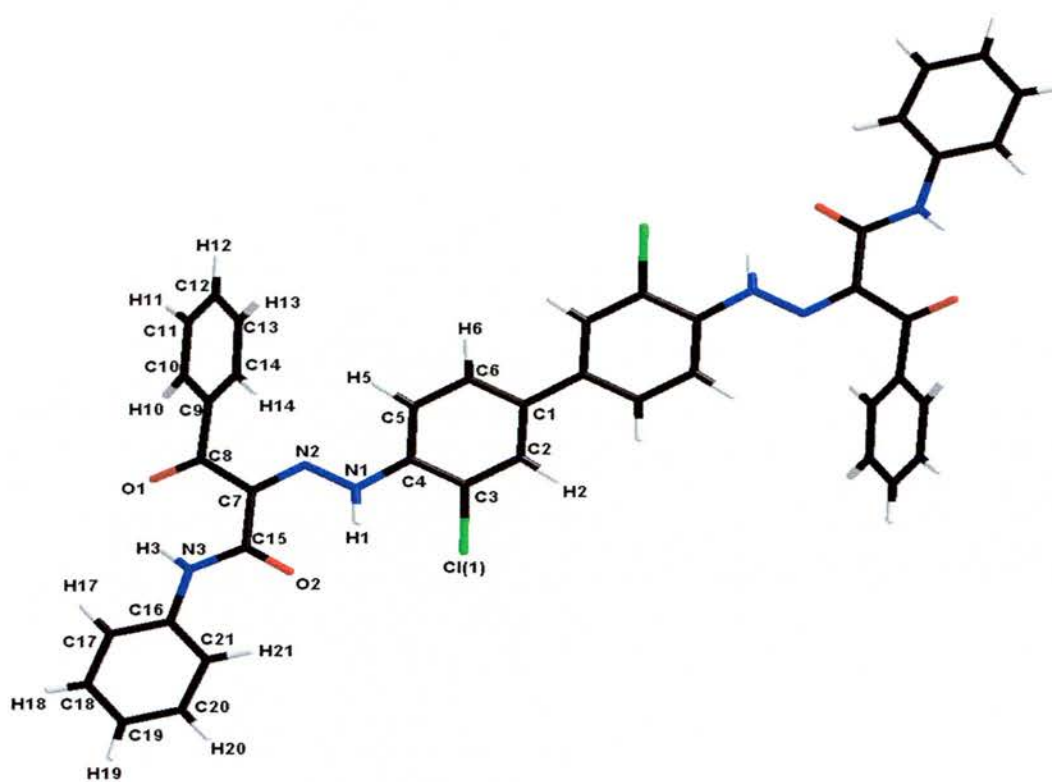
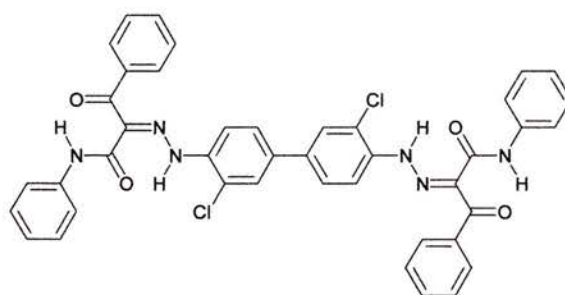


Figure 19 - Crystal structure diagram of (43)



(43)

Only one crystal structure is known to date of a non-commercial diarylide pigment (i.e. a derivative not commercially used). This derivative is identical to PY12 (42) except that a methyl group has been replaced by a phenyl group in the coupling component.

Again this pigment is centrosymmetric, as for PY13, (44) PY14 (45), PY63 (46) and PY83 (48). The molecule again exists in the ketohydrazone tautomeric form and there is weak intramolecular hydrogen bonding similar to the commercial pigments (see below). The molecule overall is non-planar and twisted and in particular there are significant non-zero torsion angles as shown. C4–N1–N2–C7 [$-178.5(5)^\circ$], C15–N3–C16–C21 [$-5(1)^\circ$], C7–C8–C9–C14 [$44.7(9)^\circ$] and C7–C8–C9–C10 [$-138.5(6)^\circ$].

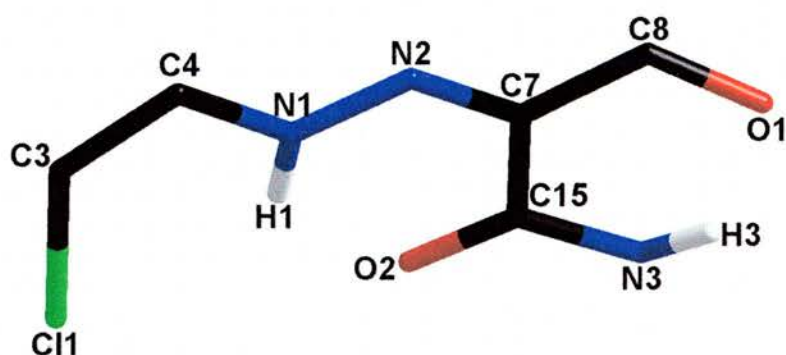


Figure 20

Atoms	Distance(Å)
Cl(1)–H1	2.38(6)
O2–H1	1.92(6)
O1–H3	1.92(6)

Table 11

3.4 Crystal Structure Analysis of Novel Diarylide Pigments

It was decided to try and obtain single crystal X-ray data for the synthetic diarylide pigments, especially for PO16 (**23**). Unfortunately this presented major problems. Due to the inherent insolubility of the pigments in the most common solvents (e.g. THF, toluene, DMSO) it proved incredibly difficult to grow crystals of suitable quality for X-ray analysis. Solvents that were able to dissolve the pigments were extremely high boiling solvents such as nitrobenzene (in which instance the pigments only dissolved at the boiling point e.g. nitrobenzene b.p. 210°C). Some superficially high-quality microcrystalline pigment crystals were grown using this method (see experimental). However none of these crystals were of sufficient quality to obtain single crystal data. Attempts were also made on the author's behalf using the Synchrotron source at both Daresbury and Grenoble but to no avail. It should be noted that workers at Ciba have also attempted to determine some of these crystal structures for several years, especially the *o*-dianisidine based ones such as PO16 (**23**) without success. It was for this reason that indirect methods were used (see below).

3.5 Synthetic Mono-Azo Analogues

The main advantage that mono-azo analogues had over their bis-azo counterparts was that they were a great deal more soluble in the normal range of solvents and therefore single crystal growth was much easier to achieve. There also exists a wealth of information on mono-azo compounds in the literature including X-ray data.^{10,11,13,16,}

⁶¹⁻⁷¹ In the absence of crystallographic data on the *o*-dianisidine-based pigments it was hoped that intramolecular hydrogen bonding, bond lengths and the extent of planarity observed in the half molecules might be extrapolated to give an approximate representation of the structure of the bis-azo pigments. It could not, of course, give any information about the overall planarity or otherwise within the molecules, or even whether or not a planar structure would be centrosymmetric. It should be noted that none of the mono-azo compounds (table 12 page 51) have been found to be fluorescent.

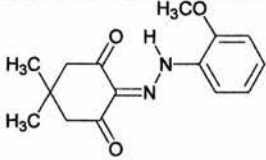
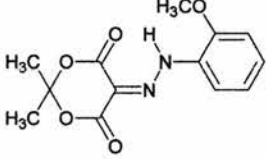
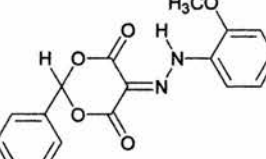
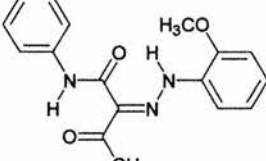
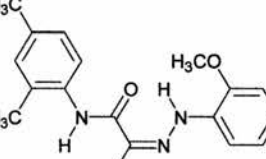
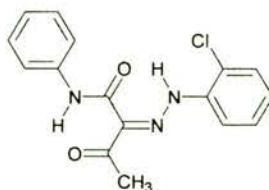
Pigment	Structure	Solid state fluorescent under uv lamp
2-[(2-Methoxyphenyl)hydrazono]-5,5-dimethylcyclohexane-1,3-dione (68)		No
5-[(2-Methoxyphenyl)hydrazono]-2,2-dimethyl-1,3-dioxan-4,6-dione (69)		No
5-[(2-Methoxyphenyl)hydrazono]-2-phenyl-1,3-dioxan-4,6-dione (70)		No
2-[(2-Methoxyphenyl)hydrazono]-3-oxo-N-phenylbutyramide (71)		No
5-[(2-Methoxyphenyl)hydrazono]-N-[2,4-dimethylphenyl]-3-oxobutyramide (72)		No

Table 12

3.5.1 2-[(2-Chlorophenyl)hydrazono]-3-oxo-N-phenylbutyramide

(73)⁵⁰



(73)

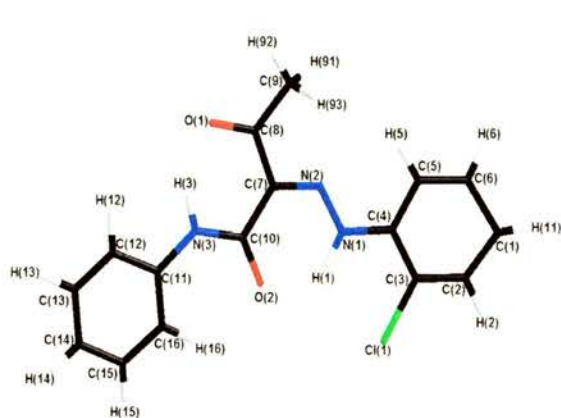


Figure 21 - crystal structure diagram of (73)

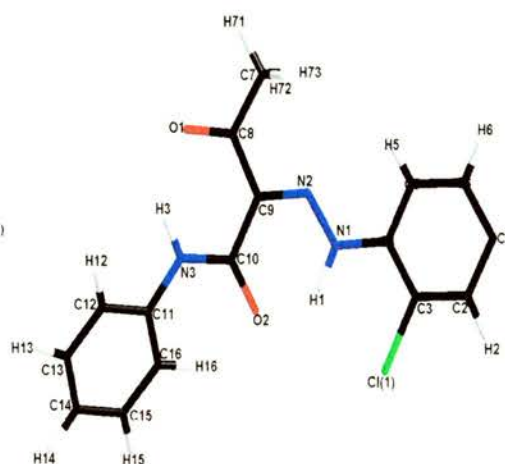


Figure 22 - crystal structure diagram of the Cl(1) half of (42)

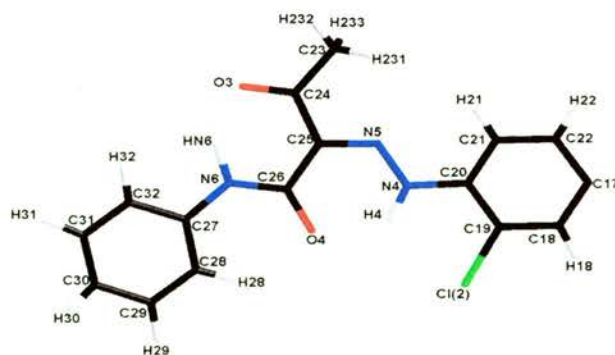


Figure 23 - crystal structure diagram of the Cl(2) half of (42)

Like its bis-azo counterpart PY12 (**42**) this derivative adopts the ketohydrazone tautomeric form. To see if there was any intramolecular hydrogen bonding correlations between the mono-azo compound and PY12 (**42**) the interatomic distances between the appropriate atoms were compared. Also various other crystal data were compared between compound (**73**) and the two “halves” of PY12 (**42**). A comparison was made to check that a comparison between the mono-azos and bis-azo compounds was justified.

Interatomic Distances/ Å (73)		Interatomic Distances/ Å of C1(1) half (42)		Interatomic Distances/ Å of C1(2) half (42)	
Cl(1)–H(1)	2.50(4)	Cl(1)–H1	2.45(8)	Cl(2)–H4	2.54(9)
O2–H1	1.92(4)	O2–H1	1.83(7)	O4–H4	1.87(7)
O1–H3	1.88(4)	O1–H3	1.95(5)	O3–HN6	1.72(7)
Bond Lengths / Å (73)		Bond Lengths/ Å of C1(1) half of (42)		Bond Lengths/ Å of C1(2) half of (42)	
C4–N1	1.39(1)	C4–N1	1.40(1)	C4'–N1'	1.42(2)
N1–N2	1.30(2)	N1–N2	1.31(1)	N1'–N2'	1.31(1)
N2–C7	1.31(1)	N2–C7	1.317(9)	N2'–C7'	1.31(9)
C7–C10	1.49(2)	C7–C10	1.51(3)	C7'–C10'	1.48(3)
C10–N3	1.34(1)	C10–N3	1.345(9)	C10'–N3'	1.34(1)
C8–O1	1.22(1)	C8–O1	1.23(1)	C8'–O1'	1.22(1)
C10–O2	1.23(2)	C10–O2	1.23(1)	C10'–O2'	1.24(1)
N3–C11	1.40(2)	N3–C11	1.41(2)	N3'–C11'	1.41(3)
Torsion Angles ^o (73)		Torsion Angles ^o (42)		Torsion Angles ^o (42)	
C4–N1–N2–C7	178.1(3)	C4–N1–N2–C7	-179.8(6)	C4'–N1'–N2'–C7'	175(2)
N1–N2–C7–C8	179.8(3)	N1–N2–C7–C8	-177.7(5)	N1'–N2'–C7'–C8'	179.7(6)
N1–N2–C7–C10	0.3(5)	N1–N2–C7–C10	0.7(9)	N1'–N2'–C7'–C10'	-1(1)
N2–C7–C8–C9	-1.0(4)	N2–C7–C8–C9	0(1)	N2'–C7'–C8'–C9'	4(1)
N2–C7–C10–N3	179.4(3)	N2–C7–C10–N3	176.4(6)	N2'–C7'–C10'–N3'	177.7(6)
C7–C10–N3–C11	-173.8(3)	C7–C10–N3–C11	-178.5(6)	C7'–C10'–N3'–C11'	-177.9(6)
C10–N3–C11–C12	171.9(3)	C10–N3–C11–C12	155.2(7)	C10'–N3'–C11'–C12'	177.9(7)
C10–N3–C11–C16	-8.3(5)	C10–N3–C11–C16	-27(1)	C10'–N3'–C11'–C16'	-1(1)

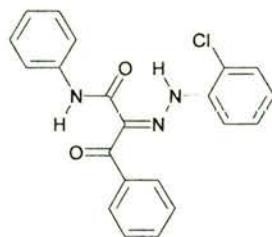
Table 13

It appears that hydrogen bonding trends are consistent between (**73**) and (**42**). The interatomic distances and bond lengths for (**73**) and both halves of (**42**) are very similar (table 13 highlighted in blue). There are significant differences in the C10–

N3–C11–C12 and C10–N3–C11–C16 torsion angles (highlighted in red on table 13), which could be a consequence of packing effects within the crystal.

3.5.2 2-[(2-Chlorophenyl)hydrazono]-3-oxo-3, N-diphenylpropionamide

(74)⁴⁵



(74)

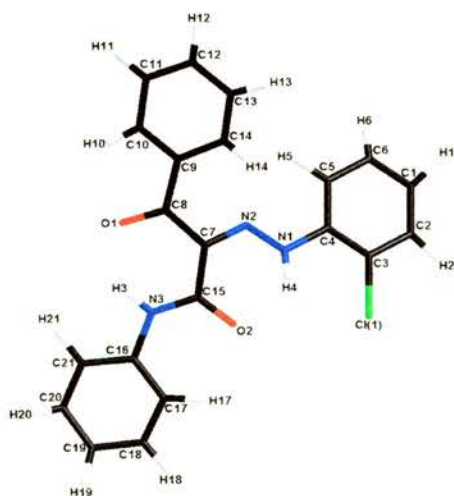


Figure 25 - crystal structure diagram of (74)

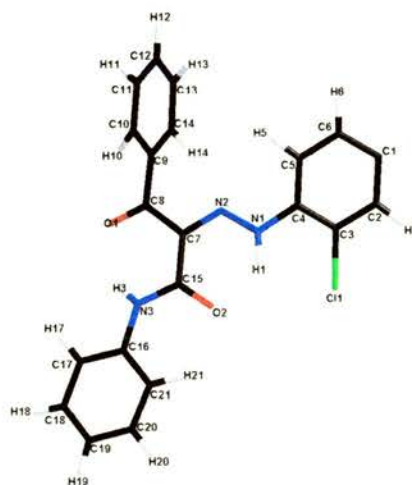


Figure 26 - crystal structure diagram of one half of (43)

Interatomic Distances/ Å (74)		Interatomic Distances/ Å (43)	
Cl(1)–H4	2.5(2)	C1(1)–H1	2.38(6)
O2–H4	1.9(3)	O2–H1	1.92(6)
O1–H3	2.0(5)	O1–H3	1.92(6)
Bond Lengths /Å (74)		Bond Lengths/Å (43)	
C4–N1	1.39(1)	C4–N1	1.37(1)
N1–N2	1.27(1)	N1–N2	1.240(7)
N2–C7	1.28(1)	N2–C7	1.29(1)
C7–C8	1.48(3)	C7–C8	1.394(8)
C7–C15	1.47(1)	C7–C15	1.48(1)
C15–N3	1.31(1)	C15–N3	1.32(1)
C8–O1	1.20(1)	C8–O1	1.19(1)
C15–O2	1.19(1)	C15–O2	1.154(8)
N3–C16	1.39(1)	N3–C16	1.41(1)
Torsion Angles/° (74)		Torsion Angles/° (43)	
C4–N1–N2–C7	176.5(8)	C4–N1–N2–C7	-178.6(6)
N1–N2–C7–C8	179(1)	N1–N2–C7–C8	174.6(6)
N1–N2–C7–C15	-2(1)	N1–N2–C7–C15	-1.6(9)
N2–C7–C8–C9	-12(4)	N2–C7–C8–C9	15.2(8)
N2–C7–C8–O1	168(3)	N2–C7–C8–O1	-161.2(6)
N2–C7–C15–O2	6(1)	N2–C7–C15–O2	-6(1)
N2–C7–C15–N3	-172.6(9)	N2–C7–C15–N3	174.4(6)
C7–C8–C9–C10	147(3)	C7–C8–C9–C10	-138.6(7)
C7–C8–C9–C14	-36(5)	C7–C8–C9–C14	44.8(9)
C7–C15–N3–C16	-177.1(9)	C7–C15–N3–C16	-178.7(6)
C8–C9–C14–C13	-175(2)	C8–C9–C14–C13	176.3(7)
C15–N3–C16–C21	-175(1)	C15–N3–C16–C21	-5(1)
C15–N3–C16–C17	6(1)	C15–N3–C16–C17	174.9(7)

Table 14

Again hydrogen bonding trends are consistent between the corresponding mono-azo phenyl analogue (74) and the bis-azo analogue (43) (interatomic distances highlighted in blue). There is a minor difference in bond length between (43) and (74) (N1–N2 highlighted in green table 14). Again planarity connections have to be treated

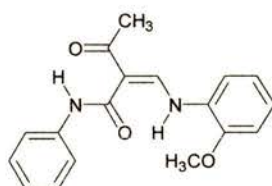
cautiously (selected torsion angles in red : see table 14) as there are major differences in the selected torsion angles.

In conclusion : reliable information about intramolecular hydrogen bonding networks and bond lengths within the molecule can generally be extrapolated from mono-azo to the corresponding bis-azo pigments. Torsion angles and overall planarity of the molecule has to be treated far more cautiously as packing effects within the crystal come into play. Crystal structure analyses on a number of pigments by Chisholm⁷² and co-workers support these observations.

3.5.3 Novel Mono-Azo Compounds

3.5.4 2-[(2-Methoxyphenyl)hydrazone]-3-oxo-N-phenylbutyramide

(71)



(71)

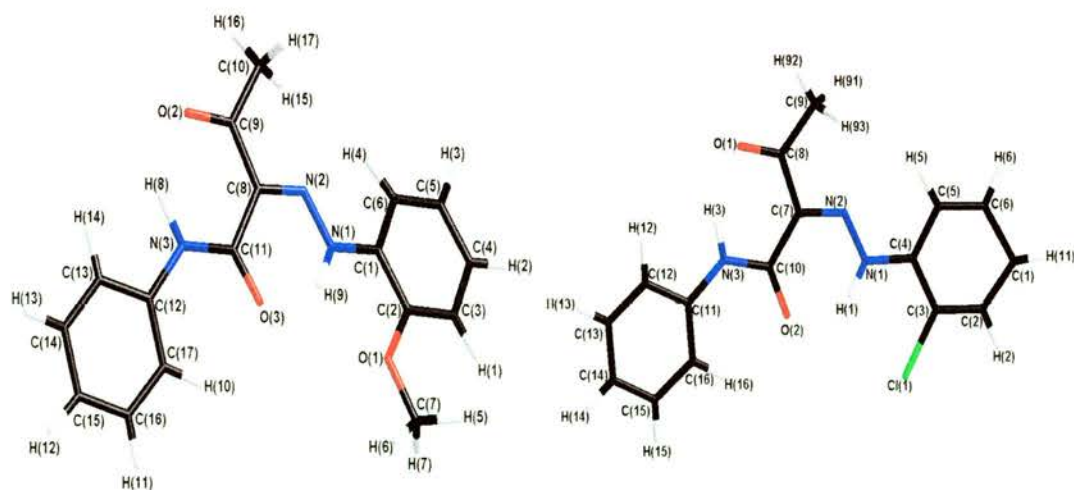


Figure 27 - crystal structure diagram of (71)

Figure 28 - crystal structure diagram of (73)

Interatomic Distances/ Å (71)		Interatomic Distances/ Å (73)	
O1–H9	2.31(4)	Cl(1)–H(1)	2.50(4)
O3–H9	1.76(4)	O2–H1	1.92(4)
O2–H8	1.93(5)	O1–H3	1.88(4)
Bond lengths/ Å (71)		Bond lengths/ Å (73)	
C1–N1	1.403(6)	C4–N1	1.39(1)
N1–N2	1.313(6)	N1–N2	1.30(2)
N2–C8	1.288(6)	N2–C7	1.31(1)
C8–C11	1.232(7)	C7–C10	1.49(2)
C11–N3	1.353(6)	C10–N3	1.34(1)
C9–O2	1.232(7)	C8–O1	1.22(1)
C11–O3	1.234(6)	C10–O2	1.23(2)
N3–C12	1.42(1)	N3–C11	1.40(2)
Torsion Angles/° (71)		Torsion Angles/° (73)	
C1–N1–N2–C8	172.0(4)	C4–N1–N2–C7	178.1(2)
N1–N2–C8–C9	172.2(4)	N1–N2–C7–C8	179.8(2)
N1–N2–C8–C11	-0.1(6)	N1–N2–C7–C10	0.2(4)
N2–C8–C11–O3	8.7(7)	N2–C7–C10–O2	0.4(4)
N2–C8–C9–O2	178.1(4)	N2–C7–C8–O1	178.5(3)
N2–C8–C9–C10	-0.8(6)	N2–C7–C8–C9	-1.0(4)
N2–C8–C11–N3	-166.2(4)	N2–C7–C10–N3	179.4(3)
C8–C11–N3–C12	172.7(4)	C7–C10–N3–C11	173.8(3)
C11–N3–C12–C13	173.1(5)	C10–N3–C11–C12	171.9(3)
C11–N3–C12–C17	-10.4(7)	C10–N3–C11–C16	-8.3(5)

Table 15

Compound number (71) is the mono-azo analogue of PO16 (23). Interatomic distances show that bifurcated hydrogen bonding is present between O1–H9 and O3–H9. Hydrogen bonding is also present between O2–H8. Comparing the data between (73) and (71), some interesting trends were observed (crystal structure diagrams of both shown on page 58). One of the interatomic distances for the two corresponding pigments were slightly different (highlighted in blue table 15). Bond lengths are reasonably consistent between the two (with the exception of the bond lengths highlighted in green table 15). There are some differences in torsion angles (see table

15: torsion angles highlighted in red) which again could be due to packing effects. Shown below (figures 29-30) are crystal packing diagrams of (71). The packing is quite complex showing a “herringbone” type packing arrangement. Molecules pack in the crystal lattice to form inclined stacks of interleaved molecules.

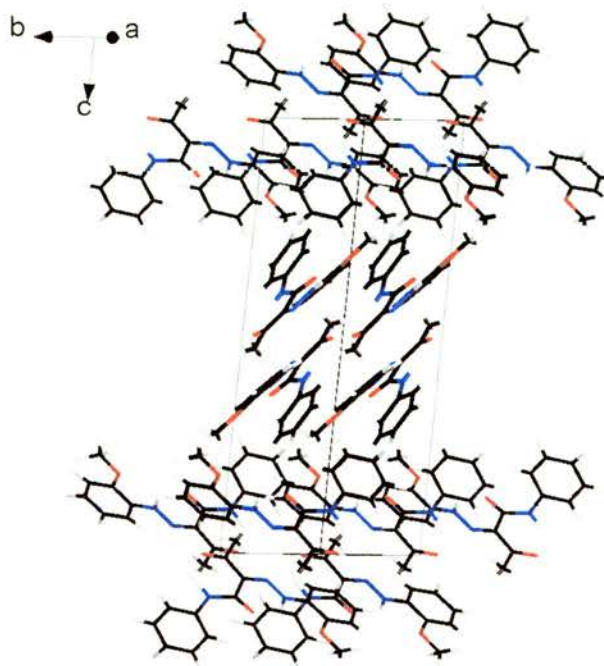


Figure 29 - crystal packing diagram of (71)

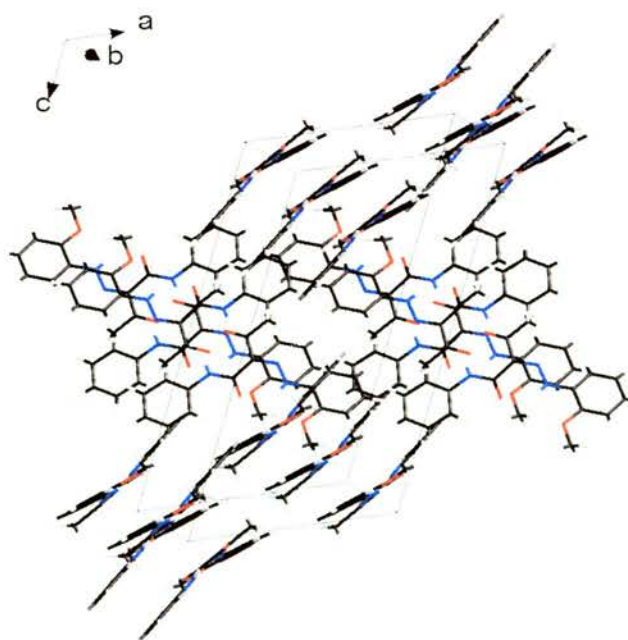
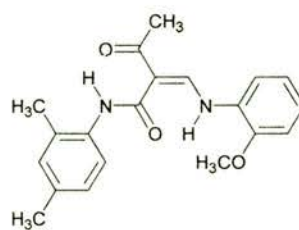


Figure 30 - alternative view of crystal packing diagram of (71)

3.5.5 2-[(2-Methoxyphenyl)hydrazone]-N-(2,4-dimethylphenyl)-3-oxobutamide (72)



(72)

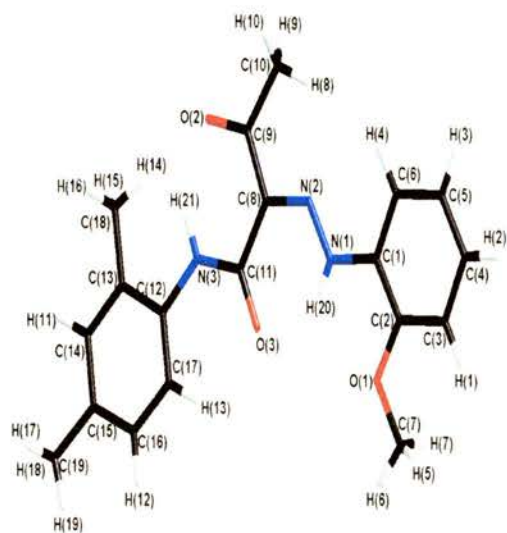


Figure 31 - crystal structure diagram of (72)

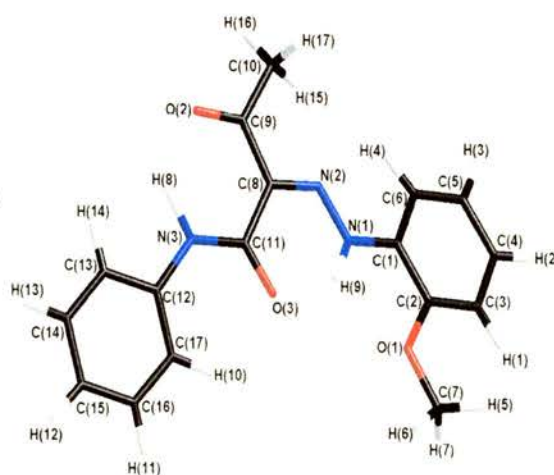


Figure 32 -crystal structure diagram of (71)

Interatomic distances between O1–H20, O3–H20 and O2–H21 indicate that intramolecular hydrogen bonding is present and that there is a bifurcated hydrogen bond between O1–H20–O3. There is quite a difference between the O3–H20 interatomic distance and the corresponding O3–H9 distance in (71) (see table 16: interatomic distances highlighted in blue). Bond lengths are reasonably consistent between (71) and (72). Again there are several differences in torsion angles (the most important ones are highlighted in red in table 16).

Interatomic Distances/ Å (72)		Interatomic Distances/ Å (71)	
O1-H20	2.34(8)	O1-H9	2.31(4)
O3-H20	2.07(8)	O3-H9	1.76(4)
O2-H21	1.95(8)	O2-H8	1.93(5)
Bond lengths/ ^o (72)		Bond lengths / ^o (71)	
C1-N1	1.40(2)	C1-N1	1.403(6)
N1-N2	1.29(1)	N1-N2	1.313(6)
N2-C8	1.32(2)	N2-C8	1.288(6)
C8-C9	1.45(1)	C8-C9	1.475(7)
C9-C10	1.52(2)	C9-C10	1.51(5)
C9-O2	1.22(2)	C9-O2	1.232(7)
C11-O3	1.22(1)	C11-O3	1.234(6)
C11-N3	1.35(2)	C11-N3	1.353(6)
N3-C12	1.44(2)	N3-C12	1.42(1)
Torsion angles/ ^o (72)		Torsion Angles/ ^o (71)	
C2-C1-N1-N2	168.7(8)	C2-C1-N1-N2	177.0(4)
C1-N1-N2-C8	178.2(8)	C1-N1-N2-C8	172.0(4)
N1-N2-C8-C9	178.3(8)	N1-N2-C8-C9	-179.2(9)
N1-N2-C8-C11	-2(1)	N1-N2-C8-C11	-0.1(6)
N2-C8-C9-C10	1(1)	N2-C8-C9-C10	-0.8(6)
N2-C8-C11-N3	177.9(8)	N2-C8-C11-N3	-166.2(4)
C11-N3-C12-C13	175.6(8)	C11-N3-C12-C13	173.1(5)
C11-N3-C12-C17	5.7(1)	C11-N3-C12-C17	10.4(7)

Table 16

The crystal packing in (72) is a good deal simpler than that of (71) (figures 33-34). The molecules pack in a two-dimensional, interleaved arrangement in contrast to the more complex “herringbone” arrangement of (71).

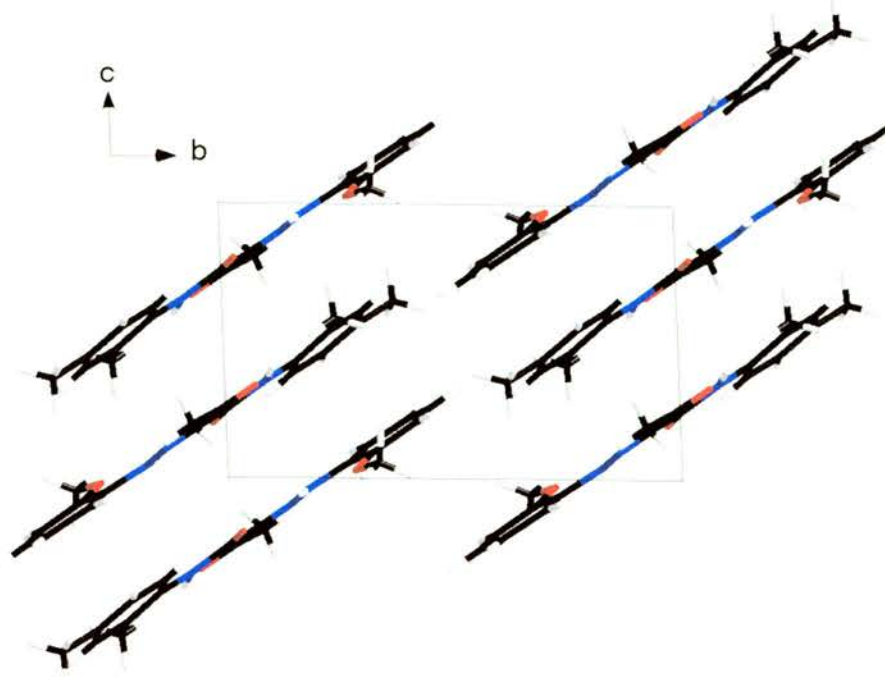


Figure 33 - crystal packing diagram of (72)

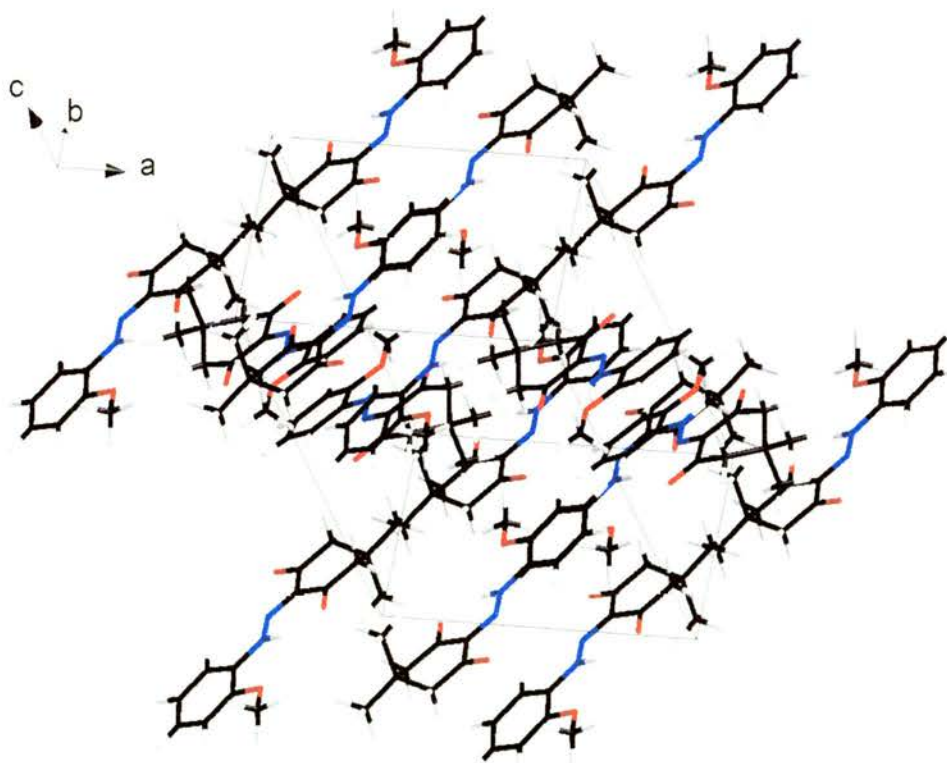


Figure 34 - alternative view of crystal packing diagram of (72)

3.5.6 2-[(2-Methoxyphenyl)hydrazono]-5,5-dimethylcyclohexane-1,3-dione (68) and 5-[(2-methoxyphenyl)hydrazono]-2,2-dimethyl-1,3-dioxan-4,6-dione (69)

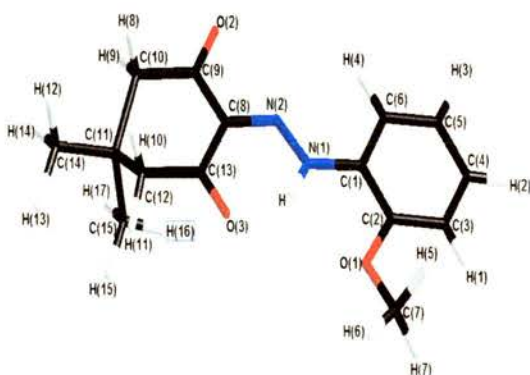
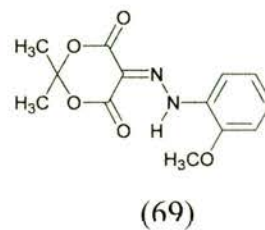
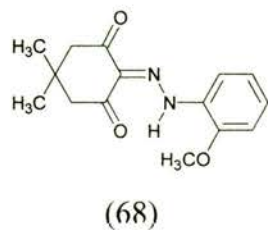


Figure 35 - crystal structure diagram of (68)

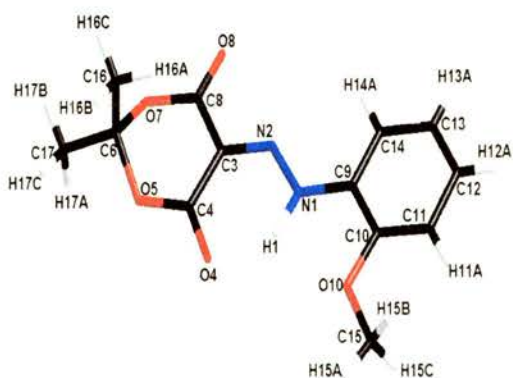


Figure 36 - crystal structure diagram of (69)

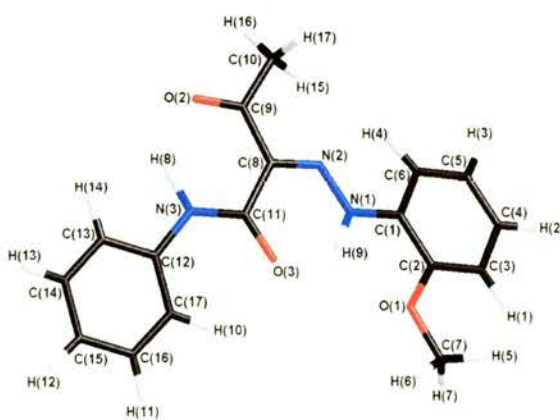


Figure 37 - crystal structure diagram of (71)

Interatomic Distances/ Å (68)		Interatomic Distances/ Å (69)		Interatomic Distances/ Å (71)	
O3–H	1.81(3)	O4–H1	1.86(3)	O3–H9	1.76(4)
O1–H	2.32(3)	O10–H1	2.39(5)	O1–H9	2.31(4)
–	–	–	–	O2–H8	1.93(5)
Bond lengths/ Å (68)		Bond lengths/ Å (69)		Bond lengths/ Å (71)	
C1–N1	1.40(1)	C9–N1	1.411(7)	C1–N1	1.403(6)
N1–N2	1.311(1)	N1–N2	1.30(1)	N1–N2	1.313(6)
N2–C8	1.32(1)	N2–C3	1.314(7)	N2–C8	1.288(6)
C8–C9	1.485(5)	C3–C8	1.480(1)	C8–C9	1.475(7)
C8–C13	1.46(1)	C3–C4	1.458(8)	C9–C10	1.51(1)
C9–O2	1.21(1)	C8–O8	1.203(8)	C9–O2	1.232(7)
C13–O3	1.237(4)	C4–O4	1.22(1)	C11–O3	1.234(6)
C11–C15	1.532(7)	C6–C16	1.50(1)	C11–N3	1.353(9)
C2–O1	1.36(1)	C15–O10	1.43(1)	N3–C12	1.42(1)
Torsion Angles/° (68)		Torsion Angles/° (69)		Torsion Angles/° (71)	
C2–C1–N1–N2	-174.0(3)	C10–C9–N1–N2	175.6(5)	C2–C1–N1–N2	177.0(4)
C1–N1–N2–C8	176.4(3)	C9–N1–N2–C3	-178.5(5)	C1–N1–N2–C8	172.0(4)
N1–N2–C8–C9	-178.5(3)	N1–N2–C3–C8	-176.4(5)	N1–N2–C8–C9	-179.2(9)
N1–N2–C8–C13	-2.4(5)	N1–N2–C3–C4	-0.5(8)	N1–N2–C8–C11	-0.1(6)
N2–C8–C9–O2	-2.9(5)	N2–C3–C8–O8	5.1(8)	N2–C8–C9–C10	-0.8(6)
N2–C8–C13–O3	4.5(6)	N2–C3–C4–O4	-6.9(9)	N2–C8–C11–N3	-166.2(4)
C8–C9–C10–C11	-31.6(5)	C3–C8–O7–C6	27.1(7)	C11–N3–C12–C13	173.1(5)
C8–C13–C12–C11	26.9(5)	C3–C4–O5–C6	-17.1(7)	C11–N3–C12–C17	10.4(7)
C13–C12–C11–C14	173.4(4)	C4–O5–C6–C17	159.4(5)	–	–
C9–C10–C11–C14	175.2(5)	C4–O5–C6–C16	-75.4(6)	–	–
C13–C12–C11–C15	67.7(4)	C8–O7–C6–C17	-165.1(5)	–	–
C9–C10–C11–C15	64.5(5)	C8–O7–C6–C16	70.2(6)	–	–

Table 17

Both (68) and (69) adopt the ketohydrazone tautomeric form. There is bifurcated hydrogen bonding observed in both (68) and (69). Both (68) and (69) are non-planar as is expected due to the geometry of the dimedone and Meldrum's acid end groups. The C2–O1 bond length in (68) is a little shorter than the equivalent C15–O10 bond length in (69) (highlighted in green table 17). The selected torsion angles

(highlighted in red: table 17) show that the two methyl groups are orientated in different directions in **(68)** and **(69)**. Both **(68)** and **(69)** pack in two dimensional, interleaved arrangements (figures 38-41). The molecules in **(68)**, however, pack in the opposite direction to **(69)** (see figures 39 and 40).

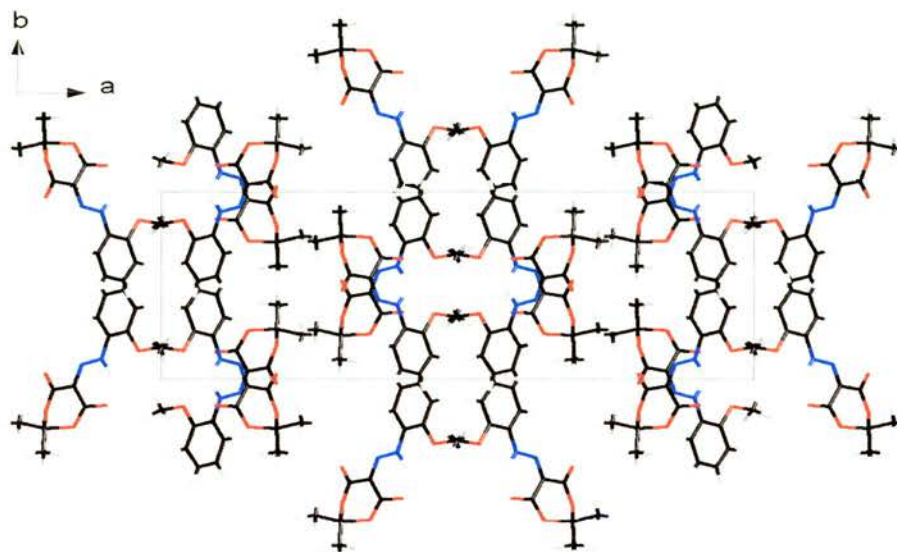


Figure 38 - crystal packing diagram of **(69)**

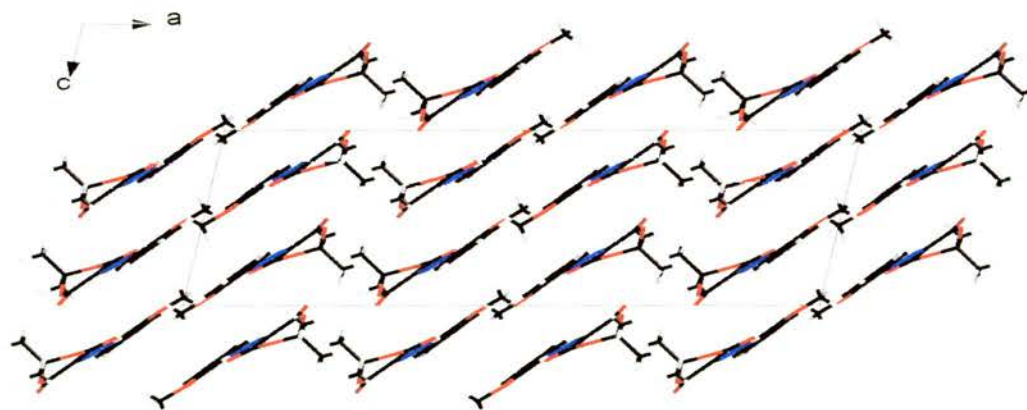


Figure 39 - alternative view of crystal packing diagram of **(69)**

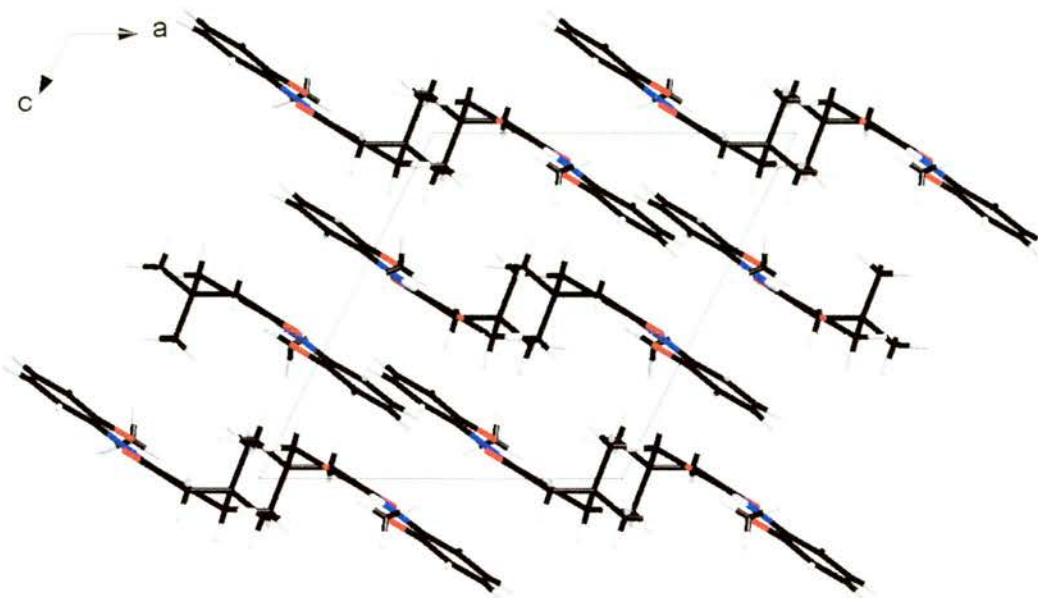


Figure 40 - alternative view of crystal packing diagram of (68)

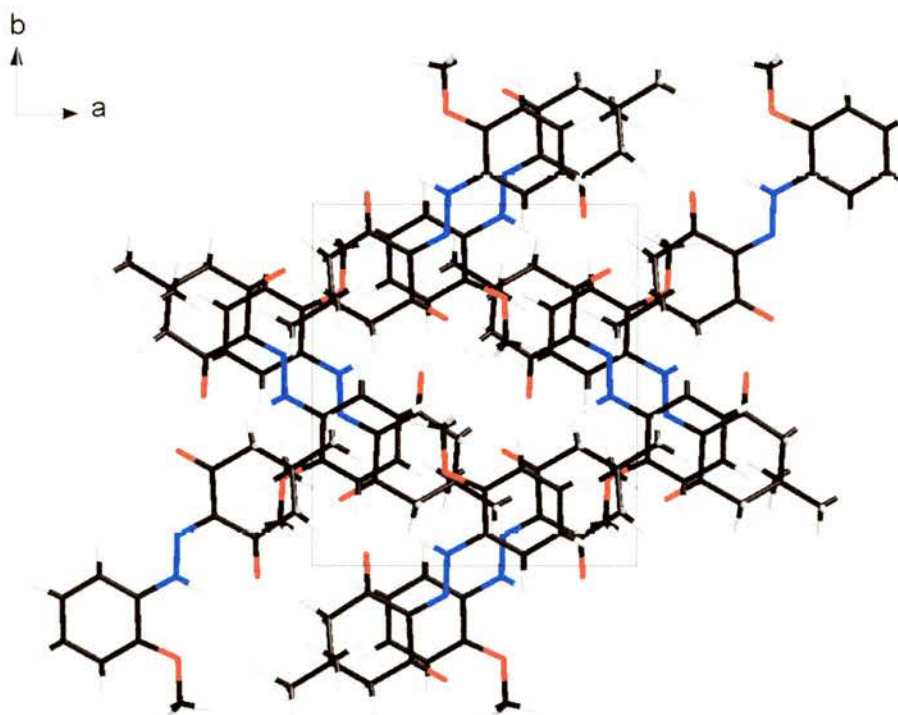
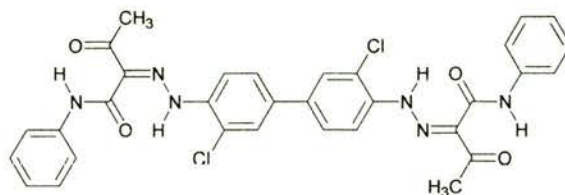


Figure 41 - alternative view of crystal packing diagram of (68)

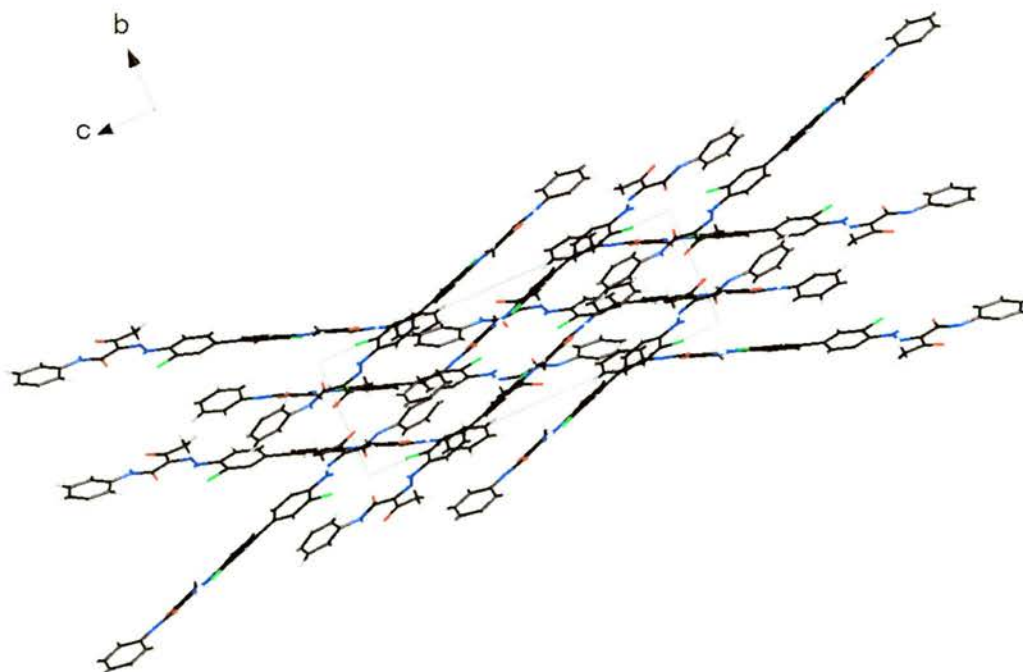
3.6 Intermolecular Interactions and Crystal Packing Trends in Known Diarylide Pigments

3.6.1 PY12 (42)^{49,50}

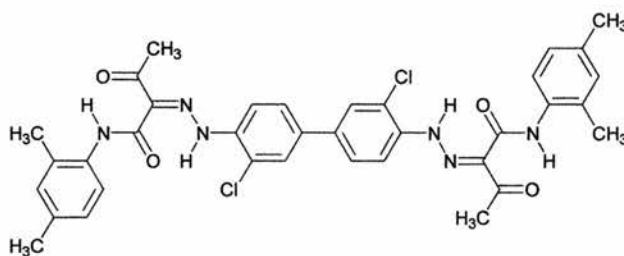


(42)

The crystal packing in PY12 (**42**) is quite complex, displaying a “herringbone” type packing arrangement. Molecules pack in the crystal lattice to form inclined stacks of interleaved molecules. The plane of the ketohydrazone group of each half of each molecule lies sandwiched between the planes of the ketohydrazone groups of the molecules that are above and below. The middle molecule is crystallographically inverted relative to those above and below. For the planar half of the molecule, the two perpendicular distances for the sandwich are: top-to-middle = 3.43(2)Å and middle-to-bottom = 3.44(1)Å. For the twisted half of the molecule the distances are respectively 3.51(2) and 3.47(2)Å.

Figure 42 - crystal packing diagram of PY12 (**42**)

3.6.2 PY13 (44)⁵⁰



(44)

In sharp contrast to PY12 (42), the packing arrangement in PY13 (44) is relatively straightforward. The molecules in PY13 (44) pack in a two-dimensional, interleaved arrangement. As previously stated (page 34) it was found that PY13 (44) did not display solid-state fluorescence, which is in stark contrast to the structurally similar PY12 (42), the only structural difference from the latter molecule being the two methyl groups at the 2 and 4 positions on each end ring. As stated above, in PY13 (44) the biphenyl moiety is planar and no solid-state fluorescence is observed whereas the PY12 (42) molecule has a central biphenyl twist. Langhals has speculated that non-interaction of adjacent chromophores can aid solid-state fluorescence.³² If two chromophores in close proximity are prevented from interacting, e.g. by being out of plane with respect to each other, fluorescence quenching could be avoided. The observations so far are in accordance with Langhals' theory. The perpendicular distance between the plane of the ketohydrazone group in one molecule and the equivalent planes in the molecules above is 3.36(3)Å and 3.23(5)Å in the molecules below which suggests that the packing efficiency in PY13 (44) is greater than that of PY12 (42) and there is a greater chance for intermolecular interactions to occur.

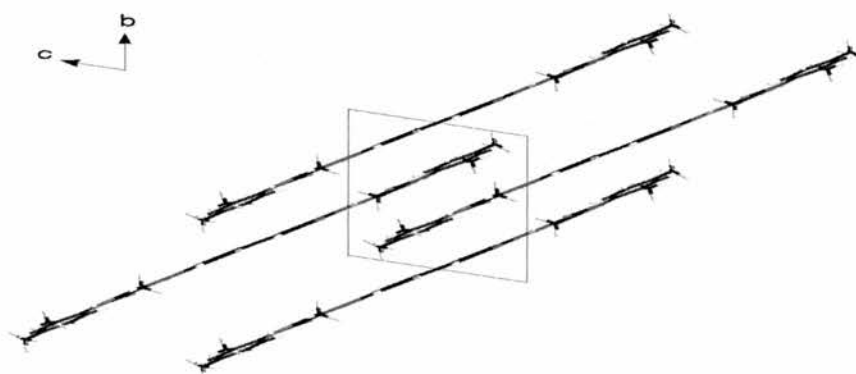
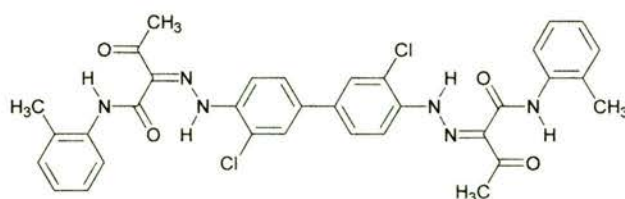


Figure 43 - crystal structure diagram of PY13 (44)

3.6.3 PY14 (45)⁵⁰



(45)

Similarly to PY13 (44), PY14 (45) packs in a two-dimensional, interleaved arrangement. However, unlike PY13 (44), PY14 (45) has been found to be fluorescent in the solid state. The packing arrangement is also unlike PY12 (42), the other solid-state fluorescent pigment mentioned. Due to the fact that the central biphenyl moiety is essentially planar this would suggest that Langhals' theory³² may not be generally applicable for the diarylide pigments. The perpendicular distances between the plane of the ketohydrazone group in one molecule and the equivalent planes in the molecules above and below are 3.43(4)Å and 3.33(6)Å. These intermolecular distances are greater than that for PY13 (44) but less than that for PY12 (42). So far the pigment with the smallest intermolecular distances has been found not to be fluorescent. How important a factor is this?

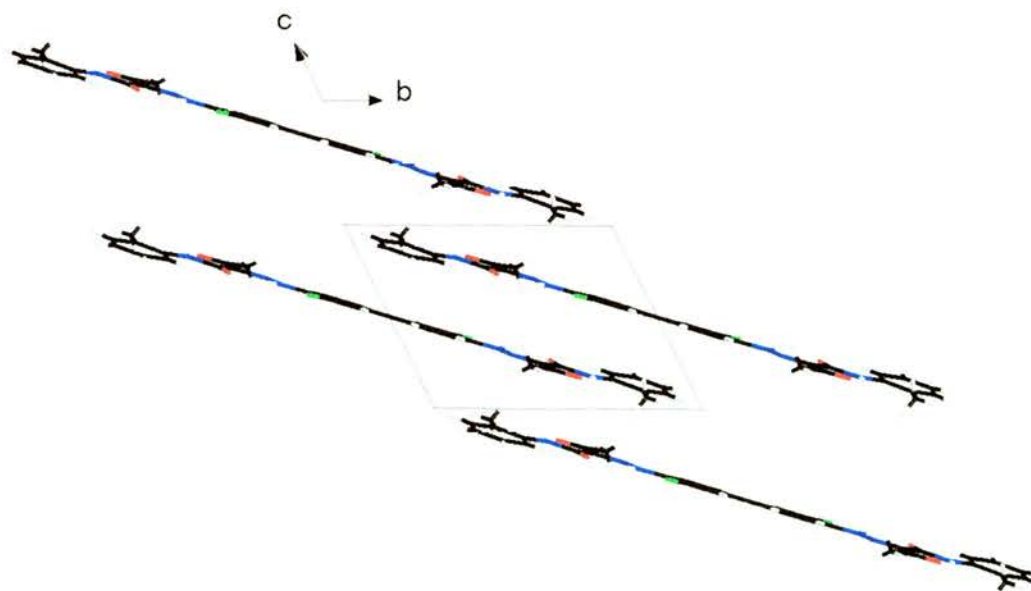
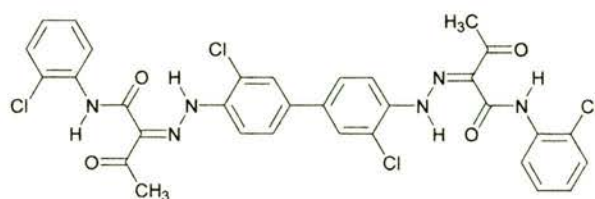


Figure 44 - crystal structure diagram of PY14 (45)

3.6.4 PY63 (46)⁵⁰



(46)

As for PY13 (44) and PY14 (45), PY63 (46) packs in a two-dimensional, interleaved arrangement. PY63 (46) has been found to be quite intensely fluorescent (page 34). Again the central biphenyl moiety is planar giving further weight to the fact that Langhals' theories²⁹ do not apply here. Looking at the intermolecular distances shows the following. The perpendicular distance between the plane of the ketohydrazone group in one molecule and the equivalent planes in the molecules above and below is 3.43(2)Å and 3.36(3)Å. This is the second greatest intermolecular distance found, behind PY12 (42). It seems that the greater the intermolecular distances are, the greater the intensity of the solid-state fluorescence.

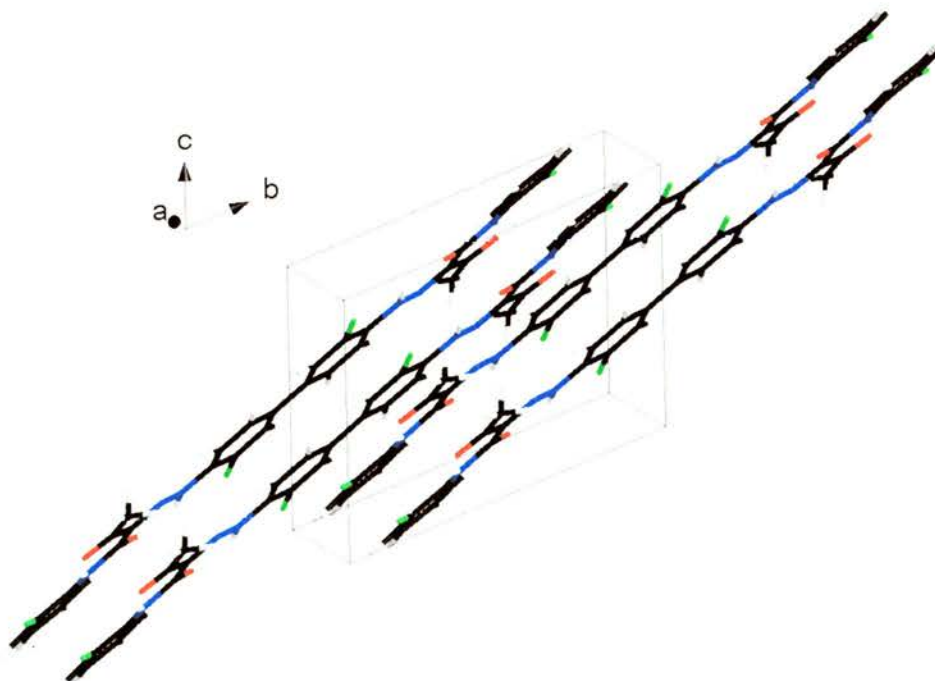
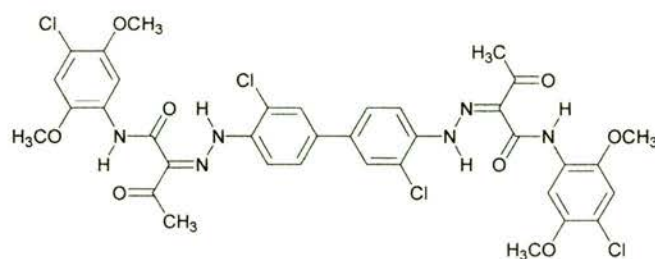


Figure 45 - crystal structure diagram of PY63 (46)

3.6.5 PY83 (48)⁴⁵



(48)

Unlike PY13 (44), PY14 (45) and PY63 (46), PY83 (48) shows a more complex packing arrangement. In some ways it is similar to PY12 (42) in that it has a “herringbone” type packing arrangement. However it does not show an interleaved type arrangement which is common to all the other pigments. The perpendicular distances between the plane of the ketohydrazone group in one molecule and the equivalent planes in the molecules above and below are both 3.35(3)Å. These are the second lowest intermolecular distances found across this series of pigments. PY83 (48) is not fluorescent in the solid state: this gives more credence to the hypothesis that intermolecular distances could be affecting solid-state fluorescence.

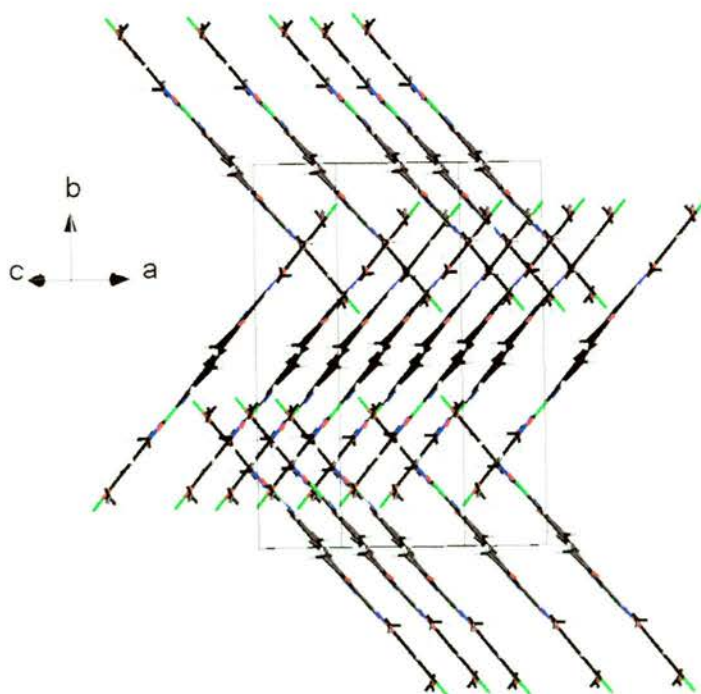
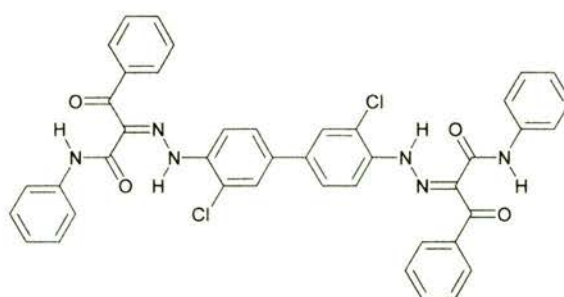


Figure 46 - crystal structure diagram of PY83 (48)

3.6.6 (43)⁴⁵

(43)

Again (43) shows a more complex packing arrangement. It is similar to PY12 (42) and PY83 (48) in that it has a “herringbone” type packing arrangement. However it does not show an interleaved type arrangement which is common to all the other pigments with the exception of PY83 (48). The perpendicular distances between the plane of the ketohydrazone group in one molecule and the equivalent planes in the molecules above and below are both 3.35(2)Å. These are quite low intermolecular distances. However this pigment was found to be fluorescent in the solid state. Perhaps the packing arrangement had more of an influence in (43).

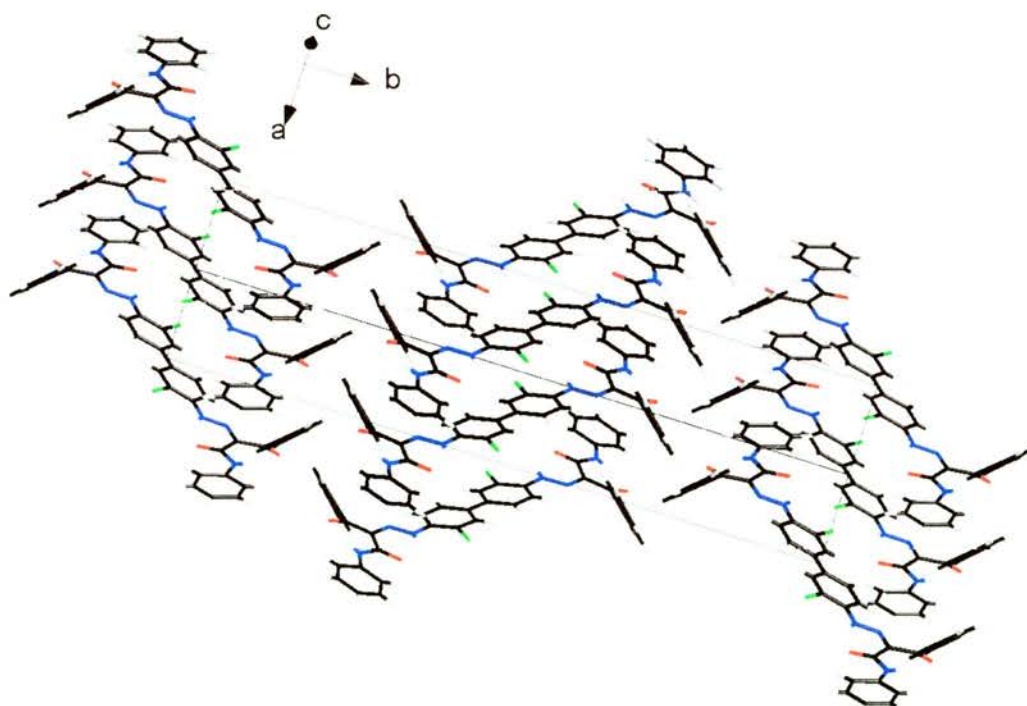


Figure 47 - crystal structure diagram of (43)

Comparing all the perpendicular distances between molecules;

Pigment	Molecule above/Å	Molecule below/Å
PY12 (42)	3.51(2), 3.47(2)	3.43(2), 3.44(1)
PY13 (44)	3.36(3)	3.23(5)
PY14 (45)	3.43(4)	3.33(6)
PY63 (46)	3.43(2)	3.36(3)
PY83 (48)	3.35(3)	3.35(3)
(43)	3.35(2)	3.35(2)

Table 18

PY13 (44) shows the smallest distance between the molecules and PY12 (42) shows the largest. PY14 (45) and PY63 (46) show similar distances between the molecules above and below the unique molecule. PY83 (48) and compound (43) show the same distances between molecules.

3.7 Quantitative Fluorescence Measurements of Pigments

Up until this point in the argument, only qualitative fluorescence measurements have been discussed. A quantitative approach was necessary to gain a handle on the fluorescence intensity and emission wavelengths of the pigments.

Initially, in collaboration with Professor J.W. Allen (School of Physics and Astronomy, University of St. Andrews) a set-up was devised to allow the quantitative measurement of fluorescence. However, several problems existed with this equipment. It was difficult to gain consistent results from this equipment due to the fact that the machine was used by several different workers and was constantly being modified. Due to consistency problems this approach was not pursued beyond this preliminary stage.

Also, some samples were submitted for testing both in Switzerland (Ciba in Basel). Again problems existed with the consistency of this approach as well as the logistical problems and timescale.

In collaboration with Professor A. Mills at the University of Strathclyde a solution was found. All samples were run under the same conditions using the absorption and fluorescence equipment in Professor Mills' laboratory.

Solid-state fluorescence measurements were made as follows. A microscope slide with double sided adhesive stuck to the top was used. A known amount of pigment (recrystallised analytically pure samples) was sprinkled on to the tape and the slide was placed in the fluorimeter. The excitation source used was set at 400nm and the slit width on the machine was set to 10nm. Solution fluorescence measurements were also made on the same instrument with the same settings. The solvent used was dichloromethane: ideally the solvent should have as little interaction with the pigment molecules as possible and the use of a non-aromatic solvent would eliminate the possibility of π - π interactions between the solvent molecules and the pigment molecules. The concentration of the solutions used was $3 \times 10^{-4} \text{ mol dm}^{-3}$. For full details, see experimental.

3.7.1 Solid-State Fluorescence

The solid-state fluorescence data are shown on pages 75-77 (tables 19-20 and figures 49-54). The order of solid-state fluorescence intensity is shown below.

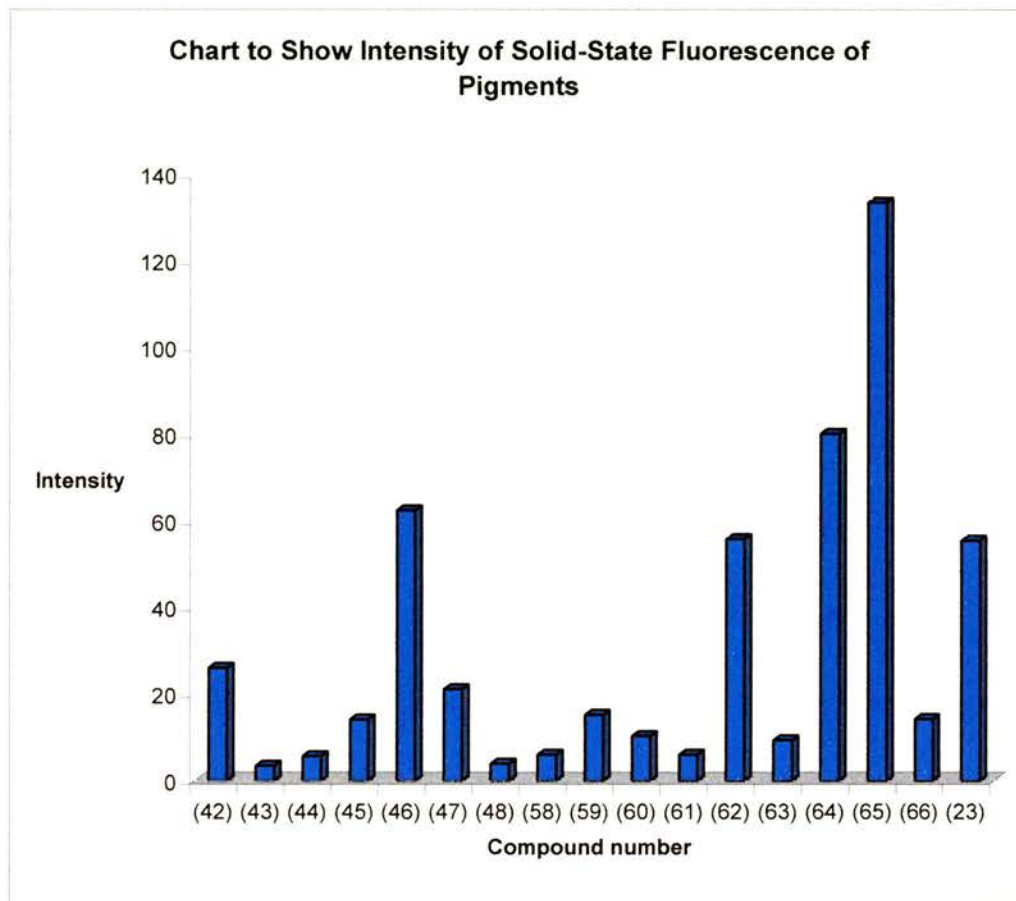


Figure 48

The solid-state fluorescence measurements show the following trends. (65) was found to be the most intensely fluorescent and the weakest was (43). The pigments in general show good fluorescence intensity with the exceptions of (43), (44), (48), (58) and (61) which gave very low readings. It was believed that particle size was also influencing the intensity of fluorescence (see section 3.10). Although pigments (43), (58) and (61) were clearly fluorescent under the naked eye they were giving very low readings in these quantitative measurements. Pigments (44) and (48) did not show solid-state fluorescence under the naked eye which accounts for the low readings of these pigments.

Pigment	Structure	λ_{max} /nm, intensity (solid-state)	Pigment	Structure	λ_{max} /nm, intensity (solid-state)
PY12 (42)		551, 26.12	PY63 (46)		546, 62.40
(43)		549, 3.40	PY81 (47)		538, 21.16
PY13 (44)		560, 5.67	PY83 (48)		553, 3.89
PY14 (45)		543, 14.10	PO16 (23)		598, 55.42

Table 19

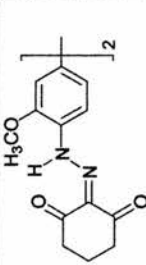
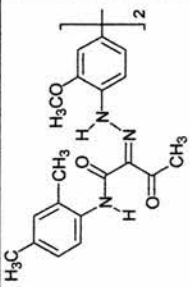
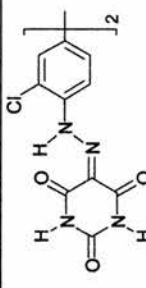
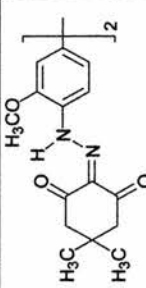
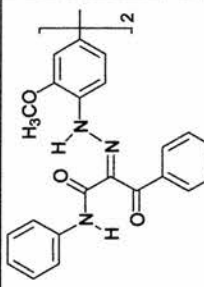
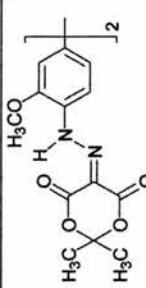
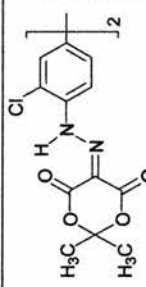
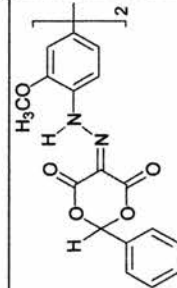
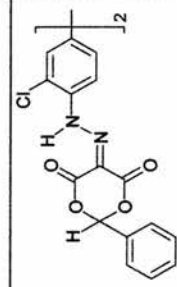
Pigment	Structure	λ_{max} /nm, intensity (solid-state)	Pigment	Structure	λ_{max} /nm, intensity (solid-state)	Pigment	Structure	λ_{max} /nm, intensity (solid-state)
(58)		603, 6.04	(62)		596, 55.75	(66)		594, 14.24
(59)		605, 15.27	(63)		600, 9.39	-	-	-
(60)		607, 10.32	(64)		548, 80.11	-	-	-
(61)		605, 5.98	(65)		570, 133.53	-	-	-

Table 20

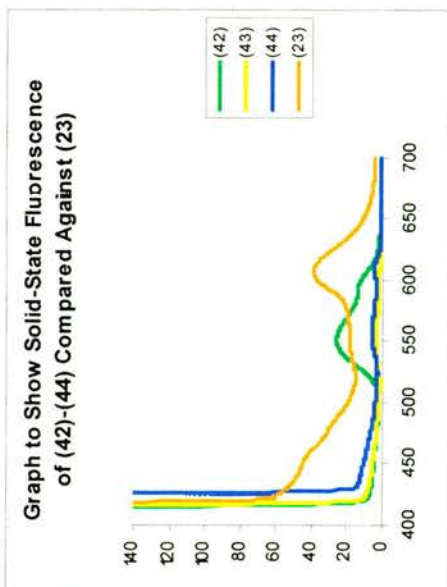


Figure 49

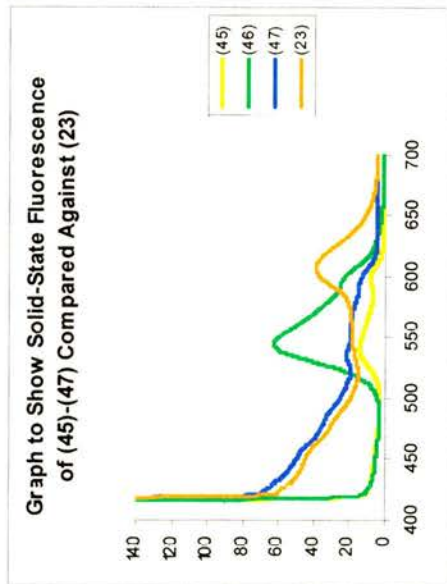


Figure 50

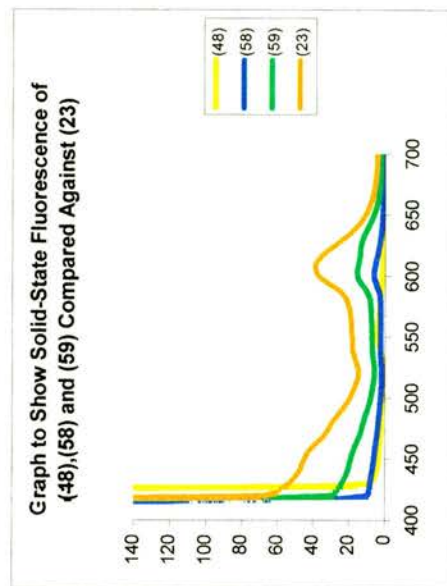


Figure 51

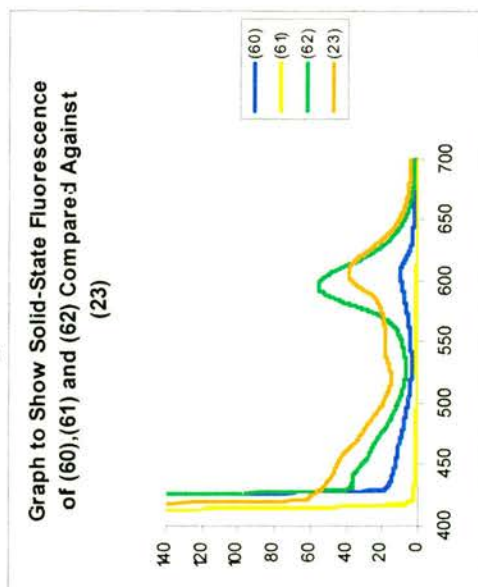


Figure 52

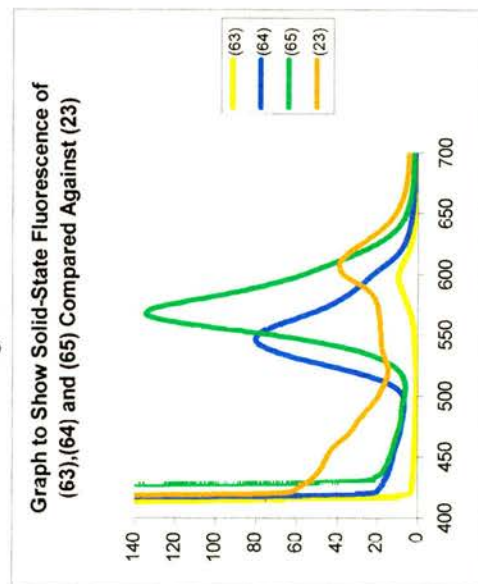


Figure 53

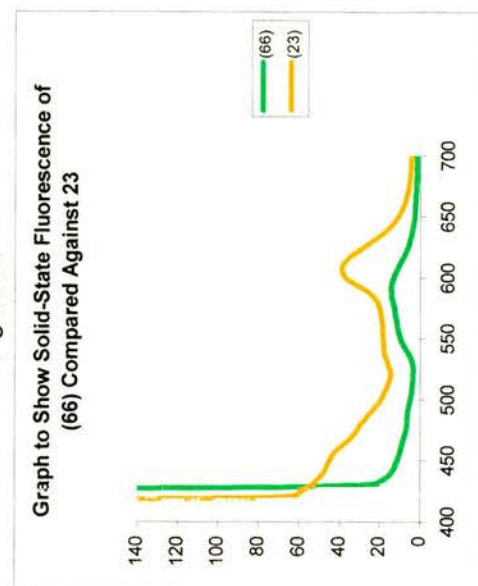


Figure 54

3.7.2 Solution Fluorescence

The solution fluorescence data are shown on pages 79-81 (tables 21-22 and figures 56-61). The order of solution fluorescence intensity is shown below.

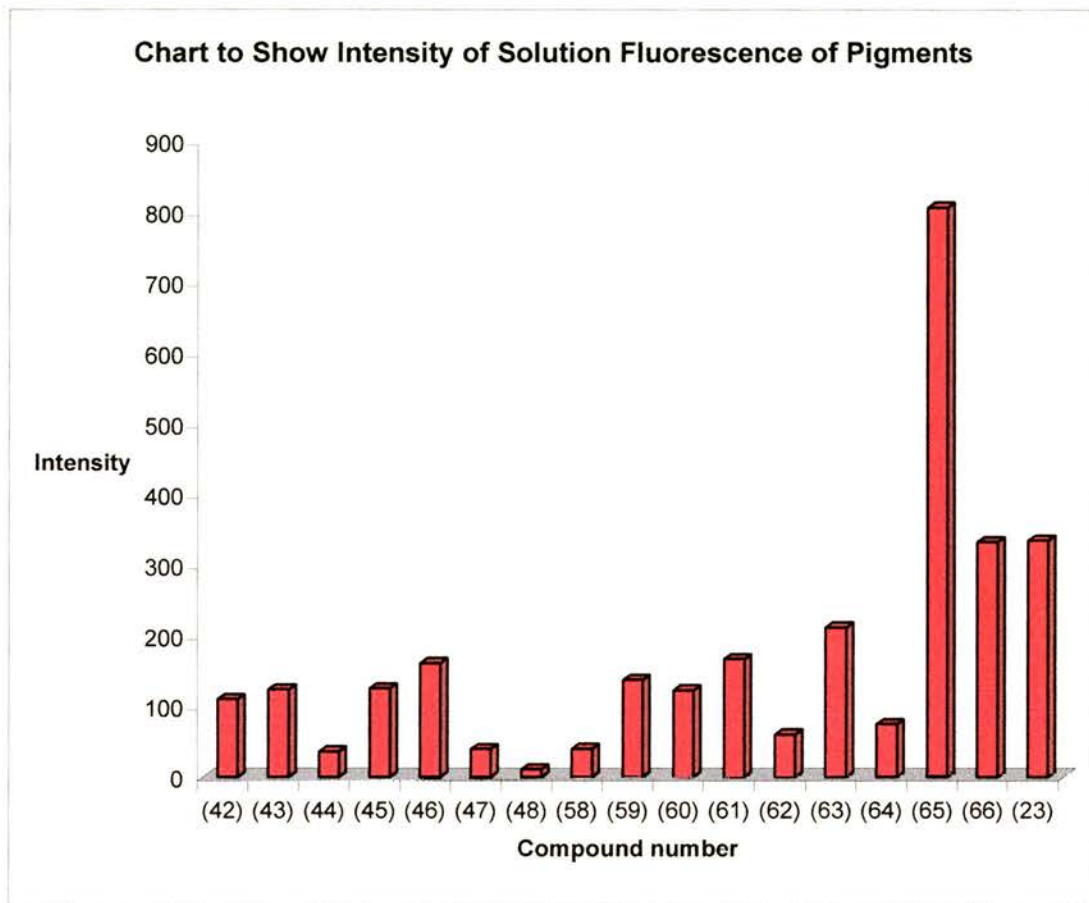


Figure 55

The solution fluorescence measurements show the following trends. The order is slightly different across the board for solution fluorescence in comparison to the solid-state order although the most intensely fluorescent pigments are still **(65)**, **(23)** and **(48)** being the most weakly fluorescent. Particle aggregation is likely to be very low due to the very low concentration of pigment within the solution so quenching effects from aggregation are expected to be minimal. There also was a possibility that the more insoluble pigments such as PO16 **(23)** were precipitating out of solution during the measuring process which could lead to erroneous readings. Reduction of intermolecular π - π interactions in solution is going to have a pronounced effect on fluorescence intensity as the solvent being used is dichloromethane (a non-aromatic non-polar solvent).

Pigment	Structure	λ_{\max}/nm , intensity (solution)	Pigment	Structure	λ_{\max}/nm , intensity (solution)
PY12 (42)		512, 110.52	PY63 (46)		504, 161.26
(43)		495, 124.02	PY81 (47)		481, 39.60
PY13 (44)		490, 36.23	PY83 (48)		511, 11.04
PY14 (45)		499, 125.60	PO16 (23)		522, 355.14

Table 21

Pigment	Structure	λ_{max}/nm , intensity (solution)	Pigment	Structure	λ_{max}/nm , intensity (solution)	Pigment	Structure	λ_{max}/nm , intensity (solution)
(58)		558, 40.02	(62)		514, 60.39	(66)		524, 332.92
(59)		552, 137.49	(63)		540, 211.9	-	-	-
(60)		542, 122.87	(64)		512, 75.07	-	-	-
(61)		543, 167.07	(65)		507, 806.69	-	-	-

Table 22

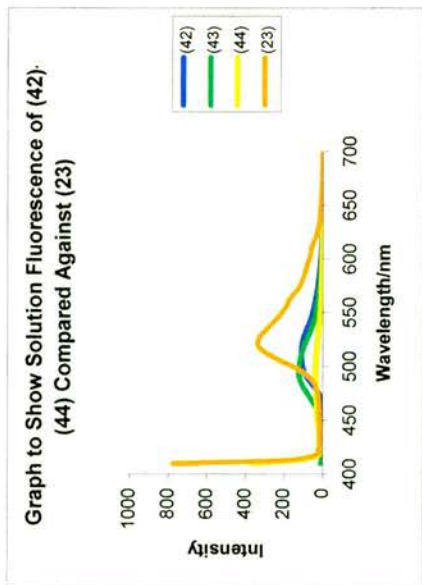


Figure 56

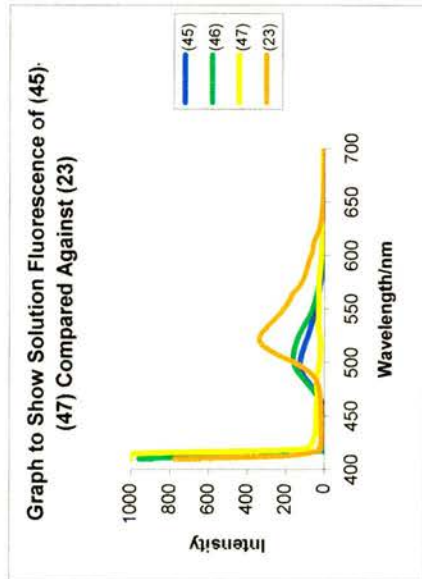


Figure 57

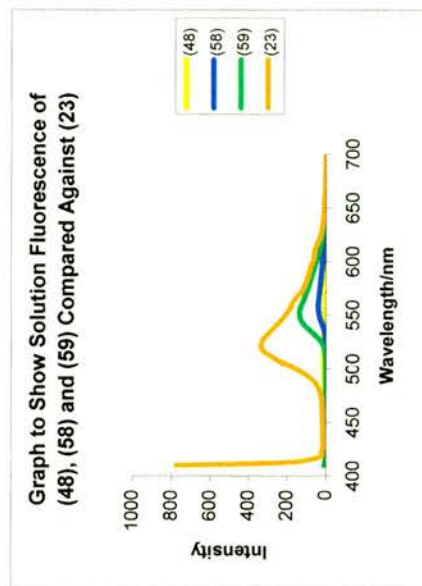


Figure 58

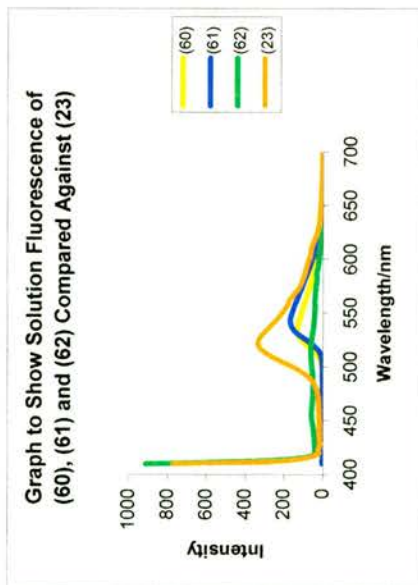


Figure 59

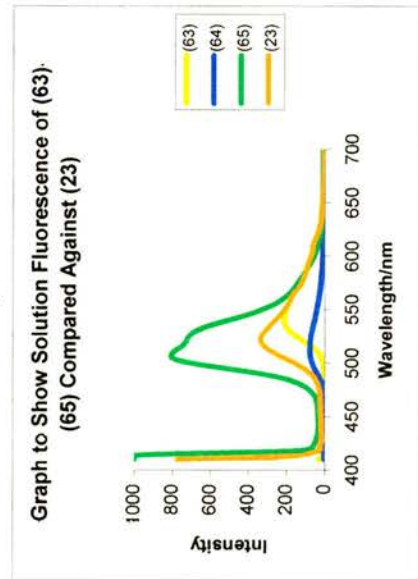


Figure 60

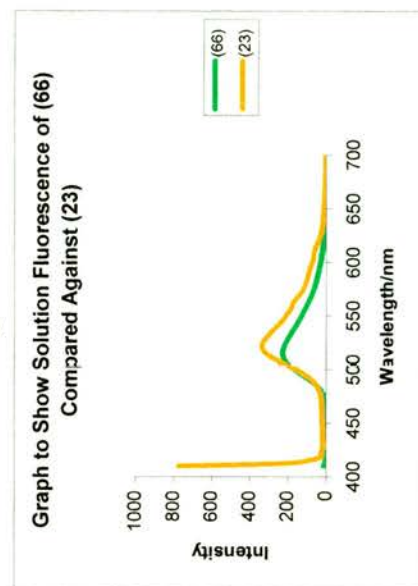


Figure 61

3.8 Quantitative Absorption Measurements of Pigments

Quantitative absorption measurements were also made for the pigments. The stock solutions that were used for the solution fluorescence measurements were also used for absorption measurements (concentration $3 \times 10^{-4} \text{ mol dm}^{-3}$). Solid-state absorption measurements were carried out as follows. The samples were prepared in the same way as a KBr disc was prepared for running IR spectra and the KBr disc was placed in a UV/visible spectrophotometer. Solution measurements were made to compare the Stokes shifts with the fluorescence measurements.

3.8.1 Solution and Solid-State Absorption Measurements

The solid-state absorption data are shown on pages 84-86. (tables 23-24 and figures 62-67). The solution absorption data is shown on pages 87-89. (tables 25-26 and figures 68-73). Stokes shifts between solid-state and solution absorption are shown on table 27 (page 90). The solution and solid-state absorption Stokes shifts are very close together (6-14nm difference) which indicates that there is no strong intermolecular interactions in the solid-state which would modify the absorption characteristics.⁷³ This is supported by the crystal structure information on (42)-(46) and (48) which indeed show no strong intermolecular interactions within the crystal lattice.

3.9 Comparison of Fluorescence and Absorption Data

All other Stokes shift data for solution and solid-state fluorescence measurements are given in tables 28 and 29 (pages 91-92). The large Stokes shift in the solid-state absorption vs. fluorescence suggest that there is significant intramolecular changes going on in the excited state, after the molecules have absorbed the light before fluorescence occurs. The Stokes shift in solution absorption vs. fluorescence is not as large as in solution, suggesting that the intramolecular changes of the excited state molecule in solution is less. It would usually be expected that the Stokes shifts in solution would be less than in the solid, since the molecules are held tightly in the

crystal lattice, so have less chance of "relaxing" prior to emission than in solution. It is possible that the emissive state in the solid is different from that in solution.

Pigment	Structure	λ_{\max}/nm , intensity (solid-state)	Pigment	Structure	λ_{\max}/nm , intensity (solid-state)
PY12 (42)		411, 0.69	PY63 (46)		415, 2.76
(43)		440, 1.52	PY81 (47)		386, 0.098
PY13 (44)		416, 0.04	PY83 (48)		394, 0.18
PY14 (45)		436, 0.094	PO16 (23)		429, 0.10

Table 23

Pigment	Structure	$\lambda_{\text{max}}/\text{nm}$, intensity (solid-state)	Pigment	Structure	$\lambda_{\text{max}}/\text{nm}$, intensity (solid-state)	Pigment	Structure	$\lambda_{\text{max}}/\text{nm}$, intensity (solid-state)
(58)		486, 0.96	(62)		428, 0.02	(66)		466, 0.6
(59)		458, 0.65	(63)		444, 0.55	-	-	-
(60)		440, 0.69	(64)		409, 0.73	-	-	-
(61)		444, 0.70	(65)		394, 0.10	-	-	-

Table 24

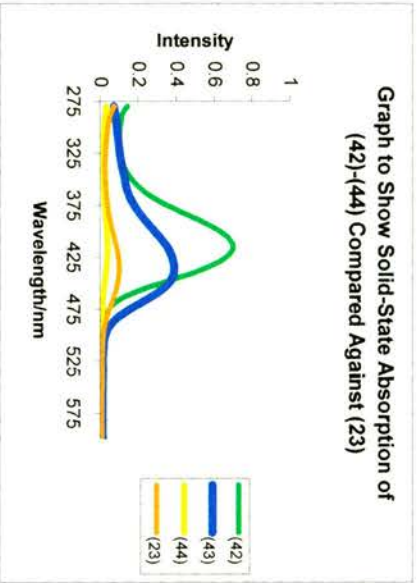


Figure 62

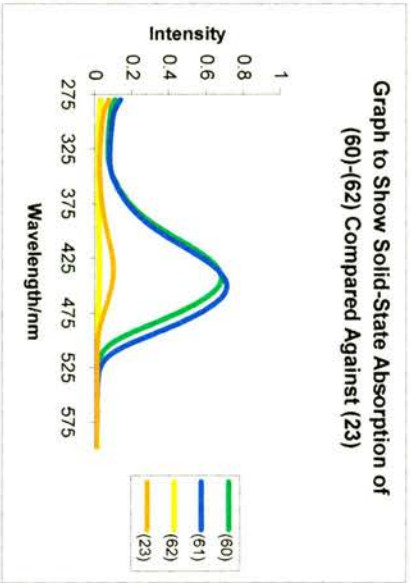


Figure 65

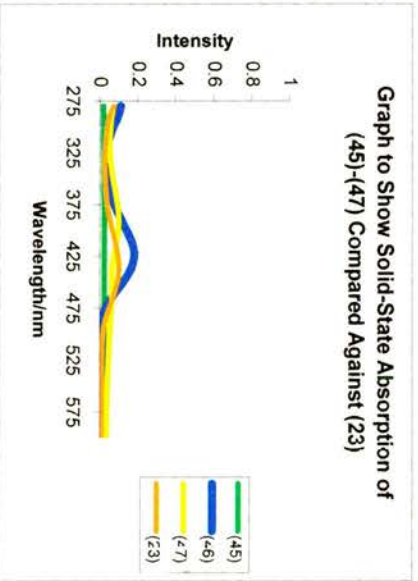


Figure 63

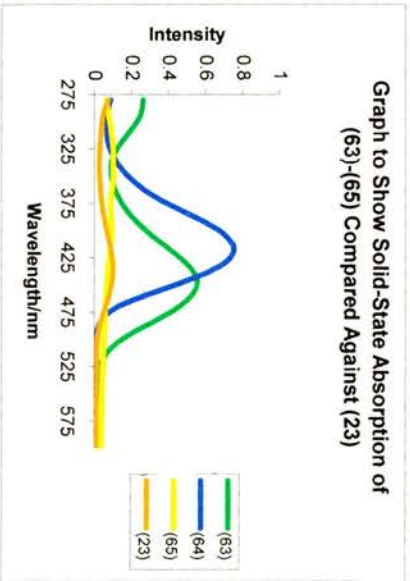


Figure 66

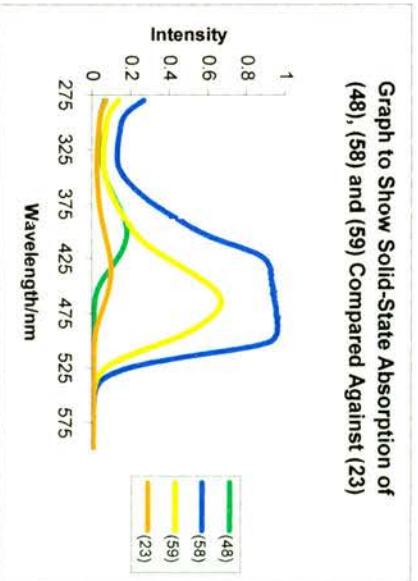


Figure 64

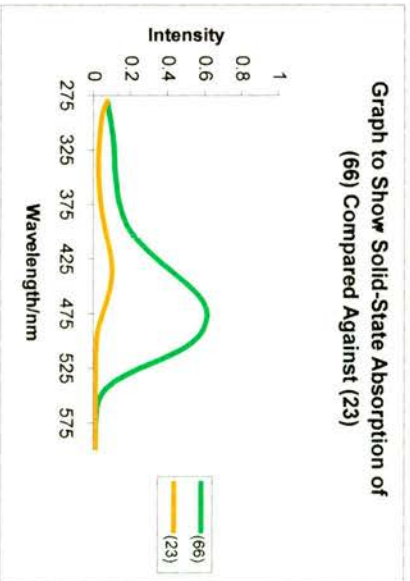


Figure 67

Pigment	Structure	λ_{max} /nm, intensity (solution)	Pigment	Structure	λ_{max} /nm, intensity (solution)
PY12 (42)		419, 2.72	PY63 (46)		426, 0.70
(43)		446, 1.54	PY81 (47)		394, 0.39
PY13 (44)		426, 0.15	PY83 (48)		402, 0.70
PY14 (45)		444, 0.09	PO16 (23)		443, 0.39

Table 25

Pigment	Structure	λ_{max} /nm, intensity (solution)	Pigment	Structure	λ_{max} /nm, intensity (solution)	Pigment	Structure	λ_{max} /nm, intensity (solution)
(58)		493, 3.78	(62)		442, 0.09	(66)		475, 2.37
(59)		471, 2.63	(63)		451, 2.22	-	-	-
(60)		449, 2.69	(64)		420, 2.92	-	-	-
(61)		456, 0.09	(65)		407, 0.36	-	-	-

Table 26

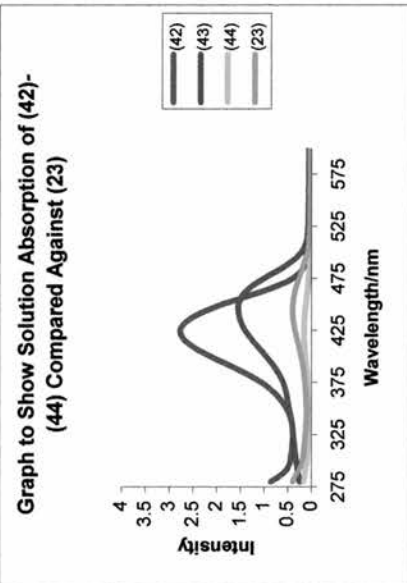


Figure 68

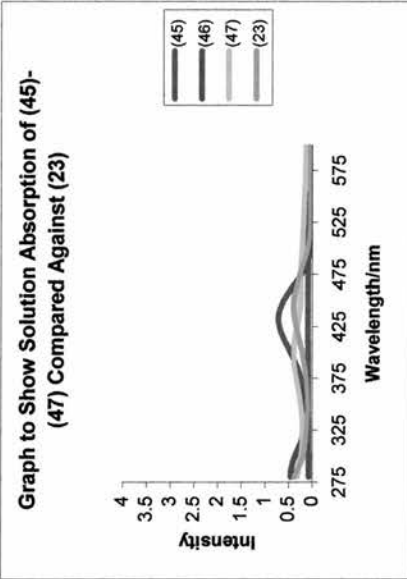


Figure 69

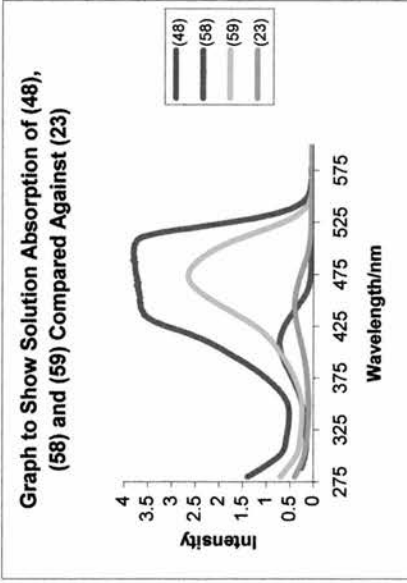


Figure 70

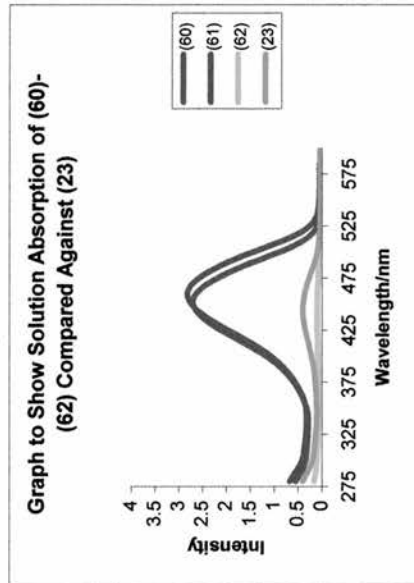


Figure 71

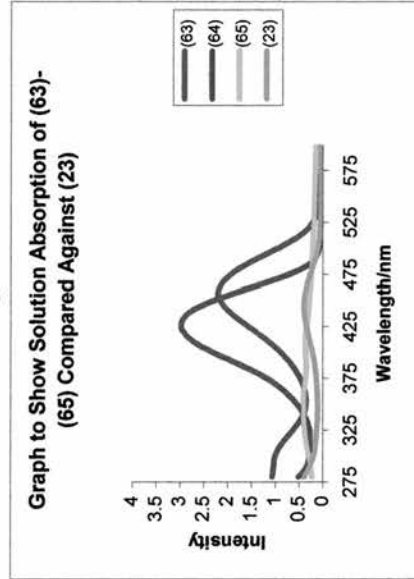


Figure 72

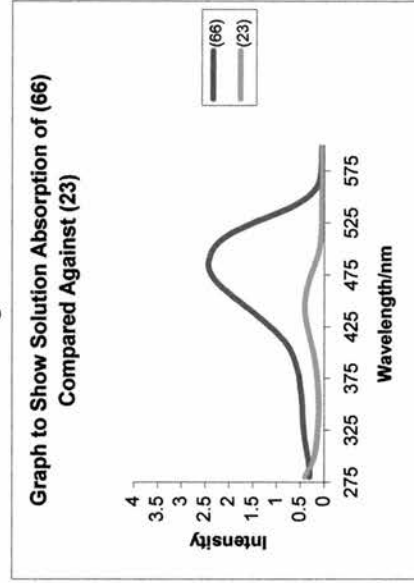


Figure 73

Pigment	$\lambda_{\text{max}}/\text{nm}$ (solid-state absorption)	$\lambda_{\text{max}}/\text{cm}^{-1}$ (solid-state absorption)	$\lambda_{\text{max}}/\text{nm}$, (solution absorption)	$\lambda_{\text{max}}/\text{cm}^{-1}$ (solution absorption)	Pigment	$\lambda_{\text{max}}/\text{nm}$ (solid-state absorption)	$\lambda_{\text{max}}/\text{cm}^{-1}$ (solid-state absorption)	$\lambda_{\text{max}}/\text{nm}$, (solution absorption)	$\lambda_{\text{max}}/\text{cm}^{-1}$ (solution absorption)	$\Delta\lambda_{\text{max}}/\text{cm}^{-1}$
PY12 (42)	411	24331	419	23866	(59)	458	21834	471	21231	603
(43)	440	22727	446	22421	(60)	440	22727	449	22272	455
PY13 (44)	416	24038	426	23474	(61)	444	22523	456	21930	593
PY14 (45)	436	22936	444	22522	(59)	428	23364	442	22624	740
PY63 (46)	415	24096	426	23474	(63)	443	22573	451	22173	400
PY81 (47)	386	25906	394	25380	(64)	409	24450	420	23810	640
PY83 (48)	394	25380	402	24875	(65)	394	25381	407	24570	811
PO16 (23)	429	23310	443	22573	(66)	466	21459	475	21053	406
(58)	486	20576	493	20284	-	-	-	-	-	-

Table 27

Pigment	$\lambda_{\text{max}}/\text{nm}$ (solid-state fluorescence)	$\lambda_{\text{max}}/\text{cm}^{-1}$ (solid-state fluorescence)	$\lambda_{\text{max}}/\text{nm}$ (solid-state absorption)	$\lambda_{\text{max}}/\text{cm}^{-1}$ (solid-state absorption)	$\Delta\lambda_{\text{max}}/\text{cm}^{-1}$	Pigment	$\lambda_{\text{max}}/\text{nm}$ (solid-state fluorescence)	$\lambda_{\text{max}}/\text{cm}^{-1}$ (solid-state fluorescence)	$\lambda_{\text{max}}/\text{nm}$ (solid-state absorption)	$\lambda_{\text{max}}/\text{cm}^{-1}$ (solid-state absorption)	$\Delta\lambda_{\text{max}}/\text{cm}^{-1}$
PY12 (42)	551	18149	411	24331	6182	(59)	605	16529	458	21834	5305
(43)	549	18215	440	22727	4512	(60)	607	16474	440	22727	6253
PY13 (44)	560	17857	416	24038	6181	(61)	605	16529	444	22523	5994
PY14 (45)	543	18416	436	22936	4520	(59)	596	16779	428	23364	6585
PY63 (46)	546	18315	415	24096	5781	(63)	600	16667	444	22523	5856
PY81 (47)	538	18587	386	25907	7320	(64)	548	18248	409	24450	6202
PY83 (48)	553	18083	394	25381	7298	(65)	570	17544	394	25381	7837
PO16 (23)	598	16722	429	23310	6588	(66)	594	16835	466	21459	4624
(58)	603	16584	486	20576	3992	-	-	-	-	-	-

Table 28

Pigment	$\lambda_{\text{max}}/\text{nm}$ (solution fluorescence)	$\lambda_{\text{max}}/\text{cm}^{-1}$ (solution fluorescence)	$\lambda_{\text{max}}/\text{nm}$ (solution absorption)	$\lambda_{\text{max}}/\text{cm}^{-1}$ (solution absorption)	$\Delta\lambda_{\text{max}}/\text{cm}^{-1}$	Pigment	$\lambda_{\text{max}}/\text{nm}$ (solution fluorescence)	$\lambda_{\text{max}}/\text{cm}^{-1}$ (solution fluorescence)	$\lambda_{\text{max}}/\text{nm}$ (solution absorption)	$\lambda_{\text{max}}/\text{cm}^{-1}$ (solution absorption)	$\Delta\lambda_{\text{max}}/\text{cm}^{-1}$
PY12 (42)	512	19531	419	23866	4335	(59)	552	18116	471	21231	3115
(43)	495	20202	446	22422	2220	(60)	542	18450	449	22272	3822
PY13 (44)	490	20408	428	23364	2956	(61)	543	18416	456	21930	3514
PY14 (45)	499	20040	444	22523	2483	(59)	514	19455	442	22624	3169
PY63 (46)	504	19841	426	23474	3633	(63)	540	18519	451	22173	3654
PY81 (47)	481	20790	394	25381	4591	(64)	512	19531	420	23810	4279
PY83 (48)	511	19569	402	24876	5307	(65)	507	19724	407	24570	4846
PO16 (23)	522	19157	443	22573	3416	(66)	524	19084	475	21053	1969
(58)	558	17921	493	20284	2363	--	--	--	--	--	--

Table 29

3.10 Particle Size Measurements

The particle sizes of the pigments were examined using transmission electron microscopy (see experimental for details). The areas were calculated by studying the photographs obtained from the microscopy. All the photographs obtained along with labels and scale bars are in the appendices section (see pages 173-189). The results are shown in the table below.

Pigment	Average Particle Area/ μm^2	Pigment	Average Particle Area/ μm^2
PY12 (42)	0.35	(59)	1.88
(43)	1.24	(60)	5.00
PY13 (44)	2.18	(61)	1.88
PY14 (45)	1.52	(62)	0.49
PY63 (46)	0.39	(63)	0.42
PY81 (47)	0.16	(64)	0.42
PY83 (48)	2.24	(65)	0.40
PO16 (23)	1.00	(66)	2.89
(58)	2.46		

Table 28

Of the pigments that did not show any solid-state fluorescence, the particle size seemed to have no bearing on its solid-state fluorescent properties. Of the pigments found to be fluorescent in the solid state, the pigments with the smaller particle size showed the greatest intensity of fluorescence. It would be logical to suggest that the greater the particle size, the greater the aggregation of particles. It has long been known that aggregation is a cause of fluorescence quenching.⁷⁴ With solution fluorescence, only dilute solutions fluoresce and the fluorescence intensity is increasingly quenched with increasing solution saturation. With increasing saturation comes increasing aggregation of the molecules in solution. The molecular stacking in such aggregated particles has been frequently cited as one of the most important reasons for fluorescence quenching.⁷⁴

3.11 Powder X-ray diffraction studies

It was hoped to gain information such as the distances between adjacent layers of molecules and side-by-side separation of molecules by looking at the dominant peaks in the powder XRD traces. By generating the calculated powder XRD pattern from single crystal data (where possible) and comparing it with the experimental pattern, it could be confirmed that the same crystal modification was being studied. Certain peaks have been indexed^{45,50} (using the calculated pattern from single crystal data) for the pigments whose structures were already known. Thus, the peaks corresponding to interplanar spacings could be identified and the interplanar distances calculated. The interplanar distances are calculated using the Bragg equation (page 117). Since there is no single crystal information for the novel compounds, these calculations cannot be carried out. The powder XRD patterns of the new compounds are so far removed from those of known structures, that comparisons between powder XRD patterns for common peaks was not possible.

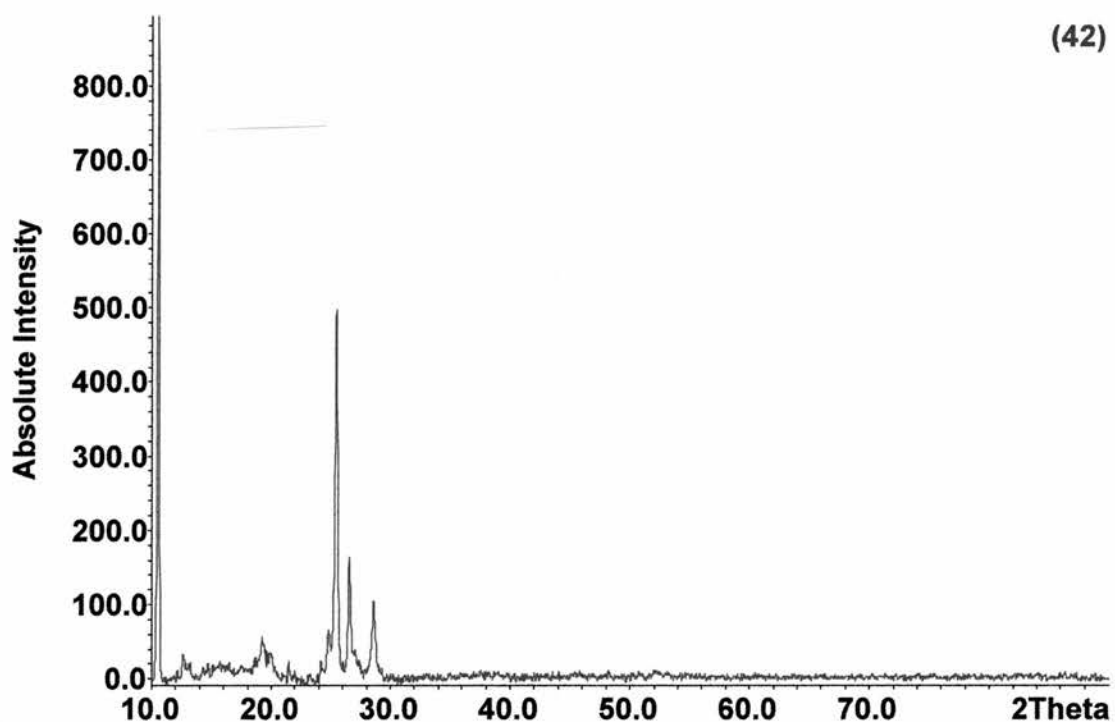
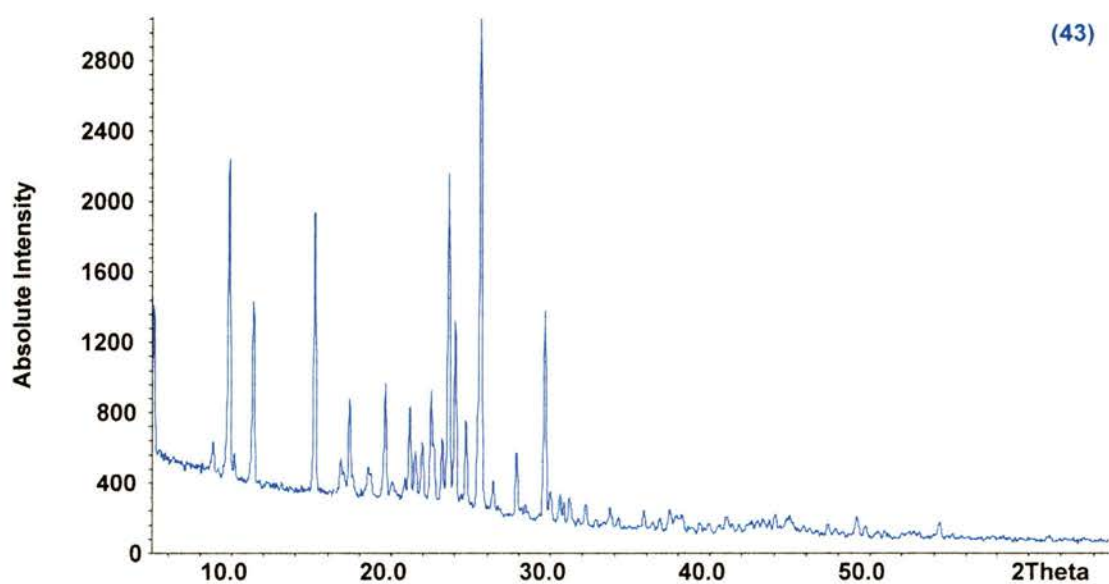


Figure 74 powder XRD diagram of PY12 (42)

d-spacing/Å	2θ/°	Relative Intensity	Absolute Intensity
8.41	10.52	100.00	974
4.60	19.27	5.44	53
3.50	25.44	52.42	511
3.36	26.54	17.90	174
3.13	28.53	11.54	112

Table 29 – powder XRD data for PY12 (42)



(43)

Figure 75 – powder XRD diagram for (43)

d-spacing /Å	2θ/°	Relative Intensity	Absolute Intensity	d-spacing /Å	2θ/°	Relative Intensity	Absolute Intensity
5.83	15.19	64.33	1946	4.05	21.92	20.57	622
5.27	16.82	17.57	532	3.95	22.48	30.32	917
5.10	17.36	28.87	873	3.77	23.59	73.44	2194
4.78	18.50	15.95	483	3.71	23.99	44.48	1329
4.52	19.62	31.60	956	3.61	24.66	25.33	757
4.43	20.05	12.97	392	3.48	25.58	100.00	2987
4.26	20.82	13.49	408	3.38	26.36	13.14	398
4.20	21.14	27.20	823	3.20	27.83	18.82	569
4.13	21.48	19.00	575	3.01	29.62	45.19	1337
4.05	21.92	20.57	622	2.92	30.56	10.12	306

Table 30 – powder XRD data for (43)

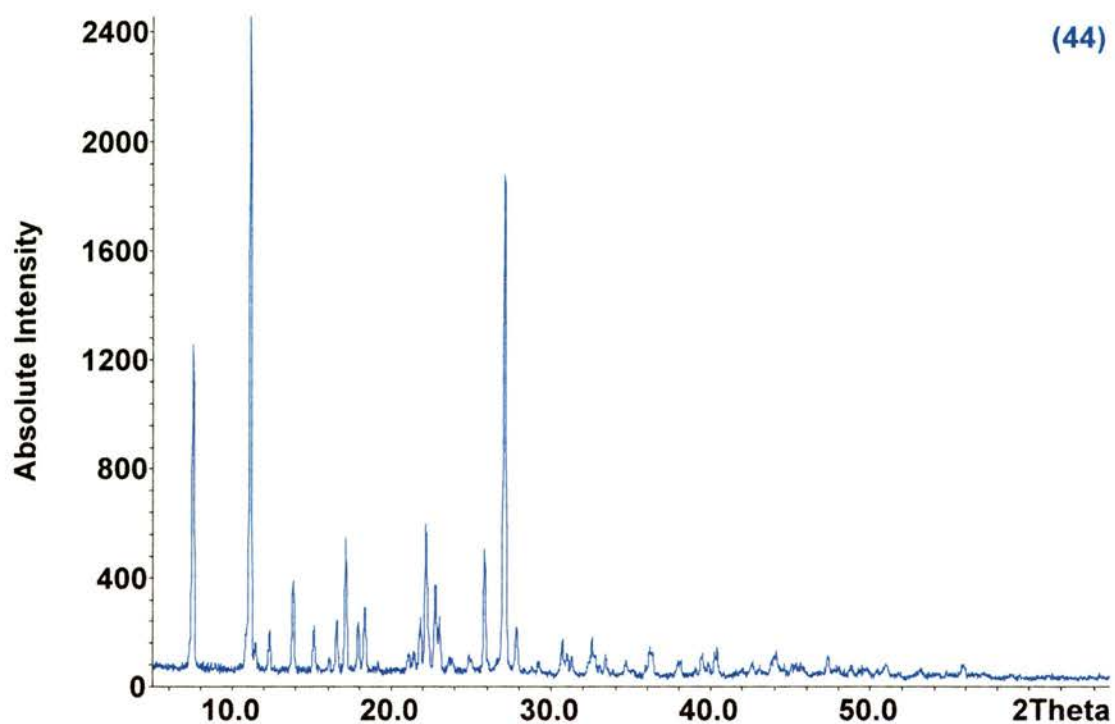


Figure 76 – powder XRD diagram for PY13 (44)

d-spacing/Å	2θ/°	Relative Intensity	Absolute Intensity
11.74	7.51	49.48	1091
7.96	11.11	100.00	2205
7.18	12.32	6.56	145
6.41	13.81	14.86	328
5.86	15.12	7.20	159
5.35	16.57	8.59	189
5.17	17.14	21.10	465
4.94	17.93	8.00	176
4.83	18.34	10.53	232
4.07	21.81	8.17	180
4.01	22.16	23.75	524
3.91	22.74	14.47	319
3.45	25.81	18.96	418
3.29	27.07	85.26	1880
3.21	27.81	7.64	168

Table 31 – powder XRD data for PY13 (44)

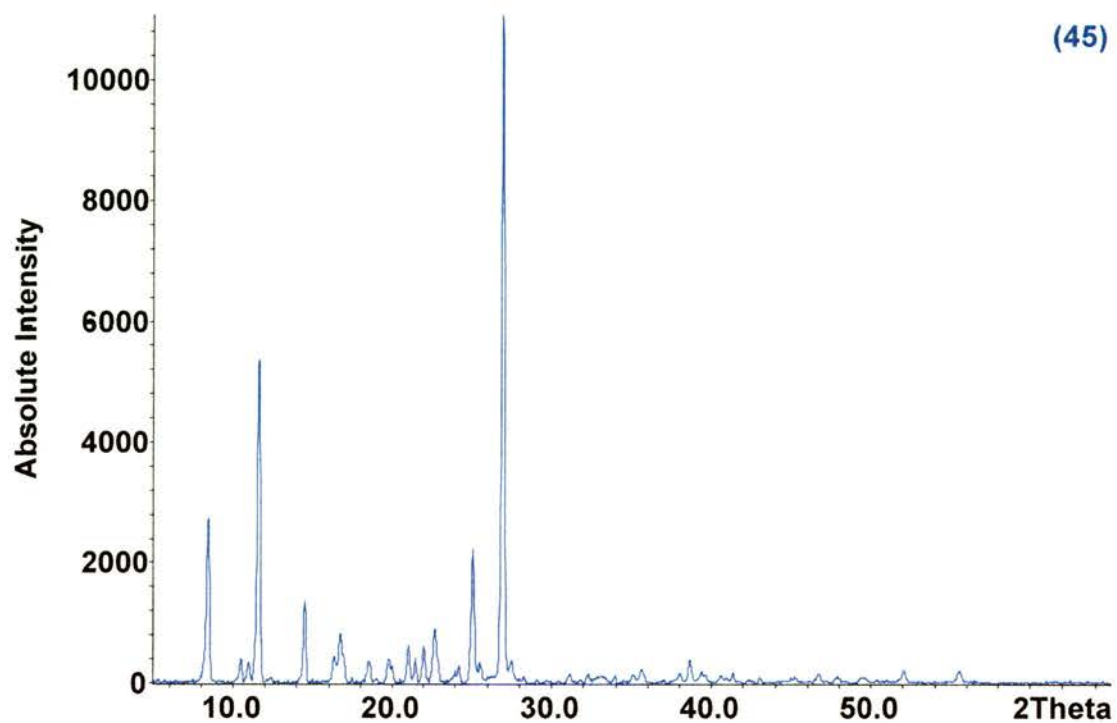


Figure 77 – powder XRD diagram for PY14 (45)

d-spacing/Å	$2\theta/^\circ$	Relative Intensity	Absolute Intensity
10.49	8.41	24.81	2735
7.64	11.58	48.36	5331
6.11	14.48	12.18	1342
5.30	16.73	7.23	797
4.22	21.02	5.61	618
4.13	21.46	3.74	413
4.04	21.99	5.47	603
3.92	22.67	7.95	876
3.55	25.06	20.12	2218
3.49	25.48	3.09	341
3.31	26.94	100.00	11024

Table 32 – powder XRD diagram for PY14 (45)

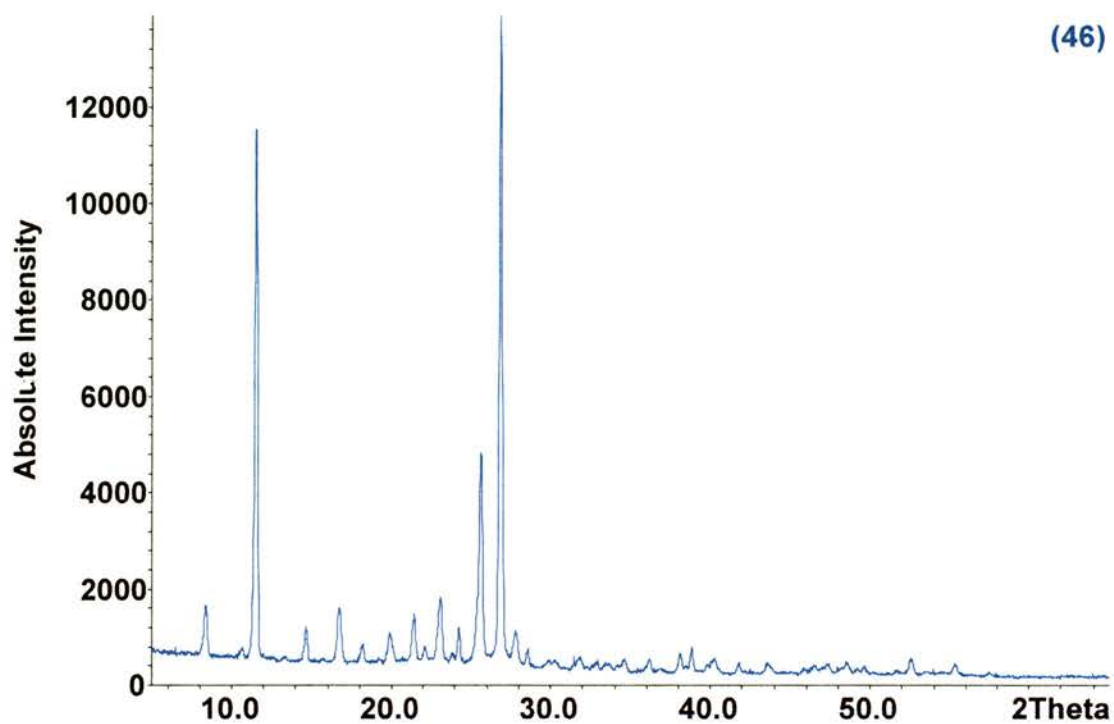


Figure 78 – powder XRD diagram for PY63 (46)

d-spacing/Å	2 θ /°	Relative Intensity	Absolute Intensity
8.45	10.46	9.41	1087
8.09	10.93	9.00	1039
7.63	11.57	52.32	6043
6.12	14.47	17.46	2016
5.42	16.35	8.92	1031
5.30	16.73	11.98	1384
4.78	18.54	8.27	955
4.48	19.80	8.08	933
4.42	21.02	10.07	1164
4.14	21.46	8.53	985
4.04	21.97	10.33	1193
3.92	22.67	12.32	1423
3.55	25.06	23.24	2685
3.31	26.93	100	11550

Table 33 – powder XRD data for PY63 (46)

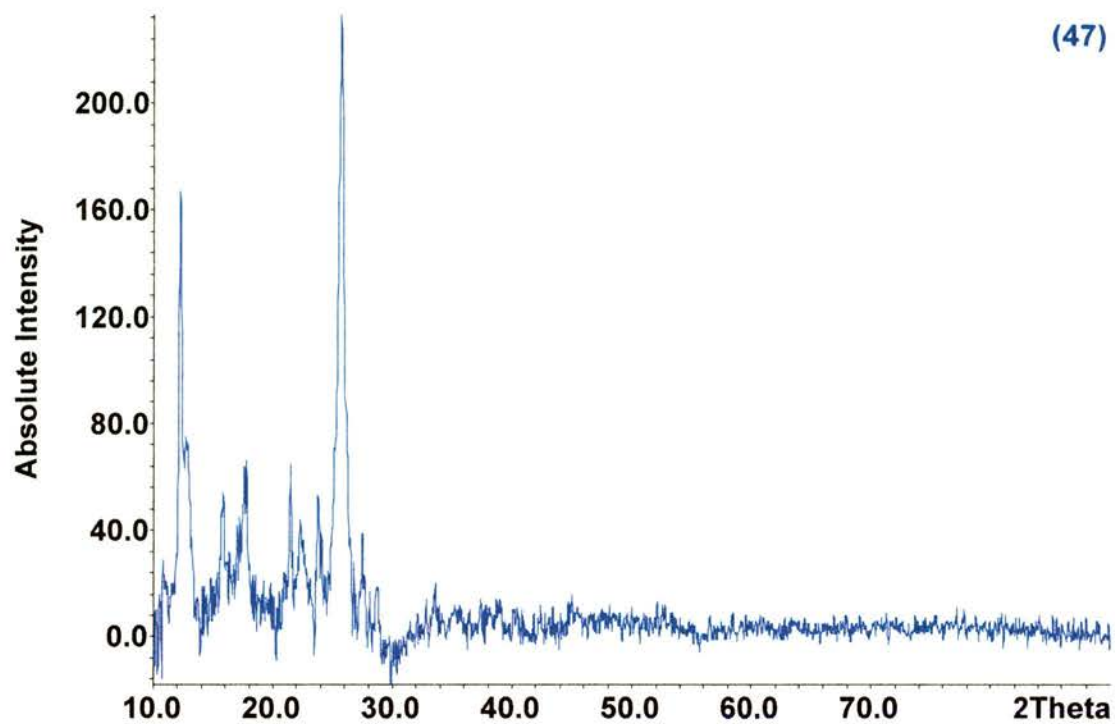


Figure 79 – powder XRD diagram for PY81 (47)

d-spacing/Å	$2\theta/^\circ$	Relative Intensity	Absolute Intensity
7.25	12.19	72.48	166
5.61	15.79	23.51	54
5.01	17.68	20.03	46
4.13	21.45	27.97	64
3.99	22.27	19.15	44
3.74	23.77	23.07	53
3.46	25.72	100.00	230

Table 34 – powder XRD data for PY81 (47)

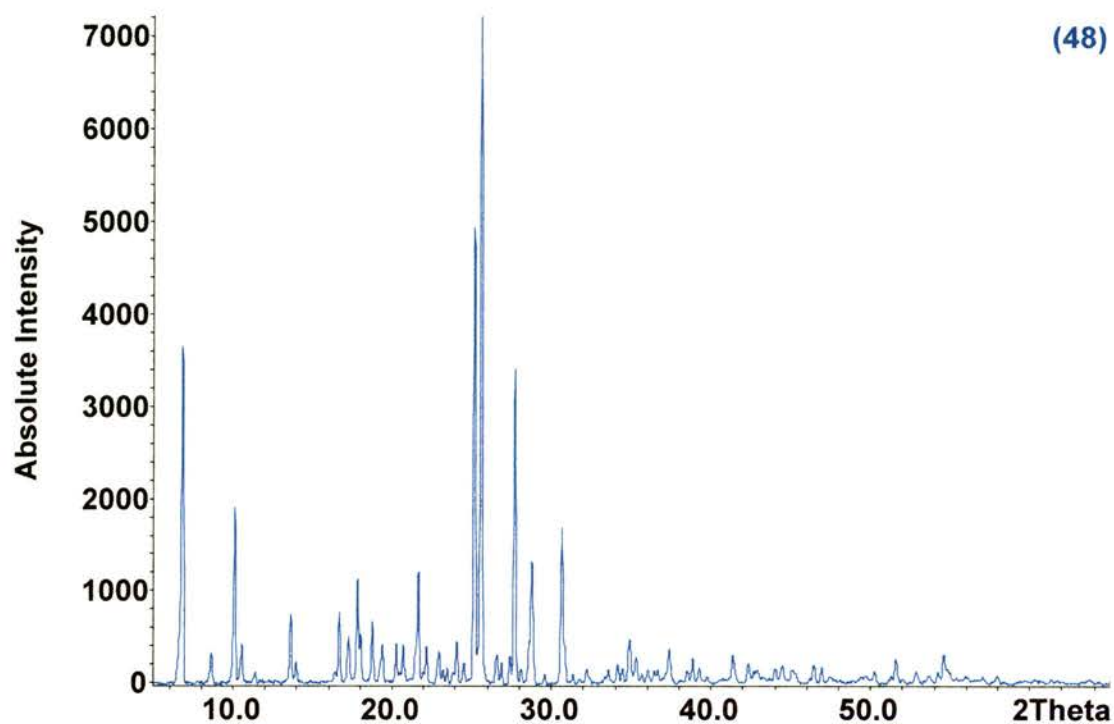


Figure 80 – powder XRD diagram for PY83 (48)

d-spacing/Å	2 θ /°	Relative Intensity	Absolute Intensity
13.00	6.80	50.19	3606
10.27	8.60	4.61	331
8.76	10.09	26.93	1913
8.39	10.53	5.88	423
6.50	13.61	10.43	749
5.31	16.69	10.79	775
5.13	17.26	6.98	502
4.97	17.83	15.63	1123
4.72	18.77	9.26	665
4.10	21.65	16.68	1198
3.53	25.16	68.41	4915
3.48	25.58	100.00	7185
3.22	27.69	47.84	3437
3.10	28.76	18.23	1309
2.92	30.64	23.45	1685

Table 35 - powder XRD data for PY83 (48)

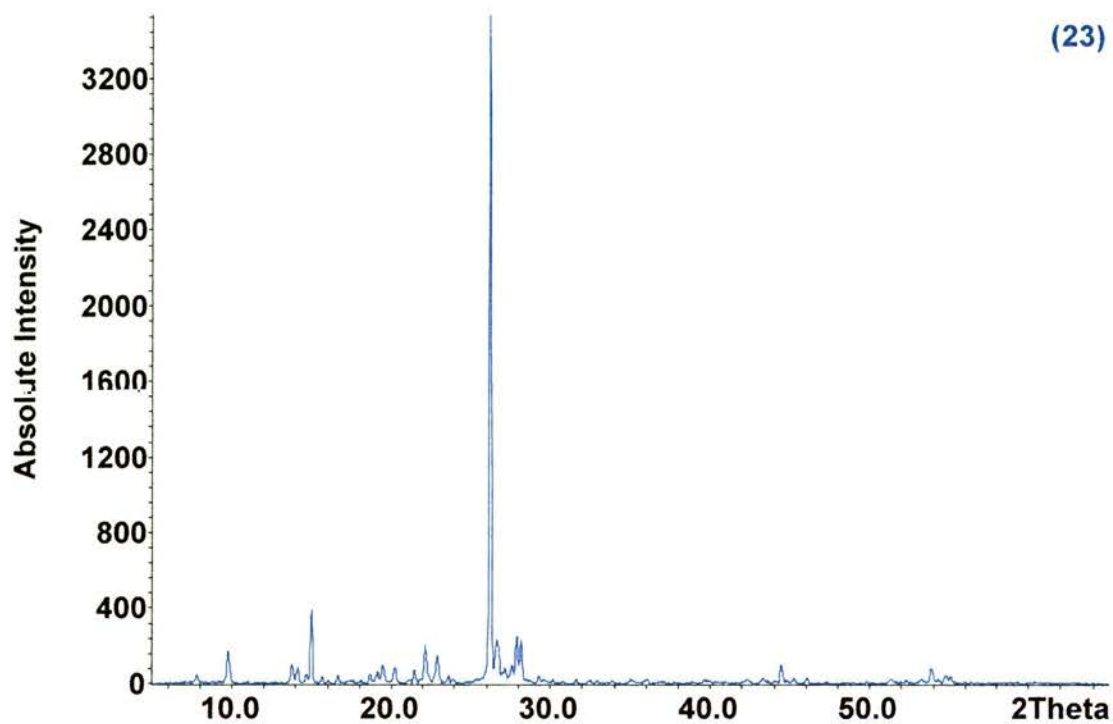


Figure 81 - powder XRD diagram for PO16 (23)

d-spacing/Å	$2\theta/^\circ$	Relative Intensity	Absolute Intensity
9.07	9.74	4.88	173
6.44	13.74	2.98	105
6.28	14.10	2.32	82
5.91	14.97	11.09	393
4.56	19.46	2.80	99
4.39	20.20	2.36	84
4.14	21.45	1.95	69
4.01	23.14	5.49	194
3.88	22.89	4.15	147
3.40	26.89	100.00	3543
3.34	26.63	6.55	232
3.20	27.88	6.99	248
3.17	28.15	6.50	230

Table 36 - powder XRD data for PO16 (23)

(58)

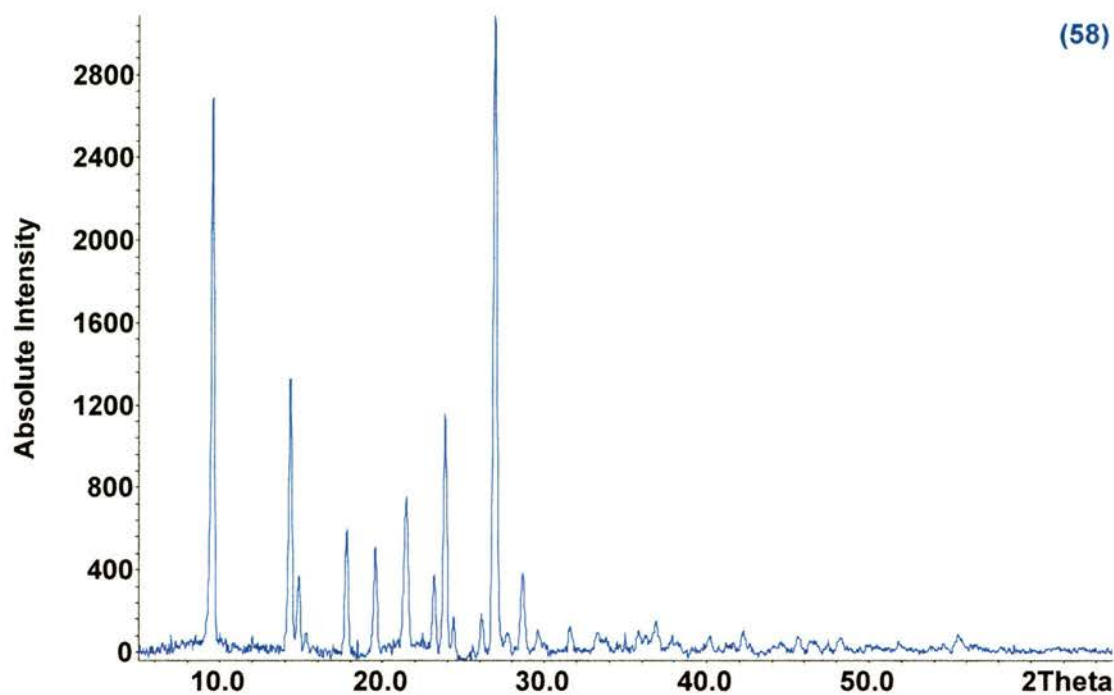


Figure 82 - powder XRD diagram for (58)

d-spacing/Å	$2\theta/^\circ$	Relative Intensity	Absolute Intensity
9.27	9.53	86.99	2685
6.18	14.31	43.40	1339
5.97	14.83	12.14	375
4.98	17.79	19.44	600
4.54	19.56	16.25	501
4.15	21.41	23.26	718
3.83	23.18	11.99	370
3.73	23.84	36.83	1137
3.65	24.37	5.59	173
3.41	26.08	5.94	183
3.31	26.92	100.00	3086
3.22	27.67	3.05	94
3.12	28.63	12.36	381

Table 37 - powder XRD data for (58)

(59)

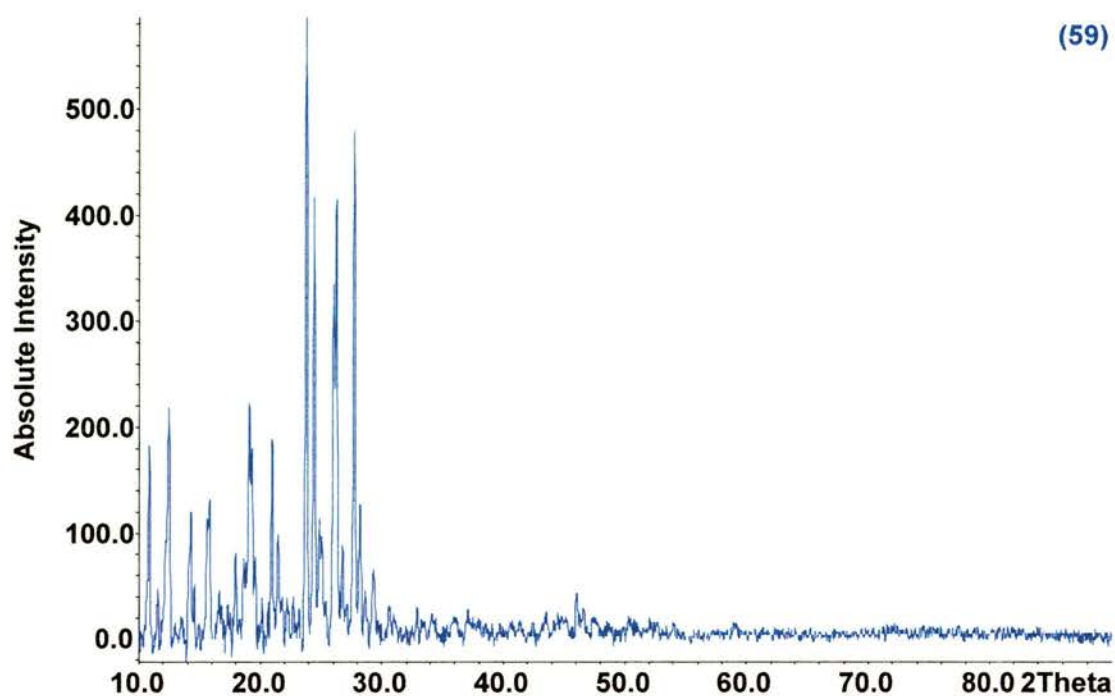


Figure 83 - powder XRD diagram for (59)

d-spacing/Å	2θ°	Relative Intensity	Absolute Intensity
8.17	10.82	31.53	184
7.12	12.42	37.35	218
6.22	14.24	20.67	120
5.63	15.74	21.26	124
4.94	17.95	13.89	81
4.65	19.08	38.09	222
4.24	20.96	32.20	188
4.14	21.45	17.15	100
3.74	23.78	100.00	582
3.64	24.42	71.23	415
3.58	24.87	19.53	114
3.42	26.03	57.41	334
3.39	26.23	70.71	412
3.33	26.77	15.31	89
3.21	27.74	81.65	476
3.16	28.22	21.63	126

Table 38 - powder XRD data for (59)

(60)

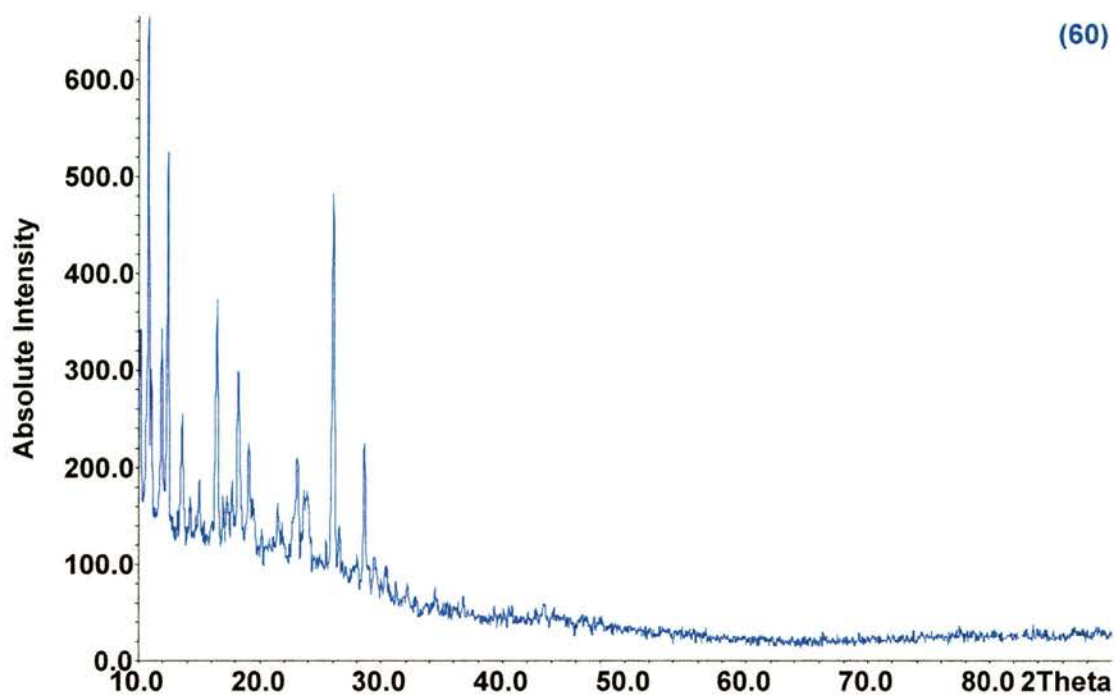


Figure 84 - powder XRD diagram for (60)

d-spacing/Å	$2\theta/^\circ$	Relative Intensity	Absolute Intensity
8.72	10.13	51.59	341
8.20	10.78	100.00	661
7.45	11.88	51.80	342
7.14	12.38	78.72	520
6.53	13.55	36.94	244
5.91	14.98	26.95	178
5.39	16.42	54.19	358
4.87	18.20	45.23	299
4.65	19.06	34.09	225
4.14	21.45	24.44	162
3.85	23.08	31.87	211
3.42	26.05	71.56	473
3.12	28.61	33.95	224

Table 39 - powder XRD data for (60)

(61)

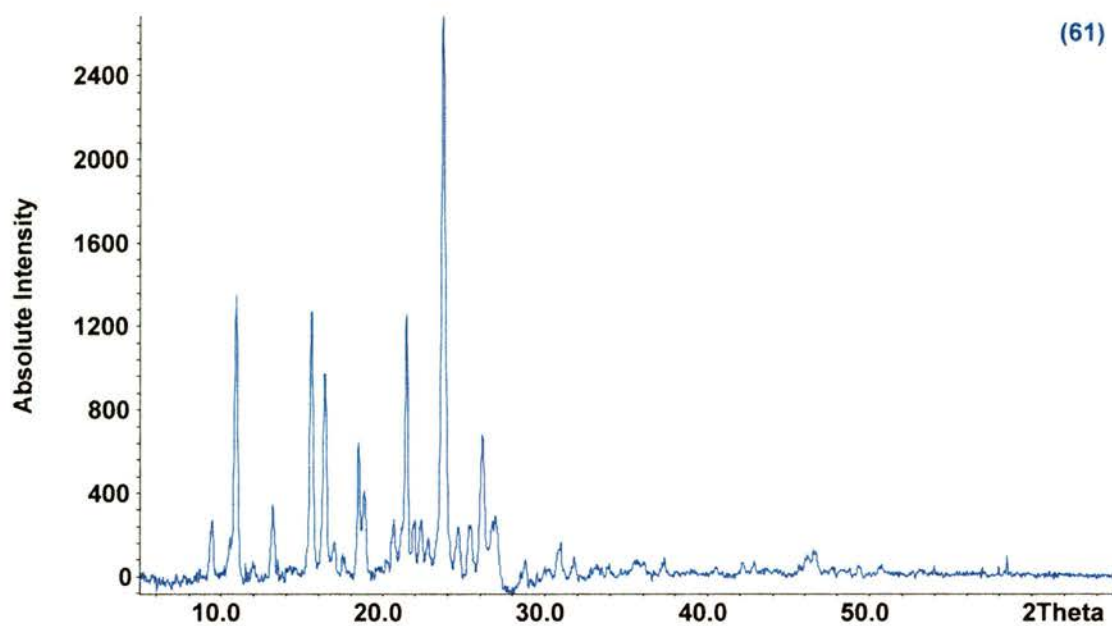


Figure 85 - powder XRD diagram for (61)

d-spacing/Å	2θ/°	Relative Intensity	Absolute Intensity
8.11	10.90	50.28	1341
6.73	13.14	13.26	354
5.69	15.57	48.02	1280
5.40	16.39	5.31	141
5.22	16.96	6.23	166
5.05	17.56	3.75	100
4.80	18.48	24.63	657
4.30	20.64	8.89	237
4.14	21.44	47.17	1257
3.97	22.37	9.64	257
3.75	23.73	100.00	2666
3.61	24.63	8.03	214
3.51	25.37	8.18	218
3.41	26.12	25.97	692
3.34	26.69	8.33	222
3.30	26.96	10.73	286
2.90	30.86	5.74	153
2.89	30.92	5.03	134

Table 40 - powder XRD data for (61)

(62)

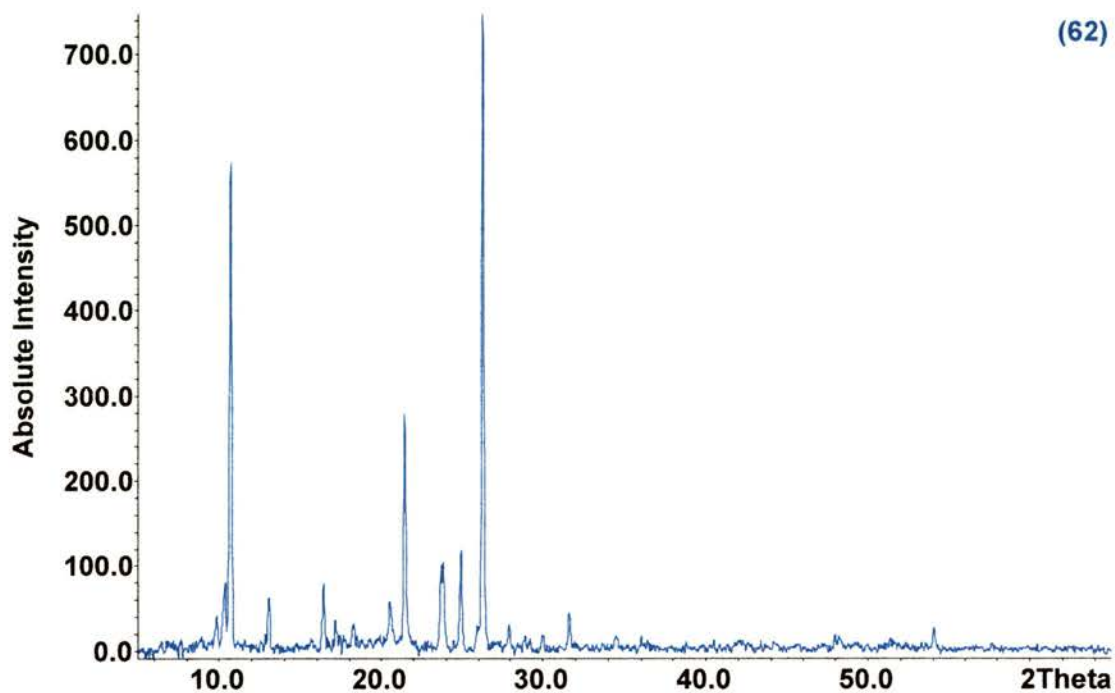


Figure 86 - powder XRD diagram for (62)

d-spacing/Å	2θ/°	Relative Intensity	Absolute Intensity
8.56	10.32	10.31	77
8.26	10.68	76.37	570
6.78	13.02	8.68	65
5.40	16.40	10.48	78
4.33	20.49	7.77	58
4.15	21.42	37.10	277
3.74	23.80	13.91	104
3.57	24.91	15.56	116
3.39	26.24	100.00	746
3.20	27.89	4.15	31

Table 41 - powder XRD data for (62)

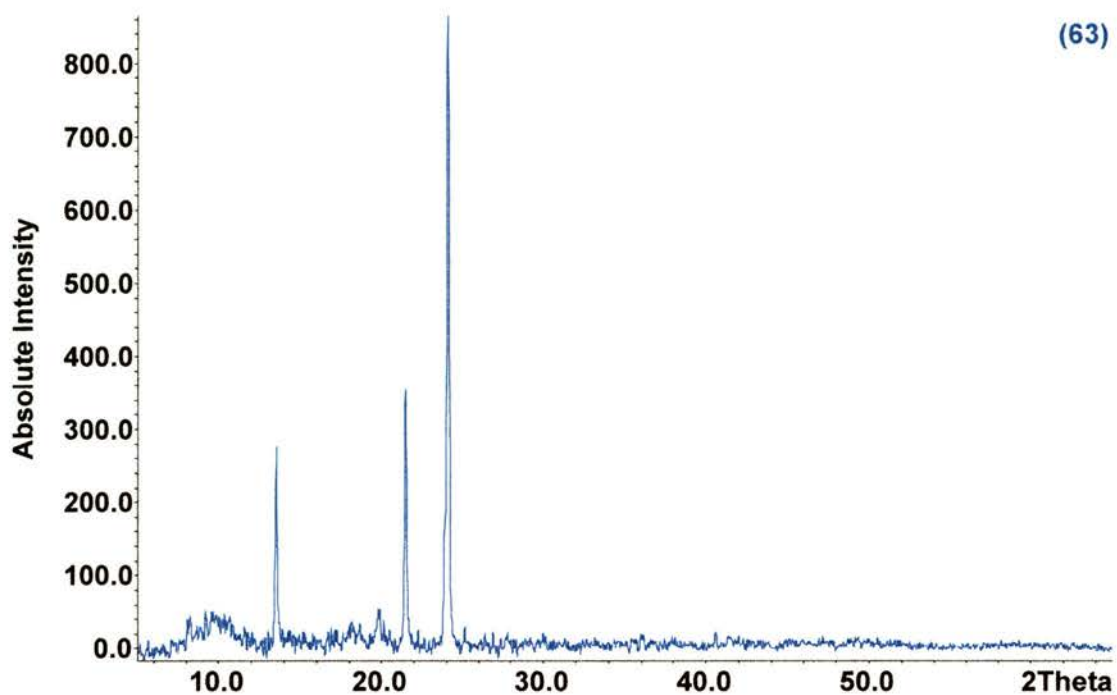


Figure 87 - powder XRD diagram for (63)

d-spacing/Å	2θ°	Relative Intensity	Absolute Intensity
6.55	13.52	34.72	302
4.14	21.44	41.20	359
3.69	24.07	100.00	871

Table 42 - powder XRD data for (63)

(64)

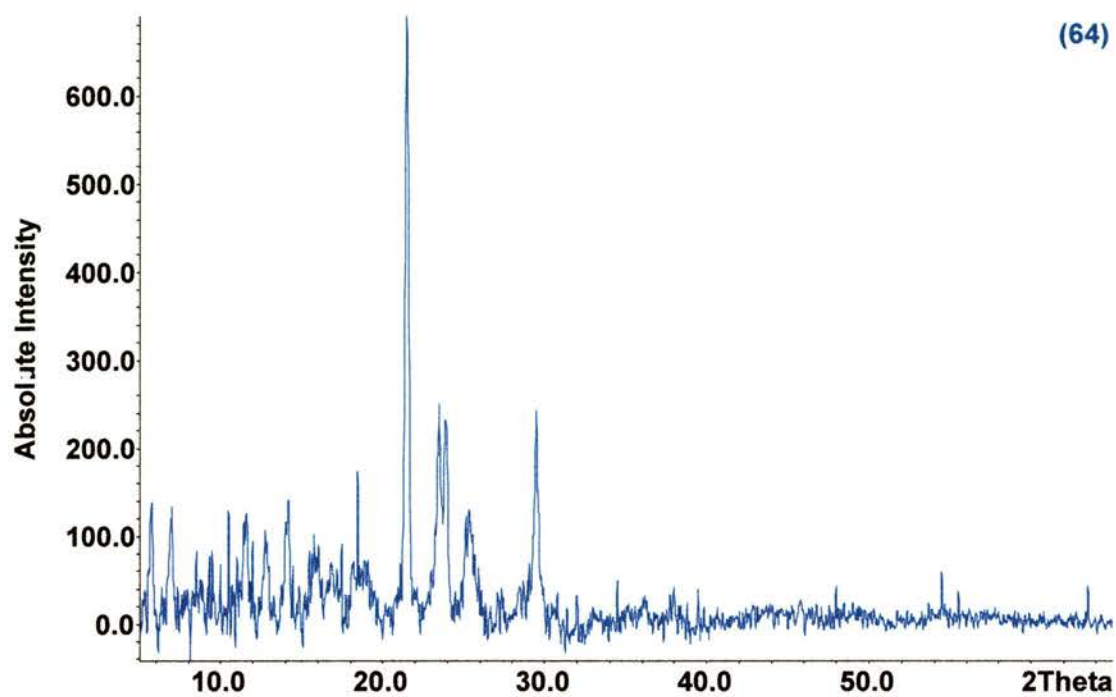


Figure 88 - powder XRD diagram for (64)

d-spacing/Å	$2\theta/^\circ$	Relative Intensity	Absolute Intensity
15.52	5.69	19.60	132
12.67	6.97	19.87	134
8.44	10.47	18.97	128
7.64	11.57	18.53	125
6.96	12.70	13.94	94
6.26	14.15	19.51	132
4.81	18.46	25.17	170
4.13	21.48	100.00	674
3.79	23.46	36.45	246
3.73	23.86	34.50	233
3.52	25.31	19.27	130
3.03	29.46	35.21	238

Table 43 - powder XRD data for (64)

(65)

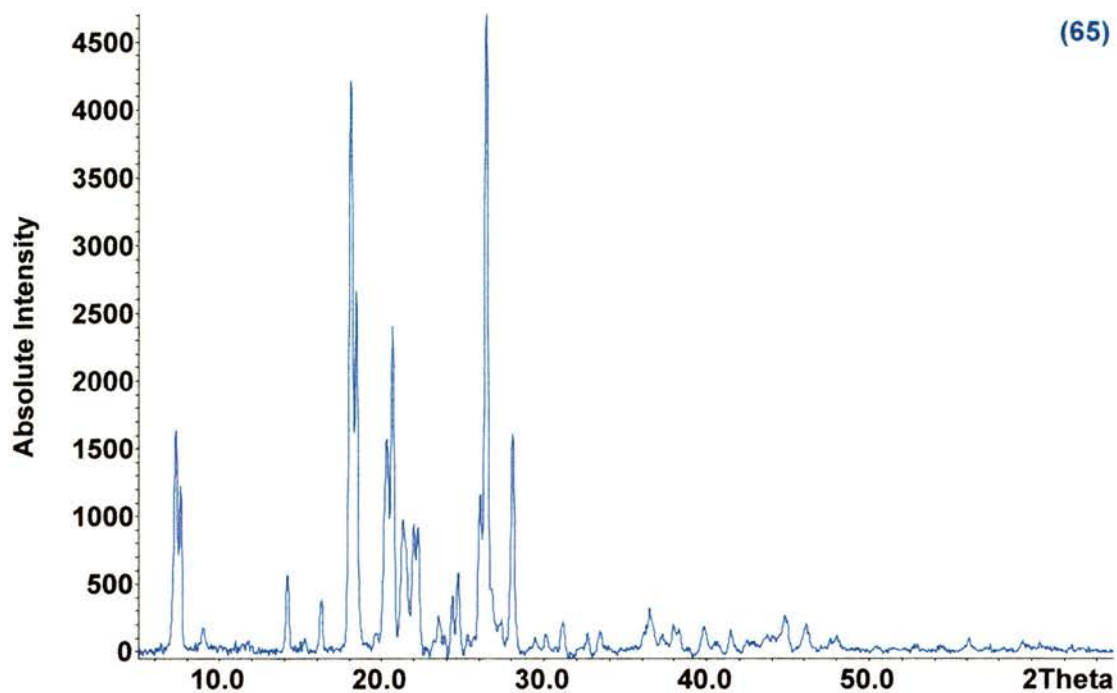


Figure 89 - powder XRD diagram for (65)

d-spacing/Å	2θ/°	Relative Intensity	Absolute Intensity
12.16	7.26	34.52	1622
11.68	7.56	26.03	1223
6.24	14.17	12.01	564
5.44	16.27	8.13	382
4.89	18.12	89.20	4192
4.37	20.31	33.23	1562
4.30	20.65	51.15	2404
4.17	21.31	20.67	971
4.04	21.98	20.13	946
3.78	23.49	5.75	270
3.65	24.36	8.71	409
3.60	24.71	12.33	579
3.42	26.05	24.59	1155
3.37	26.41	100.00	4699
3.18	28.04	34.41	1617

Table 44 - powder XRD data for (65)

(66)

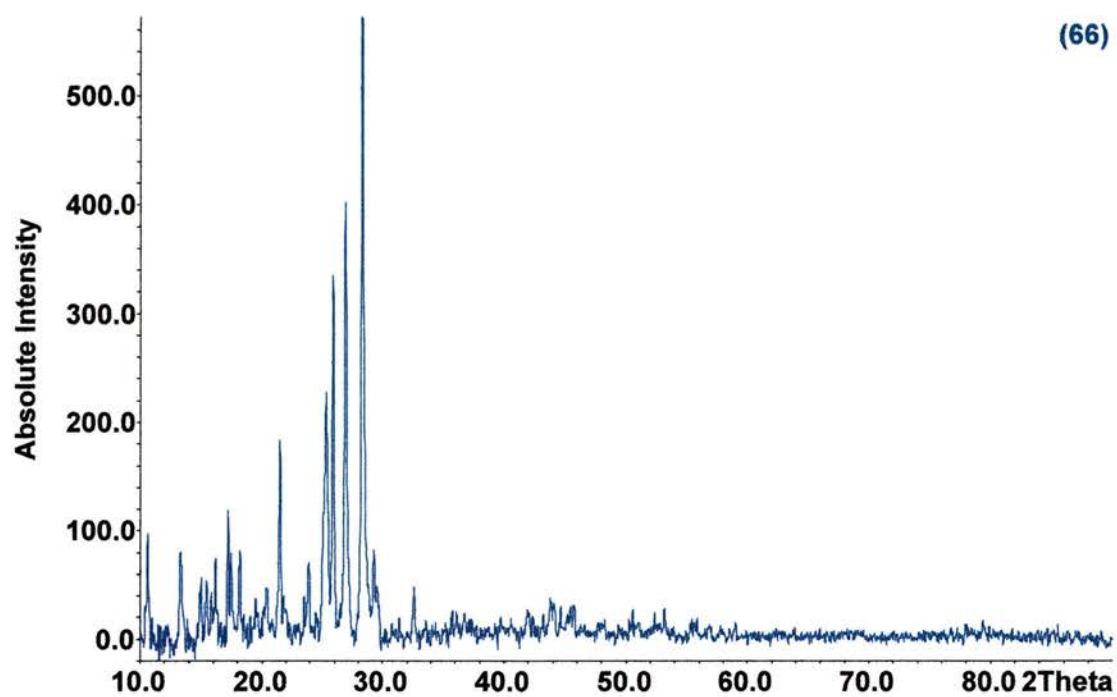


Figure 90 - powder XRD diagram for (66)

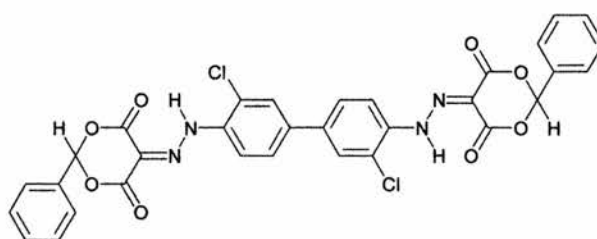
d-spacing/Å	2θ/°	Relative Intensity	Absolute Intensity
8.34	10.60	16.84	97
6.66	13.29	14.19	82
5.90	15.00	9.91	57
5.75	15.40	9.04	52
5.49	16.14	12.99	75
5.16	17.18	20.65	119
4.88	18.16	13.73	79
4.13	21.48	31.62	182
3.72	23.87	12.54	72
3.52	25.31	38.98	224
3.44	25.88	57.66	332
3.31	26.91	68.76	396
3.15	28.31	100.00	575
3.05	29.26	14.15	81
2.75	32.57	8.34	48

Table 45 - powder XRD data for (66)

From the powder XRD data obtained, there seems to be no correlation between the complexity of the powder XRD diagram and the complexity of the crystal packing within the lattice. This is clear by looking at the powder XRD patterns and the single crystal data of PY12 (42), PY13 (44), PY14 (45), PY63 (46) PY83 (48) and (43) e.g. the powder XRD pattern of PY13 (44) is quite complex whereas the crystal packing in PY13 (44) appears to be quite simple. Also, no correlation appeared between the *o*-dianisidine based and the *o*-dichlorobenzidine based pigments e.g. the *o*-dianisidine of PY13 (44), compound number (63), had a very simple powder XRD pattern whereas PY13 (44) is complex.

3.12 Conclusions

Several novel yellow, orange and red diarylide fluorescent azo pigments have been synthesised from *o*-dianisidine and 2,2'-dichlorobenzidine with coupling components based on a cyclic 1,3-diketone or 1,3-diester skeleton which may have applications in security printing, special effect printing and organic electroluminescent devices (page 30). The fluorescence and absorption properties of these pigments in solution and the solid state have been studied and compared with those of several known commercial diarylide pigments. The novel diarylide pigments show varying levels of fluorescence in the solid state and solution, the most intense being exhibited by pigment (65).



(65)

From the crystal data examined for known commercial pigments it appeared the pigments with the greater interplanar distances between the molecules had the greater fluorescence. The non or very weakly fluorescing pigments appeared to have smaller distances between the molecules.

Particle size measurements have also been studied using transmission electron microscopy. It has been shown that for those pigments that exhibited solid-state fluorescence, smaller particle sizes resulted in a greater fluorescence intensity (assuming the pigments were fluorescent in the first instance).

Monoazo analogues of the diarylide pigments have been synthesised, characterised and studied by single crystal X-ray diffraction; other monoazo analogues where the crystal structures were already known have also been studied. It is found that correlations between the mono and the corresponding bis-azo (diarylide) pigments have to be treated cautiously. Trends such as bond lengths and through-space interatomic distances are reasonably consistent, but comparisons of torsion angles and crystal packing are not necessarily meaningful.

3.12.1 Crystal Structure and Packing and Effect on Solid-State Fluorescence

From the single crystal data examined, it is clear that intramolecular hydrogen bonding has no obvious effect on fluorescence. For the pigments with solved crystal structures, all had intramolecular hydrogen bonding. Some of these pigments were fluorescent, whilst others were not. Pigments that were both planar and non-planar were found to be fluorescent. From the pigments with known structures, some have been shown to be planar and others twisted but this seemed to have no bearing on whether the pigments were fluorescent or not. The synthetic analogues, some of which could not be planar (page 36), were also found to be fluorescent. Also, the actual packing of the pigment molecules did not seem to affect whether or not the pigments were fluorescent. Similar packing arrangements are observed in pigments that are both fluorescent and non-fluorescent. Fluorescence seems to be favoured in pigments where the intermolecular distances between pigment molecules within the crystal lattice are greater. The important factor seemed to be the distances between the molecules within the lattice. The greater the distances, the less chance of intermolecular interactions. Electronic excitations can be coupled to lattice vibrations and afford a route to vibrational deactivation via internal conversion if the molecules

in the lattice are close enough. If two excited electronic states are close enough together in energy terms and their vibrational levels overlap, then the excited electron can cross over to the lower energy excited state (internal conversion IC section 1.13 pages 13-14). The molecule again loses energy by vibrational deactivation and so on until it gets back to the ground state.

Some useful information was gained from the powder XRD patterns of the pigments but these must be treated with caution. It was possible to index certain peaks in some cases where single crystal data were already available about the pigment in question. For the pigments without solved single crystal structures this was not possible. For the simple powder patterns with few peaks (e.g. figure 23) it can be confidently stated that the shortest interplanar distance within the lattice is 3.69Å. For the more complex patterns things are not so clear-cut.

3.12.2 Particle Size and Effect on Fluorescence

It has been shown that particle size has a big effect on fluorescence intensity. It has already been shown that increased aggregation of particles leads to greater particle size, which in turn leads to quenching of fluorescence.⁷⁴ During purification, particle size is very difficult to control due to the inherent insolubility of the pigments which leads to varying particle sizes across the board so growing specific particle sizes was very difficult. Using the raw pigments which are likely to have greater particle sizes was not a viable option due to the likely impurities present in the pigments. It has been shown in the past via differential scanning calorimetry (DSC)^{45,50} that there are around 5-10% impurities (generally unreacted coupling component) present in the raw pigment.

3.12.3 Absorption and Fluorescence Measurements

It is clear from the absorption measurements that there are no significant intermolecular interactions in the solid state (page 82). A large majority of the pigments studied are both fluorescent in the solid state and solution. It is possible that

the emissive state in the solid is different from that in solution (page 82) as the Stokes shift between solid-state fluorescence and absorption are greater than in solution which is surprising (page 82). One way to determine this would be to perform time resolved fluorescence studies (measuring and determining lifetimes of the excited state in solution and solid state and measuring the decay kinetics). These studies are far from trivial for solid state work.

3.13 Further Work

Further study of synthetic analogues to increase the colour range of the novel fluorescent synthetic pigments will be something that needs to be investigated. Using different substituents such as Meldrum's acid and 1,3-cyclohexanedione derivatives to see what effect this has on the colour range and the fluorescence will be the main avenue for this.

Crystal structure determination of all the novel pigments in addition to some known commercial fluorescent pigments is a crucial next step in this work to give a more rounded picture of the intermolecular interactions in the fluorescent pigments. This will prove to be very challenging due to the inherent insolubility of these compounds. Use of various solvents and crystallisation techniques should be investigated to ensure the best crystals possible can be obtained. Further use of synchrotron sources (e.g. Daresbury) for structure solution where the single crystals are too small or diffract too weakly for conventional X-ray sources should be looked into. Where this proves difficult perhaps structure solution by powder diffraction could be looked into. There have been recent reports in the literature⁷⁵ of structures being elucidated from powder data. This is another avenue that could be explored for structure determination.

Measuring the overall particle size distribution of the pigments instead will give an accurate and representative picture when combined with electron microscopy. This is

something that needs to be investigated by using photon correlation spectroscopy⁷⁶ (PCS) (also known as dynamic light scattering).

More in depth fluorescence studies (both solution and solid state) e.g. variable temperature fluorescence and time resolved fluorescent studies (both solution and solid-state to measure the decay lifetimes and study the decay kinetics) will be needed to give an insight into the properties of the emission states in solution and the solid state

4.0 Experimental

4.1 General

Melting points were determined on an Electrothermal model 9100 apparatus and are uncorrected.

NMR spectra were recorded at 200MHz for ^1H NMR and 50.3 MHz for ^{13}C spectra on a Varian Gemini NMR spectrometer, or on a Bruker AM-300 NMR spectrometer (^1H at 300MHz and ^{13}C at 75.4MHz). All coupling constants are expressed in Hertz (Hz). Chemical shifts were determined using $\text{Si}(\text{CH}_3)_4$ ($\delta_{\text{H}} = 0$) as internal standard relative to the residual solvent peak (CHCl_3 : δ 7.26. DMSO-d_6 : δ 2.5). ^{13}C NMR spectra were also recorded on a Varian Gemini NMR spectrometer or a Bruker 300MHz NMR spectrometer. Chemical shifts were determined relative to the residual solvent peak (CDCl_3 : δ 77.0; DMSO-d_6 : δ 40.6). Abbreviations for NMR results are: singlet (s), broad singlet (br s), doublet (d), multiplet (m). Organic extracts were dried over anhydrous magnesium sulfate and solvent was removed using a rotary evaporator. Samples of PY12 (**42**), PY13 (**43**), PY14 (**44**), PY63 (**45**), PY83 (**48**), PO16 (**23**) and 3,3'-dichlorobiphenyl-4,4'-bis (diazonium chloride) solution were provided by Ciba Speciality Chemicals and the pigments were purified by recrystallisation. The 3,3'-dichlorobiphenyl-4,4'-bis (diazonium chloride) solution was used as received. Dimedone, cyclohexane-1,3-dione and 5-phenylcyclohexane-1,3-dione were commercial samples and were used without further purification. Commercially available solvents were used without further purification unless stated otherwise. The term "petrol" refers to the fraction of petroleum ether which boils between 40 and 60°C.

Elemental analyses for carbon, hydrogen and nitrogen were carried out using a Carbo-Erba 1106 elemental analyser.

Electron microscopy was carried out on a Philips EM300 transmission electron microscope at the laboratory of Ciba Speciality Chemicals, Paisley. The accelerating

voltage used was 300kV. The samples were prepared by suspending the powders in ethanol and subjecting them to high frequency sound (ultrasound) for 1 minute. A small amount of the resulting suspension was transferred to a carbon coated grid to give a uniform layer. Instrumental magnification was 12,000 and photographic enlargement $\times 5$, giving a total magnification of 60,000.

Powder XRD data were recorded on a Stoe STADI/P transmission-geometry diffractometer using monochromated Cu-K α_1 radiation ($\lambda = 1.5406\text{\AA}$)

Fluorescence measurements were performed on a Perkin Elmer LS 55 Fluorimeter/Phosphorimeter. The slit width was set at 10nm. The excitation source was set at 400nm.

Absorption measurements were performed on a Perkin Elmer Lambda 20 UV/Visible spectrophotometer or a Philips PU-8730 UV/Visible spectrophotometer. The slit width was set at 10nm. Molar absorption coefficients (ϵ) are expressed in $\text{mol}^{-1}\text{dm}^3\text{cm}^{-1}$.

4.11 X-ray Diffraction

Bragg's law refers to the equation below (equation 1).

This law was derived to explain why the cleavage faces of crystals reflect X-ray beams at certain angles of incidence (θ). The distance between atomic layers in a crystal is represented by (d). The variable (λ) refers to the wavelength of the incident X-ray beam and n is an integer.⁷⁷

$$n\lambda = 2d \sin \theta \quad \text{Equation 1}$$

This law also predicts whether the interference between two diffracted beams of incident angle (λ) will be destructive / constructive.

Bragg's Law can easily be derived by considering the conditions necessary to make the phases of the beams coincide when the angle of incidence equals the angle of

reflection. The rays of the incident beam are always in phase and parallel up to the point at which the top beam strikes the top layer at atom z (figure 91). The second beam continues to the next layer where it is scattered by atom B . The second beam must travel the extra distance $AB + BC$ if the two beams are to continue travelling adjacent and parallel. This extra distance must be an integral (n) multiple of the wavelength (λ) for the phases of the two beams to be the same:

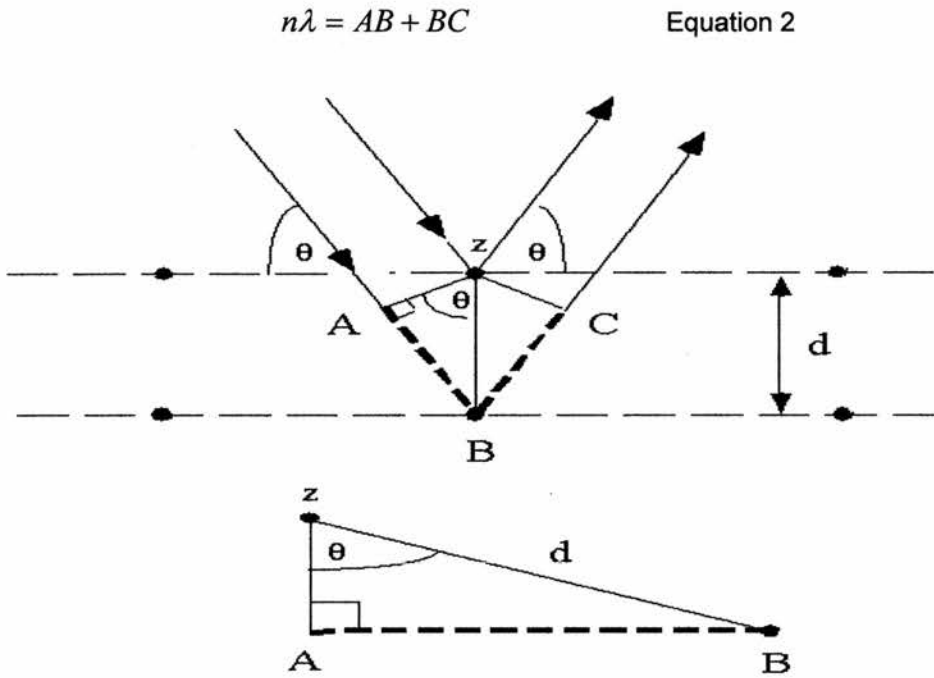


Figure 91

Recognizing d as the hypotenuse of the right triangle ABz , trigonometry can be used to relate d to the distance $(AB + BC)$. The distance AB is opposite θ so :

$$AB = d \sin \theta \quad \text{Equation 3}$$

Because $AB = BC$ equation 2 becomes :

$$n\lambda = 2AB \quad \text{Equation 4}$$

Substituting equation 3 into equation 4 gives:

$$n\lambda = 2d \sin \theta \quad \text{Equation 1}$$

Therefore Bragg's Law has been derived. The location of the surface does not change the derivation of Bragg's Law.

X-rays are scattered by electrons surrounding the atomic nuclei. The degree of scattering which occurs is termed the scattering factor and is influenced by the number of electrons surrounding the nuclei. Therefore, it increases with increasing atomic number. Reflections are represented by what are known as Miller indices (hkl) which are comprised of three numbers h , k and l that describe how the atom planes intersect with unit cell axes.

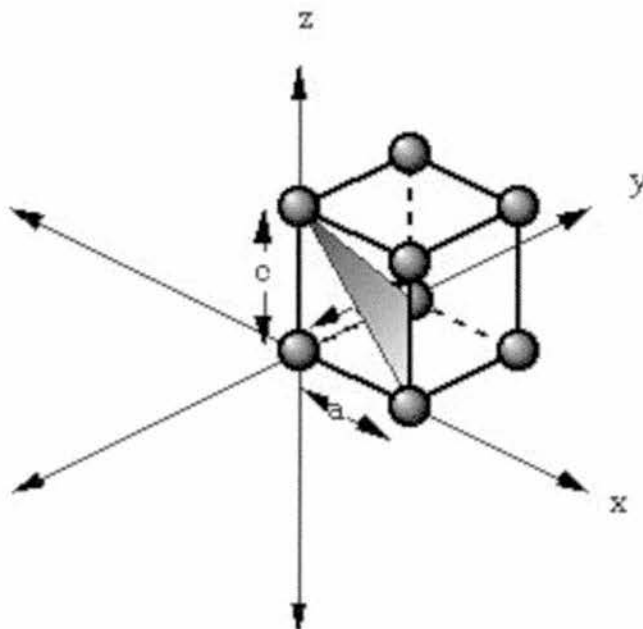


Figure 92 - example of the (111) Miller Planeⁱ

There is clearly a connection between interference patterns and crystal lattice structure. Unfortunately, one cannot deduce a lattice structure directly from this data. An approximate estimate of the structure is needed which is then refined against the X-ray data. This is achieved by using a technique known as least squares refinement⁷⁸ which involves comparing calculated and observed patterns.

X-ray intensities observed in diffraction patterns are affected by many factors. The so called "structure factor" $[F(hkl)]$ is the one that is directly related to the crystal structure and is described in terms of a single unit cell by equation 5.

ⁱ Diagram by David R. Jessey, Geosciences Dept, Cal Poly (1998)

$$F(hkl) = \sum_{j=1}^N f_j 2\pi i (hx_j + ky_j + lz_j) \quad \text{Equation 5}$$

The position of the j^{th} atom, possessing a scattering factor of f_j , is given by the coordinates (x_j , y_j and z_j) and is part of a structure with N atoms. Structure factors represent diffracted beams which have the wave properties of amplitude [$F(hkl)$] and relative phase $\Phi(hkl)$. Essentially a structure factor is a complete description of each reflection (its position, intensity and phase).

Unfortunately, the phase of the reflections cannot be determined from the diffraction pattern which is the reason why structures cannot be directly elucidated from diffraction patterns. This is referred to as the “phase problem”.

Today a technique known as “direct methods” is employed to obtain starting models for structures of a certain type.

Direct methods use the fact that the amplitude and phase of a structure factor are related by electron density. Electron density is related to both the amplitude and phase of structure factors. Therefore if one parameter is known the other can be predicted (e.g. the phase can be predicted from the amplitude). Several assumptions are necessary with regard to the electron density of the structure, namely that atoms are treated as discrete areas of electron density. This assumption rids atomic shape effects from the observed structure factors. Secondly, electron density is always positive. This removes the need to look at phases which give negative $\rho(x)$ values for given x values. Thirdly, it is assumed that $\int \rho^3(x) dV = \max$ and this applies across the entire unit cell volume and discriminates against negative electron density whilst encouraging the formation of positive peaks. This also leads directly to the probability relationships among phases and the tangent formula, which forms the basis of direct methods. Finally, all atoms are assumed to be equal which allows there to be direct relationships between structure factors. Direct methods are very useful for solving small molecule structures. Unfortunately, the statistical relationships become weaker as the number of atoms increases, and direct methods are limited to structures with, at most, a few hundred atoms in the unit cell. Also,

because of the assumption that all atoms are equal direct methods are not suited to solving structures containing heavy atoms. Structures with heavy atoms may be solved by Patterson methods.²¹ Patterson methods give a map of the vectors between atoms. So, if there is a peak of electron density for atom 1 at position \mathbf{x}_1 and a peak of electron density for atom 2 at position \mathbf{x}_2 , then the Patterson map will have peaks at positions given by $(\mathbf{x}_2 - \mathbf{x}_1)$ and $(\mathbf{x}_1 - \mathbf{x}_2)$. The height of the peak in the Patterson map is proportional to the product of the heights of the two peaks in the electron density map.

The vast majority of phase information is determined and refined to give the electron density map and figures of merit. It is from this that the most appropriate structure may be selected.

To find physical parameters such bond lengths, angles and atom types from electron density maps derived from direct methods requires structure refinement. The refinement technique used is known as least squares refinement which involves comparing experimental and calculated patterns.

Least squares refinement is a statistical technique that is used for the solution of simultaneous equations. Its most simple form is the linear case used to determine a straight line of best fit through several data points (x_i and y_i) (equation 6 or 7) (m is the gradient of the straight line and c is the y intercept, ε_i is the residual of the equation. The line of best fit has values of m and c which minimise $\sum \varepsilon_i^2$).

$$y = mx_i + c \quad \text{Equation 6}$$

or

$$\varepsilon_i = y_i - mx_i - c \quad \text{Equation 7}$$

This can be expressed in terms of vectors.

$$\begin{pmatrix} x_1 & 1 \\ x_2 & 1 \\ x_3 & 1 \\ \dots & 1 \\ \dots & 1 \\ x_i & 1 \end{pmatrix} \begin{pmatrix} m \\ c \end{pmatrix} = \begin{pmatrix} y_1 \\ y_2 \\ y_3 \\ \dots \\ \dots \\ y_i \end{pmatrix} \quad \text{Equation 8}$$

Alternatively, more concisely as :

$$Ax = b \quad \text{Equation 9}$$

(A being the left-hand-side matrix containing the x values, x being the vector of the unknowns m and c and b being the right hand-side-matrix of y values). The matrix A is termed the design matrix. The least squares solution for these equations is found by premultiplying by sides of equation 8 by the transpose of A and solving the resulting equations for x .

$$A^T Ax = A^T b \quad \text{Equation 10}$$

These values are known as the normal solutions for least squares. This can be generalised for more complex non-linear systems such as crystal structure parameters. The best fit is defined as the solution which minimises the function:

$$\sum w(F_o^2 - F_c^2) \quad \text{Equation 11}$$

Where F_o is the observed structure factor and F_c is the calculated structure factor and every reflection is given a weight w (see page 123).

To facilitate least squares solutions, the observational equations need to be in excess of the unknowns which leads to least squares matrices for crystal structures to be very large. Various statistical techniques can be used to improve the least squares fit e.g. weighting (which gives greater significance in the least squares calculation to more reliable observations), restraints (treated as experimental observations, e.g. bond lengths, bond angles and van der Waals contact distances; weights determine the strength of the applied restraint) and constraints (must be fulfilled exactly). For

example, if there are multiple copies of a molecule in the asymmetric unit of the crystal, the model can be a single copy of the molecule and replicated by rotations and translations to create the other copies. If for instance, there are three copies in the asymmetric unit, the number of adjustable parameters can be reduced by a factor of three.

Refinement progress is determined by the “minimisation function” which is expressed by several “residual factors” (R factors). The R factor most closely related to the minimisation procedure is wR^2 which considers the reflection weightings.

$$\frac{wR^2 = \sum w(F_0 - F_c)^2}{\sum wF_0^2} \quad \text{Equation 12}$$

However, R is also frequently quoted. using the $|F|$ values of “observed” reflections (those for which $F_o^2 > 2\sigma(F_o^2)$). This index was used in the past when it was commonplace to refine data against F as opposed to F^2 . It generates smaller values than wR^2 . This is less sensitive to changes in the weighting scheme so is still commonly quoted alongside wR^2

$$\frac{R = \sum \|F_0\| - \|F_c\|}{\sum \|F_0\|} \quad \text{Equation 13}$$

Several parameters can be refined. Atomic coordinates – three for each atom (x , y and z) in a general position. Atom type – correct assignment of atom types is very important as incorrect atom assignments will go lead to incorrect scattering factors, which will filter down to refinement of other parameters. Site occupancies – Generally atoms in general positions have site occupancies of one. If disorder is present in the lattice, this disorder can be modelled by refinement and fractional occupancies. Overall scale factors – used to bring experimental and calculated intensities to the same scale. and thermal displacement parameters – Isotropic atoms possess single displacement values in every direction and are defined by single parameters (U or B). Anisotropic models have thermal motion in three dimensions with the axes arbitrarily set. This gives six U values for refinement.

Estimated standard deviations (esd's) for structural parameters are calculated from the least squares matrix. Standard deviations generally involve one parameter which is measured several times over. Here, the standard deviation (σ) is the average deviation of the measured values from the mean (equation 15);

$$\sigma = \frac{1}{N} \sqrt{\sum_{i=1}^n (x_i - \bar{x})^2} \quad \text{Equation 15}$$

N is the number of measurements and \bar{x} is the average of the measurements, x_i . But crystallographic data involves only one measurement of each parameter so standard deviations must be estimated. This is possible due to the excess of data over parameters. The esd for a refined parameter P_j depends on three things ; the minimisation of the function $w_i(F_o^2 - F_c^2)_i$ (shown below as $w_i\Delta_i$), the number of data and parameters and the diagonal terms of the inverse least square matrix A^{-1} .

The esd is given by:

$$\sigma(P_j) = \sqrt{\left((A^{-1})_{jj} \frac{\sum_{i=1}^N w_i \Delta_i^2}{N - P} \right)} \quad \text{Equation 16}$$

The esd's for the bond lengths, bond angles and torsions are derived from the refined parameter esd's unless constrained in the refinement.

4.12 Single crystal X-ray diffraction

Single crystal X-ray diffraction is routinely used for elucidation of crystal structures. Data is collected from a single crystal over a range of orientations so data may be obtained for the full three-dimensional lattice structure. In a laboratory environment a four-circle diffractometer system which allows three degrees of rotational freedom for the crystal and one for the detector is used. This allows all possible crystal orientations to be obtained.⁷⁹ Detectors that are used in a four circle diffractometer have to find a peak in the diffraction pattern and then scan around it to measure the intensity, being able only to detect a single diffracted beam. Data collection on such a diffractometer is a slow process especially if the crystal in question possesses low crystallographic symmetry. The advent of high resolution charged coupled devices (CCD) chips has led to a big decrease in time needed for X-ray data collection.⁸⁰ as area detectors are able to gather many diffracted beams in a single exposure. It also allows the crystal mounting to be simplified to a two-circle set up. The intensities of the diffracted beams can be filtered from the background by appropriate thresholding software and measured by integration of the intensities.

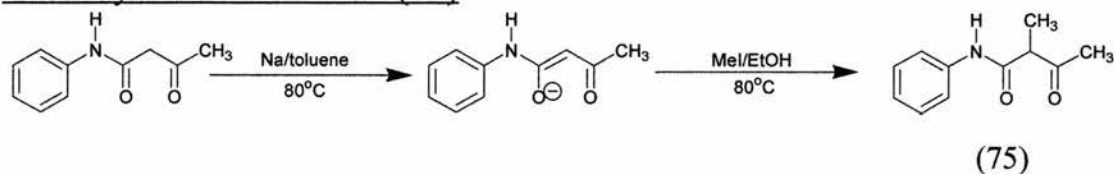
The appendices contain the details of all the X-ray crystal data, the data collection and refinements. The systematic absences allowed unique assignment of all the space groups. All intensity data were recorded at 293(1)K with a Rigaku AFC7S diffractometer [except for (72)] using graphite-monochromated Mo-K α radiation ($\lambda = 0.7101\text{\AA}$). For compound (72), the intensity data were recorded at 298(2)K with a Siemens SMART CCD diffractometer employing ω rotation with narrow frames. The structures were solved by direct methods using SIR92⁸¹ and refined by full-matrix least squares on F (except for (72)). With the exception of (75) all atoms were located by a ΔF map, and were included in the refinements as riding atoms in idealised positions with isotropic displacement parameters. For (75) hydrogen atoms bound to carbon were idealised and fixed (C-H 0.95 \AA). The NH protons were located by a ΔF map and allowed to refine anisotropically. All other atoms were located by a ΔF map and were included in the refinements as riding atoms in idealised positions with isotropic displacement parameters. All non-hydrogen atoms were refined

anisotropically. For compound (72) the structure was solved by direct methods. Non-hydrogen atoms were refined with anisotropic displacement parameters. Hydrogen atoms bound to carbon were idealised and fixed (C-H 0.95Å) and the NH proton and all other atoms were located by a ΔF map and allowed to refine anisotropically. Structural refinements were by the full-matrix least-squares method on F^2 using the program SHELXTL.⁸²

4.2 Problems with Manufacture and Synthesis of PO16 and Similar Pigments

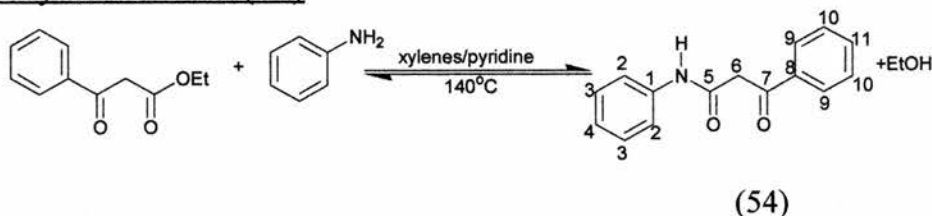
There is a problem with PO16 (**23**) and similar pigments in that one of the starting materials used in synthesis is a benzidine derivative, e.g. *o*-dianisidine, which is a suspected human carcinogen,⁸³ so precautions are necessary for its handling and containment. It was essential that it was handled and manipulated only in a designated fume hood with the sash down as far as possible. Also, when handling it, a dust mask and protective gloves were worn in addition to standard laboratory protection. Any gloves or other consumables suspected of contamination were disposed of in a designated container for *o*-dianisidine waste. The pigment itself, however, is safe to handle, as has been proven by Ciba in an extensive series of biological tests.

2-Methylacetoacetanilide (75)



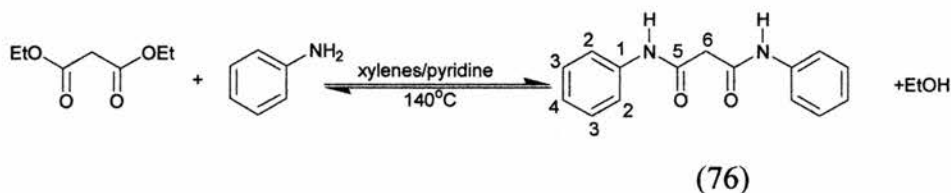
To a solution of acetoacetanilide (4.45g, 25mmol) in dry toluene (40ml) was added sodium (0.58g, 25mmol). The resulting mixture was heated under reflux for *ca.* 2h. which afforded a colour change from clear to orange with the formation of a precipitate after 1h. The toluene was removed *in vacuo*, the residue dissolved immediately in a solution of methyl iodide (4.26g, 30mmol) in absolute ethanol (50ml). The resultant brown/orange solution was gently heated under reflux for *ca.* 45 min. The ethanol was removed *in vacuo*. The minimum amount of ethanol was added to dissolve the oil. Water was then slowly added to precipitate out a light brown solid. The solid was filtered off, dried and recrystallised from ethyl acetate.

Yield 2.66g (55%), m.p.138-140°C [lit.⁸⁴ 137-139°C]; δ_{H} (CDCl₃) 8.60 (1H, bs, NH), 7.50-7.60 (2H, m, Ar-*o*), 7.25-7.40 (2H, m, Ar-*m*), 7.07-7.20 (1H, m, Ar-*p*), 3.42-3.62 (1H, m, CH), 2.62 (6H, s, 2 × CH₃).

2-Benzoylacetanilide (54)

To a mixture of freshly distilled ethyl benzoylacetate (5.65g, 29.4mmol) in xylene (40ml) and pyridine (3 drops) at 140°C was added a mixture of freshly distilled aniline (2.00g, 21.5mmol) in xylene (40ml) and pyridine (3 drops) over a period of *ca.* 2h. The xylene was constantly removed throughout the reaction by distillation. The mixture was allowed to cool to room temperature and a light yellow precipitate formed. This was filtered off, dried and recrystallised from toluene.

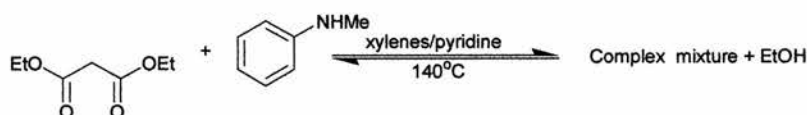
Yield 3.86g (75%), m.p. 106-108°C [lit.⁸⁵ 107-108°C]; δ_{H} (CDCl₃) 9.68 (1H, s, NH), 7.12-8.15 (10H, m, Ar), 4.08 (2H, s, CH₂); δ_{C} 194.0 (C-7), 163.9 (C-5), 137.9 (C-1), 135.0 (C-8), 134.1 (C-11), 129.6 (C-10), 128 (C-3), 124.2 (C-4), 120.0 (C-2), 43.8 (C-6).

Malondianilide (76)

To a mixture of freshly distilled diethyl malonate (3.44g, 21.5mmol) in xylene (40ml) and pyridine (3 drops) at 140°C was added a mixture of freshly distilled aniline (4.00g, 43mmol) in xylene (40ml) and pyridine (3 drops) over a period of *ca.* 2h. The xylene added and the ethanol produced were constantly removed throughout the reaction by distillation. The mixture was allowed to cool to room temperature and a white precipitate formed. This was filtered off, dried and recrystallised from aqueous ethanol.

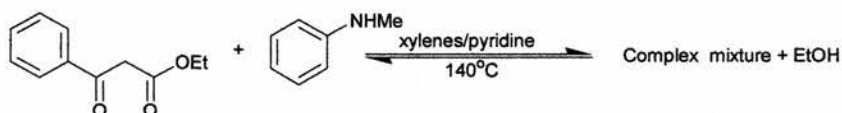
Yield 3.71g (68%), m.p. 228-232°; [lit.⁸⁶ 228-232°C]; δ_{H} (DMSO- d_6) 10.20 (2H, s, NH), 6.76-6.83 (4H, m, Ar-*o*), 6.61-6.69 (4H, m, Ar-*m*), 6.49-6.53 (2H, m, Ar-*p*), 3.48 (2H, s, CH₂); δ_{C} 166.1 (C-5), 139.4 (C-1), 129.2 (C-3), 124.0 (C-4), 119.8 (C-2), 46.6 (C-6).

Reaction of *N*-Methylaniline and diethyl malonate

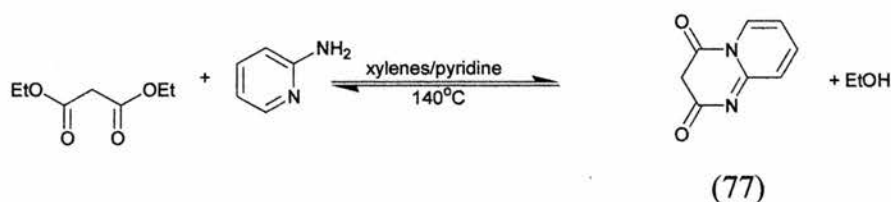


To a mixture of freshly distilled diethyl malonate (4.71g, 29.4mmol) in xylene (40ml) and pyridine (3 drops) at 140°C was added a mixture of freshly distilled *N*-methylaniline (4.00g, 43mmol) in xylene (40ml) and pyridine (3 drops) over a period of *ca.* 2h. The xylene added was constantly removed throughout the reaction by distillation. The mixture was allowed to cool. The resultant solution was extracted three times with HCl (0.1M, 40ml) and twice with water (40ml) and dried. The xylene was removed *in vacuo* to afford a brown oil. ¹H NMR showed a complex mixture of products was present.

Reaction of *N*-Methylaniline and ethyl benzoylacetate

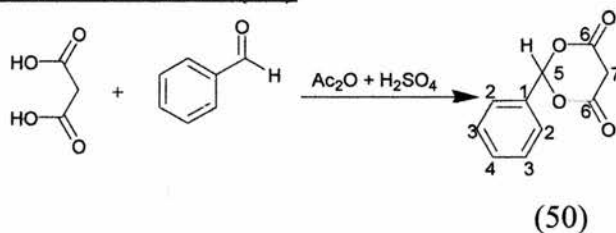


To a mixture of freshly distilled ethylbenzoylacetate (4.71g, 29.4mmol) in xylene (40ml) and pyridine (3 drops) at 140°C was added a mixture of freshly distilled *N*-methylaniline (2.00g, 43mmol) in xylene (40ml) and pyridine (3 drops) over a period of *ca.* 2h. The xylene added was constantly removed throughout the reaction by distillation. The mixture was allowed to cool. The resultant solution was extracted three times with HCl (0.1M, 40ml) and twice with water (40ml) and dried. The xylene was removed *in vacuo* and to afford a yellow oil. ¹H NMR showed a complex mixture of products was present.

2H-Pyrido-[1,2-a]pyrimidine-2,4-(3H)dione (77)

To a mixture of freshly distilled diethyl malonate (4.71g, 29.4mmol) in xylene (40ml) and pyridine (3 drops) at 140°C was added a solution of 2-aminopyridine (4.00g, 43mmol) in xylene (40ml) and 3 drops of pyridine over a period of *ca.* 2h. The xylene added was constantly removed throughout the reaction by distillation. Throughout addition a green/yellow solid precipitated out of solution. The mixture was allowed to cool to room temperature. The precipitate was filtered, dried and recrystallised from DMF to afford a fine yellow solid.

Yield 2.66g (55%) m.p. 320°C (dec.) [lit.⁸⁷ 318°C (dec.)]; δ_{H} (DMSO- d_6) 8.88-8.90 (1H, m, Ar), 8.02-8.14 (1H, m, Ar), 7.28-7.46 (2H, m, Ar), 4.96 (2H, s, CH₂).

2-Phenyl-1,3-dioxan-4,6-dione (50)

To a stirred suspension of malonic acid (5.2g, 50mmol) in acetic anhydride (15ml) was added conc. sulphuric acid (3 drops) upon which most of the malonic acid was dissolved. To the resulting solution was added benzaldehyde (5.3g, 50mmol) whilst ensuring that the temperature was maintained at 20-25°C. The resultant light brown solution was stored at 5°C for *ca.* 12h. The residual solvent was removed *in vacuo* and the resulting white solid was recrystallised from aqueous acetone.

Yield 6.02g (63%), m.p. 150°C (dec.), [lit.⁸⁸ 148°C (dec.)]; δ_{H} (DMSO- d_6) 7.48-7.63 (5H, s, Ar), 7.13 (1H, s, CH), 4.51-4.61 (1H, d, *J* 18.4 CH), 3.56-3.65 (1H, d, *J* 18.4 CH); δ_{C} 164.5 (C-6), 133.0 (C-1), 131.0 (C-3), 129.1 (C-4), 126.9 (C-2), 96.1 (C-5).

It is thought that the (C-7) carbon is hidden under the solvent peak.

3,3'-Dimethoxybiphenyl-4,4'-bis(diazonium chloride)

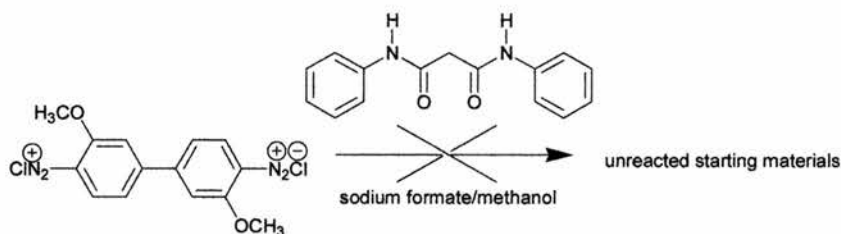
To a stirred suspension of *o*-dianisidine dihydrochloride (25.2g, 0.08mol) in water (100ml) at 0°C was added conc. HCl (19.7g, 0.2mol). Three quarters of a solution of sodium nitrite (13.1g, 0.19mol) in water was then added upon which NO₂ was evolved. Activated carbon (0.1g) and was then added. The resultant black suspension was stirred for *ca.* 20min whilst ensuring that the temperature was kept at 0-5°C. After 20 min the remaining sodium nitrite solution was added and the solution was stirred for a further 20min whilst allowing the solution to reach room temperature. The black suspension was filtered to afford a golden orange solution and sulfamic acid was added to remove excess nitrite (monitored by pH of solution).

4.3 General Method for Synthesis of Bis-azo Pigments

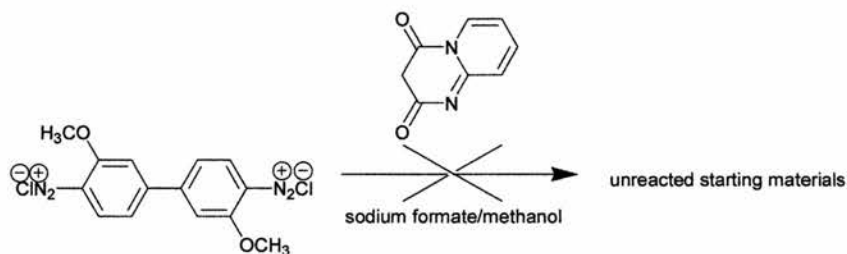
To a stirred solution of coupling component (**49-54**) (see pages 37-38) (10mmol) (2 mol. equiv.) and sodium formate (1.38g, 14mmol) (1.4mol. equiv) in methanol (70ml) was added an aqueous solution of bis-diazo component (*o*-dianisidine bis-diazo or DCB) (0.47M, 10.63ml) (1 mol. equiv.) further diluted in water (150ml) over *ca.* 50 min at 32°C. The precipitate formed was filtered off, washed with copious amounts of distilled water at 80°C and recrystallised from boiling nitrobenzene. The recrystallised pigment was then washed with petrol b.p. 40-60°C to wash away nitrobenzene and the pigment was then dried at 140°C.

2-methylacetoacetanilide and 2*H*-pyrido[1,2-*a*]pyrimidine-2,4-(3*H*)dione and malondianilide were used as coupling components. All of these attempted reactions yielded unreacted starting materials.

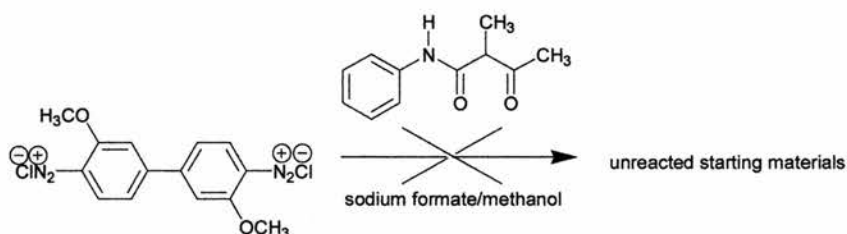
3,3'-Dimethoxybiphenyl-4,4'-bis(diazonium chloride) with (76)



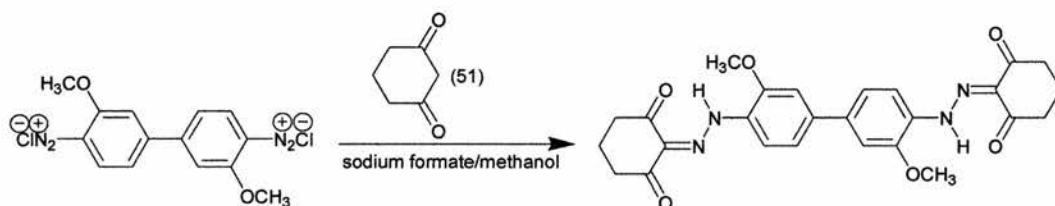
3,3'-Dimethoxybiphenyl-4,4'-bis(diazonium chloride) with (77)



3,3'-Dimethoxybiphenyl-4,4'-bis(diazonium chloride) with (75)



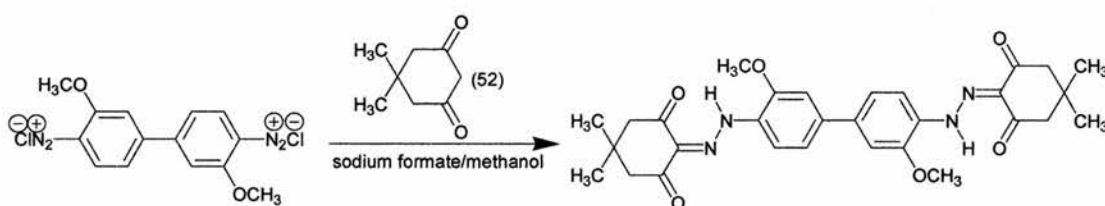
3,3'-Dimethoxybiphenyl-4,4'-bis(diazonium chloride) with (51)



(51) 1.12g, 10mol

Yield 2.22g (89%); (decomposed without melting). (Found: C, 57.6; H, 4.0; N, 11.4. $C_{26}H_{26}N_4O_6$ requires C, 57.7; H, 4.0; N, 11.2%), λ_{max} / nm (CH_2Cl_2) 493 (ϵ 12600).

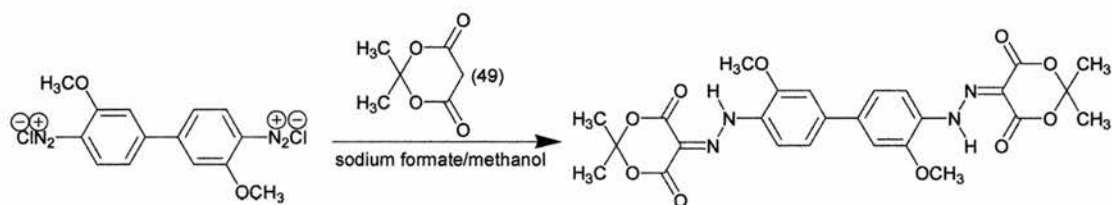
3,3'-Dimethoxybiphenyl-4,4'-bis(diazonium chloride) with (52)



(52) 1.40g, 10mmol

Yield 2.35g (86%); (decomposed without melting). (Found: C, 65.7; H, 6.3; N, 10.3. $C_{30}H_{34}N_4O_6$ requires C, 65.9; H, 6.2; N, 10.2%), λ_{\max} / nm (CH_2Cl_2) 471 (ϵ 8767).

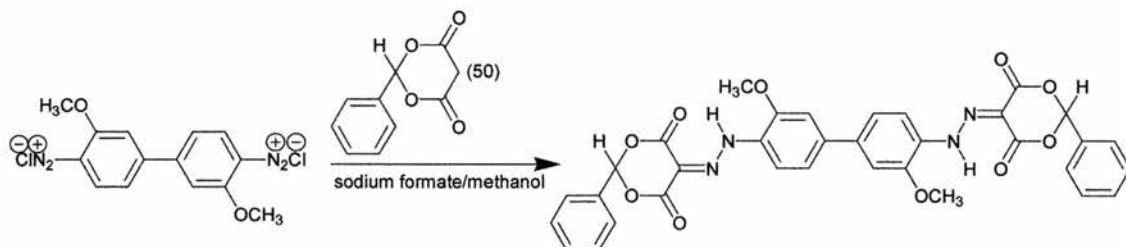
3,3'-Dimethoxybiphenyl-4,4'-bis(diazonium chloride) with (49)



(49) 1.44g, 10mmol

Yield 2.61g (94%); (decomposed without melting). (Found: C, 56.1; H, 4.8; N, 10.1. $C_{26}H_{26}N_4O_{10}$ requires C, 56.3; H, 4.7; N, 10.1%), λ_{\max} / nm (CH_2Cl_2) 449 (ϵ 8967).

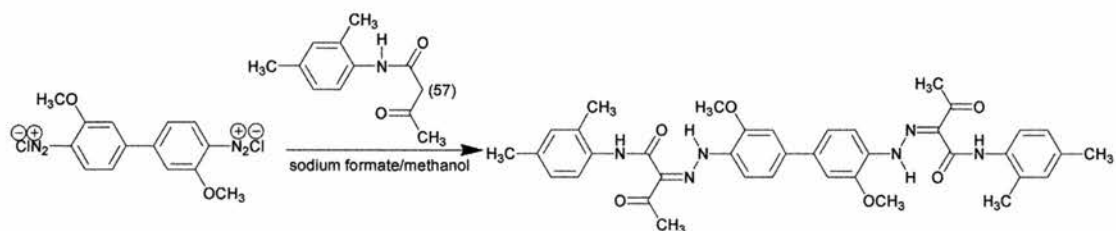
3,3'-Dimethoxybiphenyl-4,4'-bis(diazonium chloride) with (50)



(50) 1.92g, 10mmol

Yield 2.76g (85%); (decomposed without melting). (Found: C, 59.9; H, 4.3; N, 9.4. $C_{34}H_{26}N_4O_{10}$ requires C, 59.8; H, 4.4; N, 9.3%), λ_{\max} / nm (CH_2Cl_2) 456 (ϵ 300).

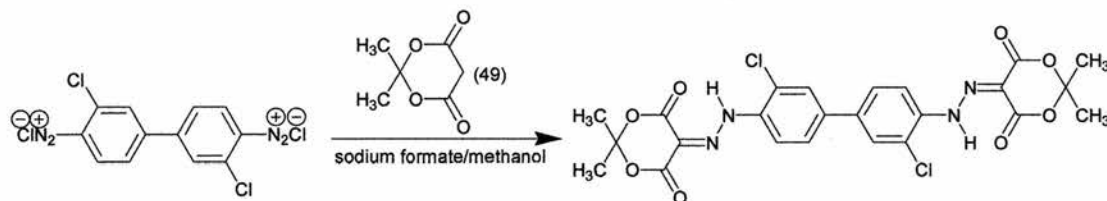
3,3'-Dimethoxybiphenyl-4,4'-bis(diazonium chloride) with (57)



(57) 2.05g, 10mmol

Yield 2.64g (78%); (decomposed without melting). (Found: C 67.2; H, 5.8; N, 12.3. $C_{38}H_{40}N_6O_6$ requires C 67.4; H, 6.0; N, 12.4%), λ_{\max} / nm (CH_2Cl_2) 442 (ϵ 300).

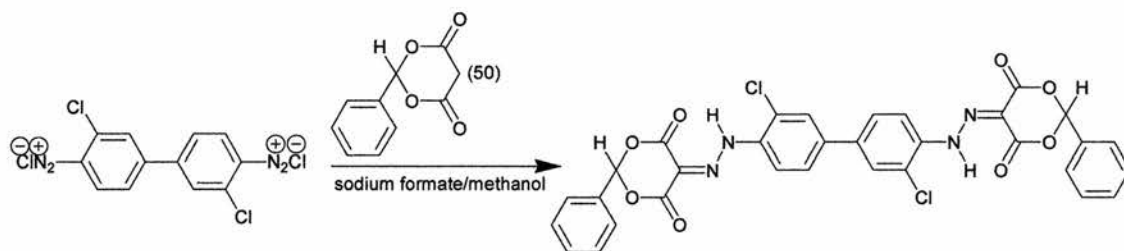
3,3'-dichlorobiphenyl-4,4'-bis(diazonium chloride) with (49)



(49) 1.44g, 10mmol

Yield 2.37g (84%); (decomposed without melting). (Found: C, 51.4; H, 3.6; N, 12.5. $C_{24}H_{20}Cl_2N_4O_8$ requires C, 51.2; H, 3.6; N, 12.6%), λ_{\max} / nm (CH_2Cl_2) 420 (ϵ 9733).

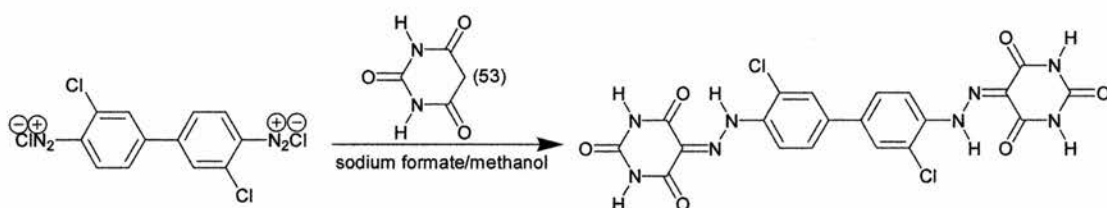
3,3'-dichlorobiphenyl-4,4'-bis(diazonium chloride) with (50)



(50) 1.92g, 10mmol

Yield 2.63g (80%); (decomposed without melting). (Found: C, 58.1; H, 3.4; N, 9.3. $C_{32}H_{20}Cl_2N_4O_8$ requires C, 58.3; H, 3.3; N, 9.2%), λ_{\max} / nm (CH_2Cl_2) 407 (ϵ 1290).

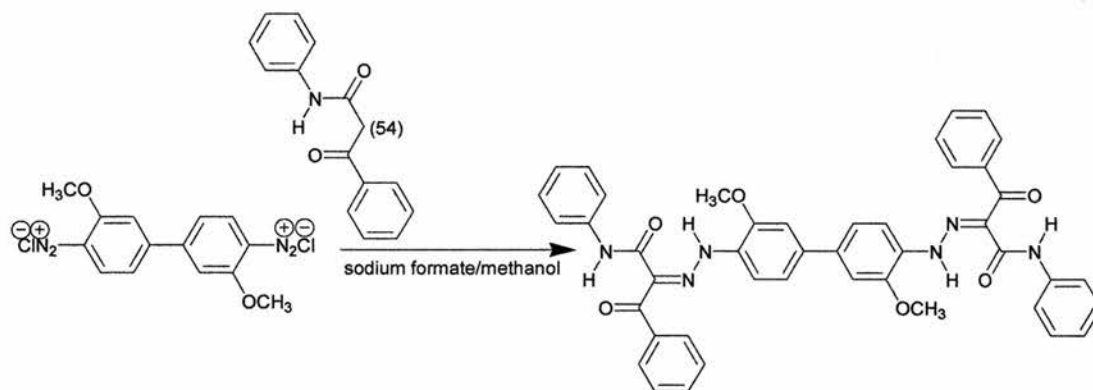
3,3'-dichlorobiphenyl-4,4'-bis(diazonium chloride) with (53)



(53) 1.28g, 10mmol

Yield 2.28g (86%); (decomposed without melting). (Found: C, 45.4; H, 2.3; N, 13.3. $C_{20}H_{12}Cl_2N_8O_6$ requires C, 45.2; H, 2.3; N, 13.4%), λ_{max} / nm (CH_2Cl_2) 475 (ϵ 7900).

3,3'-dichlorobiphenyl-4,4'-bis(diazonium chloride) with (54)



(54) 2.39g, 10mmol

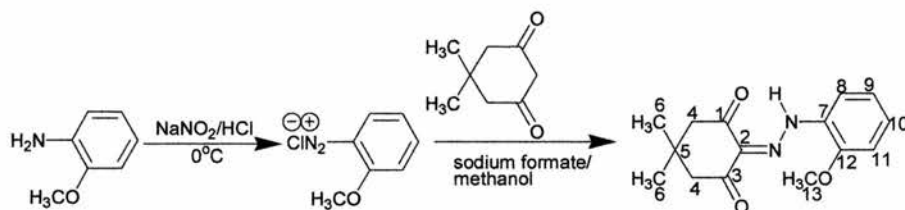
Yield 3.24g (87%); (decomposed without melting). (Found: C, 71.1; H, 5.1; N, 11.2. $C_{44}H_{36}N_6O_6$ requires C, 71.0; H, 4.9; N, 11.3%), λ_{max} / nm (CH_2Cl_2) 451 (ϵ 7400).

4.4 General Method for Synthesis of Monoazo Pigments

A mixture of conc. HCl (2.5ml) and water (20ml) was added to freshly distilled *o*-anisidine (1.23g, 10mmol). The resultant solution was stirred and cooled to 0°C and a solution of sodium nitrite (0.69g, 10mmol) in water (20ml) was added. The resultant yellow/orange solution was stirred at 0°C for 10 min. The solution was then filtered rapidly and then added to a stirred solution of sodium formate (1.36g, 20mmol) and coupling component (10mmol) in methanol (50ml) at 0°C. The solution was stirred for *ca.* 2h and the precipitated pigment was filtered and recrystallised from toluene.

2-[(2-methoxyphenyl)hydrazono]-5,5-dimethylcyclohexane-1,3-dione

(68)



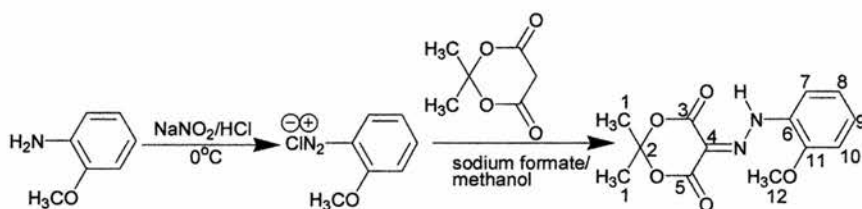
(52) 1.40g, 10mmol

Yield 2.22g (81%), m.p.155-158°C; (Found: C, 65.5; H, 6.5; N, 10.1. $C_{15}H_{18}N_2O_3$ requires C, 65.7; H, 6.6; N, 10.2%); δ_H ($CDCl_3$) 15.48 (1H, s, NH), 7.92-8.07 (1H, m, Ar), 7.18-7.31 (1H, m, Ar), 6.95-6.99 (2H, m, Ar), 3.98 (3H, s, OCH_3), 2.58 (4H, s, $2 \times CH_2$), 1.12 (6H, s, $2 \times CH_3$), δ_C 196.3 (C-1), 193.5 (C-3), 130.7 (C-12), 130.7 (C-2), 130.1 (C-7), 127.6 (C-9), 121.6 (C-10), 116.6 (C-11), 110.9 (C-8), 55.9 (C-13), 52.4 (C-4), 28.5 (C-5), 30.7 (C-6).

For single crystal X-ray data, see appendices.

5-[(2-methoxyphenyl)hydrazono]-2,2-dimethyl-1,3-dioxan-4,6-dione

(69)



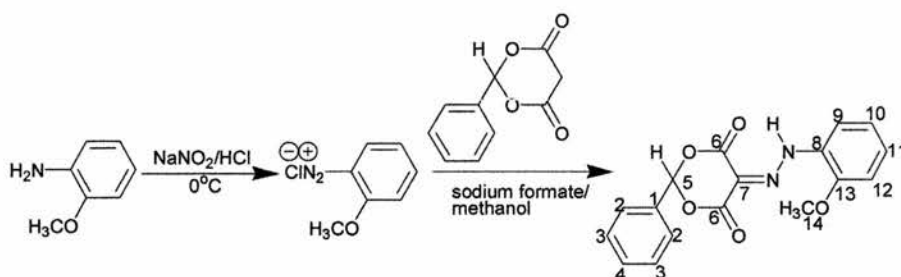
(49) 1.44g, 10mmol

Yield 2.00g (72%), m.p.141-144°C; (Found: C, 56.3; H, 5.0; N, 10.1. $C_{13}H_{14}N_2O_5$ requires C, 56.1; H, 5.1; N, 10.1%); δ_H ($CDCl_3$) 13.91 (1H, s, NH), 7.94 (1H, br s, Ar), 7.11-7.17 (1H, m, Ar), 6.93-7.04 (2H, m, Ar), 3.97 (3H, s, OCH_3), 1.40 (6H, s, $2 \times CH_3$).

× CH₃), δ_C 161.5 (C-3), 160.1 (C-5), 148.2 (C-4), 127.7 (C-6), 130.0 (C-11), 122.3 (C-8), 117.0 (C-9), 112.5 (C-7), 111.1 (C-10), 106.0 (C-2), 56.2 (C-12), 32.4 (C-1).

For single crystal X-ray data, see appendices.

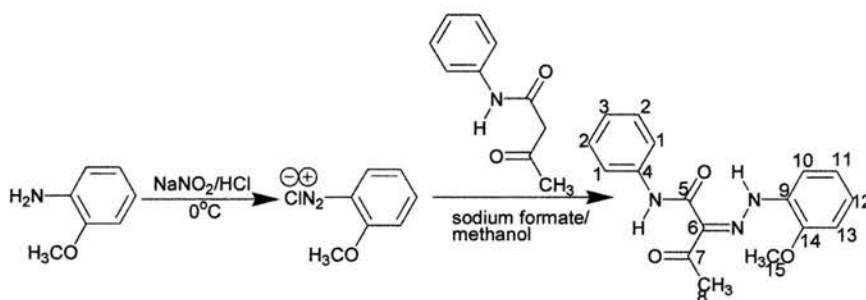
5-[(2-methoxyphenyl)hydrazono]-2-phenyl-1,3-dioxan-4,6-dione (70)



(50) 1.92g, 10mmol

Yield 2.83g (87%), m.p.142-144°C; (Found: C, 62.6; H, 4.3; N, 8.7. C₁₇H₁₄N₂O₅ requires C, 62.6; H, 4.3; N, 8.8%); δ_H (DMSO-d₆) 13.65 (1H, s, NH), 8.48 (1H, s, Ar), 8.17 (1H, d, Ar), 7.30-7.7 (7H, m, Ar), 7.23 (1H, s, CH), 4.11 (1H, s, OCH₃), δ_C 193.1 (C-6), 156.5 (C-7), 132.8 (C-13), 130.6 (C-1), 129.3 (C-8), 128.8 (C-3), 128.6 (C-4), 128.2 (C-2), 126.4 (C-10), 121.7 (C-11), 117.2 (C-9), 112.4 (C-12), 97.4(C-5), 55.0 (C-14).

2-[(2-methoxyphenyl)hydrazono]-3-oxo-N-phenylbutyramide (71)



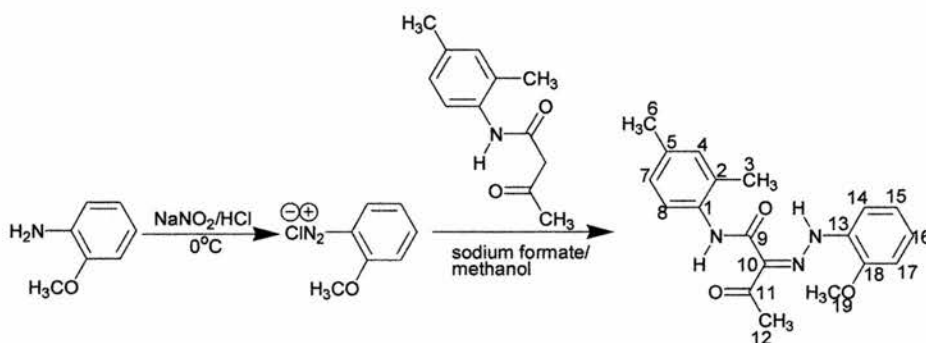
1.77g acetoacetanilide, 10mmol

Yield 2.61g (84%), m.p.143-145°C; (Found: C, 65.6; H, 5.5; N, 13.6. C₁₇H₁₇N₃O₃ requires C, 65.6; H, 5.5; N, 13.5%); δ_H (DMSO-d₆) 14.50 (1H, s, NH), 11.40 (1H, s,

NH), 7.14-7.92 (9H, m, Ar), 4.05 (3H, s, OCH₃), 2.52 (3H, s, CH₃), δ_C 198.8 (C-7), 162.1 (C-5), 148.0 (C-6), 137.0 (C-14), 130.4 (C-4), 129.0 (C-9), 126.7 (C-3), 125.6 (C-2), 124.6 (C-11), 121.5 (C-1), 120.4 (C-12), 114.4. (C-10), 112.1 (C-13), 56.2 (C-15), 26.0 (C-8).

For single crystal X-ray data, see appendices.

5-[(2-methoxyphenyl)hydrazono]-N-(2,4-dimethyl-phenyl)-3-oxo-
butyramide (78).



(54) 2.05g, 10mmol

Yield 2.98g (88%), m.p.192-195°C; (Found: C, 67.4; H, 6.5; N, 14.0. C₁₉H₂₁N₃O₃ requires C, 67.2; H, 6.2; N 14.1%); δ_H (DMSO-d₆); 14.59 (1H, s, NH), 11.32 (1H, s, NH), 7.91 (1H, d, Ar), 7.68 (1H, d, Ar), 6.98-7.34 (5H, m, Ar), 3.98 (1H, m, OCH₃), 2.50 (2H, s, 2 × CH₃), δ_C 199.0 (C-11), 162.0 (C-0), 148.0 (C-10), 133.8 (C-18), 132.9 (C-1), 130.9 (C-13), 130.4 (C-5), 128.4 (C-4), 126.8 (C-2), 125.6 (C-7), 124.6 (C-15), 121.7 (C-16), 121.4 (C-8), 114.3 (C-14), 112.0 (C-17), 56.2 (C-19), 25.9 (C-6), 20.4 (C-12), 17.5 (C-3).

For single crystal X-ray data, see appendices.

4.5 Ciba Method for Synthesis of Bis-azo Pigments⁸⁹

To a solution of sodium hydroxide (27.5g of a 47% solution) was added the coupling component (0.305mol). The solution was adjusted to pH 12.5 and maintained at room temperature. The coupling component was then precipitated, over 15min, by addition of glacial acetic acid (23.4g) in water (83ml), until the pH of the solution reached 6. The temperature was then lowered to 16°C. To this solution was added either the bis-diazonium salt of DCB or *o*-dianisidine at 0°C over the course of 1h to maintain a steady addition rate. The resultant pigment was heated in solution to 80°C for 1h, filtered, washed with copious amount of water then filtered and dried at 80°C.

4.6 Crystal Growth Techniques

Crystals of the monoazo pigments were grown by room temperature evaporation from solution over several days. Several crystallisations were performed from various solvents such as toluene and ethanol at various concentrations until suitable crystals were grown.

4.6.1 Bis-azos

A known amount of pigment was added to nitrobenzene (300ml). The suspension was heated under reflux until the pigment was fully dissolved (which always occurred at the boiling point of nitrobenzene (210°C)). The solution was then cooled very slowly to room temperature using an oil bath and a temperature controlled hot plate. The recrystallised pigment was then filtered, washed with copious amounts of petrol (b.p. 40-60°C) to wash away traces of nitrobenzene, and then dried at 140°C.

4.7 Solid-State Fluorescence Measurements

Samples were prepared as follows. Double-sided transparent adhesive tape was stuck to a glass slide. A known amount of pigment was sprinkled on the tape and the slide was mounted in the fluorimeter and the measurements were carried out. The

distribution of pigment on the tape was kept as even and consistent as possible for each measurement.

4.8 Solution Fluorescence and Absorption Measurements

For solution measurements, a solution of the pigment in dichloromethane (concentration $3 \times 10^{-4} \text{ mol dm}^{-3}$) was used.

4.9 Solid State Absorption Measurements

Solid-state absorption measurements were carried out as follows. The samples were prepared in the same way as a KBr disc for IR spectra, and the KBr disc was placed in the UV/visible spectrophotometer (n.b. KBr was the matrix used in all cases).

References

- 1 W. Herbst and K. Hunger, 'Industrial Organic Pigments, Production, Properties and Applications.', VCH Weinheim, 1997.
- 2 H. Zollinger, 'Colour Chemistry - Synthesis, Properties and Applications of Organic Dyes and Pigments.', VCH Weinheim, 1993.
- 3 A. Iqbal, B. Medingere, and R. B. McKay, 'Advances in Colour Chemistry.', ed. A. J. Peters and H. S. Freeman, Glasgow, 1996.
- 4 G. Booth, 'The Chemistry of Synthetic Dyes.', ed. Venkataraman, New York, London, 1971.
- 5 F. H. Moser and A. L. Thomas, 'Phthalocyanine compounds.', Reinhold, 1963.
- 6 W. F. Spengeman, *Paint Varn. Prod.*, 1970, **60**, 37.
- 7 S. S. Labana and L. L. Labana, *Chem. Rev.*, 1967, **67**, 1.
- 8 D. G. Farnum, G. Mehta, G. G. I. Moore, and F. P. Siegal, *Tetrahedron Lett.*, 1974, **29**, 2549.
- 9 A. Iqbal and L. Cassar, U.S. Pat. 4415685 (1983).
- 10 A. Whitaker, *Z. Kristallogr.*, 1978, **147**, 99.
- 11 A. Whitaker, *J. Soc. Dyers Colourists*, 1988, **104**, 294.
- 12 S. Zheng, D. Liu, and S. Ren, *Dyes and Pigments*, 1992, **18**, 137.
- 13 A. Whitaker, *J. Soc. Dyers Colourists*, 1978, **94**, 431.
- 14 P. Griess, *Liebigs. Ann. Chem.*, 1858, **106**, 123.
- 15 O. W. Witt, *Ber. Dtsch. Chem. Ges.*, 1876, **9**, 522.
- 16 A. Whitaker and N. P. C. Walker, *Acta Cryst.*, 1987, **C43**, 2137.
- 17 J. Griffiths, 'Colour Constitution of Organic Molecules.', Academic Press, 1976.
- 18 H. Zollinger, 'Chemie der Azfarbstoffe.', Birkhauser, 1958.
- 19 F. H. Moser and A. L. Thomas, 'The Phthalocyanines.', Boca Raton, Florida, 1983.
- 20 A. Jablonski, *Nature*, 1933, **131**, 839.
- 21 P. W. Atkins, 'Physical Chemistry.', Oxford University Press, 1990.
- 22 L. A. Tumerman, *J. Exptl. Theoret. Phys. (U. S. S. R)*, 1942, **12**, 328.
- 23 P. Ramart-Lucas, *Bull. Soc. Chim.*, 1941, **8**, 865.
- 24 M. Dolinsky, Swiss Pat. 290296 (1953); *Chem. Abstr.*, **48**, 7310.

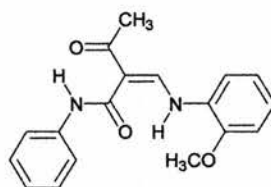
- 25 M. Dolinsky, Swiss Pat. 293879 (1954); *Chem. Abstr.*, **49**, 12844.
- 26 Ciba Specialty Chemicals, personal communication, 1997.
- 27 P. A. Merchak, R. J. Schwartz, M. Z. Gregorio, and A. Zwirgzdas, U. S. Pat. 5863459 (1999).
- 28 P. A. Merchak, R. J. Schwartz, M. Z. Gregorio, and A. Zwirgzdas, U. S. Pat. 5904878 (1999).
- 29 H. Langhals, T. Potrawa, H. Noth, and G. Linti, *Angew. Chem. Int. Ed. Engl.*, 1989, **28**, 478.
- 30 H. Langhals, S. Demmig, and T. Potrawa, *J. Prakt. Chem.*, 1991, **333**, 733.
- 31 H. Langhals and F. Submeier, *J. Prakt. Chem.*, 1999, **341**, 309.
- 32 H. Langhals and W. Jona, *Angew. Chem. Int. Ed. Engl.*, 1998, **37**, 952.
- 33 H. Langhals, J. Funfschilling, D. Glatz, and I. Schokke-Granacher, *Spectrochimica Acta*, 1988, **A44**, 311.
- 34 J. Otani, personal communication to Ciba Specialty Chemicals, 1996.
- 35 K. Shirai, M. Matsuoka, and K. Fukunishi, *Dyes and Pigments*, 1999, 95.
- 36 F. D. Lewis, J.-S. Yang, and C. L. Stern, *J. Am. Chem. Soc.*, 1996, **118**, 12029.
- 37 J. C. MacDonald and G. M. Whitesides, *Chem. Rev.*, 1994, **94**, 2383.
- 38 Z. Hao, J. S. Zambounis, and A. Iqbal, U. S. Pat. 5874580 (1999).
- 39 Z. Hao, J. S. Zambounis, and A. Iqbal, U. S. Pat. 5886160 (1999).
- 40 J. J. Segura, *Acta Polym.*, 1998, **49**, 319.
- 41 J. H. Burroughes, D. D. C. Bradley, A. R. Brown, R. N. Marks, K. Mackey, R. H. Friend, P. L. Burn, and A. B. Holmes, *Nature*, 1990, **347**, 539.
- 42 J. Su, T. Xu, K. Chen, and H. Tian, *Synthetic Metals*, 1997, 249.
- 43 C. W. Tang and S. A. VanSlyke, *Appl. Phys. Lett.*, 1987, **51**, 913.
- 44 I. Kennosuke, Jap. Pat. 54066930 (1979).
- 45 T. D. Badcock, Ph. D. Thesis, Napier University, 1994.
- 46 A. A. Fadda, M. M. Yousf, A. M. Housini, and M. S. Housini, *Indian J. Text. Res.*, 1984, **9**, 115.
- 47 D. Davidson and S. A. Bernhard, *J. Am. Chem. Soc.*, 1948, **70**, 3426.
- 48 T. Tomoyuki and A. Hiroto, Jap. Pat. 500262999 (1993).
- 49 M. J. Barrow, R. M. Christie, A. J. Lough, J. E. Monteith, and P. N. Standring, *Dyes and Pigments*, 2000, 153.

- 50 J. Monteith, Ph. D. Thesis, Napier University, 1989.
- 51 G. P. Charbonneau and Y. Delugeard, *Acta Cryst.*, 1977, **B33**, 1586.
- 52 A. Hargreaves, *Acta Cryst.*, 1962, **15**, 365.
- 53 G. B. Robertson, *Nature*, 1961, **191**, 593.
- 54 J. Trotter, *Acta Cryst.*, 1961, **14**, 1135.
- 55 G. P. Charboneau and Y. Delugeard, *Acta Cryst.*, 1976, **B32**, 1420.
- 56 J. L. Baudour, *Meth. Struct. Anal. Modulated Struct. Quasicrystals*, 1991, 383.
- 57 H. Callieau, J. L. Baudour, and C. M. E. Zeyen, *Acta Cryst.*, 1979, **B35**, 426.
- 58 J. L. Baudour and M. Sanquer, *Acta Cryst.*, 1983, **B39**, 75.
- 59 J. L. Baudour, L. Toupet, Y. Delugeard, and S. Ghemid, *Acta Cryst.*, 1986, **C42**, 1211.
- 60 G. C. Pimental and A. L. McCellan, 'The Hydrogen Bond.', 1960.
- 61 A. Whitaker, *Z. Kristallogr.*, 1985, **170**, 213.
- 62 A. Whitaker, *Z. Kristallogr.*, 1977, **145**, 271.
- 63 A. Whitaker, *Z. Kristallogr.*, 1978, **146**, 173.
- 64 A. Whitaker, *Z. Kristallogr.*, 1983, **163**, 19.
- 65 A. Whitaker, *Z. Kristallogr.*, 1983, **163**, 139.
- 66 A. Whitaker, *Z. Kristallogr.*, 1984, **166**, 177.
- 67 A. Whitaker, *Z. Kristallogr.*, 1984, **167**, 225.
- 68 A. Whitaker, *Z. Kristallogr.*, 1985, **171**, 7.
- 69 A. Whitaker, *Z. Kristallogr.*, 1985, **171**, 17.
- 70 A. Whitaker, *Acta Cryst.*, 1986, **C42**, 1566.
- 71 A. Whitaker, *Acta Cryst.*, 1987, **C43**, 2141.
- 72 G. Chisholm, A. R. Kennedy, S. Wilson, and S. J. Teat, *Acta Cryst.*, 2000, **B56**, 1046.
- 73 J. Mizuguchi, G. Rihs, and H. R. Karfunkel, *J. Phys. Chem.*, 1995, **99**, 16217.
- 74 H. Langhals, R. Ismael, and O. Yuruk, *Tetrahedron*, 2000, **30**, 5435.
- 75 E. J. MacLean, M. Tremayne, B. M. Kariuki, K. D. M. Harris, A. F. M. Iqbal, and Z. Hao., *J. Chem. Soc. Perkin Trans. 2*, 2000, **6**, 1513.
- 76 H. J. Carmichael, P. Kochan, and B. C. Sanders, *Phys. Rev. Lett.*, 1996, **77**, 631.
- 77 A. Guinier, 'X-ray Diffraction.', W. Freeman and Co., 1963.

- 78 D. Viterbo, 'Fundamentals of Crystallography.', ed. C. Giacovazzo, Oxford, 1992.
- 79 H. L. Monaco, 'Fundamentals of Crystallography.', ed. C. Giacovazzo, Oxford, 1992.
- 80 A. M. Z. Slawin, *Chem. Brit.*, 1998, **34**, 31.
- 81 A. Altomare, G. Cascarano, C. Giacovazzo, and A. Guagliardi, *J. Appl. Crystallogr.*, 1993, **26**.
- 82 SHELXTL, Structure Solution and Determination Package, Bruker AXS, Madison WI, 1999.
- 83 J. Barek, A. Berka, and H. Skokankova, *Microchemical Journal*, 1984, **29**, 350.
- 84 A. L. Searles and H. G. Lindwall, *J. Am. Chem. Soc.*, 1946, **68**, 988.
- 85 J. Buckingham and S. M. Donaghy, 'Dictionary of Organic Compounds.', ed. J. Buckingham and S. M. Donaghy, 1982.
- 86 N. S. Vulfson, *Zhur. Obshchei. Khim.*, 1949, **19**, 1904.
- 87 G. R. Lappin, Q. R. Petersen, and C. E. Wheeler, *J. Org. Chem.*, 1950, **15**, 377.
- 88 A. Michael and N. Weiner, *J. Am. Chem. Soc.*, 1936, **58**, 680.
- 89 K. Ventataraman, 'The Chemistry of Synthetic Dyes.', London Academic Press, 1952 .

Appendices

2-[(Methoxyphenyl)hydrazono]-3-oxo-*N*-phenylbutyramide (74)



(71)

Crystal data

Formula	C ₁₇ H ₁₇ N ₃ O ₃
<i>M</i>	311.34
Space group	<i>P</i> 2 ₁ / n (no. 14)
Crystal system	Monoclinic
Temperature/K	293(1)
<i>a</i> /Å	12.802(6)
<i>b</i> /Å	5.358(3)
<i>c</i> /Å	22.582(4)
<i>α</i> /°	90
<i>β</i> /°	103.14(2)
<i>γ</i> /°	90
<i>V</i> /Å ³	1508.3(9)
<i>Z</i>	4
<i>D_c</i> / g cm ⁻³	1.296
<i>F</i> ₀₀₀	656
<i>μ</i> (Mo- <i>k</i> _α)/cm ⁻¹	0.96
Max. 2 <i>θ</i> (°) for reflections	50
Measured reflections	2928
Reflections with [<i>I</i> > 3 <i>σ</i> (<i>I</i>)]	1558
<i>R</i>	0.056
<i>wR</i>	0.057
Solution method	Direct Methods (SIR92)
No. of variables in LS	277
Density max in final ΔF -map (eÅ ⁻³)	0.25

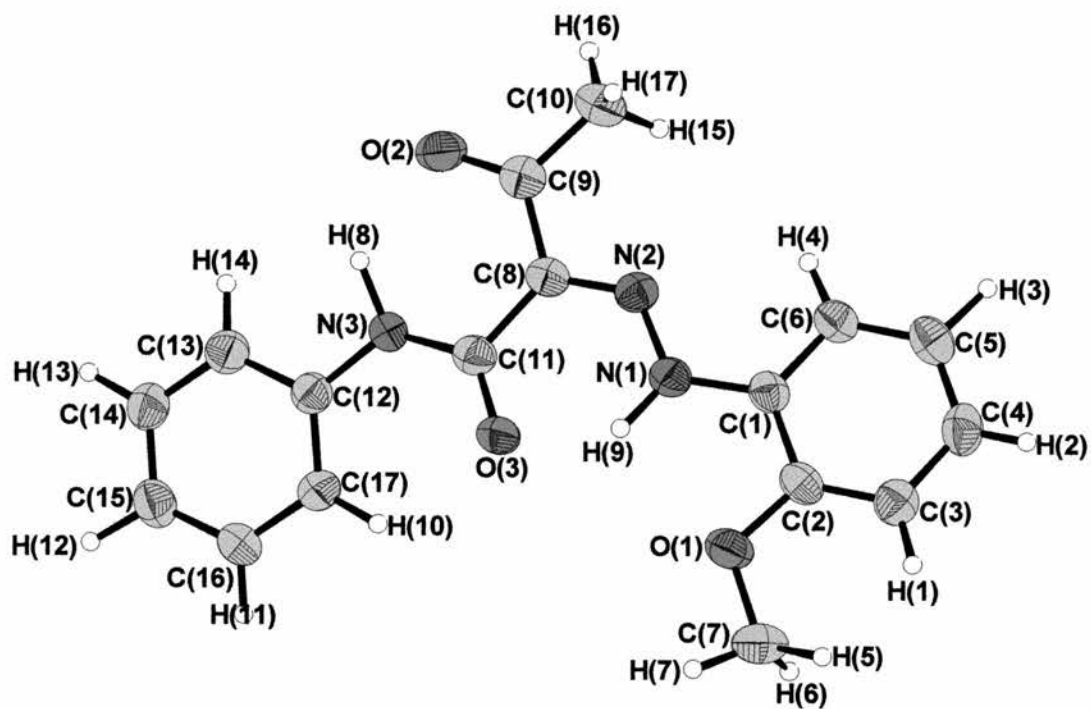


Figure 93 - ORTEP Diagram of (74)

Atomic Coordinates and Isotropic Displacement Parameters (in Å²)

Atom	x	y	Z	U _{eq}
O(1)	0.3077(2)	0.2864(6)	0.6789(1)	0.045(1)
O(2)	0.1075(3)	-0.7778(6)	0.5026(1)	0.050(1)
O(3)	0.1132(2)	-0.2256(6)	0.6343(1)	0.045(1)
N(1)	0.2832(3)	-0.0866(7)	0.6012(2)	0.037(1)
N(2)	0.2639(3)	-0.2672(7)	0.5609(1)	0.035(1)
N(3)	0.0451(3)	-0.6086(7)	0.6006(2)	0.038(1)
C(1)	0.3769(3)	0.0569(8)	0.6083(2)	0.034(1)
C(2)	0.3915(3)	0.2557(9)	0.6499(2)	0.036(1)
C(3)	0.4789(4)	0.4068(10)	0.6577(2)	0.041(2)
C(4)	0.5591(4)	0.353(1)	0.6259(2)	0.049(2)
C(5)	0.5469(4)	0.155(1)	0.5863(2)	0.047(2)
C(6)	0.4586(4)	0.002(1)	0.5782(2)	0.042(2)
C(7)	0.3205(5)	0.486(1)	0.7228(2)	0.050(2)
C(8)	0.1853(3)	-0.4204(8)	0.5578(2)	0.034(1)
C(9)	0.1766(4)	-0.6136(9)	0.5104(2)	0.039(1)
C(10)	0.2572(5)	-0.611(1)	0.4708(3)	0.051(2)
C(11)	0.1086(4)	-0.4070(9)	0.6001(2)	0.038(1)
C(12)	-0.0244(3)	-0.6539(9)	0.6403(2)	0.036(1)
C(13)	-0.0900(4)	-0.8603(10)	0.6277(2)	0.042(2)
C(14)	-0.1602(4)	-0.921(1)	0.6646(2)	0.047(2)
C(15)	-0.1619(4)	-0.7786(10)	0.7155(2)	0.046(2)
C(16)	-0.0956(4)	-0.575(1)	0.7283(2)	0.047(2)
C(17)	-0.0252(4)	-0.5116(10)	0.6917(2)	0.047(2)
H(1)	0.477(4)	0.558(10)	0.682(2)	0.08(2)
H(2)	0.616(3)	0.468(7)	0.629(2)	0.03(1)
H(3)	0.617(3)	0.115(8)	0.566(2)	0.04(1)
H(4)	0.448(4)	-0.15(1)	0.555(2)	0.09(2)
H(5)	0.356(4)	0.667(10)	0.713(2)	0.08(2)
H(6)	0.378(3)	0.451(8)	0.759(2)	0.04(1)
H(7)	0.243(4)	0.48(1)	0.729(2)	0.09(2)
H(8)	0.023(4)	-0.738(9)	0.563(2)	0.08(2)
H(9)	0.223(3)	-0.047(8)	0.623(2)	0.05(1)
H(10)	0.019(3)	-0.356(8)	0.702(2)	0.03(1)
H(11)	-0.096(3)	-0.477(9)	0.766(2)	0.06(1)
H(12)	-0.222(3)	-0.824(7)	0.740(2)	0.04(1)
H(13)	-0.203(3)	-1.083(8)	0.655(2)	0.04(1)
H(14)	-0.080(4)	-0.970(9)	0.595(2)	0.07(2)
H(15)	0.329(4)	-0.566(10)	0.495(2)	0.07(2)
H(16)	0.274(5)	-0.78(1)	0.459(3)	0.12(2)
H(17)	0.236(5)	-0.49(1)	0.441(3)	0.10(2)

Anisotropic Displacement Parameters (in Å²)

Atom	U_{11}	U_{22}	U_{33}	U_{12}	U_{13}	U_{23}
O(1)	0.053(2)	0.047(2)	0.041(2)	0.000(2)	0.021(2)	-0.003(2)
O(2)	0.067(2)	0.046(2)	0.041(2)	-0.009(2)	0.019(2)	-0.009(2)
O(3)	0.051(2)	0.042(2)	0.049(2)	-0.007(2)	0.025(2)	-0.013(2)
N(1)	0.041(2)	0.040(3)	0.033(2)	-0.002(2)	0.011(2)	0.000(2)
N(2)	0.041(2)	0.036(2)	0.028(2)	0.000(2)	0.006(2)	0.003(2)
N(3)	0.036(2)	0.041(3)	0.039(2)	-0.006(2)	0.014(2)	-0.006(2)
C(1)	0.038(3)	0.037(3)	0.030(3)	-0.001(2)	0.010(2)	0.007(2)
C(2)	0.039(3)	0.039(3)	0.033(3)	0.005(2)	0.013(2)	0.009(2)
C(3)	0.046(3)	0.037(3)	0.041(3)	-0.002(3)	0.010(2)	0.006(3)
C(4)	0.046(3)	0.049(4)	0.052(3)	-0.011(3)	0.012(3)	0.007(3)
C(5)	0.048(3)	0.052(3)	0.048(3)	-0.001(3)	0.021(3)	0.008(3)
C(6)	0.043(3)	0.045(3)	0.039(3)	0.000(3)	0.015(2)	0.001(3)
C(7)	0.071(4)	0.042(4)	0.040(3)	0.005(3)	0.018(3)	-0.003(3)
C(8)	0.036(3)	0.036(3)	0.030(2)	0.005(2)	0.007(2)	0.003(2)
C(9)	0.040(3)	0.041(3)	0.035(3)	0.006(2)	0.006(2)	0.004(2)
C(10)	0.055(4)	0.059(4)	0.042(3)	0.004(3)	0.020(3)	-0.002(3)
C(11)	0.039(3)	0.041(3)	0.033(3)	0.002(3)	0.009(2)	0.000(3)
C(12)	0.034(3)	0.036(3)	0.039(3)	0.001(2)	0.008(2)	-0.001(2)
C(13)	0.039(3)	0.039(3)	0.048(3)	0.002(3)	0.010(2)	-0.004(3)
C(14)	0.045(3)	0.042(3)	0.057(3)	-0.008(3)	0.015(3)	-0.005(3)
C(15)	0.045(3)	0.043(3)	0.056(3)	-0.002(3)	0.021(3)	0.003(3)
C(16)	0.042(3)	0.054(4)	0.051(3)	-0.002(3)	0.020(3)	-0.010(3)
C(17)	0.052(3)	0.043(3)	0.050(3)	-0.013(3)	0.020(3)	-0.014(3)

Bond Lengths

Atoms	Distance/Å
O(1)—C(2)	1.38(1)
O(1)—C(7)	1.442(6)
O(2)—C(9)	1.232(7)
O(3)—C(11)	1.234(6)
N(1)—N(2)	1.313(6)
N(1)—C(1)	1.403(6)
N(2)—C(8)	1.288(6)
N(3)—C(11)	1.353(6)
N(3)—C(12)	1.42(1)
C(1)—C(2)	1.404(7)
C(1)—C(6)	1.40(1)
C(2)—C(3)	1.360(7)
C(3)—C(4)	1.41(1)
C(4)—C(5)	1.373(7)
C(5)—C(6)	1.375(8)
C(8)—C(9)	1.475(7)
C(8)—C(11)	1.51(1)
C(9)—C(10)	1.51(1)
C(12)—C(13)	1.379(8)
C(12)—C(17)	1.391(7)
C(13)—C(14)	1.39(1)
C(14)—C(15)	1.384(7)
C(15)—C(16)	1.372(8)
C(16)—C(17)	1.39(1)

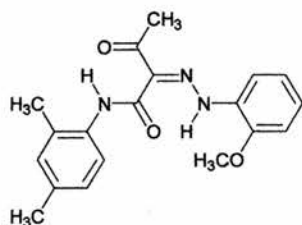
Bond Angles

C(2)—O(1)—C(7)	115.6(3)
N(2)—N(1)—C(1)	120.3(3)
N(1)—N(2)—C(8)	121.9(3)
C(11)—N(3)—C(12)	127.2(4)
N(1)—C(1)—C(2)	118.1(3)
N(1)—C(1)—C(6)	122.8(3)
C(2)—C(1)—C(6)	118.8(4)
O(1)—C(2)—C(1)	113.9(3)
O(1)—C(2)—C(3)	124.7(3)
C(1)—C(2)—C(3)	121.2(4)
C(2)—C(3)—C(4)	119.0(4)
C(3)—C(4)—C(5)	120.0(4)
C(4)—C(5)—C(6)	121.0(4)
C(1)—C(6)—C(5)	119.4(4)
N(2)—C(8)—C(9)	114.5(3)
N(2)—C(8)—C(11)	122.9(3)
C(9)—C(8)—C(11)	122.4(3)
O(2)—C(9)—C(8)	122.5(4)
O(2)—C(9)—C(10)	119.1(4)
C(8)—C(9)—C(10)	118.2(4)
O(3)—C(11)—N(3)	124.5(4)
O(3)—C(11)—C(8)	119.0(3)
N(3)—C(11)—C(8)	116.2(4)
N(3)—C(12)—C(13)	116.5(4)
N(3)—C(12)—C(17)	123.9(4)
C(13)—C(12)—C(17)	119.4(4)
C(12)—C(13)—C(14)	120.5(4)
C(13)—C(14)—C(15)	120.0(4)
C(14)—C(15)—C(16)	119.1(4)
C(15)—C(16)—C(17)	121.3(4)
C(12)—C(17)—C(16)	119.2(4)

Torsion Angles

Atoms	Angle/°
O(1)–C(2)–C(1)–N(1)	-0.7(6)
O(1)–C(2)–C(3)–C(4)	179.3(4)
O(2)–C(9)–C(8)–C(11)	-0.9(7)
O(3)–C(11)–C(8)–N(2)	8.7(7)
N(1)–N(2)–C(8)–C(9)	-179.2(4)
N(1)–C(1)–C(2)–C(3)	177.0(4)
N(2)–N(1)–C(1)–C(2)	8.7(7)
N(2)–C(8)–C(9)–C(10)	-0.8(6)
N(3)–C(11)–C(8)–C(9)	12.8(6)
N(3)–C(12)–C(17)–C(16)	-178.9(4)
C(1)–C(2)–O(1)–C(7)	178.9(4)
C(1)–C(6)–C(5)–C(4)	3.5(8)
C(2)–C(3)–C(4)–C(5)	2.0(7)
C(3)–C(2)–C(1)–C(6)	5.3(7)
C(8)–C(11)–N(3)–C(12)	172.7(4)
C(11)–N(3)–C(12)–C(13)	173.1(5)
C(12)–C(13)–C(14)–(15)	2.2(8)
C(13)–C(12)–C(17)–(16)	2.5(7)
C(14)–C(13)–C(12)–(17)	2.7(7)
O(1)–C(2)–C(1)–C(6)	-177.4(4)
O(2)–C(9)–C(8)–N(2)	178.1(4)
O(3)–C(11)–N(3)–C(12)	-1.9(8)
O(3)–C(11)–C(8)–C(9)	-172.3(4)
N(1)–N(2)–C(8)–C(11)	-0.1(6)
N(1)–C(1)–C(6)–C(5)	178.4(4)
N(2)–N(1)–C(1)–C(6)	-6.5(7)
N(2)–C(8)–C(11)–N(3)	-166.2(4)
N(3)–C(12)–C(13)–C(14)	179.4(4)
C(1)–N(1)–N(2)–C(8)	172.0(4)
C(1)–C(2)–C(3)–C(4)	-3.7(7)
C(2)–C(1)–C(6)–C(5)	-5.1(7)
C(3)–C(2)–O(1)–C(7)	-3.9(6)
C(3)–C(4)–C(5)–C(6)	-1.9(8)
C(10)–C(9)–C(8)–C(11)	-179.8(4)
C(11)–N(3)–C(12)–C(17)	-10.4(7)
C(12)–C(17)–C(16)–C(15)	1.8(8)
C(13)–C(14)–C(15)–C(16)	1.4(8)
C(14)–C(15)–C(16)–C(17)	-1.2(8)

2-[(2-Methoxyphenyl)hydrazono]-N-(2,4-dimethylphenyl)-3-oxo-butylamide (75)



(75)

Crystal data

Formula	C ₁₉ H ₂₁ N ₃ O ₃
<i>M</i>	339.39
Space group	<i>P</i> $\bar{1}$ (no. 2)
Crystal system	Triclinic
Temperature/K	293(1)
<i>a</i> /Å	8.514(2)
<i>b</i> /Å	13.463(3)
<i>c</i> /Å	8.456 (3)
α /°	98.14(3)
β /°	110.64(3)
γ /°	73.63(3)
<i>V</i> /Å ³	869.4(4)
<i>Z</i>	2
<i>D</i> _c / g cm ⁻³	1.296
<i>F</i> ₀₀₀	360
μ (Mo- <i>k</i> α)/cm ⁻¹	0.83
Max. 2 θ (°) for reflections	50
Measured reflections	3259
Reflections with [<i>I</i> > 3 σ (<i>I</i>)]	1968
<i>R</i>	0.104
<i>wR</i>	0.127
Solution method	Direct Methods (SIR92)
No. of variables in LS	234
Density max in final ΔF -map (eÅ ⁻³)	0.45

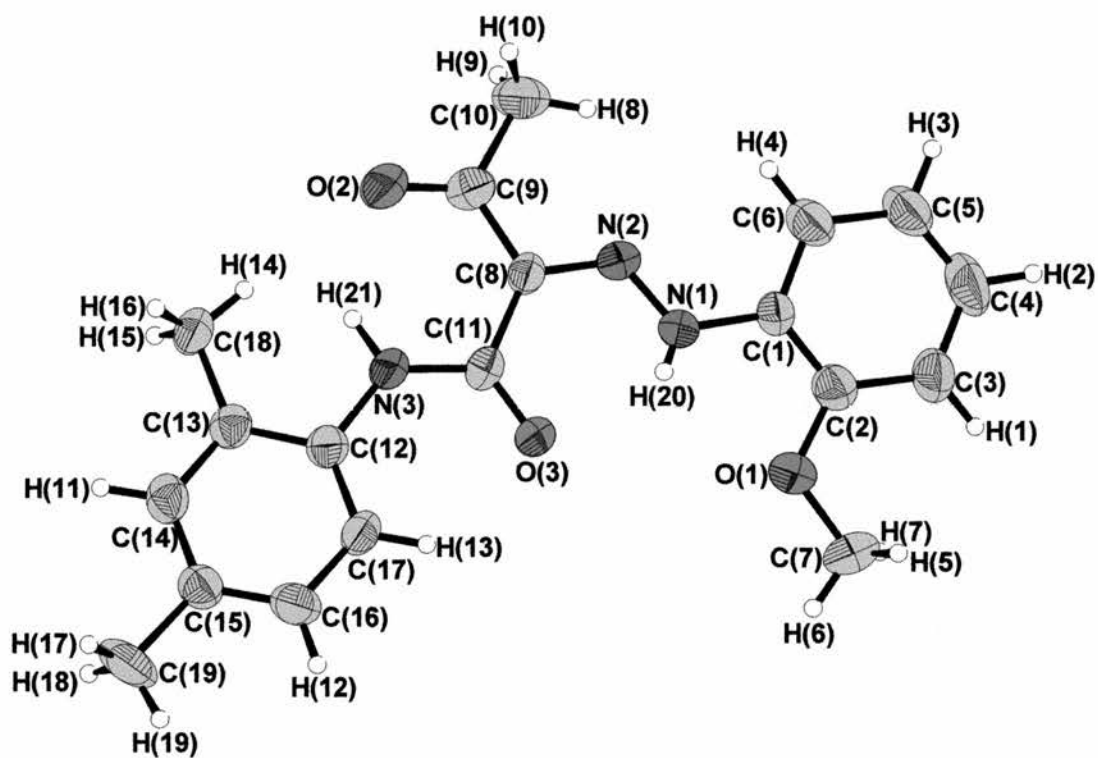


Figure 94 - ORTEP diagram for (75)

Atomic Coordinates and Isotropic Displacement Parameters (in Å²)

Atom	x	y	z	U _{eq}
O(1)	0.7470(8)	0.2799(5)	0.0274(9)	0.062(2)
O(2)	0.2109(9)	-0.0668(5)	-0.3367(10)	0.069(2)
O(3)	0.6709(7)	0.0295(4)	-0.1979(8)	0.049(2)
N(1)	0.507(1)	0.1781(6)	-0.039(1)	0.041(2)
N(2)	0.3774(8)	0.1355(5)	-0.0992(8)	0.039(2)
N(3)	0.5233(9)	-0.0885(5)	-0.3526(10)	0.044(2)
C(1)	0.494(1)	0.2710(6)	0.0594(10)	0.036(2)
C(2)	0.618(1)	0.3229(7)	0.096(1)	0.047(3)
C(3)	0.614(1)	0.4143(7)	0.201(1)	0.059(3)
C(4)	0.474(2)	0.4514(7)	0.260(1)	0.070(4)
C(5)	0.348(1)	0.4009(7)	0.219(1)	0.058(3)
C(6)	0.354(1)	0.3089(7)	0.119(1)	0.051(3)
C(7)	0.877(1)	0.3343(8)	0.057(1)	0.067(4)
C(8)	0.3846(10)	0.0495(6)	-0.196(1)	0.036(2)
C(9)	0.229(1)	0.0121(7)	-0.247(1)	0.045(3)
C(10)	0.077(1)	0.0751(8)	-0.191(2)	0.071(4)
C(11)	0.541(1)	-0.0032(6)	-0.2489(10)	0.037(2)
C(12)	0.648(1)	-0.1576(6)	-0.424(1)	0.040(2)
C(13)	0.587(1)	-0.2352(6)	-0.537(1)	0.040(2)
C(14)	0.703(1)	-0.3057(6)	-0.608(1)	0.046(3)
C(15)	0.873(1)	-0.2981(6)	-0.564(1)	0.044(3)
C(16)	0.927(1)	-0.2204(7)	-0.455(1)	0.054(3)
C(17)	0.814(1)	-0.1486(6)	-0.381(1)	0.046(3)
C(18)	0.405(1)	-0.2461(6)	-0.583(1)	0.049(3)
C(19)	0.994(2)	-0.3768(8)	-0.646(2)	0.080(4)
H(1)	0.70360	0.44930	0.23100	0.0711
H(2)	0.46680	0.51310	0.33060	0.0840
H(3)	0.25180	0.42880	0.25840	0.0692
H(4)	0.26570	0.27310	0.09330	0.0613
H(5)	0.93540	0.34080	0.17470	0.0800
H(6)	0.95780	0.29710	0.00200	0.0800
H(7)	0.82420	0.40130	0.01250	0.0800
H(8)	0.10810	0.13350	-0.12230	0.0852
H(9)	-0.02020	0.09790	-0.28760	0.0852
H(10)	0.04980	0.03340	-0.12790	0.0852
H(11)	0.66590	-0.35920	-0.68580	0.0550
H(12)	1.04260	-0.21470	-0.42830	0.0644
H(13)	0.85210	-0.09510	-0.30360	0.0547
H(14)	0.34370	-0.19350	-0.52420	0.0594
H(15)	0.34880	-0.23950	-0.70170	0.0594
H(16)	0.40850	-0.31220	-0.55330	0.0594
H(17)	1.00420	-0.44480	-0.61890	0.0966
H(18)	0.94840	-0.37150	-0.76560	0.0966
H(19)	1.10550	-0.36270	-0.60520	0.0966
H(20)	0.578(9)	0.159(6)	-0.06(1)	0.02(3)
H(21)	0.420(9)	-0.105(5)	-0.402(9)	0.03(2)

Anisotropic Displacement Parameters (in Å²)

Atom	U_{11}	U_{22}	U_{33}	U_{12}	U_{13}	U_{23}
O(1)	0.059(4)	0.062(4)	0.084(5)	-0.025(3)	0.045(4)	-0.022(4)
O(2)	0.060(4)	0.053(4)	0.113(6)	-0.030(3)	0.046(4)	-0.027(4)
O(3)	0.038(3)	0.047(4)	0.067(4)	-0.019(3)	0.024(3)	-0.018(3)
N(1)	0.035(5)	0.044(5)	0.050(5)	-0.013(4)	0.020(4)	-0.010(4)
N(2)	0.036(4)	0.041(4)	0.043(4)	-0.013(3)	0.015(3)	0.001(3)
N(3)	0.042(4)	0.036(4)	0.061(5)	-0.018(3)	0.022(4)	-0.011(4)
C(1)	0.039(5)	0.032(4)	0.036(5)	-0.008(4)	0.011(4)	-0.002(4)
C(2)	0.051(6)	0.041(5)	0.053(6)	-0.010(4)	0.023(5)	-0.002(4)
C(3)	0.082(7)	0.044(5)	0.066(7)	-0.027(5)	0.037(6)	-0.015(5)
C(4)	0.100(9)	0.038(5)	0.079(8)	-0.010(6)	0.048(7)	-0.016(5)
C(5)	0.067(7)	0.045(6)	0.068(7)	-0.005(5)	0.040(6)	-0.006(5)
C(6)	0.056(6)	0.044(5)	0.059(6)	-0.006(4)	0.031(5)	-0.002(5)
C(7)	0.053(6)	0.077(7)	0.087(8)	-0.035(6)	0.031(6)	-0.007(6)
C(8)	0.035(4)	0.032(4)	0.042(5)	-0.011(4)	0.011(4)	-0.004(4)
C(9)	0.040(5)	0.046(5)	0.053(6)	-0.013(4)	0.015(4)	0.006(5)
C(10)	0.063(7)	0.058(6)	0.115(10)	-0.019(5)	0.056(7)	-0.009(6)
C(11)	0.040(5)	0.031(4)	0.039(5)	-0.014(4)	0.009(4)	0.000(4)
C(12)	0.041(5)	0.032(4)	0.051(6)	-0.009(4)	0.018(4)	0.000(4)
C(13)	0.046(5)	0.034(5)	0.042(5)	-0.013(4)	0.015(4)	0.003(4)
C(14)	0.060(6)	0.033(5)	0.050(6)	-0.014(4)	0.022(5)	-0.001(4)
C(15)	0.047(5)	0.040(5)	0.047(5)	-0.009(4)	0.020(4)	0.001(4)
C(16)	0.055(6)	0.047(5)	0.072(7)	-0.012(5)	0.038(5)	-0.002(5)
C(17)	0.037(5)	0.041(5)	0.058(6)	-0.017(4)	0.012(4)	-0.010(4)
C(18)	0.045(5)	0.043(5)	0.062(6)	-0.020(4)	0.016(5)	-0.013(5)
C(19)	0.102(9)	0.058(7)	0.11(1)	-0.014(6)	0.086(8)	-0.015(7)

Bond Lengths

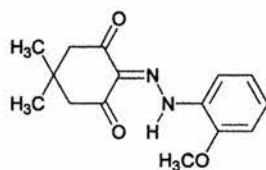
Atoms	Distance/Å
O(1)—C(2)	1.36(1)
O(1)—C(7)	1.42(1)
O(2)—C(9)	1.22(2)
O(3)—C(11)	1.22(1)
N(1)—N(2)	1.295(9)
N(1)—C(1)	1.40(2)
N(2)—C(8)	1.32(2)
N(3)—C(11)	1.35(2)
N(3)—C(12)	1.44(2)
C(1)—C(2)	1.35(1)
C(1)—C(6)	1.39(1)
C(2)—C(3)	1.41(2)
C(3)—C(4)	1.39(2)
C(4)—C(5)	1.34(2)
C(5)—C(6)	1.39(2)
C(8)—C(9)	1.45(1)
C(8)—C(11)	1.50(2)
C(9)—C(10)	1.52(2)
C(12)—C(13)	1.39(2)
C(12)—C(17)	1.36(1)
C(13)—C(14)	1.40(2)
C(13)—C(18)	1.50(1)
C(14)—C(15)	1.39(1)
C(15)—C(16)	1.36(2)
C(15)—C(19)	1.53(2)
C(16)—C(17)	1.40(2)

Bond Angles

Atoms	Angle ^o
C(2)—O(1)—C(7)	117.5(7)
N(2)—N(1)—C(1)	120.7(7)
N(1)—N(2)—C(8)	121.9(7)
C(11)—N(3)—C(12)	128.4(6)
N(1)—C(1)—C(2)	119.4(7)
N(1)—C(1)—C(6)	119.9(7)
C(2)—C(1)—C(6)	120.6(8)
O(1)—C(2)—C(1)	115.5(8)
O(1)—C(2)—C(3)	123.1(7)
C(1)—C(2)—C(3)	121.2(8)
C(2)—C(3)—C(4)	117.6(8)
C(3)—C(4)—C(5)	120(1)
C(4)—C(5)—C(6)	121.7(8)
C(1)—C(6)—C(5)	117.8(7)
N(2)—C(8)—C(9)	113.9(7)
N(2)—C(8)—C(11)	122.2(7)
C(9)—C(8)—C(11)	123.8(8)
O(2)—C(9)—C(8)	123.6(8)
O(2)—C(9)—C(10)	117.6(8)
C(8)—C(9)—C(10)	118.6(8)
O(3)—C(11)—N(3)	124.6(7)
O(3)—C(11)—C(8)	121.2(8)
N(3)—C(11)—C(8)	114.0(7)
N(3)—C(12)—C(13)	114.9(6)
N(3)—C(12)—C(17)	122.3(8)
C(13)—C(12)—C(17)	122.6(8)
C(12)—C(13)—C(14)	117.5(7)
C(12)—C(13)—C(18)	122.8(7)
C(14)—C(13)—C(18)	119.6(8)
C(13)—C(14)—C(15)	120.3(8)
C(14)—C(15)—C(16)	120.3(8)
C(14)—C(15)—C(19)	118.1(9)
C(16)—C(15)—C(19)	121.4(7)
C(15)—C(16)—C(17)	120.7(7)
C(12)—C(17)—C(16)	118.3(8)

Torsion Angles

Atoms	Angle/°
O(1)—C(2)—C(1)—N(1)	1(1)
O(1)—C(2)—C(3)—C(4)	178.7(9)
O(2)—C(9)—C(8)—C(11)	0(1)
O(3)—C(11)—C(8)—N(2)	3(1)
N(1)—N(2)—C(8)—C(9)	178.3(8)
N(1)—C(1)—C(2)—C(3)	-177.1(8)
N(2)—N(1)—C(1)—C(2)	-168.7(8)
N(2)—C(8)—C(9)—C(10)	1(1)
N(3)—C(11)—C(8)—C(9)	1(1)
N(3)—C(12)—C(13)—C(14)	-178.9(7)
C(1)—N(1)—N(2)—C(8)	178.1(8)
C(1)—C(2)—C(3)—C(4)	-2(1)
C(2)—C(1)—C(6)—C(5)	0(1)
C(3)—C(2)—O(1)—C(7)	-3(1)
C(3)—C(4)—C(5)—C(6)	1(1)
C(10)—C(9)—C(8)—C(11)	-177.4(9)
C(11)—N(3)—C(12)—C(17)	5(1)
C(12)—C(17)—C(16)—C(15)	-1(1)
C(13)—C(14)—C(15)—C(16)	-1(1)
C(14)—C(13)—C(12)—C(17)	0(1)
C(15)—C(14)—C(13)—C(18)	-178.6(8)
C(17)—C(16)—C(15)—C(19)	179(1)
O(1)—C(2)—C(1)—C(6)	-178.4(8)
O(2)—C(9)—C(8)—N(2)	-179.8(8)
O(3)—C(11)—N(3)—C(12)	0(1)
O(3)—C(11)—C(8)—C(9)	-177.5(8)
N(1)—N(2)—C(8)—C(11)	-2(1)
N(1)—C(1)—C(6)—C(5)	178.9(8)
N(2)—N(1)—C(1)—C(6)	11(1)
N(2)—C(8)—C(11)—N(3)	-177.9(8)
N(3)—C(12)—C(17)—C(16)	179.0(8)
C(1)—C(2)—O(1)—C(7)	177.5(8)
C(1)—C(6)—C(5)—C(4)	-1(1)
C(2)—C(3)—C(4)—C(5)	0(1)
C(3)—C(2)—C(1)—C(6)	2(1)
C(8)—C(11)—N(3)—C(12)	-178.9(8)
C(11)—N(3)—C(12)—C(13)	-175.6(8)
C(12)—C(13)—C(14)—C(15)	0(1)
C(13)—C(12)—C(17)—C(16)	0(1)
C(13)—C(14)—C(15)—C(19)	-179.7(9)
C(14)—C(15)—C(16)—C(17)	2(1)
C(17)—C(12)—C(13)—C(18)	179.2(8)

2-[(2-Methoxyphenyl)hydrazono]-5,5-dimethylcyclohexane-1,3-dione

(71)

Crystal data

Formula	C ₁₅ H ₁₈ N ₂ O ₃
<i>M</i>	274.32
Space group	<i>P</i> 2 ₁ / n (no. 14)
Crystal system	Monoclinic
Temperature/K	293(1)
<i>a</i> /Å	11.418(4)
<i>b</i> /Å	11.515(4)
<i>c</i> /Å	12.320 (4)
α /°	90
β /°	116.28(2)
γ /°	90
<i>V</i> /Å ³	1452.3(9)
<i>Z</i>	4
<i>D</i> _c / g cm ⁻³	1.254
<i>F</i> ₀₀₀	584
μ (Mo- <i>k</i> _α)/cm ⁻¹	0.88
Max. 2θ (°) for reflections	50
Measured reflections	2840
Reflections with [<i>I</i> > 3σ (<i>I</i>)]	1728
<i>R</i>	0.050
<i>wR</i>	0.054
Solution method	Direct Methods (SIR92)
No. of variables in LS	254
Density max in final Δ <i>F</i> -map (eÅ ⁻³)	0.18

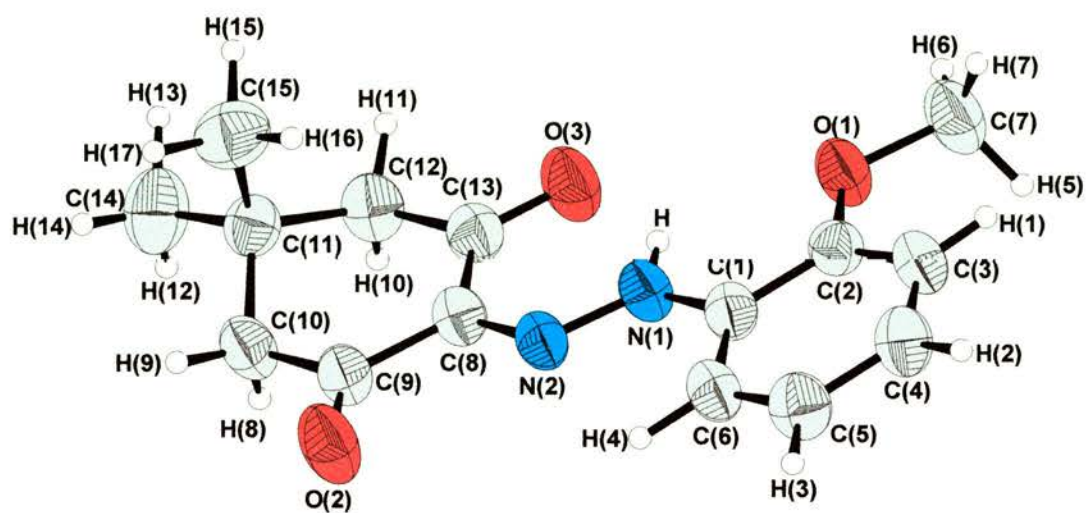


Figure 95 - ORTEP diagram of (71)

Atomic Coordinates and Isotropic Displacement Parameters (in Å²)

Atom	x	y	z	U _{eq}
O(1)	0.4098(2)	0.2575(2)	0.1163(2)	0.0572(7)
O(2)	0.4098(2)	-0.3162(2)	0.0796(3)	0.0733(8)
O(3)	0.1665(2)	0.0307(2)	-0.0344(2)	0.0674(8)
N(1)	0.4162(3)	0.0313(2)	0.0928(2)	0.0477(8)
N(2)	0.4126(3)	-0.0824(2)	0.0874(2)	0.0455(8)
C(1)	0.5349(3)	0.0887(3)	0.1619(3)	0.0437(9)
C(2)	0.5310(3)	0.2091(3)	0.1740(3)	0.0440(9)
C(3)	0.6446(4)	0.2677(3)	0.2439(3)	0.051(1)
C(4)	0.7621(4)	0.2099(3)	0.2986(3)	0.055(1)
C(5)	0.7658(4)	0.0905(3)	0.2841(3)	0.056(1)
C(6)	0.6522(3)	0.0301(3)	0.2162(3)	0.049(1)
C(7)	0.4032(5)	0.3818(3)	0.1120(5)	0.067(1)
C(8)	0.2989(3)	-0.1358(3)	0.0273(3)	0.0443(9)
C(9)	0.3066(3)	-0.2646(3)	0.0302(3)	0.0476(9)
C(10)	0.1803(4)	-0.3290(3)	-0.0338(4)	0.055(1)
C(11)	0.0616(3)	-0.2685(3)	-0.0340(3)	0.0481(9)
C(12)	0.0513(3)	-0.1478(3)	-0.0891(3)	0.056(1)
C(13)	0.1730(3)	-0.0766(3)	-0.0314(3)	0.048(1)
C(14)	-0.0635(5)	-0.3369(5)	-0.1108(5)	0.076(2)
C(15)	0.0751(5)	-0.2582(5)	0.0950(4)	0.070(1)
H	0.337(3)	0.070(3)	0.051(3)	0.05(1)
H(1)	0.640(3)	0.346(3)	0.255(3)	0.05(1)
H(2)	0.844(3)	0.250(3)	0.352(3)	0.06(1)
H(3)	0.852(3)	0.053(3)	0.322(3)	0.06(1)
H(4)	0.652(3)	-0.055(3)	0.201(3)	0.052(9)
H(5)	0.472(4)	0.413(4)	0.078(4)	0.11(2)
H(6)	0.310(3)	0.398(3)	0.064(3)	0.07(1)
H(7)	0.436(4)	0.416(3)	0.198(4)	0.09(1)
H(8)	0.166(4)	-0.334(3)	-0.114(3)	0.09(1)
H(9)	0.196(3)	-0.403(3)	0.005(3)	0.08(1)
H(10)	0.032(4)	-0.158(4)	-0.173(4)	0.09(1)
H(11)	-0.024(3)	-0.097(3)	-0.089(3)	0.07(1)
H(12)	-0.073(4)	-0.345(4)	-0.192(4)	0.09(2)
H(13)	-0.160(5)	-0.290(4)	-0.118(4)	0.14(2)
H(14)	-0.058(4)	-0.411(4)	-0.081(4)	0.11(2)
H(15)	-0.007(4)	-0.218(4)	0.094(4)	0.10(2)
H(16)	0.154(3)	-0.214(3)	0.150(3)	0.07(1)
H(17)	0.090(4)	-0.339(4)	0.134(4)	0.10(1)

Anisotropic Displacement Parameters (in Å²)

Atom	U_{11}	U_{22}	U_{33}	U_{12}	U_{13}	U_{23}
O(1)	0.052(1)	0.036(1)	0.074(2)	0.002(1)	0.020(1)	0.000(1)
O(2)	0.056(2)	0.042(1)	0.102(2)	0.005(1)	0.017(1)	0.002(1)
O(3)	0.062(2)	0.040(1)	0.089(2)	0.007(1)	0.024(1)	0.008(1)
N(1)	0.053(2)	0.035(1)	0.048(2)	0.000(1)	0.022(1)	0.000(1)
N(2)	0.051(2)	0.036(1)	0.052(2)	0.002(1)	0.019(1)	0.001(1)
C(1)	0.051(2)	0.039(2)	0.040(2)	-0.004(1)	0.020(2)	-0.001(1)
C(2)	0.049(2)	0.041(2)	0.044(2)	0.001(1)	0.022(2)	0.002(1)
C(3)	0.060(3)	0.036(2)	0.055(2)	-0.003(2)	0.023(2)	-0.005(2)
C(4)	0.056(2)	0.048(2)	0.052(2)	-0.008(2)	0.016(2)	-0.001(2)
C(5)	0.052(2)	0.052(2)	0.055(2)	0.004(2)	0.016(2)	0.006(2)
C(6)	0.058(2)	0.036(2)	0.052(2)	0.001(2)	0.023(2)	0.001(2)
C(7)	0.065(3)	0.039(2)	0.087(3)	0.008(2)	0.024(3)	0.004(2)
C(8)	0.047(2)	0.039(2)	0.042(2)	-0.002(1)	0.016(1)	-0.001(1)
C(9)	0.048(2)	0.040(2)	0.052(2)	-0.001(2)	0.019(2)	-0.001(2)
C(10)	0.059(2)	0.040(2)	0.063(2)	-0.003(2)	0.024(2)	-0.008(2)
C(11)	0.047(2)	0.049(2)	0.046(2)	-0.006(2)	0.018(1)	-0.001(2)
C(12)	0.048(2)	0.053(2)	0.055(2)	0.002(2)	0.013(2)	0.005(2)
C(13)	0.050(2)	0.043(2)	0.053(2)	0.001(2)	0.023(2)	0.002(2)
C(14)	0.062(3)	0.072(3)	0.075(3)	-0.02(2)	0.014(2)	-0.001(3)
C(15)	0.076(3)	0.082(3)	0.059(2)	0.003(3)	0.035(2)	0.005(2)

Bond Lengths

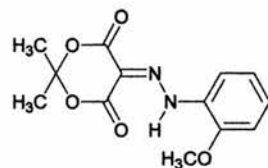
Atoms	Distance/Å
(1)—C(2)	1.36(1)
O(1)—C(7)	1.433(4)
O(2)—C(9)	1.21(1)
O(3)—C(13)	1.237(4)
N(1)—N(2)	1.311(3)
N(1)—C(1)	1.40(1)
N(2)—C(8)	1.32(1)
C(1)—C(2)	1.397(5)
C(1)—C(6)	1.38(1)
C(2)—C(3)	1.37(1)
C(3)—C(4)	1.37(1)
C(4)—C(5)	1.389(5)
C(5)—C(6)	1.38(5)
C(8)—C(9)	1.485(5)
C(8)—C(13)	1.46(1)
C(9)—C(10)	1.49(1)
C(10)—C(11)	1.523(6)
C(11)—C(12)	1.528(5)
C(11)—C(14)	1.53(1)
C(11)—C(15)	1.532(7)
C(12)—C(13)	1.49(1)

Bond Angles

Atoms	Angle/°
C(2)—O(1)—C(7)	116.8(2)
N(2)—N(1)—C(1)	120.0(2)
N(1)—N(2)—C(8)	119.4(2)
N(1)—C(1)—C(2)	117.6(3)
N(1)—C(1)—C(6)	122.1(3)
C(2)—C(1)—C(6)	120.2(3)
O(1)—C(2)—C(1)	115.0(3)
O(1)—C(2)—C(3)	125.7(3)
C(1)—C(2)—C(3)	119.2(3)
C(2)—C(3)—C(4)	120.9(3)
C(3)—C(4)—C(5)	119.5(3)
C(4)—C(5)—C(6)	120.1(3)
C(1)—C(6)—C(5)	119.8(3)
N(2)—C(8)—C(9)	114.6(2)
N(2)—C(8)—C(13)	124.4(3)
C(9)—C(8)—C(13)	120.8(3)
O(2)—C(9)—C(8)	122.2(3)
O(2)—C(9)—C(10)	121.0(3)
C(8)—C(9)—C(10)	116.6(3)
C(9)—C(10)—C(11)	115.0(3)
C(10)—C(11)—C(12)	108.0(2)
C(10)—C(11)—C(14)	110.5(3)
C(10)—C(11)—C(15)	110.6(3)
C(12)—C(11)—C(14)	108.9(3)
C(12)—C(11)—C(15)	110.0(3)
C(14)—C(11)—C(15)	108.5(3)
C(11)—C(12)—C(13)	114.5(2)
O(3)—C(13)—C(8)	120.9(3)
O(3)—C(13)—C(12)	120.1(3)
C(8)—C(13)—C(12)	118.9(3)

Torsion Angles

Atoms	Angle/°
O(1)—C(2)—C(1)—N(1)	0.2(5)
O(1)—C(2)—C(3)—C(4)	179.8(3)
O(2)—C(9)—C(8)—C(13)	-179.1(3)
O(3)—C(13)—C(8)—N(2)	4.5(6)
O(3)—C(13)—C(12)—C(11)	-153.6(3)
N(1)—N(2)—C(8)—C(13)	-2.4(5)
N(1)—C(1)—C(6)—C(5)	-179.4(3)
N(2)—N(1)—C(1)—C(6)	6.3(5)
N(2)—C(8)—C(13)—C(12)	-175.9(3)
C(1)—C(2)—O(1)—C(7)	-171.6(3)
C(1)—C(6)—C(5)—C(4)	0.5(6)
C(2)—C(3)—C(4)—C(5)	-0.7(6)
C(3)—C(2)—C(1)—C(6)	-2.2(5)
C(8)—C(9)—C(10)—C(11)	-31.6(5)
C(9)—C(8)—C(13)—C(12)	-0.1(5)
C(9)—C(10)—C(11)—C(14)	175.2(4)
C(10)—C(9)—C(8)—C(13)	2.3(5)
C(13)—C(12)—C(11)—C(14)	-173.4(3)
O(1)—C(2)—C(1)—C(6)	179.9(3)
O(2)—C(9)—C(8)—N(2)	-2.9(5)
O(2)—C(9)—C(10)—C(11)	149.8(4)
O(3)—C(13)—C(8)—C(9)	-179.6(3)
N(1)—N(2)—C(8)—C(9)	-178.5(3)
N(1)—C(1)—C(2)—C(3)	178.1(3)
N(2)—N(1)—C(1)—C(2)	-174.0(3)
N(2)—C(8)—C(9)—C(10)	178.5(3)
C(1)—N(1)—N(2)—C(8)	176.4(3)
C(1)—C(2)—C(3)—C(4)	2.1(6)
C(2)—C(1)—C(6)—C(5)	0.9(5)
C(3)—C(2)—O(1)—C(7)	10.7(5)
C(3)—C(4)—C(5)—C(6)	-0.6(6)
C(8)—C(13)—C(12)—C(11)	26.9(5)
C(9)—C(10)—C(11)—C(12)	56.1(4)
C(9)—C(10)—C(11)—C(15)	-64.5(5)
C(10)—C(11)—C(12)—C(13)	-53.2(4)
C(13)—C(12)—C(11)—C(15)	67.7(4)

5-[(2-methoxyphenyl)hydrazono]-2,2-dimethyl-1,3-dioxan-4,6-dione**(72)****(72)****Crystal Data**

Formula	C ₁₃ H ₁₄ N ₂ O ₅
<i>M</i>	278.26
Space group	<i>C</i> 2 / <i>c</i> (no.15)
Crystal system	Monoclinic
Temperature/K	298(2)
<i>a</i> /Å	26.87(1)
<i>b</i> /Å	10.656(7)
<i>c</i> /Å	9.631(6)
<i>α</i> /°	90
<i>β</i> /°	100.56(1)
<i>γ</i> /°	90
<i>V</i> /Å ³	2711(3)
<i>Z</i>	8
<i>D</i> _c / g cm ⁻³	1.363
<i>F</i> ₀₀₀	1168
<i>μ</i> (Mo- <i>k</i> _α)/cm ⁻¹	1.06
Measured reflections	5573
Reflections [<i>I</i> > 2σ (<i>I</i>)]	1881
<i>R</i>	0.1180
<i>wR</i>	0.3907
Solution method	SHELX-97
Density max in final Δ <i>F</i> -map (eÅ ⁻³)	0.66

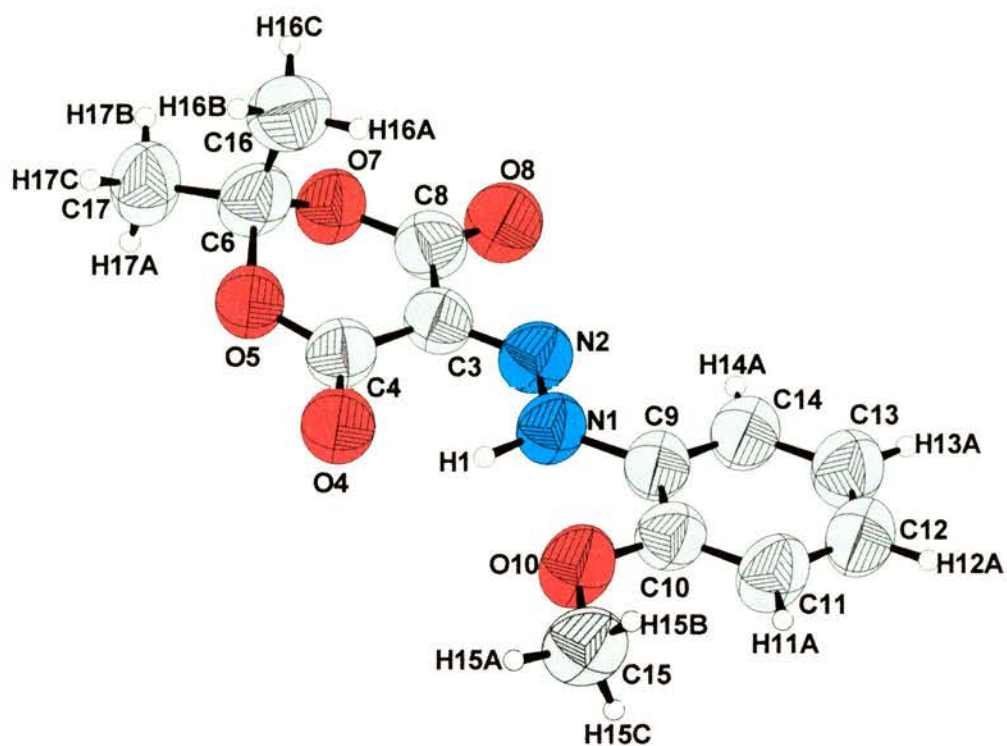


Figure 96 - ORTEP Diagram of (72)

Atomic Coordinates and Isotropic Displacement Parameters (in Å²)

Atom	x	y	z	U _{eq}
N1	0.3991(1)	0.3964(4)	0.2208(5)	0.082(1)
H1	0.415(1)	0.470(3)	0.187(5)	0.09(1)
N2	0.3667(1)	0.4227(4)	0.3023(4)	0.083(1)
C3	0.3536(1)	0.5396(5)	0.3198(5)	0.075(1)
C4	0.3727(2)	0.6488(5)	0.2549(6)	0.083(1)
O4	0.4067(1)	0.6441(3)	0.1866(5)	0.097(1)
O5	0.3526(1)	0.7607(3)	0.2766(4)	0.094(1)
C6	0.3047(2)	0.7665(5)	0.3270(6)	0.090(1)
O7	0.3052(1)	0.6781(3)	0.4407(4)	0.086(1)
C8	0.3191(2)	0.5575(5)	0.4216(6)	0.084(1)
O8	0.3058(1)	0.4757(4)	0.4929(4)	0.101(1)
C9	0.4120(2)	0.2702(5)	0.2003(6)	0.081(1)
C10	0.4441(2)	0.2462(5)	0.1044(6)	0.082(1)
O10	0.4618(1)	0.3502(3)	0.0439(5)	0.102(1)
C11	0.4571(2)	0.1235(5)	0.0773(7)	0.095(1)
H11A	0.47850	0.10610	0.01410	0.1150
C12	0.4368(3)	0.0269(6)	0.1479(8)	0.105(2)
H12A	0.44470	-0.05580	0.12990	0.1260
C13	0.4058(3)	0.0497(5)	0.2420(7)	0.100(2)
H13A	0.39310	-0.01630	0.28840	0.1200
C14	0.3935(2)	0.1722(5)	0.2678(7)	0.094(1)
H14A	0.37230	0.18850	0.33200	0.1130
C15	0.4989(2)	0.3317(6)	-0.0444(7)	0.105(2)
H15A	0.50840	0.41140	-0.07780	0.1580
H15B	0.48470	0.28000	-0.12340	0.1580
H15C	0.52810	0.29120	0.00900	0.1580
C16	0.2617(2)	0.7356(6)	0.2081(7)	0.111(2)
H16A	0.26590	0.65200	0.17510	0.1670
H16B	0.26150	0.79410	0.13220	0.1670
H16C	0.23020	0.74120	0.24140	0.1670
C17	0.3021(3)	0.8947(5)	0.3912(8)	0.107(2)
H17A	0.33080	0.90620	0.46590	0.1600
H17B	0.27150	0.90190	0.42870	0.1600
H17C	0.30250	0.95760	0.32010	0.1600

Anisotropic Displacement Parameters (in Å²)

Atom	U_{11}	U_{22}	U_{33}	U_{12}	U_{13}	U_{23}
N1	0.089(3)	0.077(3)	0.087(3)	0.007(2)	0.033(3)	0.003(2)
N2	0.088(3)	0.089(3)	0.080(3)	0.007(2)	0.031(2)	0.002(2)
C3	0.076(3)	0.078(3)	0.077(3)	-0.003(2)	0.025(3)	0.004(2)
C4	0.083(4)	0.081(4)	0.092(4)	0.003(3)	0.032(3)	-0.003(3)
O4	0.099(3)	0.090(3)	0.115(3)	0.0004(19)	0.050(3)	0.002(2)
O5	0.092(3)	0.077(2)	0.126(3)	0.0005(18)	0.052(2)	0.001(2)
C6	0.094(4)	0.088(4)	0.099(4)	0.013(3)	0.041(3)	-0.001(3)
O7	0.097(3)	0.080(2)	0.092(3)	0.005(1)	0.038(2)	-0.001(1)
C8	0.080(3)	0.087(4)	0.089(4)	-0.001(3)	0.025(3)	-0.005(3)
O8	0.109(3)	0.100(3)	0.105(3)	0.003(2)	0.048(2)	0.013(2)
C9	0.083(3)	0.069(3)	0.096(4)	0.002(2)	0.024(3)	0.001(3)
C10	0.081(3)	0.082(4)	0.090(4)	0.005(3)	0.026(3)	0.006(3)
O10	0.120(3)	0.091(3)	0.112(3)	0.014(2)	0.063(3)	0.011(2)
C11	0.108(4)	0.084(4)	0.106(5)	0.017(3)	0.050(4)	-0.001(3)
C12	0.110(5)	0.077(4)	0.131(5)	0.009(3)	0.032(4)	0.001(3)
C13	0.106(4)	0.085(4)	0.118(5)	0.004(3)	0.042(4)	0.006(3)
C14	0.095(4)	0.078(4)	0.114(5)	0.006(3)	0.029(3)	0.004(3)
C15	0.107(5)	0.116(5)	0.105(5)	0.013(3)	0.051(4)	0.008(3)
C16	0.099(4)	0.116(5)	0.121(5)	0.009(3)	0.025(4)	0.003(4)
C17	0.123(5)	0.078(4)	0.135(5)	0.002(3)	0.065(4)	-0.006(4)

Bond Lengths

Atoms	Distance/Å
N1—N2	1.30(1)
N1—C9	1.411(7)
N2—C3	1.314(7)
C3—C4	1.458(8)
C3—C8	1.48(1)
C4—O4	1.22(1)
C4—O5	1.341(7)
O5—C6	1.459(9)
C6—O7	1.442(7)
C6—C16	1.50(1)
C6—C17	1.506(8)
O7—C8	1.359(6)
C8—O8	1.203(8)
C9—C14	1.371(9)
C9—C10	1.39(1)
C10—O10	1.378(7)
C10—C11	1.390(8)
O10—C15	1.43(1)
C11—C12	1.39(1)
C12—C13	1.36(1)
C13—C14	1.380(8)

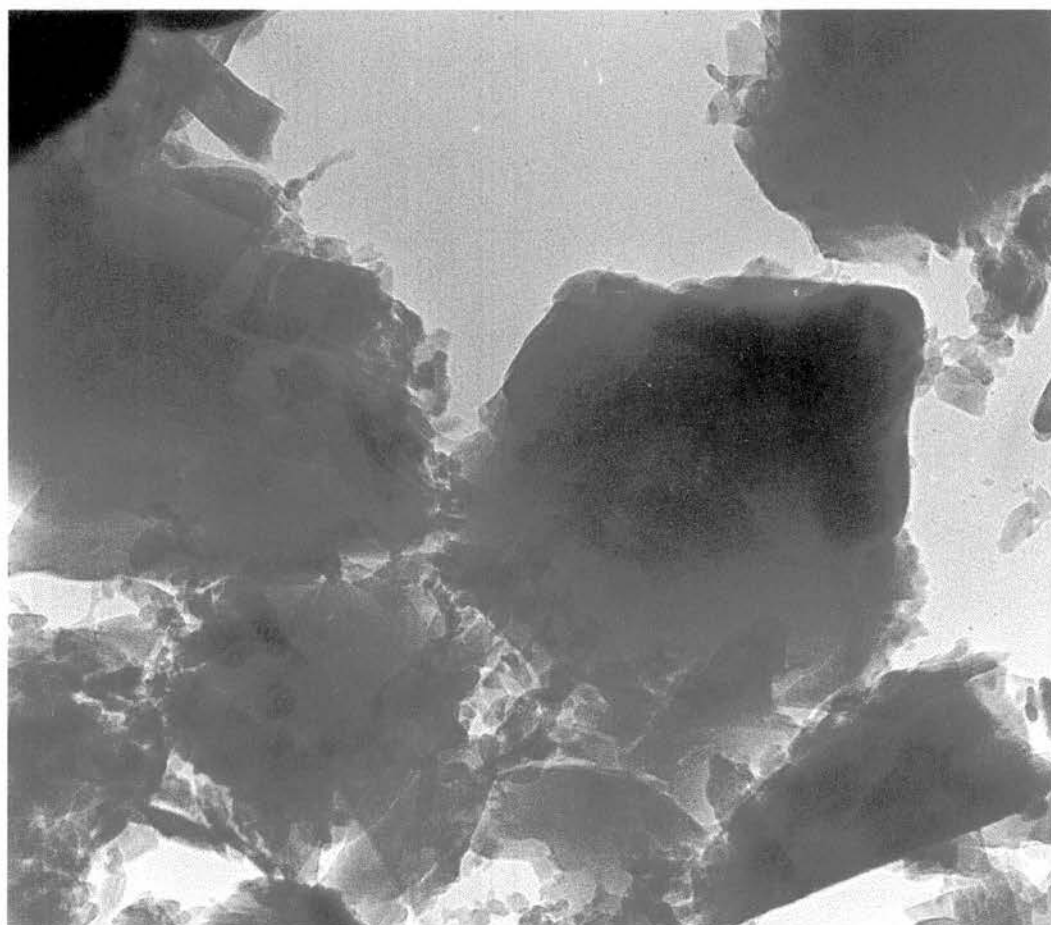
Bond Angles

Atoms	Angle/°
N2—N1—C9	119.7(4)
N1—N2—C3	120.3(4)
N2—C3—C4	125.2(4)
N2—C3—C8	115.0(4)
C4—C3—C8	119.5(4)
O4—C4—O5	118.8(4)
O4—C4—C3	123.(5)
O5—C4—C3	117.3(4)
C4—O5—C6	119.6(4)
O7—C6—O5	109.7(4)
O7—C6—C16	109.5(4)
O5—C6—C16	109.8(4)
O7—C6—C17	105.9(4)
O5—C6—C17	106.5(4)
C16—C6—C17	115.0(5)
C8—O7—C6	118.6(3)
O8—C8—O7	119.3(4)
O8—C8—C3	124.8(5)
O7—C8—C3	115.5(4)
C14—C9—C10	119.6(5)
C14—C9—N1	122.6(4)
C10—C9—N1	117.6(4)
O10—C10—C11	123.9(4)
O10—C10—C9	115.8(4)
C11—C10—C9	120.1(5)
C10—O10—C15	118.1(4)
C10—C11—C12	117.8(5)
C13—C12—C11	122.2(6)
C12—C13—C14	119.0(5)
C9—C14—C13	121.0(5)

Torsion Angles

Atoms	Angle/°
C3—C4—O5—C6	-17.1(7)
C4—O5—C6—O7	45.0(6)
O5—C6—O7—C8	-50.4(6)
C6—O7—C8—C3	27.1(7)
C4—O5—C6—C16	-75.4(6)
C4—O5—C6—C17	159.4(5)
O5—C6—C17—H17C	61.7(7)
O5—C6—C16—H16C	-178.9(5)
C3—N2—N1—H1	8(2)
N2—C3—C8—O8	5.1(8)
N2—C3—C4—O4	-6.9(9)
N2—C3—C8—O7	179.9(4)
N2—C3—C4—O5	175.6(5)
N1—N2—C3—C8	-176.4(5)
N1—N2—C3—C4	-0.5(8)
C9—N1—N2—C3	-178.5(5)
C3—N2—N1—C9	-178.5(5)
N2—N1—C9—C14	-2.9(8)
N2—N1—C9—C10	175.6(5)
N1—C9—C14—C13	178.1(6)
N1—C9—C10—C11	-178.4(5)
C9—C14—C13—C12	0(1)
C9—C10—C11—C12	0.5(9)
C9—C10—O10—C15	173.9(5)
C14—C13—C12—C11	0(1)
C14—C9—C10—C11	0.2(8)
C13—C12—C11—C10	0(1)
C13—C14—C9—C10	-0.4(9)
C11—C10—C9—C14	0.2(8)
C11—C12—C13—C14	0(1)
N1—C9—C14—H14A	-1.8(9)
O10—C10—C9—C14	-178.5(5)
C11—C10—O10—C15	-4.8(8)

Electron Microscopy Photographs



1 μm

Figure 97 - Electron Microscopy Photograph of (23)

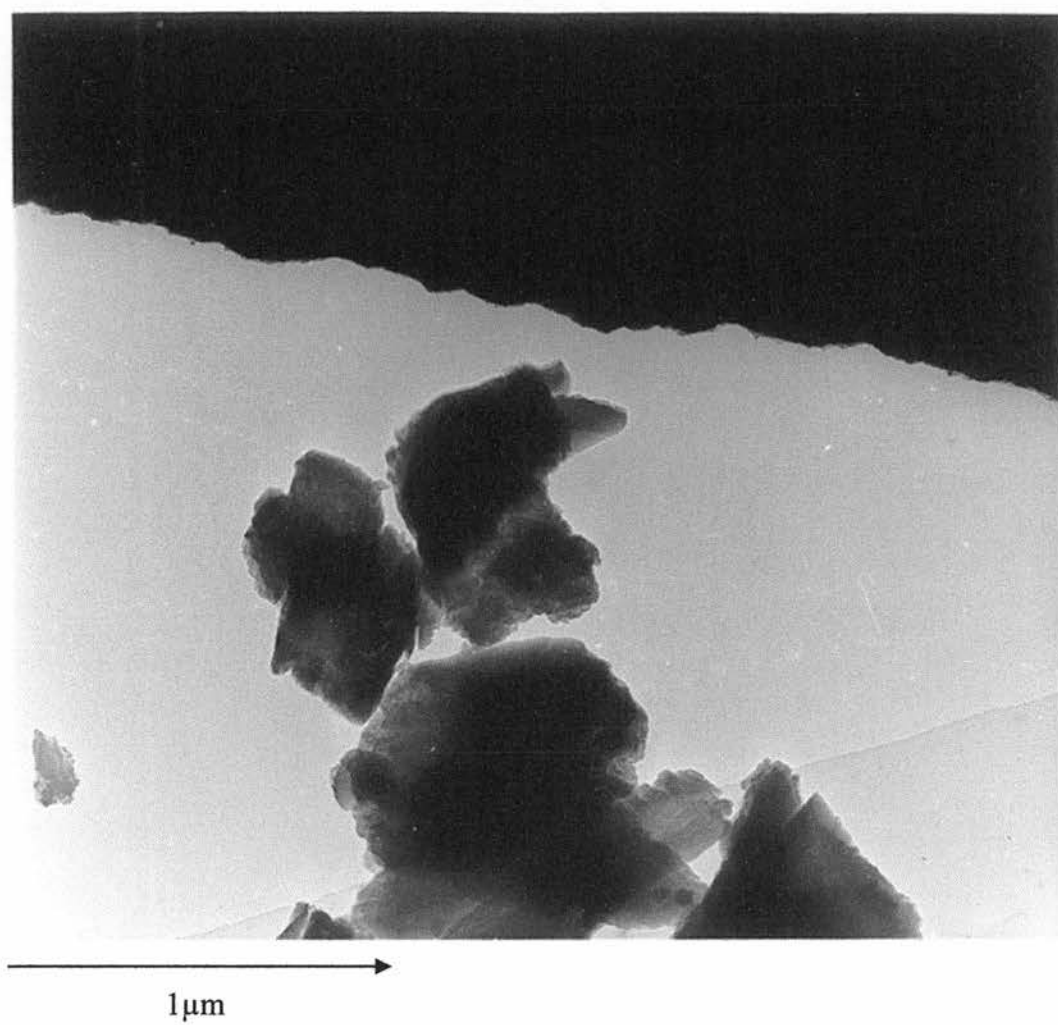


Figure 98 - Electron Microscopy Photograph of (42)

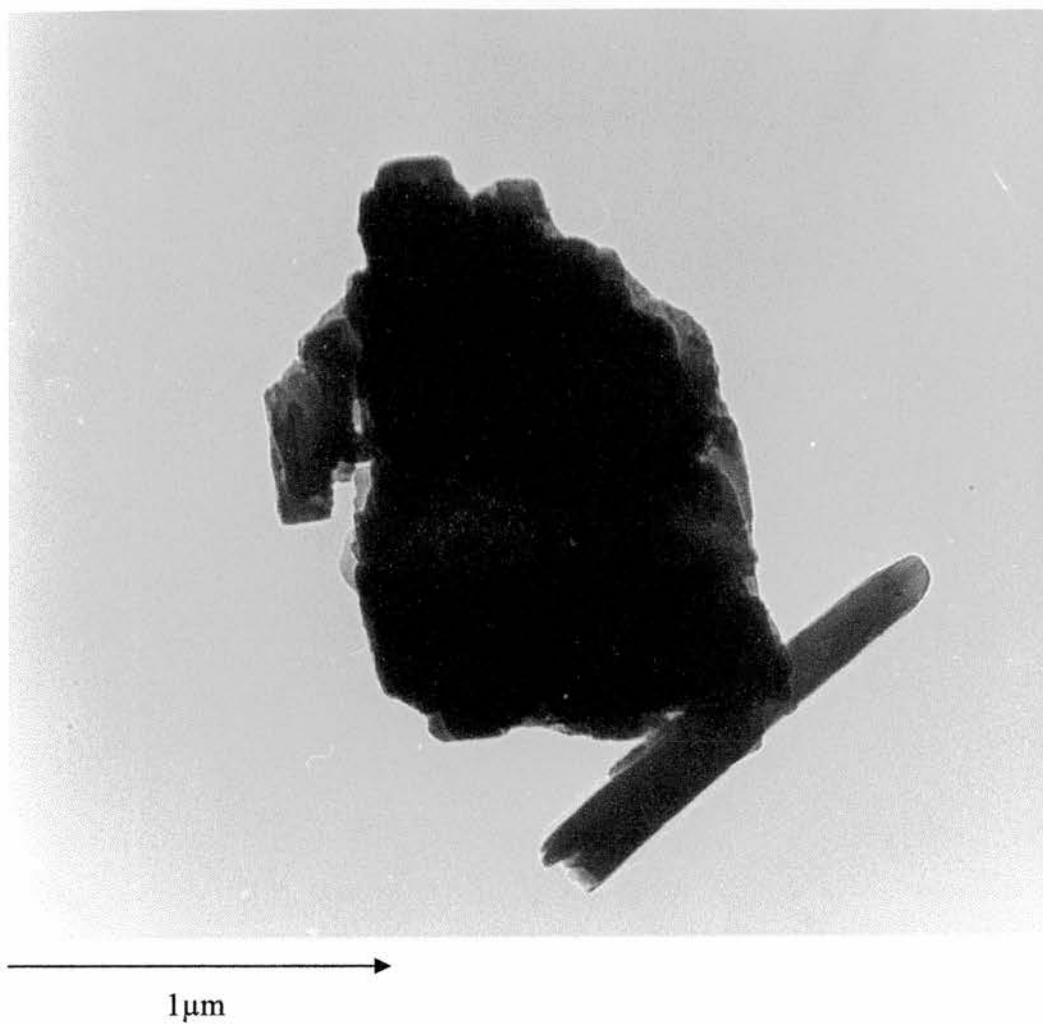


Figure 99 - Electron Microscopy Photograph of (43)

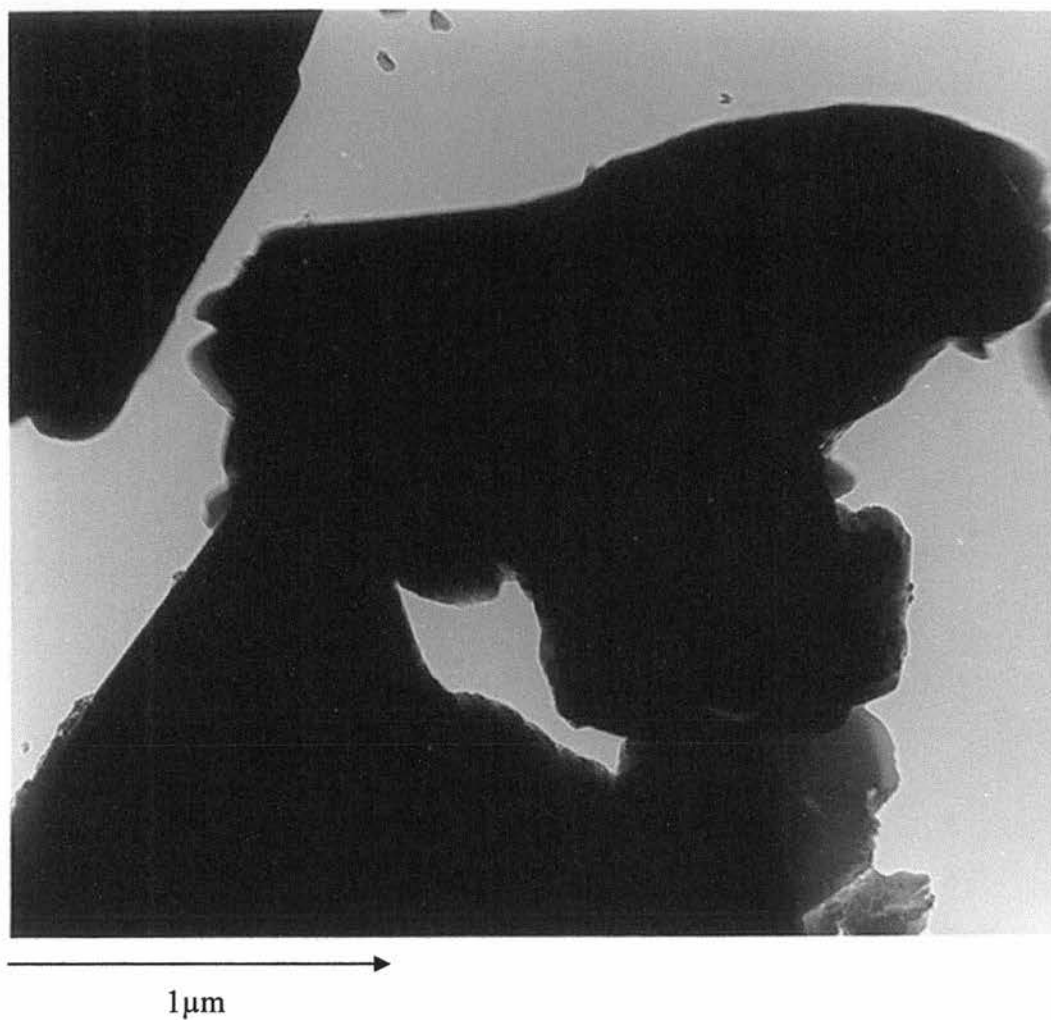


Figure 100 - Electron Microscopy Photograph of (44)

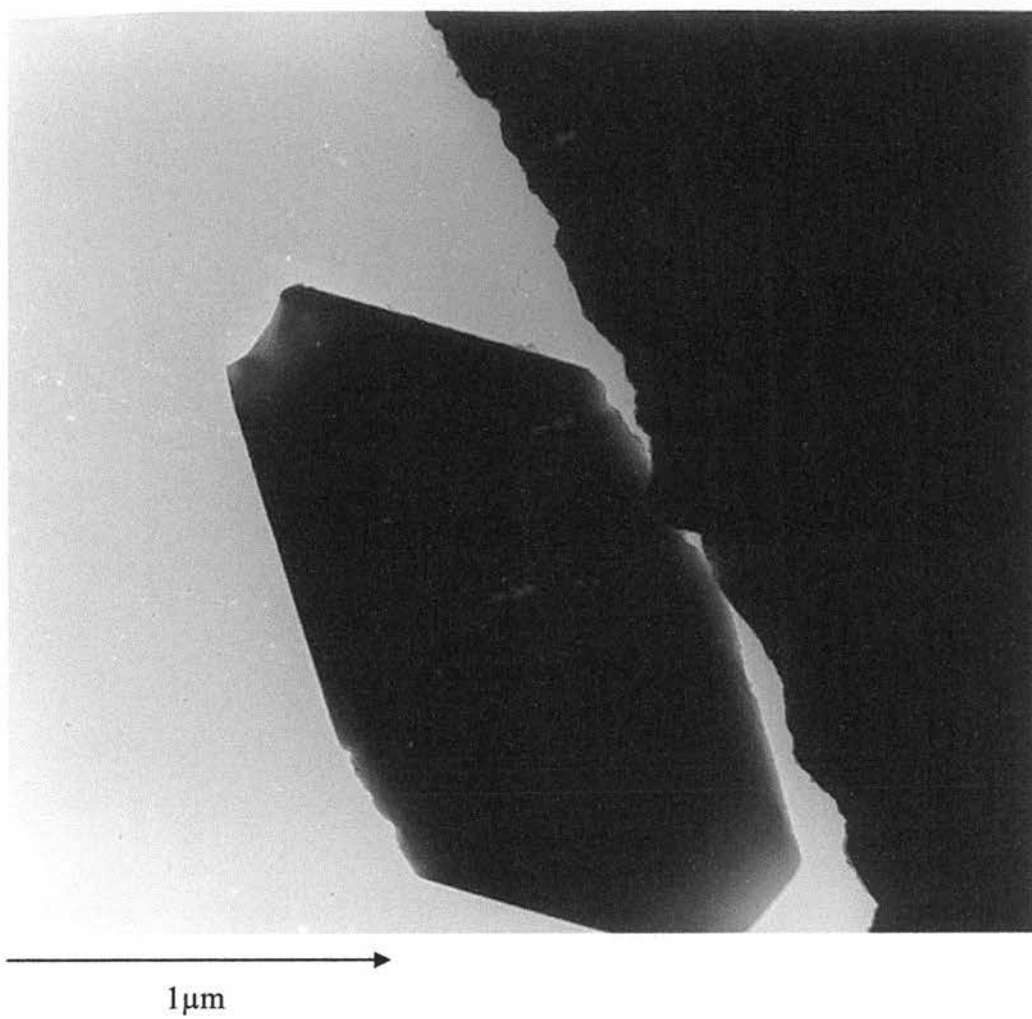


Figure 101 - Electron Microscopy Photograph of (45)

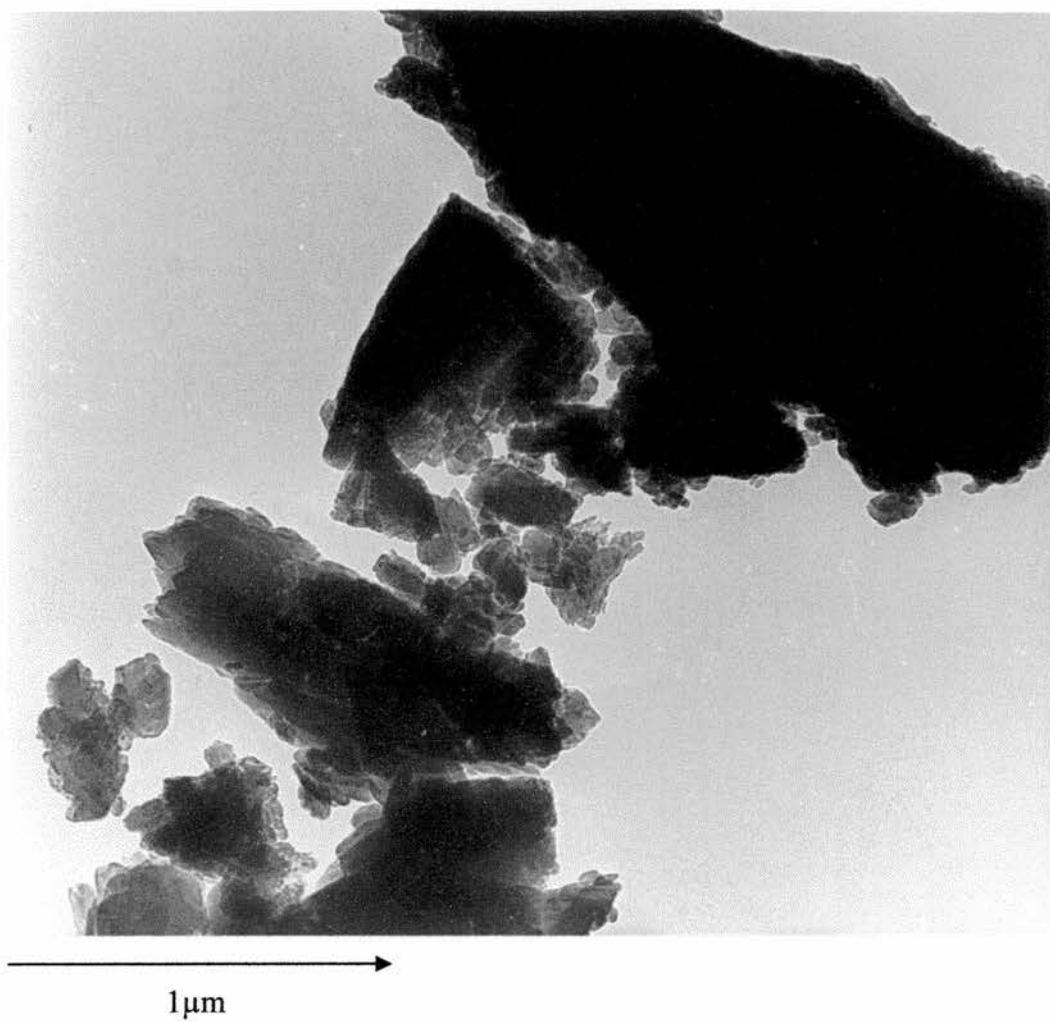


Figure 102 - Electron Microscopy picture of (46)

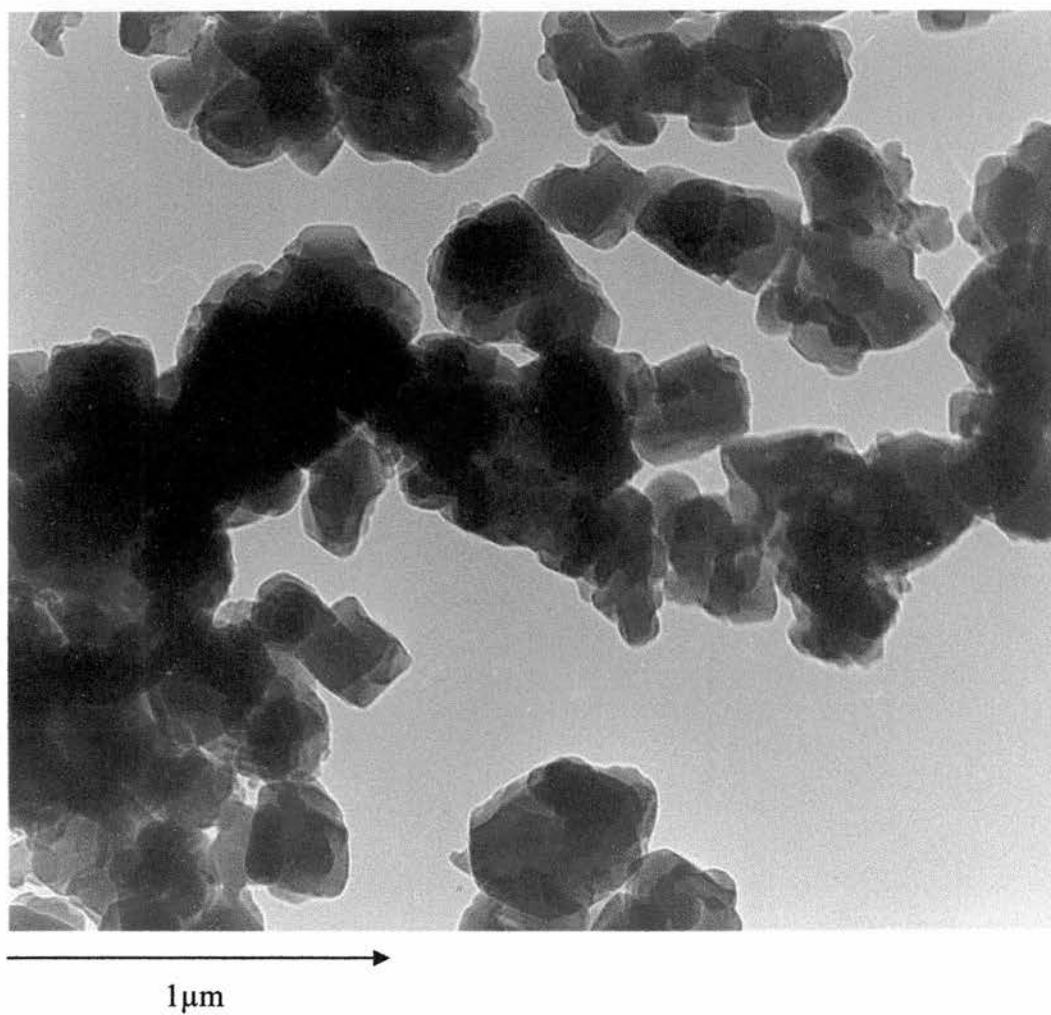


Figure 103 - Electron Microscopy Photograph of (47)

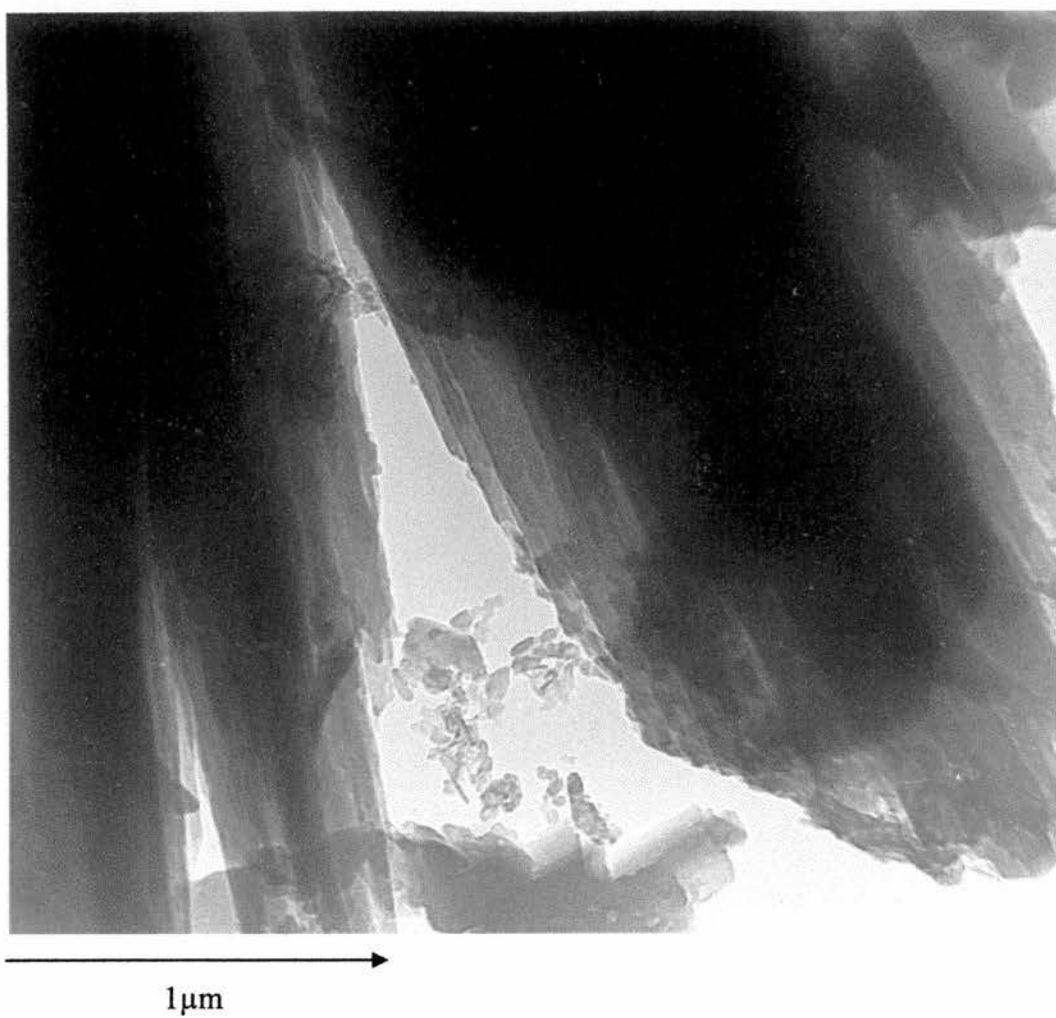


Figure 104 - Electron Microscopy Photograph of (48)

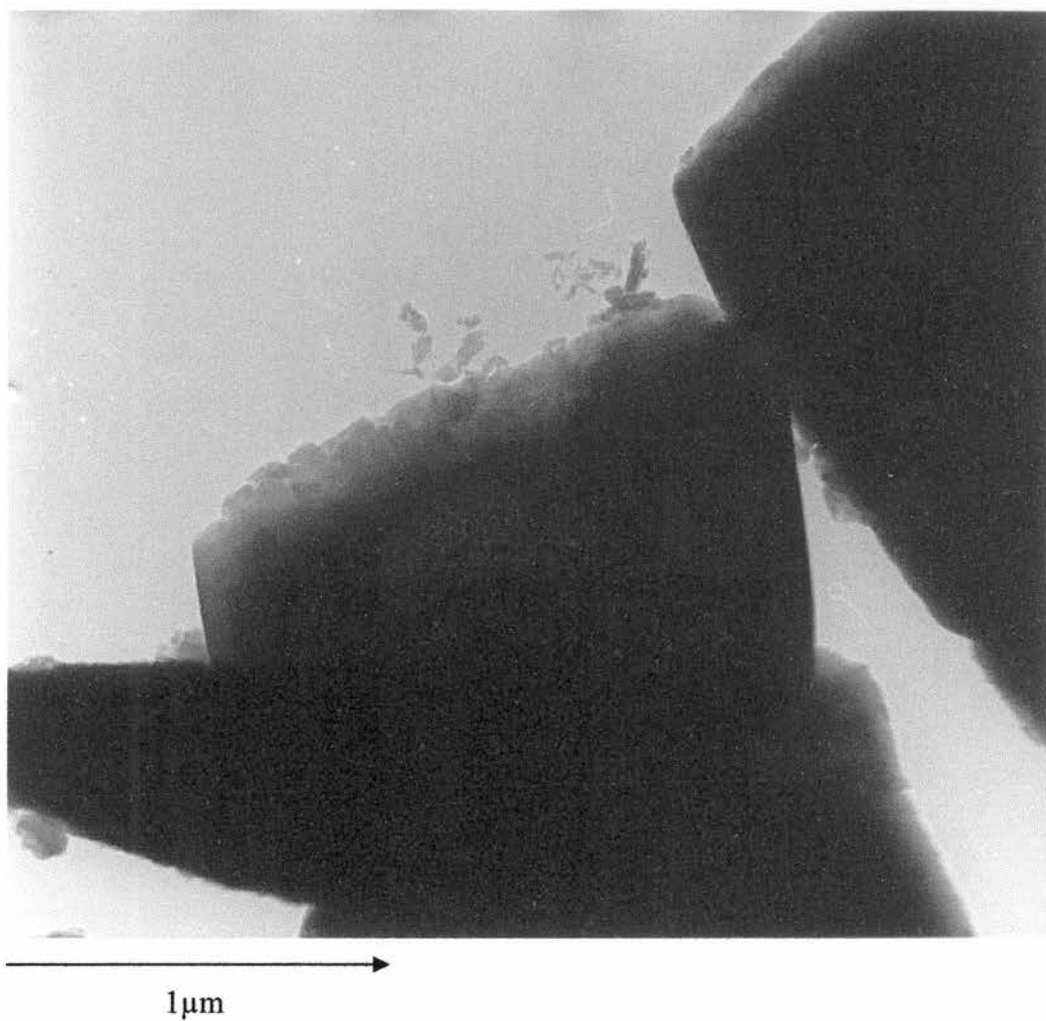


Figure 105 - Electron Microscopy Photograph of (58)

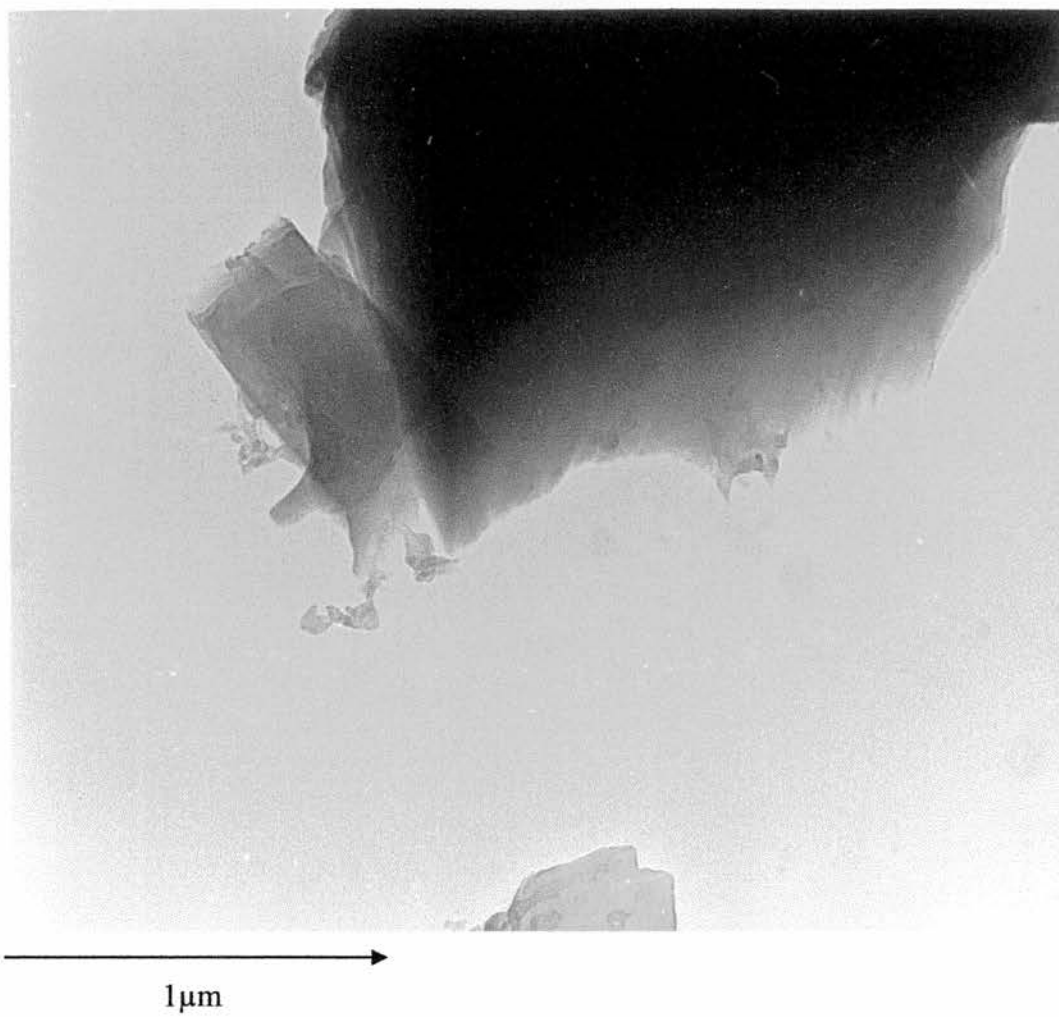


Figure 106 - Electron Microscopy Photograph of (59)

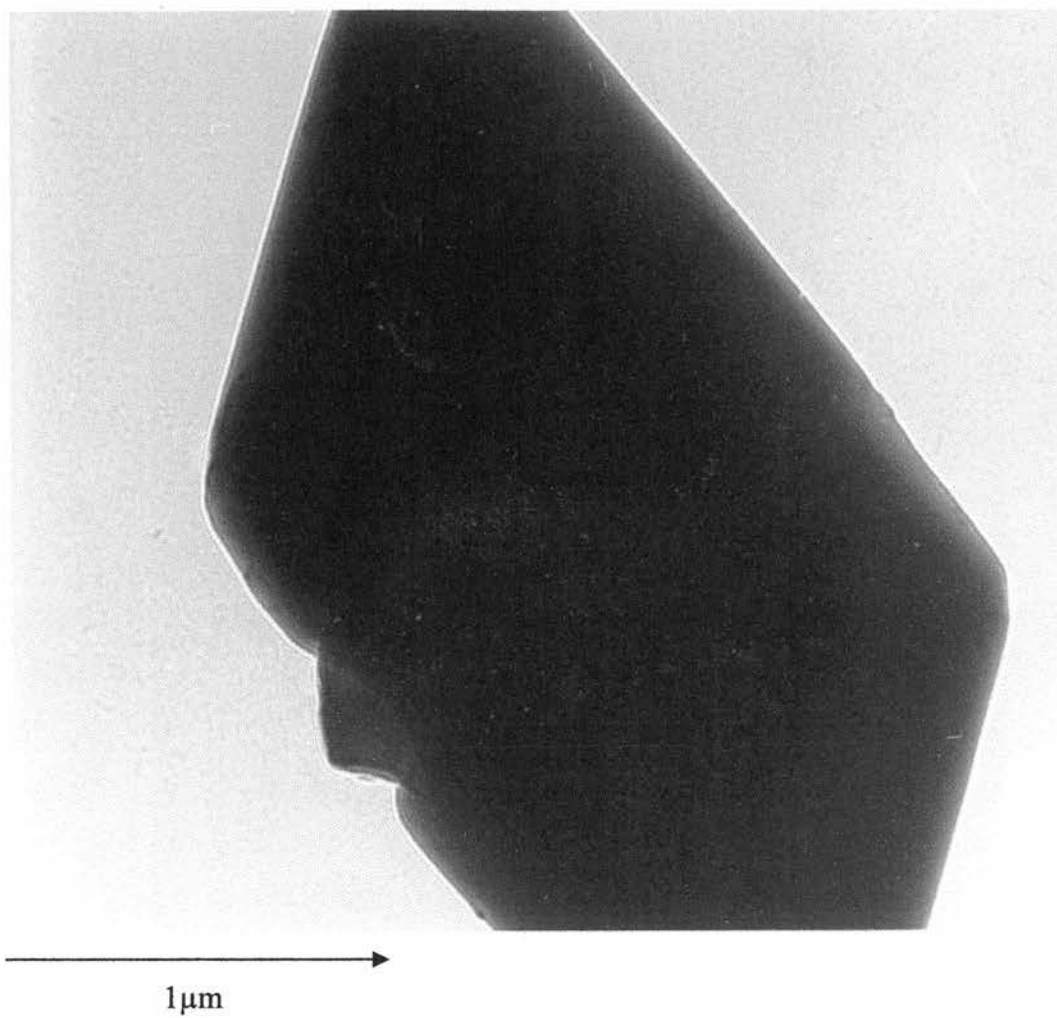
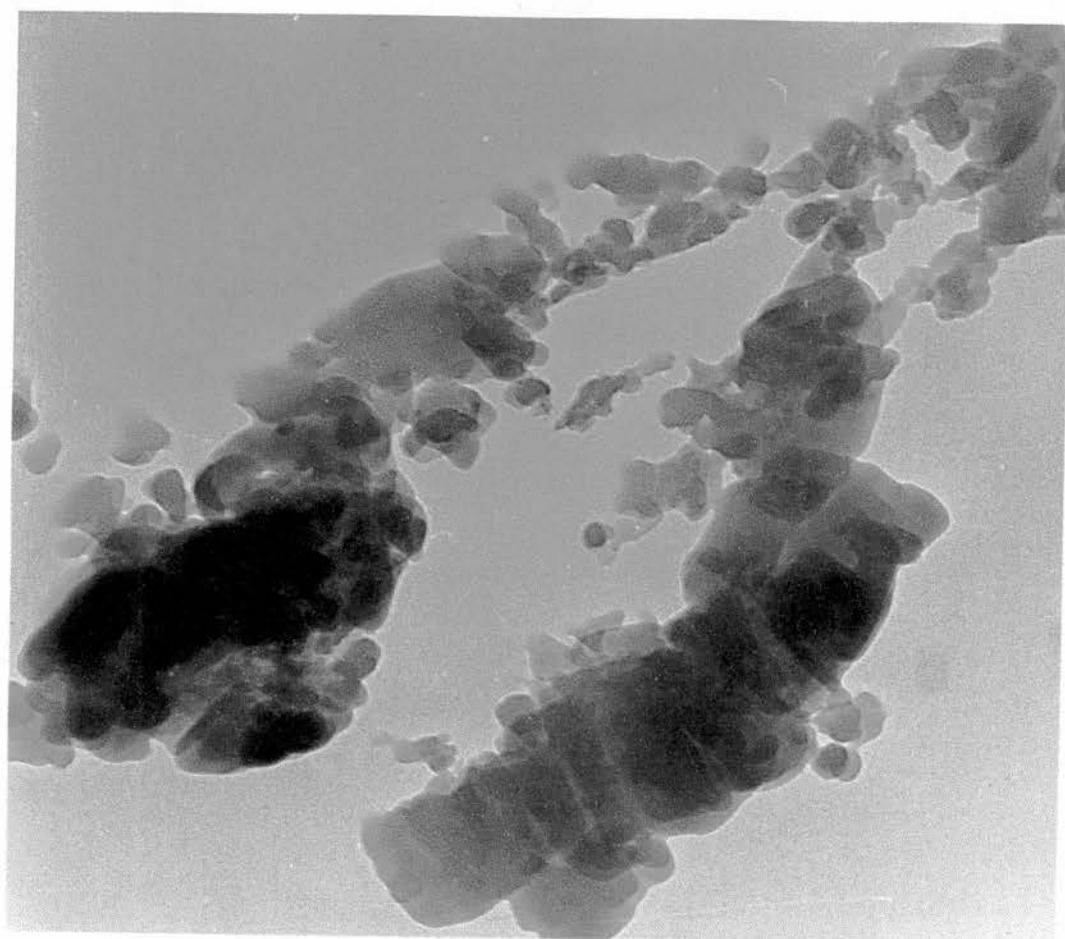


Figure 107 - Electron Microscopy Photograph of (60)



1 μm

Figure 108 - Electron Microscopy Photograph of (61)



1 μm

Figure 109 - Electron Microscopy Photograph of (62)

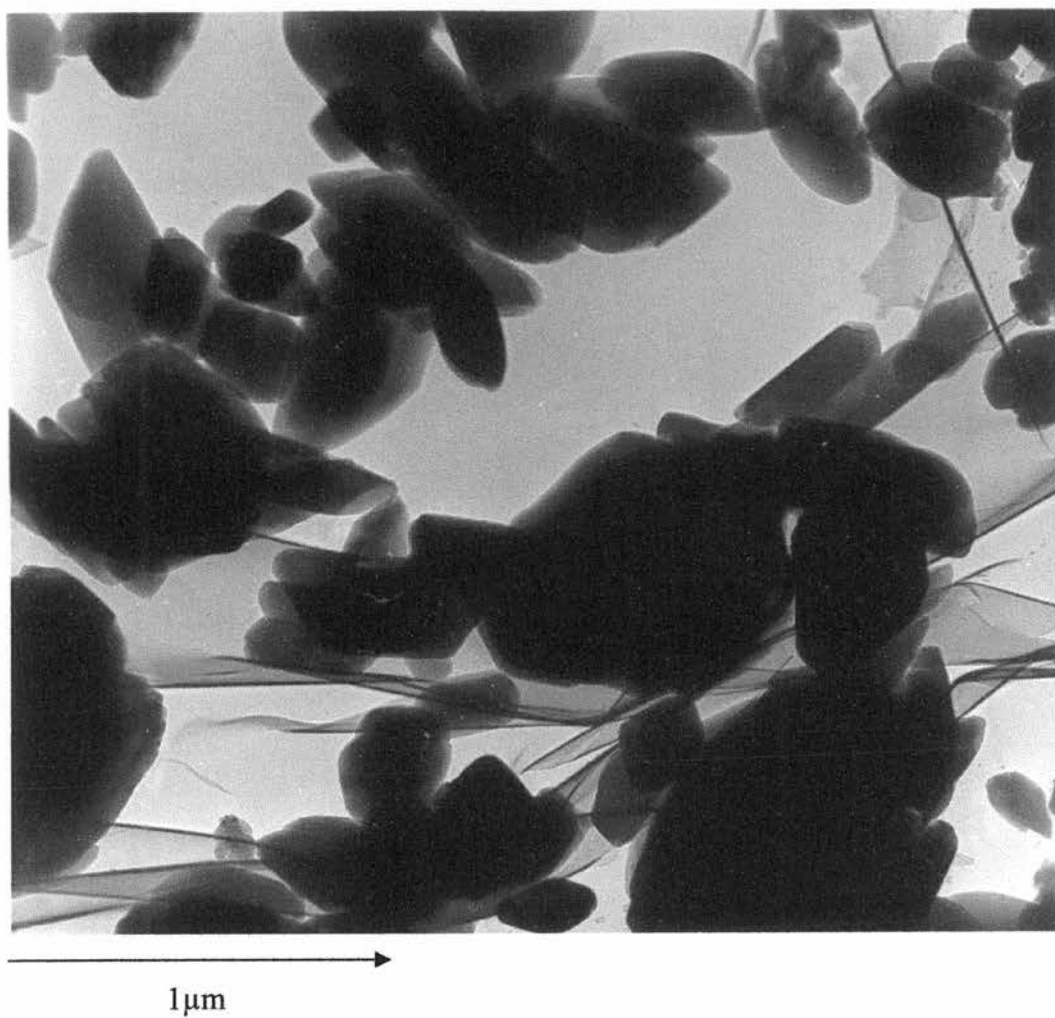


Figure 110 - Electron Microscopy Photograph of (63)

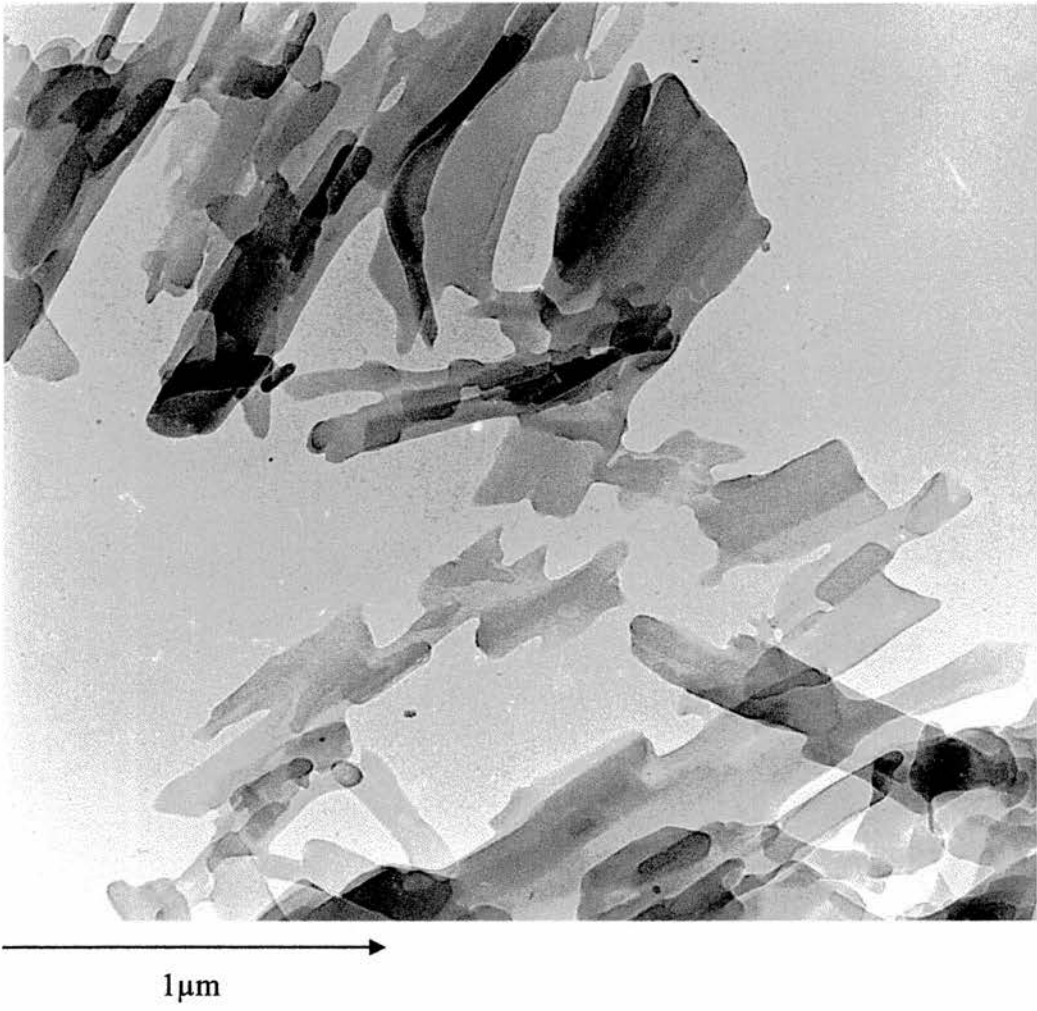


Figure 111 - Electron Microscopy Photograph of (64)

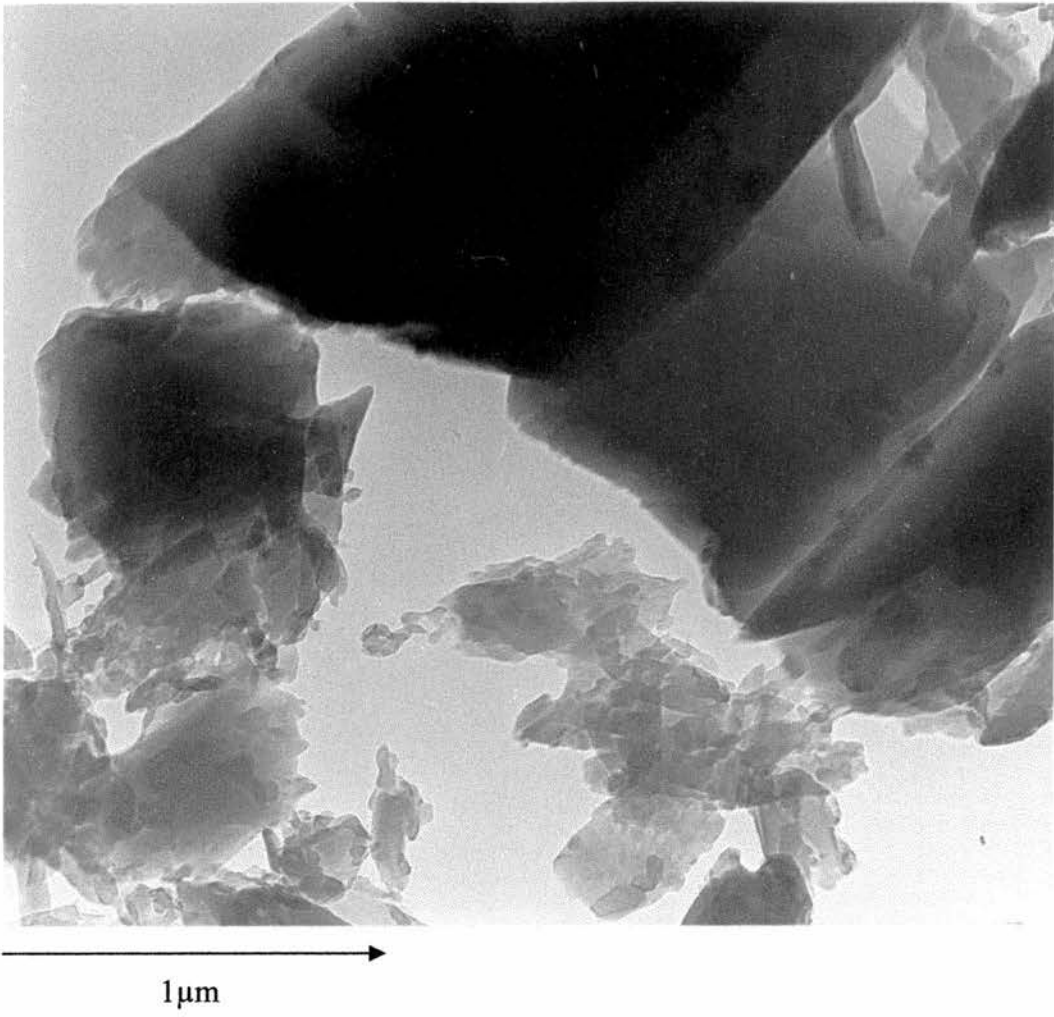


Figure 112 - Electron Microscopy Photograph of (65)